

# Preparation and Characterization of Nanoporous Membranes with Optimized Pore Structure for the Separation of Practice-Relevant Binary Gas Mixtures

Von der Naturwissenschaftlichen Fakultät der  
Gottfried Wilhelm Leibniz Universität Hannover

zur Erlangung des Grades

Doktor der Naturwissenschaften (Dr. rer. nat.)

genehmigte Dissertation

von

Alexander Mundstock, Diplom-Nanostrukturwissenschaftler

2021

Referent: Prof. Dr. rer. nat. Jürgen Caro

Korreferentin: Prof. Dr. rer. nat. Heidemarie Weinhart

Tag der Promotion: 25.02.2021

*"Wenn wir als Wissenschaftler immer wüssten, was wir tun,  
dann würde man das nicht Forschung nennen."*

- ALBERT EINSTEIN

*"The most exciting phrase to hear in science, the one that heralds new discoveries,  
is not «Eureka!» (I found it!) but «That's funny ...»"*

- ISAAC ASIMOV

---



---

## Danksagung

Mit Danksagungen ist das immer so eine Sache. Mir persönlich, und ich glaube damit bin ich nicht alleine, bereitet das Schreiben dieser paar Zeilen fast mehr Probleme als das der eigentlichen Arbeit, der sie eigentlich nur einleitend vorstehen sollen. Da der damit zum nochmaligen Ausdruck gebrachte Dank aber ohne Zweifel mehr als berechtigt und verdient ist, stelle ich mich dieser Herausforderung jedoch immer wieder gerne.

An allererster Stelle möchte ich natürlich Herrn Prof. Dr. Jürgen Caro für die herzliche Aufnahme in seinen Arbeitskreis, die Bereitstellung eines sowohl spannenden als auch fordernden Themas und das damit zum Ausdruck gebrachte Vertrauen in mich sowie seine Geduld danken. Sein Fördern und Fordern, die ausgezeichnete Betreuung, die vielen lebhaften Diskussionen in Kombination mit seinem unglaublichen (für uns "Normalsterbliche") Wissens- und Erfahrungsschatz als auch ganz einfach seine Art haben die letzten Jahre zu einer Erfahrung werden lassen, die ich um Nichts in der Welt missen möchte und die mir in Zukunft sicher noch des Öfteren von Nutzen sein wird.

Ich danke des Weiteren Frau Prof. Dr. Marie Weinhart für die Übernahme des Koreferats sowie Herrn Prof. Dr. Josef-Christian Buhl, der sich als Drittprüfer/Prüfungsvorsitzender zur Verfügung gestellt hat.

Ob man letztendlich gerne zur Arbeit geht oder nicht, hängt zu einem großen Teil von den Menschen ab, die einen dort erwarten. Aus diesem Grund gilt mein Dank auch allen meinen aktuellen und ehemaligen Kollegen (Mitdoktoranden, Sekretariat, Werkstatt, Kooperations-/Industriepartner, Bachelor- und Masteranden usw.) mit denen ich in den letzten Jahren zusammen arbeiten durfte und die ein Arbeitsklima geschaffen haben, in dem man auch gerne mal Überstunden gemacht hat. Möchte jetzt eigentlich noch irgendjemand meine Resturlaubstage kaufen?

Besonders Frank Steinbach sei an dieser Stelle auch noch einmal für seine präparativen Wunder, die Einweisung in alles Mögliche und das geheime REM-Steuerpult gedankt.

Um den täglichen Wahnsinn, den eine Promotion zwangsläufig mit sich bringt, "relativ" unbeschadet überstehen zu können, braucht es Freunde die einen daran erinnern, dass es auch noch so etwas wie ein Privatleben neben der Uni gibt (wenn nötig auch in der Uni). Ich danke euch, wo auch immer ihr gerade rumfliegen mögt und gelobe Besserung was das "Lass dich mal wieder blicken"-Problem angeht. Auch in Hannover hatte ich wieder das unbeschreiblich große Glück, dass aus einigen meiner Kollegen im Laufe der Zeit sehr gute Freunde wurden, bei denen kein Problem, egal ob fachlicher oder privater Natur, auf taube Ohren stieß. Sie tragen eine große Mitschuld daran, dass die Jahre hier wie im Fluge vergangen sind. Danke für Alles. Insbesondere die Abende am runden Tisch werde ich nie vergessen.

Und den Uhu. Und leider auch die Ananas.

---

Für zwei meiner "Mitpflegefälle", Basti und Benni, gilt Letzteres jedoch noch einmal in besonderem Maße. Wer bei seiner Arbeit so viel zu lachen hat, kann sich glücklich schätzen und muss irgendetwas richtig gemacht haben. Mit Leuten wie euch (und natürlich ein paar Bierchen und Dittmann) ist Alles so viel einfacher und Nichts unmöglich.

Auf euch! Man sieht sich.

Als dann auch noch Inca zu uns gestoßen ist, meine erste "Doktorandin" und jemand der eindeutig vom selben Planeten stammt wie ich (wenn auch einem anderen Kontinent), wurde Alles nur noch besser. Freu mich schon auf all die Postkarten aus den entferntesten Ecken dieser Welt.

Nichtsdestotrotz schuldest du mir immer noch ein Currywurst-Frühstück!

Besonderer Dank gilt zu guter Letzt natürlich meinen Eltern Eva-Maria und Peter sowie meinen Großeltern Margot und Joachim für die Möglichkeit, meinen eigenen Weg zu gehen und ihre immerwährende und unerschütterliche Unterstützung auf diesem.

Und ja, jetzt komme ich auch mal wieder etwas länger nach Hause.

---

---

## Abstract

The present thesis is dedicated to the preparation and characterization of a series of supported nanoporous membranes, featuring various materials (metal-organic frameworks (MOFs), zeolites and polymers) and designs (single-component, multilayer and mixed matrix membranes (MMIMs)), as well as the subsequent evaluation of their gas separation capabilities (Wicke-Kallenbach), using the binary gas mixtures propylene/propane and  $H_2/CO_2$  as model systems.

In the case of MOF-74, the right orientation of its 1D channels (perpendicular to the corundum support surface in the best case) inside the dense layers is of utter importance and was eventually achieved to some extent, for the first time ever, by further developing known synthesis procedures. Unfortunately, all resulting Mg-MOF-74 membranes were only able to separate  $H_2$  and  $CO_2$  due to a previously unknown adsorption-founded blockage/self-hindrance in the case of propylene/propane. Neat zeolite type X (NaX) membranes, on the other hand, oftentimes suffer from severe structural issues which could be avoided by pre-synthetically modifying the supports with either PDA (polydopamine) or APTES (3-amino-propyltriethoxysilane), thus simultaneously improving their separation efficiency for both gas mixtures.

In order to investigate the possible benefits of using multilayered instead of monolayered systems for separating hydrogen from carbon dioxide, some of the PDA/NaX membranes were subsequently coated with a Matrimid top layer to create a novel kind of sandwich membrane. The same polyimide was also used to fabricate MMIMs with good  $H_2/CO_2$  separation capabilities, where it serves as flexible and protective matrix for the embedded separation-active zeolite X particles (inorganic filler phase).

Furthermore, it could be shown that using post-synthetic pore optimizations like ion-exchanged faujasite particles (PbX, CuX, NiX and CoX) instead of NaX in the Matrimid-based MMIMs as well as modifying the open Mg sites inside MOF-74's 1D channels with amine groups results in remarkably enhanced hydrogen selectivity due to stronger internal  $CO_2$ -ion/amine interactions. By studying large Co-MOF-74 crystals and their gas uptake behavior before and after the contact with humid air (via infrared microscopy) it was eventually found that even a very short exposure to humidity causes a surface pore blockage (phase transition), completely preventing the adsorption of even small guest molecules, which could be subsequently annealed in a methanol atmosphere.

The thesis includes six publications (three with me as lead author), published in subject-specific, nationally and internationally renowned journals, which are reprinted and arranged in logical, rather than a chronological order.

**Keywords:** Gas Separation,  $H_2/CO_2$ , Olefin/Paraffin, Porous Membranes, MOF-74, Zeolite X, Mixed Matrix Membranes, Matrimid, Amine-Functionalization, Ion-Exchange, Pore Blockade

---





---

## Zusammenfassung

Die vorliegende Dissertation befasst sich mit der Präparation und Charakterisierung einer Serie von geträgerten nanoporösen Membranen in diversen Material- (metallorganische Gerüststrukturen (MOFs), Zeolithe und Polymere) und Designvarianten (Einkomponenten-, Mehrlagen- und Mischphasen-Membranen (MIMMs)) sowie der anschließenden Evaluierung ihrer Gastrennungsvermögen am Beispiel der binären Modellsysteme Propen/Propan und  $H_2/CO_2$ .

Im Falle von MOF-74 spielt dabei die Ausrichtung der 1D Kanäle (bestenfalls senkrecht zur Trägeroberfläche) innerhalb der dichten Schichten eine entscheidende Rolle, welche hier erstmalig durch eine Weiterentwicklung der Syntheseprozedur annähernd erzielt werden konnte. Dennoch zeigten die MOF Membranen aufgrund von bis dato unbekannten adsorptionbedingten Blockierungen bzw. Verengungen nicht das vorausgegangene Olefin/Paraffin-Trennvermögen, sondern waren nur in der Lage,  $H_2$  und  $CO_2$  zu separieren. Andererseits leiden reine Zeolith-Typ X- (NaX) Membranen oft unter schwerwiegenden strukturellen Problemen, welche durch Modifizierungen der Trägeroberflächen mittels PDA (Polydopamin) oder APTES (3-Aminopropyltriethoxysilan) vermieden werden konnten, was gleichzeitig deren Trenneffizienz für beide Gasgemische erheblich verbesserte.

Des Weiteren wurden, um die etwaigen Vorzüge von mehrlagigen Systemen hinsichtlich der Aufreinigung von Wasserstoff untersuchen zu können, neuartige Sandwichmembranen durch das nachträgliche Beschichten der angefertigten PDA/NaX-Membranen mit einer Matrimid-Deckschicht kreiert. Ebenjenes Polyimid wurde anschließend außerdem noch zur Herstellung neuartiger MIMMs mit gutem  $H_2/CO_2$  Trennvermögen benutzt, wo es als flexible und schützende Matrix für die eingebetteten trennungsaktiven Zeolith X-Partikel (anorganische Füllphase) fungiert.

In weiteren Experimenten konnte gezeigt werden, dass postsynthetische Porenoptimierungen wie die Benutzung von ionenausgetauschten FAU-Partikeln (PbX, CuX, NiX und CoX) anstelle von NaX als Füller in Matrimid-basierten MIMMs oder die Modifizierung der offenen Mg-Zentren innerhalb der 1D Kanäle von Mg-MOF-74 mit Aminogruppen in deutlich verbesserten Wasserstoffselektivitäten resultieren. Untersuchungen des Gasaufnahmeverhaltens großer Co-MOF-74 Kristalle vor und nach dem Kontakt mit feuchter Luft (via Infrarotmikroskopie) führten letztendlich zu der Erkenntnis, dass selbst ein sehr kurzer Kontakt mit Luftfeuchtigkeit zu einer Blockierung der Oberflächenporen durch Phasenumwandlung führt, welche die Adsorption selbst kleiner Gastmoleküle vollständig verhindert.

Diese Doktorarbeit enthält sechs Artikel (drei davon mit mir als Erstautor), welche in national und international renommierten Fachzeitschriften veröffentlicht und hier in logischer statt chronologischer Reihenfolge aufgeführt sind.

**Schlagworte:** Gastrennung,  $H_2/CO_2$ , Olefin/Paraffin, Poröse Membranen, MOF-74, Zeolith X, Mischmatrixmembranen, Matrimid, Aminofunktionalisierung, Ionenaustausch, Porenblockierung

---



---

## Table of Contents

<i>Danksagung</i> .....	III
<i>Abstract</i> .....	V
<i>Zusammenfassung</i> .....	VII
<b>I Setting the Scene</b> .....	1
<b>II Motivation</b> .....	2
Separation Principles and Techniques .....	3
Olefins and Paraffins .....	6
Hydrogen and Carbon Dioxide .....	9
<b>III Separation-Active Materials</b> .....	16
Zeolites .....	16
Type X .....	19
Metal-Organic Frameworks .....	21
MOF-74 .....	25
Mixed Matrix Membranes .....	27
Matrimid .....	31
<b>III Measurement Method and Important Physical Quantities</b> .....	34
<b>II Why finding an Olefin/Paraffin-Selective Material is only half the Battle</b> .....	39
<b>III Ethene/Ethane and Propene/Propane Separation via the Olefin and Paraffin     Selective Metal-Organic Framework Adsorbents CPO-27 and ZIF-8</b> .....	41
<b>III Propylen/Propan-Trennung im Festbettadsorber und durch     Membranpermeation</b> .....	51
<b>III Propane/Propene Permeation through Na-X Membranes: The Interplay of     Separation Performance and Pre-Synthetic Functionalization</b> .....	58
<b>III Material Optimizations and their Impact on the H<sub>2</sub>/CO<sub>2</sub> Separation Capability</b> .....	68
<b>III On comparing Permeation through Matrimid-Based Mixed Matrix and     Multilayer Sandwich FAU Membranes: H<sub>2</sub>/CO<sub>2</sub> Separation, Support     Functionalization and Ion Exchange</b> .....	70

---

III.II Amine-Modified Mg-MOF-74/CPO-27-Mg Membrane with Enhanced H <sub>2</sub> /CO <sub>2</sub> Separation .....	81
IV. An Example for the Love-Hate Relationship between MOFs and Humidity .....	92
IV.I Idiosyncrasies of Co <sub>2</sub> (dhtp): In Situ-Annealing by Methanol .....	93
V. Conclusions .....	101
VI Summary .....	101
VII Discussion and Outlook .....	102
<i>Appendix</i> .....	XI
<i>List of Abbreviations</i> .....	XI
<i>Publications</i> .....	XIII
<i>Oral Presentations</i> .....	XVI
<i>Poster Presentations</i> .....	XVII
<i>Patent Applications</i> .....	XVIII
<i>Curriculum Vitae</i> .....	XIX

---

---

## I. Setting the Scene

*"With the colloid septum properly supported, as by a stucco plate in the diffusimeter covered by a thin film of rubber, a considerable separation of mixed gases can be effected"<sup>[1]</sup>*

- SIR THOMAS GRAHAM  
1866

Over one hundred and fifty years have passed since GRAHAM conducted his seminal systematic study on the permeation and separation of various gases (H<sub>2</sub>, CO<sub>2</sub>, CH<sub>4</sub>, O<sub>2</sub>, N<sub>2</sub>, CO ...) through membranes (mostly caoutchouc) <sup>[1]</sup>, which was inspired by the previous works of MITCHELL about the penetrativeness of gases <sup>[2]</sup> and is considered the very first of its kind <sup>[3,4]</sup>, but, at a first glance, surprisingly little seems to have changed regarding the basic means of separation since then. The layered (asymmetric) design mentioned in the quote above, featuring an as thin as possible separation-active/selective layer in combination with a stabilizing/protective porous support, is still today one of the most commonly used and researched on ones for gas separation membranes <sup>[eg. 5, 6]</sup> (and mine are no exemption).

However, not only did GRAHAM play a substantial role in laying the sound technical and scientific foundation for the relatively new field of membrane-based gas separation, e.g. by discovering GRAHAM's law of gas effusion or performing the first quantitative measurements of the rate of gas permeation <sup>[4]</sup>, he also started <sup>[1]</sup> what has been occupying and haunting generations of scientists (including me) ever since, namely the systematic search for the most suitable/selective membrane material for specific separation issues. But while back in the middle of the 19<sup>th</sup> century the high tech materials of choice were mostly processed "natural products" like India/Malay-rubber in varying thicknesses and shapes (vulcanized and untreated), rubberized silk, gelatin as well as membranes made out of platinum and palladium <sup>[1,4]</sup>, today's focus nearly completely lies on specially tailored and fabricated separation-active materials like functionalized metal-organic frameworks (MOFs) and advanced polymers (individually or as mixed matrix membranes (MMM)). And because the scientific, technological and therefore civilisatory progress always was, is and will be directly interwoven with the increasingly demanding need to separate, at first glance inseparable matter like water and salt for desalination, blood and toxins by dialysis (the basic principle was also invented by

---

[1] T. Graham, *J. Chem. Soc.*, 20, 1867, 235-288. (From the Philosophical Transactions for 1866)

[2] J. K. Mitchell, *On the Penetrativeness of Fluids*, Philadelphia: R. A. Skerrett, 1830.

[3] J. Philibert, *Diffusion Fundamentals*, 4, 2006, 6.1 - 6.19.

[4] D. R. Paul, Y. P. Yampol'skii, *Polymeric Gas Separation Membranes*, CRC Press, USA, 1994.

[5] D. F. Sanders, Z. P. Smith, R. Guo, L. M. Robeson, J. E. McGrath, D. R. Paul, B. D. Freeman, *Polymer*, 54, 2013, 4729 - 4761.

[6] N. Rangnekar, N. Mittal, B. Elyassi, J. Caro, M. Tsapatsis, *Chem. Soc. Rev.*, 44, 2015, 7128 - 7154.

GRAHAM<sup>[3]</sup>), uranium isotopes for enrichment or enantiomers for pharmaceutical applications, every new generation of separation materials/techniques has to meet even higher demands.

The nonexistent shortage on either old/novel separation challenges and newly discovered/invented materials is what in turn perpetuates the already mentioned neverending systematic trial-and-error cycle of testing, evaluating and eventually finding the best possible material/method for one (or all?) of those issues. This quest usually tends to be rather resource-consuming and tedious but nevertheless worthwhile, because it could help with some of humanities existing or looming major problems like global warming, pollution and energy production/storage<sup>[7]</sup>.

And due to obvious reasons (i.e. their volatility and very good miscibility in combination with entropy) the separation of different gases, especially very similar ones (comparable weight, size, affinity as well as reactivity), is one of the most difficult tasks at hand and highly desired by chemical industry and therefor science alike.

## II Motivation

But why exactly is our modern world's potential or even well-being to some extent interwoven with and hinged on a few elusive gases?

Ever since the Industrial Revolution, the chemical industry is hooked on fossil fuels as raw material for their efforts to create core basic chemicals (like synthesis gas (CO/H<sub>2</sub>), aromatics and olefins) which literally and figuratively drive our society since then and enable the progress and prosperity we are all accustomed to. While this revolution once started with coal, there has been a gradually shift in the past century to crude oil and natural gas as the main ingredients due to their lower prices, better availability, simpler logistics and the much more versatile spectrum of possible applications<sup>[8]</sup>. The primary cause for the latter one are the available conversion technologies which transform these raw materials into the first core elements of the chemical value-added chain.

Amongst the most important conversion reactions is the so-called steam cracking, where the longer alkanes of *Naphtha* (a distillation fraction of crude oil) are broken down at high temperatures (around 850 °C) and with the dilution of steam into smaller, often unsaturated, hydrocarbons like ethylene and propylene as well as aromatics like toluene and benzene (Fig. 1). Syngas (CO/H<sub>2</sub> + traces of CO<sub>2</sub>) on the other hand, the general-purpose building-block for the chemical industry, can essentially be created from nearly all carboniferous compounds but is mainly produced by steam reforming. Hidden behind this technical term is the high temperature (700 - 1100 °C) nickel-catalyzed reaction of natural gas (up to 98% methane<sup>[8]</sup>) with steam (H<sub>2</sub>O) (Fig. 1) which is responsible for most of today's commercial bulk hydrogen.

---

[7] P. Silva, S. I. f. Vilela, J. P. C. Tome, F. A. Almeida Paz, *Chem. Soc. Rev.*, 44, 2015, 6774 - 6803.

[8] R. Diercks, J.-D. Arndt, S. Freyer, R. Geier, O. Machhammer, J. Schwartz, M. Volland, *Chem. Eng. Technol.*, 31 No. 5, 2008, 631 - 637.

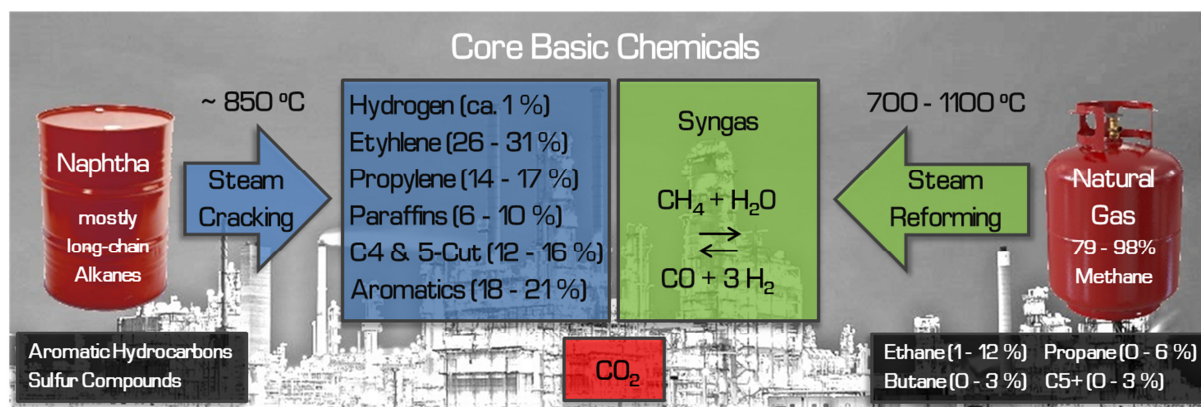


Fig. 1 Important raw materials, conversion techniques and the resulting core basic chemicals of the petrochemical industry (data was derived from [8]).

But as with all good things, they come at a price. Besides the pollution related with the initial mining and drilling and the enormous energy costs of the high temperature conversion reactions, there is one more thing that all fossil fuel based technologies have in common, namely the greenhouse gas CO<sub>2</sub>. Be it as a byproduct of the conversions or from using the final products (e.g. burning diesel in a VW), carbon dioxide is a constant companion of this technology and will be a threat for the world climate as long as we still use fossil fuels and most probably for some time afterwards. Unless, of course, we find new ways of storing or even harnessing this renewable carbon source. [9]

The much more fundamental issue, however, stems directly from the fact that the majority of the important conversion products is gaseous in nature (see Fig. 1). This brings us right back to the topic of this thesis, because, as it is common for many chemical reactions, those products (wanted or not) are received as mixtures and anything but pure. However, their individual purity is exactly what is mandatory for many consecutive reactions, the risk-free use or an unproblematic storage of those conversion products. And considering the energy-intensive nature of the "production"-steps so far, a suitable separation approach should be both effective and energy/resource-saving at the same time.

## Separation Principles and Techniques

Whether or not a separation attempt is successful in the first place, almost entirely depends on how clever the distinct properties of the individual mixture components are exploited by the chosen combination of technique and separation-active material. But no matter how simple or sophisticated the means to this end are right now or will become in the future (from ordinary pinholes via tailored nanoporous frameworks to matrix/compound materials), the underlying and usable fundamental principles are always either kinetic or thermodynamic in nature. [10]

[9] T. Sakakura, J.-C. Choi, H. Yasuda, *Chem. Rev.*, 107, 2007, 2365 - 2387.

[10] A. Mundstock, N. Wang, S. Friebe, J. Caro, *Micropor. Mesopor. Mater.*, 215, 2015, 20 - 28.

A separation achieved by the former one, on the one hand, basically takes advantage of the particle motion and all related physical attributes of the molecules in question like their weight (e.g. effusion) or size (e.g. molecular sieving Fig. 2A). Especially the dimensions of the mixture components are, however, a double-edged sword in a way because they "suffer" from a certain intrinsic flexibility due to the chemical composition/bonding of the compounds, what is eventually taken into account by the so-called critical diameter. This crucial parameter is defined as the smallest possible diameter of a theoretical cylinder which can circumscribe the considered molecule in its most favorable equilibrium conformation <sup>[11]</sup>. It therefore not only simultaneously indicates the smallest pore size this molecule can fit through and by that greatly facilitates the selection of a suitable sieve but is also fundamental to the functioning of the desired separation due to the fact that even small differences in the critical diameter can eventually cause tremendously different diffusion rates of the individual mixture components (e.g. H<sub>2</sub>/propane <sup>[12]</sup>) through the pores of the chosen separation-active material <sup>[13]</sup>. And due to its simplicity, there is no need for extra heating or any electrically driven parts (like it's the case with gas centrifuges), this size exclusion method is by far one the most energy efficient separation technique at hand.

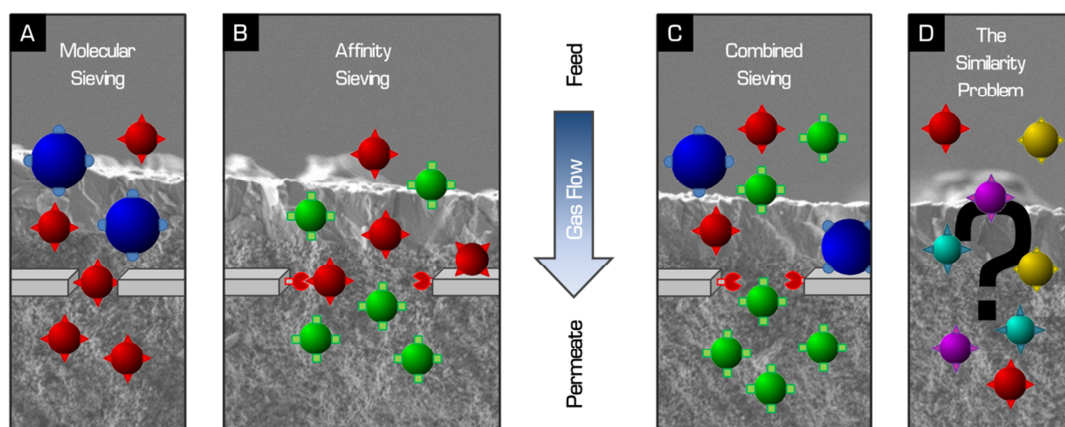


Fig. 2 Schematic representation of the fundamental principles behind molecular sieving (A), affinity sieving (B), the combination of both (C) and the arising similarity problem (D).

Unfortunately, molecular sieving only brings you that far. As soon as the gases in question become too similar in their physical properties, and many of the most important mixtures components are, a separation based solely on kinetic effects is either nearly impossible (e.g. propylene/propane) or not effective enough to be profitable (e.g. H<sub>2</sub>/CO<sub>2</sub>). But even if two guest species with different chemical compositions happen to be nearly indistinguishable in those physical terms, they most probably still show diverging chemical behaviors like different reactivities, solubilities (e.g. scrubbing),

[11] N. Y. Chen, T. F. Degnan Jr., C. Morris Smith, *Molecular Transport and Reaction in Zeolites - Design and Application of Shape Selective Catalysts*, WILEY-VCH, USA, 1994.

[12] A. Huang, Q. Liu, N. Wang, J. Caro, *J. Mater. Chem. A*, 2, 2014, 8246 - 8251.

[13] Z. Song, Y. Huang, L. Wang, S. Li, M. Yu, *Chem. Commun.*, 51, 2015, 373 - 375.



adsorptivities and/or affinities (e.g. chromatography), which can be exploited in thermodynamically driven approaches. The underlying key mechanism behind most of these is thereby that points of molecular interaction, like for example functional groups (i.a. amine, nitrate, carboxylate), free ions or coordinatively unsaturated metal centers within a porous stationary phase (usually membranes or packed powder), can cause equilibrium-based fractionations (affinity sieving Fig. 2B) due to the different mixed gas adsorption equilibria of the individual components.<sup>[10]</sup> As one might expect, the interaction points are boon and bane of this separation method because, while they enable the material to excel in one or a few very specific tasks, they in some cases simultaneously impair it in others, complicate the overall more expensive synthesis (glove-box, post functionalization etc.), pose a threat to the material's stability and make the whole process less energy-efficient due to the necessary activation steps (mostly heat in combination with vacuum or an inert gas flow).

In the end, it is the combination of both complementary fundamental principles mentioned above (Fig. 2C) which has bestowed us with some of the currently best-known and widely-used gas separation techniques like, first and foremost, the so-called pressure swing adsorption (PSA). This process in particular utilizes the sieve effect and large specific surface area inherent to highly porous materials (i.a. zeolites, molecular sieves, activated carbon) in conjunction with the increased adsorption at higher pressures to recover (e.g. H<sub>2</sub>, NH<sub>3</sub>) or remove (e.g. CO<sub>2</sub>) specific gases from industry-relevant mixtures. Naturally, it is impossible to solely adopt the benefits of both separation principles (kinetic and thermodynamic) without suffering from at least some of the known and mentioned drawbacks but, all members of this procedure family (PSA, TSA (temperature) and VSA (vacuum)) are commonly applied nowadays despite the necessary eponymous energy consuming pressure/heat/vacuum generation because of their nevertheless unrivaled cost efficiency, wide range of applications and, once again, the simple lack of alternatives.

That finally leaves us with the worst-case scenario in form of a mixture composed of gases with very similar dimensions as well as affinities (Fig. 2D), like it's the case with olefins and paraffins. Simply put, none of the countless efforts and ideas pursued so far has yielded a comparably reliable (easy scalability and maintenance, high capacity ...) but more reasonable/sustainable separation technique than cryogenic distillation (CD) to satisfactorily solve this kind of similarity problem.<sup>[14]</sup> As the name implies, this process, which was (in its basic form) invented<sup>[15]</sup> and pioneered by LINDE for the purpose of air separation in the late 1800s/early 1900s, basically uses subzero temperatures to at first liquefy the gaseous mixture components and subsequently separate them via distillation, utilizing their different boiling points. The hard-won separation achieved by this means, however, is, due to the inherent nature of the indispensable process itself (mainly the necessary cooling), yet again bought at the expense of a tremendous parasitic resource, time and energy consumption.

Summing up, it seems that most of the currently applied ("state of the art") separation procedures are, quite frankly, nothing more than a compromise between satisfying the industry's enormous

---

[14] J. R. Alcantara-Avila, F. I. Gomez-Castro, J. G. Segovia-Hernandez, K.-I. Sotowa, T. Horikawa, *Chem. Eng. Process*, 82, 2014, 112 - 122.

[15] C. Linde, *Ann. Phys.*, 293 (2), 1896, 328 - 332.

hunger for pure basic chemicals and their resource inefficiency, which is, without much ado, readily tolerated for the sake of prosperity and progress. However, in the light of the facts that the demand for this kind of raw materials is not likely to decrease or even stay at the present level in the years to come and this world's resources are dwindling at a disquieting pace, the need and consequential search for novel separation-active materials, usable in well-known as well as future separation processes, has become a major scientific concern. And because they represent/suffer from a multitude of the above-mentioned challenges, two of today's most prominent and pressing separation issues are especially well-suited to serve as guinea pigs in this regard.

## Olefins and Paraffins

As already mentioned in passing earlier, short chain ( $C_2/C_3$ ) hydrocarbons are a by-/main product of various petrochemical processes (e.g. steam cracking (see Fig. 1 and 3)) and a highly sought after core resource.<sup>[8]</sup> How fundamental especially the olefins have become to modern industry/society is evidenced by the fact that many complimentary processes, with the sole purpose of providing more and more ethylene and propylene, have been developed over the years like for example the catalytic conversion of MeOH (methanol-to-olefins process (MTO)) or dehydrogenation of alkanes, which in turn are mainly obtained from natural gas and coal liquefaction/hydrogenation via the Fischer-Tropsch process (see Fig. 3). The interplay between these manifold generation possibilities and the steady rise in demand for  $C_2H_4$  and  $C_3H_6$  has led to ever-growing annual production figures in the current range of roughly  $1.5 \times 10^8$  t and  $8 \times 10^7$  t, respectively (data from 2009<sup>[16]</sup>).

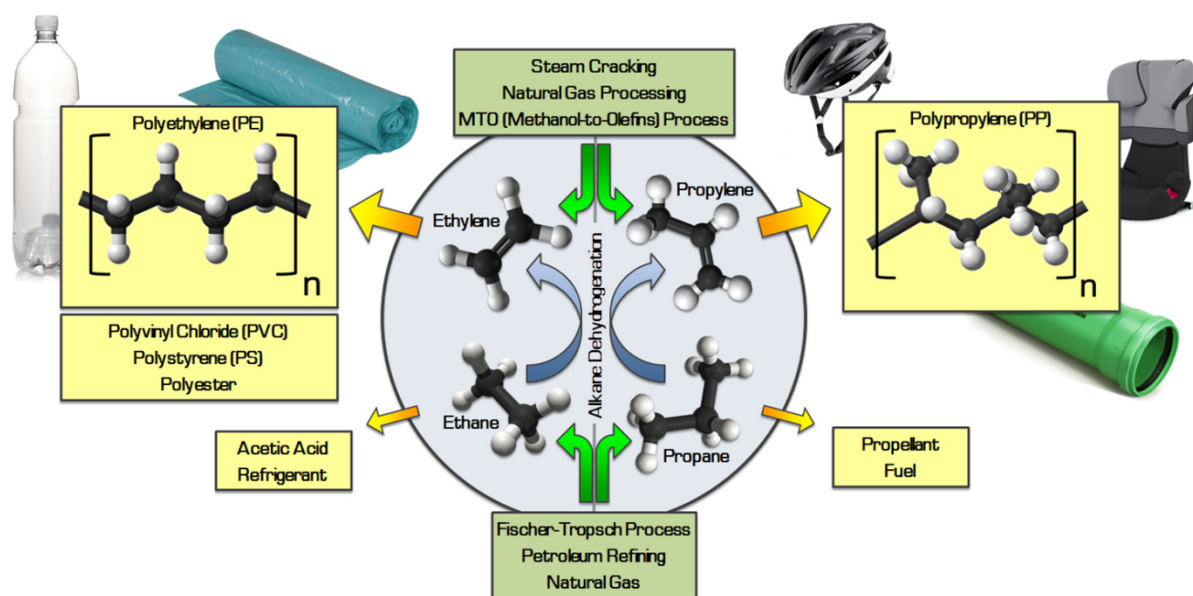


Fig. 3 Main sources, production routes, applications as well as derived products of/from  $C_2$  -  $C_3$  olefins and paraffins.

Their popularity, however, is not mainly rooted in a direct usability, as it is the case with e.g. hydrogen, methane or solvents in general, but rather in the ability to form polyolefin polymers, which account for 62% (2013 <sup>[17]</sup>) of all plastic materials in use right now, by means of a catalyzed (ionic, radical or coordinative double-bond opening) chain polymerization reaction. <sup>[18]</sup> But like so many world-shaking and -shaping scientific achievements, polyethylene (PE), and consequently many subsequent findings in the field of polymers, was discovered by pure chance and contaminated educts.

What started as 0.4 g of an unknown "*Waxy solid found in reaction tube*" by FAWECKETT and GIBSON (ICI Research in Winnington, Cheshire, England) after a high pressure reaction (1900 atmospheres, 170 °C) of benzaldehyde and ethylene (with enough oxygen to initiate the free radical polymerization) in 1933 has actually sounded the bell for a "polymer age" and developed into a global industry producing over 80 million tons of PE per year (in 2013). <sup>[18]</sup> In the end, it took another 20 years after this first step before HOGAN and BANKS (Phillips Petroleum), after a neck-and-neck race with a hand full of other scientists like NATTA, BAXTER and VANDENBERG, were able to reliably synthesize crystalline polypropylene (PP) using a chromium catalyst (and another 32 years before the patent was issued), thereby helping to create the second polymeric pillar (86 million tons/year estimated for 2018) our modern world is built on. <sup>[18]</sup> Whereas the latter is mainly used for e.g. cable coatings, pipes, insulations, bicycle helmets, furniture and, in general, everything where sturdiness and/or a certain heat resistance comes in handy, PE shines when a high chemical resistance, good electrical conductivity or better pliability/flexibility (at the expense of its mechanical properties) is needed, as is the case with chemical containers, anti-static protection as well as all "essentials" for a throwaway society such as bags (shopping, garbage etc.), bottles, foils and packaging. The feature, however, which all polymers, including other "products" of ethylene like PVC, PS or polyesters (Fig. 3), have in common and what makes this substance class so unique and ubiquitous, is their easy processability (e.g. injection molding, extrusion or melt spinning) in combination with a nearly limitless moldability.

But no matter how pedestrian or elaborate the final product might be, it all starts, stands and falls with the one key requirement no chemical reaction or manufacturing process can work around and function without, namely the right quality/purity of the educts in question. As already shown in Fig. 1 and the associated text passages, the raw products provided by the leading petrochemical conversion reactions like *Naphtha* cracking (thermal or catalytic) are far from pure (mixtures of C<sub>2</sub> - C<sub>5</sub> olefins and paraffins, hydrogen, aromatics etc. <sup>[8]</sup>) and therefor need to undergo a whole cascade of subsequent purification steps (distillations, fractioning or splitting) before they can be of any further use. In the case of olefins, this is done until everything but 6 - 10% of the corresponding paraffin is removed from the individual main product, the so-called chemical grade <sup>[19]</sup>, which represents a negligible amount of impurity for many consecutive reactions and processes (e.g. the

---

[17] *Polyolefins Report*, IHS Chemicals, 2014.

[18] M. Al-Ali AIMa'adeed, I. Krupa, *Polyolefin Compounds and Materials Fundamentals and Industrial Applications*, VI, Springer, 2016.

[19] V. Spallina, I. C. Velarde, J. A. Medrano Jimenez, H. R. Godini, F. Gallucci, M. Van Sint Annaland, *Energy Convers. Manag.*, 154, 2017, 244 - 261.

production of acrylonitrile, oxo-alcohols or propylene oxide). The catch, however, is that polymerization is one of the few exceptions thereof, requiring even higher purities of about 99.5% (PP) and > 99.9% (PE)<sup>[19]</sup>, as well as the fact that those "normal" purification procedures simply can't provide such values when it comes to gases with this grade of similarity (see Table 1).

**Table 1** Separation-relevant parameters of ethane, ethylene, propane and propylene (data from<sup>[20]</sup>)

Gas	Normal boiling point / °C	Critical temperature / °C	Critical volume /cm <sup>3</sup> mol <sup>-1</sup>	Critical pressure /bar	Kinetic diameter /Å	Polarizability x10 <sup>25</sup> /cm <sup>3</sup>
Ethane	-88.60	32.17	145.50	48.72	4.443	44.3 - 44.7
Ethylene	-103.73	9.19	131.10	50.41	4.163	42.52
Propane	-42.13	96.68	200	42.48	4.3 - 5.118	62.9 - 63.7
Propylene	-47.69	91.75	184.6	46	4.678	62.6

The only feasible way to reliably conquer this similarity problem and, thereby, ensure a perpetual supply of polymer grade olefins at the moment is by cryogenic distillation whose very nature enables the separation but simultaneously makes it one of the most energy-intensive petrochemical processes in use, consuming (for example) up to 85% of the overall power required throughout the entire olefin generation process.<sup>[21]</sup> Because this number obviously represents a huge savings potential in terms of money, resources, time and plant space, as well as the perfect "adjusting screw" for greatly enhancing the environmental sustainability of the polymer production in its entirety, it comes as no surprise that there has been an ongoing effort/struggle by industry and science alike to replace CD with a more reasonable olefin/paraffin separation method.

Amongst all the various approaches devised during this quest, including e.g. extractive distillation, chemisorption of the olefins by immobilized metal complexes/complexing solutions (sparged vessel)<sup>[22]</sup> as well as supported liquid membranes<sup>[23]</sup>, the "simple" permeation through nanoporous materials (natural or tailored) with their inherent ability to thermodynamically (affinities) and/or kinetically (pore size) overcome said similarity problem seems to harbor the most potential in this regard. Recent research examples for this kind of separation-active substances in their most common form of deployment, as thin composite membranes, are polysulfone hollow fibers<sup>[24]</sup>,

[20] J.-R. Li, J. Kuppler, H.-C. Zhou, *Chem. Soc. Rev.*, 38, 2009, 1477 - 1504.

[21] A. Van Miltenburg, W. Zhu, F. Kapteijn, J. A. Moulijn, *Chem. Eng. Res. Des.*, 84 (5), 2006, 350 - 354.

[22] R. B. Eldridge, *Ind. Eng. Chem. Res.*, 32, 1993, 2208 - 2212.

[23] B. Jiang, H. Dou, B. Wang, Y. Sun, Z. Huang, H. Bi, L. Zhang, H. Yang, *ACS Sustainable Chem. Eng.*, 5, 2017, 6873 - 6882.

[24] A. Ovcharova, V. Vasilevsky, I. Borisov, S. Bazhenov, A. Volkov, A. Bidyukevich, V. Volkov, *Sep. Purif. Technol.*, 183, 2017, 162 - 172.

MgO nanosheets in a comb copolymeric matrix <sup>[25]</sup>, boron embedded carbon <sup>[26]</sup>, NaX zeolite (membranes <sup>[10]</sup> or beads <sup>[27]</sup>) and metal-organic frameworks like polycrystalline ZIF-8 (zeolitic imidazolate framework) <sup>[28]</sup>, Cu-BTC (trimesic acid) <sup>[29]</sup> or MOF-74 <sup>[30]</sup>. What strikes the eye is that most of those porous materials (e.g. the latter two) as well as many of the alternatives exploit one and the same mechanism in order to gain their olefin/paraffin separation potential, namely the ability of the incorporated metal-ions/unsaturated metal centers to form weak chemical bonds with unsaturated hydrocarbons via  $\pi$ -complexation <sup>[31]</sup>.

But despite all the extensive research done in the field of permeation-based olefin/paraffin separation over the last decades and the occasional "false" beacon of hope, which, for example, meets the commercial viability limit for the propene/propylene separation factor (SF) of about 35 <sup>[32]</sup> but only by applying resource-intensive high sweep gas fluxes (e.g. ZIF-8,  $SF_{\text{propylene/propane}} > 150$ , 100 cc/min argon sweep <sup>[28]</sup>) and utilizing the resulting counter-diffusion, no feasible replacement has been found for cryogenic distillation so far. Considering their nearly limitless customizability (pre- and post-synthetic), easy combinability with other materials (coatings, polymer matrices etc.) as well as increasingly well understood internal workings and possibilities (like breathing or switching), however, the potential of nanoporous separation-active substances like MOFs (still "relatively" new) and zeolites is far from being exhausted yet.

## Hydrogen and Carbon Dioxide

Whereas the previously discussed olefins and paraffins only play a rather minor and indirect role regarding the (nowadays omnipresent) man-made climate change, mainly arising from their elaborate separation needs, two other gases are particularly associated with this very complex scientific, political and even social hot topic, namely hydrogen, with its promise of clean energy, and the greenhouse gas carbon dioxide. The latter is, despite all the "recent" fuss, no novelty or purely artificial phenomenon but has many natural sources like erupting volcanoes, geysers, aerobic respiration, decay as well as fermentation and remains essential for this planets capability to sustain life as we know it because plants require it to perform photosynthesis. As any chemist can

---

[25] C. H. Park, J. H. Lee, J. P. Jung, J. H. Kim, *J. Membr. Sci.*, 533, 2017, 48 - 56.

[26] K.-S. Liao, S. Japip, J.-Y. Lai, T.-S. Chung, *J. Membr. Sci.*, 534, 2017, 92 - 99.

[27] G. Narin, V. F. D. Martins, M. Campo, A. M. Ribeiro, A. Ferreira, J. C. Santos, K. Schumann, A. E. Rodrigues, *Sep. Purif. Technol.*, 133, 2014, 452 - 475.

[28] M. J. Lee, H. T. Kwon, H.-K. Jeong, *J. Membr. Sci.*, 529, 2017, 105 - 113.

[29] A. Luna-Triguero, J. M. Vicent-Luna, P. Gomez-Alvarez, S. Calero, *J. Phys. Chem. C*, 121, 2017, 3126 - 3132.

[30] U. Böhme, B. Barth, C. Paula, A. Kuhnt, W. Schwieger, A. Mundstock, J. Caro, M. Hartmann, *Langmuir*, 29, 2013, 8592 - 8600.

[31] R. T. Yang, E. S. Kikkinides, *AIChE Journal*, 41, 1995, 509 - 517.

[32] C. H. Colling, G. Bartels, US 20040004040 A1, 2004.

confirm, however, usefulness/harmlessness always depends on concentration (PARACELTUS) and the 32.3 Gt/a of  $\text{CO}_2$  (2016) <sup>[33]</sup> which are emitted as by-product of many vital industrial/day-to-day processes (combustion of fossil fuels for transportation and energy generation (around 65% <sup>[34]</sup>), water-gas shift reaction, production of bioethanol or cement (see Fig. 4) are enough to noticeably change the climate and threaten the habitability (for humans) of this world in the long run, even if they are not toxic to animal life on their own yet. Hydrogen, on the other hand, is always a very welcome, versatile and "green" product/resource sought after by nature (e.g. the anaerobic hydrogen cycle or water splitting by photosynthetic bacteria/algae via hydrogenase <sup>[35]</sup>) and humanity alike, mostly (in our case) regardless of the effort and repercussions involved. Today, after nearly 350 years of artificial  $\text{H}_2$  generation (ROBERT BOYLE first described the reaction between iron and acid in 1671 <sup>[36]</sup>), the annual production amounts to over 65 million tons (55 Mt in 2013 with a 6% increase per year) from various sources like oil/naphtha reforming (30%), coal gasification (18%) and water electrolysis (3.9%). <sup>[37]</sup> The dilemma with the remaining close to 50% is that they are procured solely by means of steam reforming (Fig. 1) and the subsequent so-called water-gas shift (WGS) (Fig. 4), a highly temperature (mostly a high- and low- $T$  stage) and catalyst (stage-specific composition) dependent reaction of carbon monoxide and water vapor which indeed delivers the desired hydrogen at justifiable efforts but, unfortunately, always contaminated with a considerable amount of the aforementioned greenhouse gas  $\text{CO}_2$  (above 20% <sup>[38]</sup>).

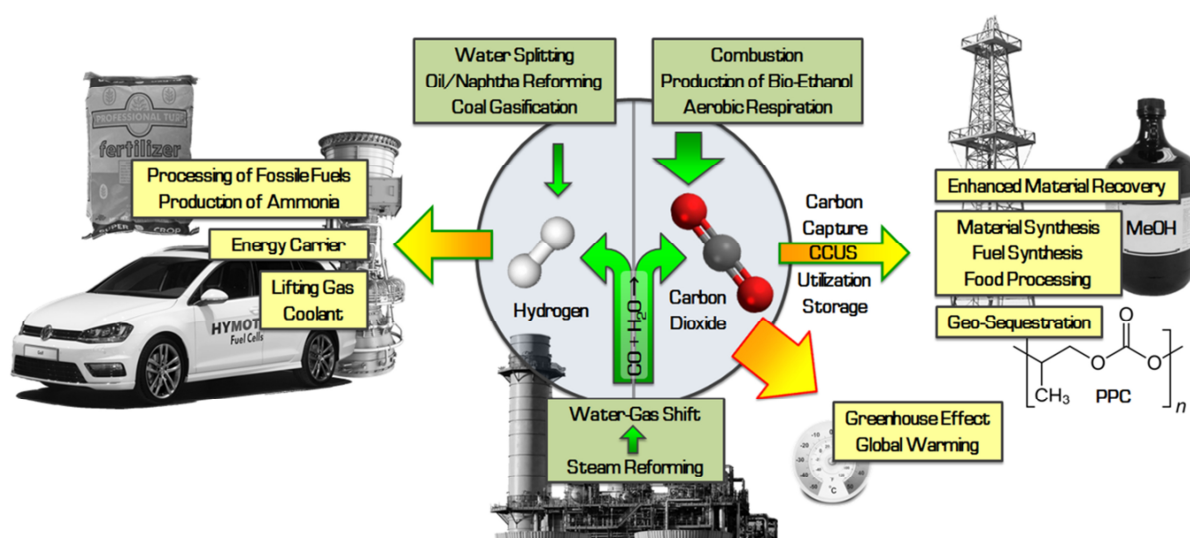


Fig. 4 Main sources, production routes, applications as well as derived products of/from hydrogen and carbon dioxide.

[33] J. F. D. Tapia, J.-Y. Lee, R. E. H. Ooi, D. C. Y. Foo, R. R. Tan, *Sust. Prod. Cons.*, 13, 2018, 1 - 15.

[34] X. Chen, G. Huang, C. An, Y. Yao, S. Zhao, *Chem. Eng. J.*, 335, 2018, 921 - 935.

[35] A. P. Batista, L. Gouveia, P. A. S. S. Marques, *Renew. Energ.*, 119, 2018, 203 - 209.

[36] A. Midilli, M. Ay, I. Dincer, M. A. Rosen, *Renew. Sust. Energ. Rev.*, 9, 2005, 255 - 271.

[37] C. M. Kalamaras, A. M. Efstathiou, *Hindawi Conference Papers in Energy*, 2013, 1 - 8.

[38] D. Y. C. Leung, G. Caramanna, M. M. Maroto-Valer, *Renew. Sust. Energ. Rev.*, 39, 2014, 426 - 443.

Seemingly foolish tradeoffs like this, considering the current debate surrounding carbon dioxide, are always justified by the plethora of indispensable applications of hydrogen in today's industry and, above all else, its imminent future as a "green" energy carrier. The figurehead of the latter are the well discussed/researched fuel cells (FC), electrochemical devices which internally convert the chemical energy of a redox reaction between e.g. hydrogen (fuel) and oxygen (oxidizing agent) to usable electricity and are thereby perfectly suited to jumpstart the aspired "decarbonization" of economy, energy/heat generation and transportation (the global passenger vehicle fleet is expected to grow to 2.5 billion by 2050<sup>[39]</sup>) alike. Once problems like durability, cost, range anxiety, storage and the lack of a hydrogen infrastructure are solved<sup>[39]</sup>, FCs could power not only cars/busses, but also planes, ships, trains, power plants and even common buildings (combined heat and power units (CHP)<sup>[40]</sup>) with the only thing coming out of the exhaust pipes/chimneys being water. Ironically, this bright future is partially overshadowed by some of the other industrial applications of hydrogen like as a raw feedstock for the production of ammonia/fertilizer (the Haber-Bosch process consumes 3 - 5% of the global natural gas, accounts for nearly 2% of the global energy output and releases 1% of the global greenhouse gas<sup>[41]</sup>), methanol and polymers as well as the refinement of crude oil into gasoline/diesel, coolant for generators, and corrosion protection of pipelines (Fig. 4). One of the things many of these still prevalent hydrogen utilizations have in common are their not-so-green implications like the subsequent release of carbon dioxide.

To the same extend the knowledge about the dangerous nature of atmospheric CO<sub>2</sub> increases and spreads, more and more ways to either prevent/circumvent its generation and emission by e.g. replacing the conventional by renewable (wind, sun and water) and environment-friendly (H<sub>2</sub>) energy sources or render it harmless/useful by "Carbon Capture, Storage and Utilization" (CCSU, Fig. 4) are being discussed and evaluated. Although the first way seems to be the logical and most promising one for the future, sadly, it is no contemporary solution for the problems at hand. Besides high costs, lacking coverage and intermittency, one of the main reasons for this is the missing storage technology which can supply electricity on demand from fluctuating sources like wind and sun.<sup>[42, 43]</sup> CCSU, on the other hand, has its own problems like tremendous logistic and energy penalties for the CO<sub>2</sub> capture and sequestration, because the most commonly used ad/absorbates like alkaline metal oxides or corrosive liquids like aqueous monoethanolamine solutions (MEA) need high temperature thermal swings for their regeneration.<sup>[42 - 45]</sup> Safely storing only a small amount of the annually produced (approx.) 33 billion tons of CO<sub>2</sub><sup>[46]</sup> is no easy feat either, be it in salt water, sedimentary

---

[39] B. G. Pollet, S. S. Kocha, I. Staffell, *Curr. Opin. Electrochem.*, 16, 2019, 90 - 95.

[40] T. H. Kwan, Y. Shen, Q. Yao, *Appl. Energy*, 251, 2019, 113318.

[41] Q. Wang, J. Guo, P. Chen, *J. Energy. Chem.*, 36, 2019, 25 - 36.

[42] P. Folger, Carbon Capture and Sequestration: Research, Development and Demonstration at the US, in *C.R. Service (Ed.), Department of Energy*, 2014.

[43] A. Evans, V. Strezov, T. J. Evans, *Renewable Sustainable Energy Rev.*, 16, 2012, 4141 - 4147.

[44] A. Samanta, A. Zhao, G. K. H. Shimizu, P. Sakar, R. Gupta, *Int. Eng. Chem. Res.*, 51, 2012, 1439 - 1463.

[45] P. A. Webley, *Adsorption*, 20, 2014, 225 - 231.

[46] L. Bigli, U. B. Celebi, *Environ. Ecol. Res.*, 5 (2), 2017, 112 - 116.

layers on the seabed or by injection into geological formations like inaccessible coal deposits or depleted gas and oil reservoirs. The latter ones are generally summarized under the term EMR (enhanced material recovery) where the CO<sub>2</sub> is simultaneously used to more effectively exploit oil (EOR), coal bed methane (ECBM) and shale gas (ESGR) reserves as well as permanently sequestered into the earth.<sup>[33]</sup> Especially in recent years, the focus of CO<sub>2</sub>-related science has shifted noticeably from "Out of sight, out of mind"-solutions towards seeing it as a potent feedstock for the chemical industry with possible applications as educt for the production of synthetic fuels via SNG (synthetic natural gas) and methanol<sup>[47, 48]</sup> or new materials like poly(propylene carbonate) (PPC), a copolymer catalytically derived from propylene oxide and CO<sub>2</sub><sup>[49]</sup> (see Fig. 4).

But as with the olefins and paraffins before, most of those applications demand very high educt purities, regardless of whether the final product is a high-grade polymer, a simple injection agent or clean energy from a fuel cell, and therefor raise the issue of how to effectively/energy-efficiently remove carbon dioxide from other gases like (primarily) hydrogen. The three main scenarios for CO<sub>2</sub> capture in the predominantly affected energy sector, which are considered technologically feasible right now, are post-combustion, pre-combustion and oxyfuel combustion.<sup>[50]</sup> While the latter refers to processes where pure oxygen instead of air is used in the energy conversion, resulting in flue gas comprised of high purity CO<sub>2</sub>, and pre-combustion transforms fossil fuels (oil, coal, natural gas) into synthesis gas (H<sub>2</sub>/CO<sub>2</sub> mixture) via a sequence of partial oxidations and reforming steps, post-combustion encompasses all efforts to separate carbon dioxide from the resulting flue gas after the actual power generation.<sup>[51]</sup> Unlike the already discussed short-chain hydrocarbons, carbon dioxide and hydrogen have very little in common regarding their fundamental physical and chemical properties (see Table 2), making a mixture of both, in theory, considerably more separation-friendly.

Somewhat surprisingly, the slightest difference between the two gases when it comes to separation-relevant parameters happens to be their kinetic diameter, with CO<sub>2</sub> only being about 0.04 - 0.05 nm "bigger" than H<sub>2</sub>. Although this miniscule difference makes a size exclusion-based

**Table 2** Separation-relevant parameters of hydrogen and carbon dioxide (data from<sup>[20]</sup>)

Gas	Normal boiling point / °C	Critical temperature / °C	Critical volume /cm <sup>3</sup> mol <sup>-1</sup>	Critical pressure /bar	Kinetic diameter /Å	Polarizability x10 <sup>25</sup> /cm <sup>3</sup>
Hydrogen	- 252.88	- 240.17	64.20	12.93	2.83 - 2.89	8.024
Carbon Dioxide	- 56.6	30.97	94.07	73.74	3.3	29.11

[47] G. Centi, E. A. Quadrelli, S. Perathoner, *Energy Environ. Sci.*, 6, 2013, 1711 - 1731.

[48] M. Behrens, *Angew. Chem. Int. Ed.*, 53, 2014, 12022 - 12024.

[49] Y. Qin, X. Wang, *Biotechnol. J.*, 5, 2010, 1164 - 1180.

[50] H. Hasse, *CIT*, 85, 2013, 1401.

[51] M. Kanniche, R. Gros-Bonnivard, J. Valle-Marcos, J.-M. Amann, *Appl. Therm. Energ.*, 30, 2010, 53 - 62.



separation very challenging, the number of publications concerning new experimental concepts for molecular sieves, some with very promising separation capabilities under laboratory conditions, has been steadily growing over the last few years. Recent examples for this trend include membranes made from electropolymerized polythiophene<sup>[52]</sup>, 2D graphene oxide<sup>[53]</sup> or even lamellar stacked transition metal nitride, carbonitride or carbide nanosheets (so-called MXenes, e.g.  $Ti_3C_2T_x$  with  $T_x$ : =O, -OH and -F) with a  $H_2/CO_2$  separation capability (selectivity > 160,  $H_2$  permeability > 2200 Barrer) superior to other state of the art materials<sup>[54]</sup>. The latter two do not simply rely on the "classical" inherent and separation-relevant material properties like pore diameter, channel geometry and functional groups for an enhanced selectivity, but rather use the highly ordered and tailorable subnanometer spacings between the partially/completely impermeable layers (about 0.35 nm in the case of MXene) as the "mesh" through which the gases are separated.<sup>[54, 55]</sup> Although the huge potential of such highly effective but somewhat limited membrane concepts is evidenced by those first proof of principle result, they are still in their infancy, with all the practical issues new materials always suffer from like overcomplicated/expensive preparation processes and questionable stability, and only time will tell whether a purely size-based  $H_2/CO_2$  separation method will ever reach market maturity or not.

Fortunately, for climate and scientist alike, the two gases in question have other, and more importantly, easier exploitable idiosyncrasies to offer like carbon dioxides chemical reactivity or hydrogens ability to "travel within certain metals", and both of them are utilized in some of today's predominant industrial solutions for this specific contamination problem. With the first patent dating back as far as 1916<sup>[56, 57]</sup>, dense palladium-based (pure or as an alloy together with Ce, Cu Fe, Pt, Ru, Ag or Y) membranes are considered to be the most scrutinized and commercialized inorganic system for  $H_2$  purification due to their simplicity, high permeability and almost infinite selectivity (only  $H_2$  can pass, SF >> 1000)<sup>[57, 58]</sup> which is rooted in the diffusion of dissociated atomic hydrogen through the metal lattice (solution-diffusion mechanism) by hopping between tetrahedral interstitial sites<sup>[59]</sup>. This incredible advantage over every other separation-active material in combination with numerous successful applications in e.g. steam methane reforming (SMR)<sup>[60]</sup> or WGS reactions<sup>[61]</sup>

---

[52] M. Zhang, X. Jing, S. Zhao, P. Shao, Y. Zhang, S. Yuan, Y. Li, C. Gu, Y. Ye, X. Feng, B. Wang, *Angew. Chem. Int. Ed.*, 131, 2019, 8860 - 8864.

[53] J. Shen, G. Liu, K. Huang, Z. Chu, W. Jin, N. Xu, *ACS nano*, 10 (3), 2016, 3398 - 3409.

[54] L. Ding, Y. Wie, L. Li, T. Zhang, H. Wang, J. Xue, L.-X. Ding, S. Wang, J. Caro, Y. Gogotsi, *Nat. Commun.*, 155 (9), 2018, 1 - 7.

[55] Q. Liu, K. M. Gupta, Q. Xu, G. Liu, W. Jin, *Sep. Purif. Technol.*, 209, 2019, 419 - 425.

[56] W. O. Snelling, *Apparatus for separating gases*, US patent 1174631, 7 March 1916.

[57] S. P. Cardoso, I. S. Azenha, Z. Lin, I. Portugal, A. Rodrigues, C. S. Silva, *Sep. Purif. Rev.*, 47, 2018, 229 - 266.

[58] K. Ramasubramanian, Y. Zhao, W. S. W. Ho, *AIChE J.*, 59, 2013, 1033 - 1045.

[59] T. L. Ward, T. Dao, *J. Membr. Sci.*, 153 (2), 1999, 211 - 231.

[60] H. W. A. El Hawa, S. T. Lundin, N. S. Patki, J. D. Way, *J. Hydrogen Energy*, 41 (24), 2016, 10193 - 10201.

[61] A. Brunetti, A. Caravella, E. Fernandez, D. A. P. Tanaka, F. Gallucci, E. Drioli, E. Curcio, J. L. Viviente, G. Barbieri, *J. Hydrogen Energy*, 40 (34), 2015, 10883 - 10893.

raise the logical question of why Pd (Ni or V and their alloys are promising candidates too <sup>[57]</sup>) isn't used every time this separation issue arises and the simple but inconvenient answer is, again, because of severe industry-relevant handicaps like the metal's price, availability and the consequential difficult scale up (e.g. more or less defect-free deposited on porous stainless-steel (PSS) by sputtering, CVD, PVD, ELP or spray pyrolysis <sup>[62]</sup>) as well as sulfur poisoning and hydrogen embrittlement (Pd lattice shrinkage caused by a phase shift in the presence of H<sub>2</sub>) <sup>[57, 63]</sup>. Nearly none of all the weaknesses mentioned so far in this chapter applies to the few existing non-membrane-based approaches like, first and foremost, the highly effective chemisorption of CO<sub>2</sub> (carbon capture) via alkaline metal oxides or aqueous amine-containing solutions (e.g. monoethanolamine (MEA)) primarily used on a large scale in power plants for the so-called scrubbing. <sup>[42 - 46, 64]</sup> This process, however, in which the flue gas from burning fossil fuels is simply passed through said scrubbing solutions where the CO<sub>2</sub> (also used against SO<sub>2</sub>) is selectively bound while all the other components come out unhindered, suffers from two major drawbacks of its own in the form of corroding equipment/pipelines and the very expensive parasitic power consumption related to the thermal regeneration of the chemisorbents <sup>[64]</sup> (CO<sub>2</sub> carbon capture cost is about 55 Euro/ton <sup>[65]</sup>, integration of a MEA process to a power plant (coal) increases the cost of electricity by 86% <sup>[66]</sup>). Unfortunately, those flawed "solutions" and their continuing use will stay a necessary evil for the foreseeable future due to the already familiar lack of viable alternatives.

So it should come as no surprise that the climatic impact of especially hydrogen and carbon dioxide along with the insufficient contemporary separation methods has become a huge driving force behind the hunt for new H<sub>2</sub>/CO<sub>2</sub> separation-active materials recently, focusing almost exclusively on membrane-based approaches and their better cost-effectiveness, lower energy consumption and operational simplicity. Although the results of this endeavor include many promising proton conducting ceramics (100% H<sub>2</sub>-selective, ambipolar diffusion mechanism of protons and electrons through the membrane) like perovskites <sup>[67]</sup> (SrCeO<sub>3</sub>, BaCeO<sub>3</sub> or SrZrO<sub>3</sub>), pyrochlores (e.g. La<sub>2</sub>Zr<sub>2</sub>O<sub>7</sub>) <sup>[68]</sup> or acceptor doped rare earth ortho-niobates/tantalates (LnNbO<sub>4</sub>/LnTaO<sub>4</sub>) <sup>[69]</sup> as well as modified polymers (e.g. electropolymerized polythiophene <sup>[52]</sup>, polyimides with naphthalene groups <sup>[70]</sup> and polyvinylamine/poly(allylamine) <sup>[71]</sup>), a great deal of hope again seems to rest on old and

---

[62] S. Liguori, A. Iulianelli, F. Dalena, F. Drago, M. Broglia, Y. Hunang, A. Basile, *Membranes*, 4, 2014, 143 - 162.

[63] J. Gabitto, C. Tsouris, *Int. Rev. Chem. Eng.*, 1, 2009, 394 - 411.

[64] R.-B. Lin, S. Xiang, H. Xing, W. Zhou, B. Chen, *Coord. Chem. Rev.*, 378, 2019, 87 - 103.

[65] L. M. Romeo, I. Bolea, J. M. Escosa, *Appl. Therm. Eng.*, 28, 2008, 1039 - 1046.

[66] J. M. Klara, Cost and Performance Baseline for Fossil Energy Plants, *U.S. Department of Energy*, 2010, DOE/NETL-2010/1397.

[67] M. Cai, S. Liu, K. Efimov, J. Caro, A. Feldhoff, H. Wang, *J. Membr. Sci.*, 343 (1 - 2), 2009, 90 - 96.

[68] T. Omata, S. Otsuka-Yao-Matsuo, *Solid State Ionics*, 148 (12), 2001, 475 - 482.

[69] R. Haugrud, T. Norby, *Nat. Mater.*, 5 (3), 2006, 193 - 196.

[70] T. Li, J. Liu, S. Zhao, Z. Chen, H. Huang, R. Guo, Y. Chen, *J. Membr. Sci.*, 585, 2019, 282 - 288.

[71] Y. Han, W. S. W. Ho, *Chin. J. Chem. Eng.*, 2018, 2238 - 2254.

new micro/nanoporous materials, ranging from amorphous silica [72] over carbon (CMSs (carbon molecular sieves from polymeric precursors) [73], CNTs (carbon nanotubes) [74] etc.) to Zeolites (e.g. NaX [75], MFI [76]) and metal-organic frameworks (ZIF-8 [77], Mg-MOF-74 [78] etc.). This group of substance classes is mainly characterized by their huge surface areas on the one hand, which provide various possibilities for the reversible (more energy-efficient) physisorption of guests like CO<sub>2</sub> with its high polarizability (see Table 2) and quadrupole moment, as well as their modular design/functionalizability on the other hand, making it very easy to provide/incorporate specific functional polar groups (-CHO [79], -NH<sub>2</sub> [78], etc.), open metal sites (e.g. ion exchanged NaX [75], Mg-MOF-74 [80]) or tailor the pore sizes [81] to further enhance their intrinsic CO<sub>2</sub> affinity/H<sub>2</sub> selectivity. However, since membrane materials for industrial applications should also feature a high thermal, chemical (H<sub>2</sub>S, SO<sub>2</sub>, NH<sub>3</sub> etc.), environmental (moisture) and mechanical/pressure (high pressure = larger driving force) stability as well as an easy upscalability/malleability, and many of these are not a particularly strong suit of said substances, the general idea of encapsulating separation-active nanoparticle inside of a protective but still permeable/selective polymeric matrix (e.g. Matrimid [75], PEBAX-1657 [82]) has gained more and more traction over the last decades. The challenge now, given the fact that even the most recent and effective representatives of these so-called mixed matrix membranes are still about 100 times less selective (for example: SF<sub>H<sub>2</sub>/CO<sub>2</sub></sub> = 32.9 with a CO<sub>2</sub> permeability of 120.2 Barrer [82]) than the mentioned Pd membranes, is "simply" to find/create the blend of materials best suited for the job.

---

[72] N. W. Ockwig, T. M. Nenoff, *Chem. Rev.*, 107 (10), 2007, 4078 - 4110.

[73] A. F. Ismail, L. I. B. David, *J. Membr. Sci.*, 193, 2001, 1 - 18.

[74] W. Mi, Y. S. Lin, Y. Li, *J. Membr. Sci.*, 304 (1 - 2), 2007, 1 - 7.

[75] A. Mundstock, S. Friebe, J. Caro, *Int. J. Hydrog. Energy*, 42, 2017, 279 - 288.

[76] M. Zhou, D. Korelskiy, P. Ye, M. Grahn, J. Hedlund, *Angew. Chem. Int. Ed.*, 53, 2014, 3492 - 3495.

[77] A. Huang, Q. Liu, N. Wang, J. Caro, *J. Mater. Chem. A*, 2, 2014, 8246 - 8251.

[78] N. Wang, A. Mundstock, Yi. Liu, A. Huang, J. Caro, *Chem. Eng. Sci.*, 124, 2015, 27 - 36.

[79] A. Huang, W. Dou, J. Caro, *J. Am. Chem. Soc.*, 132 (44), 2010, 15562 - 15564.

[80] X. Kong, E. Scott, W. Ding, J. A. Mason, J. R. Long, J. A. Reimer, *J. Am. Chem. Soc.*, 134 (35), 2012, 14341 - 14344.

[81] Z. Kang, M. Xue, L. Fan, L. Huang, G. Wei, B. Chen, S. Qiu, *Energy Environ. Sci.*, 7, 2014, 4053 - 4060.

[82] L. Fan, Z. Kang, Y. Shen, S. Wang, H. Zhao, H. Sun, X. Hu, H. Sun, R. Wang, D. Sun, *Cryst. Growth Des.*, 18 (8), 2018, 4365 - 4371.

## III Separation-Active Materials

After mainly focusing on WHAT needs to be separated, WHY and HOW it's currently done in the previous chapters, the next section will take a closer look at promising experimental separation-active materials which have the potential to revolutionize this energy-intensive branch of industry and what enables them to do so. The ever-expanding variety of such substances, as intimated by the long but not exhaustive list of examples given so far, is both a blessing and a curse, for it makes finding the haystack's proverbial needle very cumbersome as well as worthwhile due to the promising idiosyncrasies all the candidates contribute to the "separation-toolbox" like modularity, pore size/geometry, stability, flexibility/stiffness, crosslinkability, interpenetration, post synthetic functionalizability or even switchability. However, since it would otherwise go beyond the scope of this thesis, only directly relevant material classes and their used representatives will make an appearance in this next part, starting with one of the best known/longest serving assets in the separation/purification business.

### Zeolites

"Boiling stones", or rather its greek equivalent zeolites (*zeo* meaning "to boil" and *lithos* translates to "stone"), was the term the Swedish mineralogist ALEX FREDRIK CRONSTEDT coined for the vast family of hydrated tectosilicates after discovering Stilbite in 1756 due to the fact that upon rapid heating, the characteristically adsorbed water is released from the highly porous material in the form of steam.<sup>[83]</sup> While the majority of natural zeolites are an indirect result of volcanic activity, born from reactions between hot lava and salt water over millennia<sup>[84]</sup>, it only took scientists 106 years to obtain the first synthetic representative<sup>[85]</sup> and until 1948 for RICHARD MALING BARRER to synthesize a novel zeolitic material without natural counterpart (Barrerite)<sup>[86]</sup>.

In general and regardless of whether they are naturally occurring or man-made, zeolites are hydrothermally created crystalline aluminosilicates composed of oxygen-bridged electro-neutral  $\text{SiO}_4^{4-}$  and negatively charged  $\text{AlO}_4^{5-}$  tetrahedra (see Fig. 5) whose ratio (Si/Al) fundamentally determines their structure (LOEWENSTEIN rule = no Al-O-Al linkages), type and properties (Table 3).<sup>[83, 85, 87]</sup> Those tetrahedral primary building units (PBUs), in turn, form so-called SBUs (secondary building units), a term recently rediscovered in connection with MOFs, in the shape of cycles or simple polyhedra like hexagonal prisms, octahedra and cubes which then ultimately assemble into a complex 3D framework (Fig. 5). Depending on zeolite type and composition, the actual structure features cage- or tube-like voids interconnected by 1D, 2D or 3D channel systems (Table 3) and occupied by water

---

[83] L. Bacova, M. Vandrovcova, I. Kopova, I. Jirka, *Biomater. Sci.*, **6**, 2018, 974 - 989.

[84] M. Moshoeshe, M. S. Nadiye-Tabbiruka, V. Obuseng, *Am. J. Mater. Sci.*, **7** (5), 2017, 196 - 221.

[85] S. P. Cardoso, I. S. Azenha, Z. Lin, A. E. Rodrigues, C. M. Silva, *Sep. Purif. Rev.*, **47**, 2018, 229 - 266.

[86] R. M. Barrer, *J. Chem. Soc.*, **3**, 1948, 127 - 132.

[87] M. Matasukata, K. Sawamura, Y. Sekine, E. Kikuchi, *Mater. Sci. Technol.*, **14**, 2011, 175 - 193.

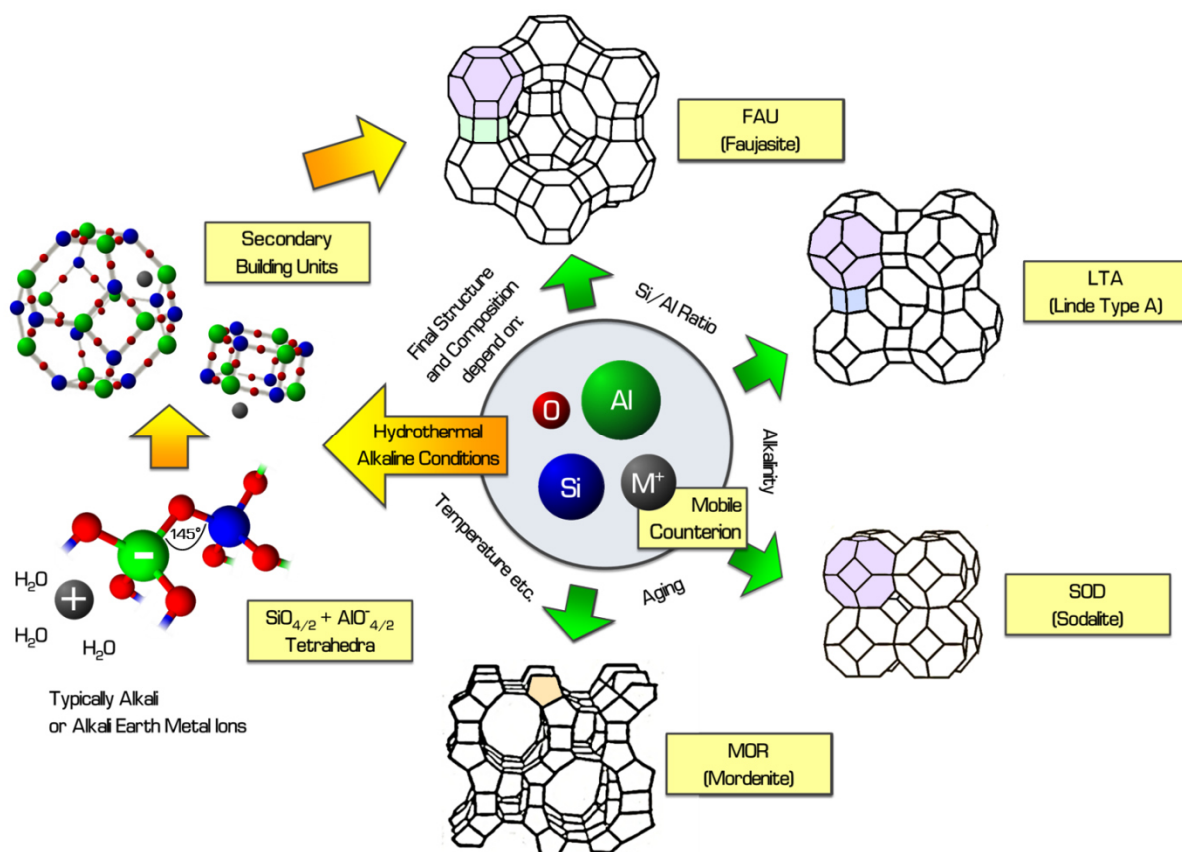


**Fig. 5** Schematic illustration of the basic building blocks, general synthesis process and structures of some well-known zeolite framework types.

molecules as well as exchangeable mobile counterions (typically alkali and alkali earth metals) to balance the negative framework charge (see Fig. 5). According to their size, one of the most crucial qualities when it comes to separation capability, the zeolite channels/windows are categorized as either small (8-ring, 3.5 - 4.5 Å), medium (10-ring, 4.5 - 6.0 Å) or large (12-ring, 6.0 - 8.0 Å), enabling, in most cases, an unhindered and fully reversible dehydration, guest and ion exchangeability.<sup>[85, 88]</sup>

Besides the latter one, which on its own is a powerful tool for adjusting a zeolite's properties (molecular sieving, catalytic, sorption etc.) through the cations location, site occupancy, valency and radius (directly influences the pore size: e.g. zeolite A with Na/K = 4/3 Å<sup>[89]</sup> <sup>[90]</sup>, tectosilicates are characterized by their large inner surface (~100 m<sup>2</sup> g<sup>-1</sup> <sup>[83]</sup>) as well as a remarkable mechanical (including a high framework stiffness), chemical and thermal stability (e.g. zeolite A and X up to 800 °C <sup>[91]</sup> <sup>[85]</sup>). This is furthermore complimented by the tunable BRØNSTED acidity (generated by

[88] R. M. Barrer, *Zeolites*, 1, 1981, 130 - 140.

[89] C. Feng, K. C. Khulbe, T. Matsuura, R. Farnood, A. F. Ismail, *JSMR*, 1, 2015, 49 - 72.

[90] Z. Sarbak, *Cryst. Res. Technol.*, 28 (7), 1993, 979 - 987.

[91] N. M. Musyoka, L. F. Petrik, E. Hums, A. Kuhnt, W. Schwioger, *Res. Chem. Intermed.*, 41, 2015, 575 - 582.

hydroxyl groups between Al and Si), lattice oxygen basicity, hydrophilic/hydrophobic character, element interchangeability and the consequential framework polarity (a high Al amount (Si/Al around one) equals a high polarity, making the zeolite more selective (stronger adsorption) towards polar molecules and the other way around<sup>[85]</sup>) of those materials<sup>[92]</sup>, opening up a wide field of possible applications.

**Table 3** Well-known zeolites and their structural properties (data from<sup>[87]</sup>)

Zeolite (counter cation)	Topology	Crystal system	Si/Al ratio	Window size/Å	Channel dimensionality
Sodalite (Na)	SOD	cubic	~ 10	2.5	0D
X (Na)	FAU	cubic	10 - 14	7.4	3D
Y (Na)	FAU	cubic	15 - 4.7	7.4	3D
A (Na)	LTA	cubic	10 - 13	4.2	3D
Chabazite (Ca)	CHA	trigonal	1.9 - infinity	3.7 x 4.2	3D
ZSM-5 (Na)	MFI	orthorhombic	7.5 - infinity	5.1 x 5.5	3D
DD3R	DDR	trigonal	infinity	3.6 x 4.4	2D
Mordenite (Na)	MOR	orthorhombic	5.0 - 13.5	6.7 x 7	2D

Given such a versatile, stable and easily produced class of materials, it comes a no surprise that industrial commercialization started soon after BARRERs pioneering work (mainly synthesis and adsorption), with Union Carbide introducing their synthetic zeolites as drying agent for refrigerant and natural gas (1954) as well as isomerization catalyst (zeolite Y, 1959).<sup>[85]</sup> But despite their topological variety, 231 framework types are known today, only about 5% are industrially relevant (among them FAU, BEA, MFI, FER and LTA)<sup>[85]</sup> and implemented in the most frequent application fields of zeolites, namely water/soil/air purification/decontamination (e.g. ion exchange with heavy metals<sup>[93]</sup>, sorption of ammonium-nitrogen<sup>[94]</sup> or cesium/strontium<sup>[95]</sup>), catalysis (cracking of hydrocarbons<sup>[96]</sup>, pyrolysis of rubbers<sup>[97]</sup>, conversion of syngas to light olefins<sup>[98]</sup> etc.) and gas separation (CO<sub>2</sub> from flue gas with SAPO-34<sup>[99]</sup>, O<sub>2</sub> from air with zeolite 4A@PDMS MIMs<sup>[100]</sup>,

[92] G. A. Ozin, A. Kuperman, A. Stein, *Angew. Chem. Int. Ed.*, 28 (3), 1989, 359 - 376.

[93] M. Jovanovic, N. Rajic, B. Obradovic, *J. Hazard. Mater.*, 57, 2012, 233 - 234.

[94] G. Hunang, F. Liu, Y. Yang, W. Deng, S. Li, Y. Huang, X. Kong, *J. Environ. Manage.*, 154, 2015, 1 - 7.

[95] A. V. Voronina, M. O. Blinova, V. S. Semishchev, D. K. Gupta, *J. Environ. Radioact.*, 144, 2015, 103 - 112.

[96] A. Kostyniuk, M. Grlic, B. Likozar, *Ind. Eng. Chem. Res.*, 59 (19), 2019, 7690 - 7705.

[97] J. Yu, S. Liu, A. Cardoso, Y. Han, K. Bikane, L. Sun, *Energy*, 188, 2019, 116117.

[98] J. Su, H. Zhou, S. Liu, C. Wang, C. Liu, Y. Ye, L. Zhang, Y. Zhao, H. Liu, D. Wang, W. Yang, Z. Xie, M. He, *Nat. Commun.*, 10 (1), 2019, 1297.

[99] B. Liu, C. Tang, X. Li, B. Wang, R. Zhou, *Micropor. Mesopor. Mater.*, 292, 2020, 109798.

[100] P. K. Prajapati, A. M. Kansara, V. K. Aswal, P.S. Singh, *J. Appl. Polym.*, 136 (42), 2019, 48047.

xenon recovery with DDR3<sup>[101]</sup>, CH<sub>4</sub>/N<sub>2</sub> with Ag<sup>+</sup> exchanged clinoptilolite<sup>[102]</sup>). Furthermore, zeolites are tested as/used for less prominent purposes like heat harvesting, adsorption refrigeration, human detoxification, separation of biomolecules, biosensors, drug/gene delivery, biomaterial coating, batteries, data storage or simply as laundry detergent<sup>[83, 85, 92]</sup>, proving again and again that they are more than just steam spewing stones.

## Type X

As one of the most commercially significant artificial zeolites, created solely by and for industry (UNION CARBIDE), X was discovered/first synthesized by D. W. BRECK and coworkers as one of a group of 20 new crystalline minerals (including e.g. zeolites A, Y and the synthetic counterparts of chabazite) between 1949 and 1953 (patented in 1959<sup>[103]</sup>) and introduced as early as 1962 by MOBILE OIL as a hydrocarbon cracking catalyst due to its beneficial chemical composition and faujasite-like structure.<sup>[104]</sup> Characteristically synthesized following a hydrothermal route under alkaline conditions using a low Si/Al ratio of 1.0 - 1.4 (see Table 3), this tectosilicate features a stiff framework constructed from two distinct SBUs in the form of sodalite cages (truncated octahedrons) and interconnecting hexagonal prisms (see Fig. 6) which encompasses a uniform 3D pore system easily accessible through 12-membered oxygen rings with an aperture diameter of 7.4 Å.<sup>[10, 87]</sup>

Inhabited are those channels by more than 64 mobile, charge-compensating extraframework cations per unit cell (normally Na<sup>+</sup> and water molecules in the hydrated state), carefully distributed among ten different crystallographic sites (located on the prism faces (I), open hexagonal faces (II) or on the walls of the supercage (III) etc.<sup>[105]</sup>, see Fig. 6) in order to achieve a minimal electrostatic ion-ion repulsion while maximizing their interaction with the oxygens of the surrounding framework.<sup>[106]</sup> Fortunately, said ion-framework interplay is still weak enough to allow for one of zeolite X's most important and sought-after properties, namely the ability to post-synthetically exchange its inherent Na<sup>+</sup> counterions against a variety of different alternatives like Cs<sup>+</sup>, K<sup>+</sup>, Rb<sup>+</sup>, Li<sup>+</sup>, Cu<sup>2+</sup>, Co<sup>2+</sup>, Ni<sup>2+</sup>, Pb<sup>2+</sup> or Sr<sup>2+</sup><sup>[75, 106]</sup> and thereby tailor the zeolites intrinsic capabilities regarding catalysis, adsorption or separation. Other convenient features for industrial applications besides this "open door policy" of the 3D pore system when it comes to ions or other molecular guests are a sound structural rigidity (fixed window size) in combination with high mechanical, chemical (acid is the biggest weakness) and

---

[101] X. Wang, Y. Zhang, X. Wang, E. Andres-Garcia, P. Du, L. Giordano, L. Wang, Z. Hong, X. Gu, S. Murad, F. Kapteijn, *Angew. Chem. Int. Ed.*, 58 (43), 2019, 15518 - 15525.

[102] D. A. Kennedy, M. Khanafer, F. H. Tezel, *Micropor. Mesopor. Mater.*, 281, 2018, 123 - 133.

[103] W. Lutz, *Adv. Mater. Sci. Eng.*, 2014, 724248.

[104] D. W. Breck, W. G. Eversole, R. M. Milton, *J. Am. Chem. Soc.*, 78 (10), 1956, 2338 - 2339.

[105] Y. Yang, N. Burke, J. Zhang, S. Huang, S. Lim, Y. Zhu, *RSC Adv.*, 4, 2014, 7279 - 7287.

[106] T. Frising, P. Leflaive, *Micropor. Mesopor. Mater.*, 114, 2008, 27 - 63.

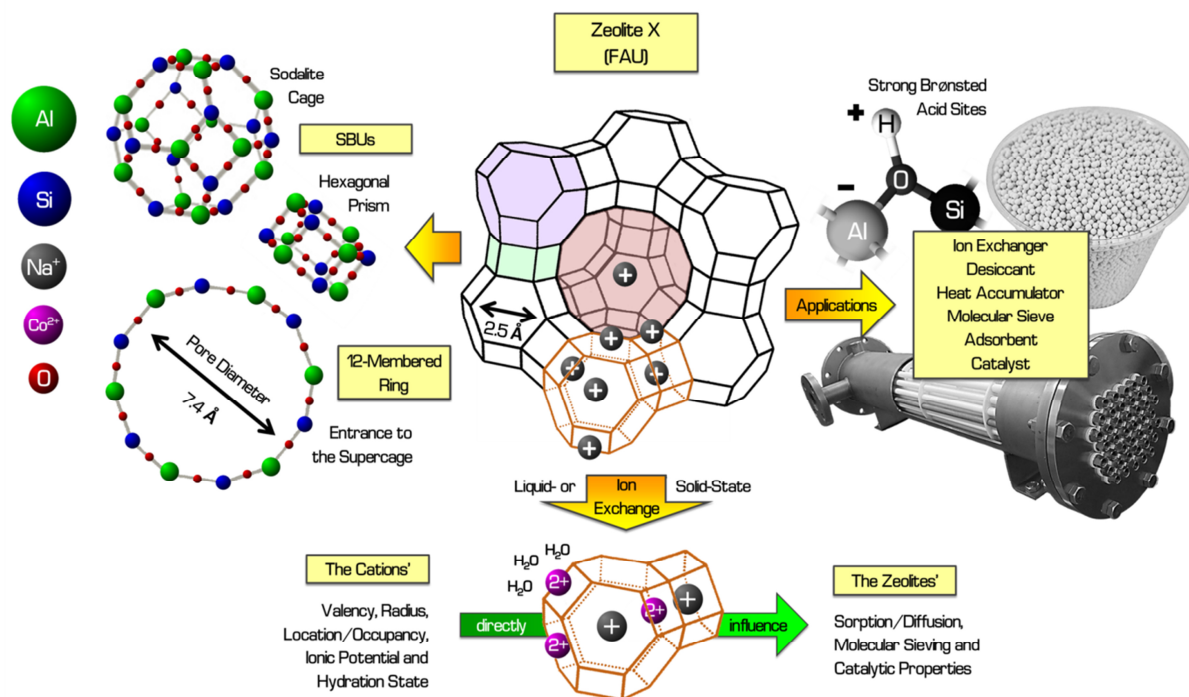


Fig. 6 Schematic depiction of the basic building blocks, pore sizes, extraframework cation distribution and exchangeability, as well as important application fields of Zeolite X.

thermal stability (up to 800 °C<sup>[91]</sup>), a tunable acido-basicity (Lewis acidity of the Na<sup>+</sup>/framework Al<sup>3+</sup>, Brønsted acidity of the protonated form (see Fig. 6), basicity of certain oxygen atoms<sup>[107]</sup>) as well as the innate polarity/hydrophilicity (both due to the low Si/Al ratio)<sup>[10, 85]</sup>, making zeolite X a very versatile material.

Not surprisingly, this overall flexibility is directly reflected in the sheer amount of possible industrial and scientific applications which are being applied/pursued right now like as a support for iron oxide nanoparticles (simultaneous ammonia and phosphate removal from water bodies)<sup>[108]</sup>, carrier for laccase immobilization<sup>[109]</sup>, for the removal of antibiotics (CuX)<sup>[110]</sup>, adsorption of aromatics (C<sub>6</sub>-C<sub>8</sub>, BaX)<sup>[111]</sup>, as antimicrobial agent (Cu/ZnX)<sup>[112]</sup>, part of an anticorrosion coating<sup>[113]</sup>, catalyst for the isobutane/2-butene alkylation (Cu-modified rare earth X-type)<sup>[114]</sup>, isomerization of 1-butene,

[107] G. Busca, *Micropor. Mesopor. Mater.*, 254, 2017, 3 - 16.

[108] Q. Xu, W. Li, L. Ma, D. Cao, G. Owens, Z. Chen, *Sci. Total Environ.*, 703, 2020, 135002.

[109] H. R. Wehaidy, M. A. Naby, H. M. El-Hennawi, H. F. Youssef, *Biocatal. Agr. Biotechnol.*, 19, 2019, 101135.

[110] A. Rahimi, B. Bayati, M. Khamforoush, *Arab. J. Sci. Eng.*, 44, 2019, 5381 - 5397.

[111] Q. Shi, J. C. Goncalves, A. F. P. Ferreira, A. E. Rodrigues, *Chem. Eng. Technol.*, 42 (11), 2019, 2410 - 2418.

[112] G. Yao, W. Zhang, Z. Sun, S. Zheng, S. Komameni, *Environ. Sci. Pollut. Res. Int.*, 26 (3), 2019, 2782 - 2793.

[113] A. H. Abdel Aziz, T. S. Jamil, M. S. Shalaby, A. M. Shaban, E. R. Souaya, N. A. Abdel Ghany, *Int. J. Ind. Chem.*, 10, 2019, 175 - 191.

[114] H. Zang, J. Xu, H. Tang, Z. Yang, R. Liu, S. Zhang, *Ind. Eng. Chem.*, 58, 2019, 9690 - 9700.



alkylation of toluene and cycloaddition of carbon dioxide to ethylene oxide <sup>[115]</sup> or as membrane for the alcohol dehydration by pervaporation <sup>[116]</sup>. Finally, and despite a relatively big pore size, zeolite X can be used to separate binary mixtures of small gases such as CH<sub>4</sub>/N<sub>2</sub> (X/AC composite) <sup>[117]</sup>, CO<sub>2</sub>/N<sub>2</sub> <sup>[118]</sup>, N<sub>2</sub>/O<sub>2</sub> (polyvalent cation form) <sup>[119]</sup>, propylene/propane <sup>[120]</sup> and H<sub>2</sub>/CO<sub>2</sub> (utilizing the higher ionic potentials of e.g. Co exchanged type X), relying solely on the its advanced adsorption behavior (affinity sieving) for this purpose unlike many of the zeolite's modern wannabe successors.

## Metal-Organic Frameworks

Multiple organ failure <sup>[120]</sup> was the most common meaning behind the acronym MOF before OMAR YAGHI started to coin it in 1995 <sup>[121]</sup> for his highly porous crystalline organic-inorganic hybrid materials, better known today as metal-organic frameworks (a term already used in the late 80's by PALMER et al. for crystalline porphyrinic molecular metals <sup>[122]</sup>). This substance class in particular (occasionally also called porous coordination polymers (PCPs)/porous coordination networks (PCNs) <sup>[123]</sup>), as well as the special branch of reticular (netlike) chemistry it belongs to, emerged as the logical evolution from the historical field of metal-containing coordination compounds like Prussian Blue (Fe<sub>4</sub>[Fe(CN)<sub>6</sub>]<sub>3</sub>, the first modern artificial pigment), WERNER complexes (e.g. [Co(NH<sub>3</sub>)<sub>4</sub>Cl<sub>2</sub>]Cl) or HOFMANN clathrates (2D metal cyanide sheets), and nowadays contains more than 20.000 distinct materials <sup>[124]</sup>. Since all of these need a proper moniker (some have even more than one: MOF-74 = CPO-27 = M<sub>2</sub>dhtp or HKUST-1 = CuBTC) and share some of their structural DNA with zeolites, the same naming convention (three letters-one number) applies to MOFs in most cases, leading to abbreviations derived from, for example, their university of origin (CPO = coordination polymer of Oslo, HKUST = Hon-Kong University of Science and Technology, MIL = matériaux de l'institut Lavoisier, DUT = Dresden University of Technology, CAU = Christian-Albrecht-University of Kiel etc.).

What all metal-organic frameworks, no matter how "creatively" named, have in common is that they self-assemble from organic multidentate linker molecules (mainly acids and imidazoles, or rather their conjugate bases (see Table 4)) and inorganic nodes made of discrete metal-ions or metal-

---

[115] F. R. Ribeiro, *Zeolites: Science and technology*, 1984, Martinus Nijhoff, The Hague.

[116] H. Zhou, D. Korelsky, M. Grahn, J. Tanskanen, J. Hedlund, *J. Membr. Sci.*, 399 - 400, 2012, 106 - 111.

[117] C. L. Xue, W. P. Chen, W. M. Hao, J. H. Ma, R. F. Li, *J. Chem.*, 2019, 2078360.

[118] A. Villarreal, G. Garbarino, E. Finocchio, B. Bosio, J. Ramirez, G. Busca, *J. CO<sub>2</sub> Util.*, 19, 2017, 266 - 275.

[119] C. G. Cop, G. E. Parris, R. Srinivas, S. R. Auvil, *Stud. Surf. Sci. Catal.*, 28 (C), 1986, 1033 - 1040.

[120] M. Fukui, T. Furakawa, M. Kurosawa, H. Sato, H. Tomaru, T. Narisawa, I. Sugimura, C. Sekiya, M. Namiki, *Kanzo*, 28 (11), 1987, 1507 - 1514.

[121] O. M. Yaghi, H. Li, *J. Am. Chem. Soc.*, 117, 1995, 10401 - 10402.

[122] S. M. Palmer, J. L. Stanton, B. M. Hoffman, J. A. Ibers, *Inorg. Chem.*, 25, 1986, 2296 - 2300.

[123] S. R. Batten, N. R. Champness, X.-M. Chen, J. Garcia-Martinez, S. Kitagawa, L. Oehrstroem, M. O'Keeffe, M. P. Suh, J. Reedijk, *Pure Appl. Chem.*, 85 (8), 2013, 1715 - 1724.

[124] H. Furukawa, K. E. Cordova, M. O'Keeffe, O. Yaghi, *Science*, 341, 2013, 1230444.

containing clusters/chains (aka. secondary building units (SBUs), see Fig. 7)<sup>[125]</sup> via a multitude of different synthesis methods, ranging from slow diffusion, solvothermal, electrochemical, mechanochemical, microwave assisted, ultrasonic to one-pot<sup>[126]</sup>. The wealth of functionalizability this modular design enables (e.g. by choosing specialized (with functional groups, Fig. 7) or elongated (principle of isorectularity: "same" topology, bigger pores<sup>[127]</sup>) linkers and metal-ions with different radii/coordination spheres/states of saturation) is, however, far from being exhausted after the initial synthesis, because the resulting highly ordered frameworks (mono- or mixed-metal/linker) can be further tailored using post-synthetic modification technics like, for example, metal/ligand exchange (PSME/PSLE), elimination or installation, as well as polymerization, oxidation<sup>[128]</sup> and the infiltration

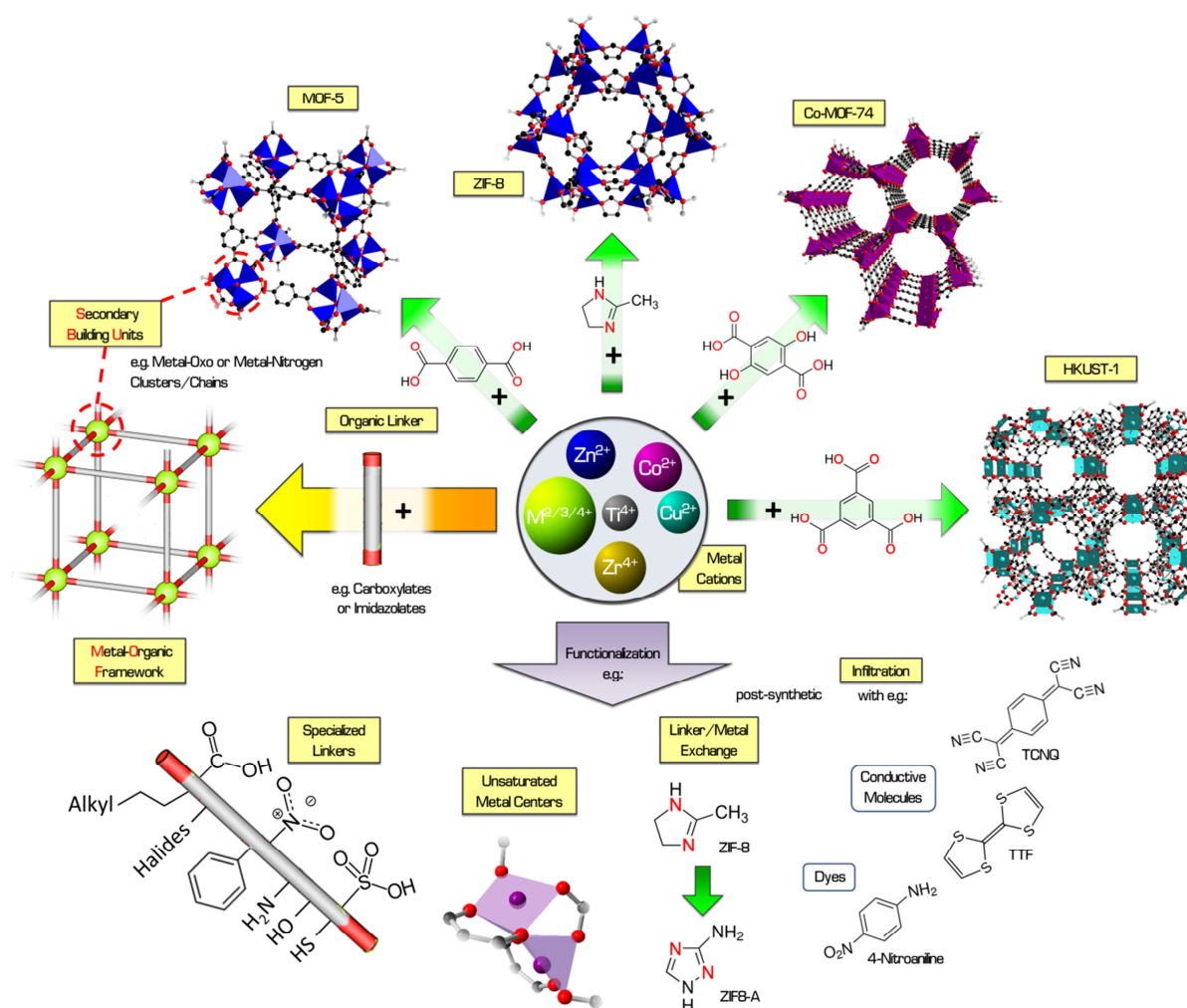


**Fig. 7** Schematic overview of the basic building blocks and functionalization possibilities for MOFs, as well as the crystal structures of some well-known representatives.

[125] G. Férey, *Chem. Soc. Rev.*, 37, 2008, 191 - 214.

[126] P. Silva, S. M. F. Vilela, J. P. C. Tome, F. A. Almeida Paz, *Chem. Soc. Rev.*, 44, 2015, 6774 - 6803.

[127] H. Deng, S. Grunder, K. E. Cordova, C. Valente, H. Furukawa, M. Hmadeh, F. Gandara, A. C. Whalley, Z. Liu, S. Asahina, H. Kazumori, M. O'Keeffe, O. Terasaki, J. F. Stoddart, O. M. Yaghi, *Science*, 336, 2012, 1018 - 1023.

[128] Z. Yin, S. Wan, J. Yang, M. Kurmoo, M.-H. Zeng, *Coord. Chem. Rev.*, 378, 2019, 500 - 512.

with instrumental conductive (e.g. TTF = tetrathiafulvalene, TCNQ = tetra-cyanoquinodimethane <sup>[129]</sup>) or dye (4-nitroaniline <sup>[130]</sup>, methylene blue, rose bengal <sup>[131]</sup> etc.) molecules (Fig. 7).

With this degree of flexibility, it comes as no surprise that no MOF is like the other and their properties, be it hydrophobicity, magnetism, catalytic activity, sorption, luminescence, structure or overall stability etc., are somewhat all over the place, with the latter one, for example, being especially high in zeolitic imidazolate frameworks (e.g. ZIF-8, due to the zeolite-like topology/bridging angle <sup>[132]</sup>) and zirconium/titania-based materials like UiO-66/MIL-125 (built from 12-coordinated Zr<sub>6</sub>/Ti<sub>6</sub>-clusters <sup>[133]</sup>). Among the most inherent and important properties of nearly every MOF, however, are a consistent nanoporosity, responsible for the very high inner surface areas (as high as 10400 m<sup>2</sup>/g (Langmuir) for MOF-210 <sup>[134]</sup>) and featuring a wide range of aperture/pore sizes <sup>[135]</sup> (see Table 4), but also a fundamental framework flexibility (MOFs are "soft matter" and subject to

Table 4 Well-known MOFs and their structural properties (data adapted from <sup>[134 and 135]</sup>)

MOF	Metal ion	Linker	Window size in Å	Pore system dimensionality	Langmuir surface area in m <sup>2</sup> /g
MOF-5	Zn <sup>2+</sup>	Terephthalate	~8.0	3D	~3800
ZIF-8	Zn <sup>2+</sup> (Co <sup>2+</sup> = ZIF-67)	2-Methyl-imidazolate	~3.4	3D	~1800
HKUST-1	Cu <sup>2+</sup>	Benzene-1,3,5-tricarboxylate	~9.0, ~5 and ~3.5 (trimodal)	3D	~2200
MOF-74	Co <sup>2+</sup> , Cu <sup>2+</sup> , Mg <sup>2+</sup> , Ni <sup>2+</sup> , Fe <sup>2+</sup> , Mn <sup>2+</sup>	2,5-Dioxido-terephthalate	~11.0	1D	~1400 (Co) ~1600 (Ni) ~1900 (Mg)
UiO-66	Zr <sup>4+</sup>	Terephthalate	~6.0	3D	~1100
ZIF-90	Zn <sup>2+</sup>	Imidazolate-2-carbaldehyde	~3.5	3D	~1300
ZIF-7	Zn <sup>2+</sup>	Benzimidazolate	~3.0	3D	~400

[129] I. Strauss, A. Mundstock, M. Treger, K. Langem S. Hwang, C. Chmelik, P. Rusch, N. C. Bigall, T. Pichler, H. Shiozawa, J. Caro, *ACS Appl. Mater. Interfaces*, 11, 2019, 14175 - 14181.

[130] R. Medishetty, J. K. Zareba, M. Samoc, R. A. Fischer, *Chem. Soc. Rev.*, 46, 2017, 4976 - 5004.

[131] H.-Y. Chi, S.-H. Hung, M.-Y. Kan, L.-W. Lee, C. H. Lam, J.-J. Chen, D.-Y. Kang, *Cryst. Eng. Comm.*, 20, 2018, 5465 - 5474.

[132] K. S. Park, Z. Ni, A. P. Cote, J. Y. Choi, R. Huang, F. J. Uribe-Romo, H. K. Chae, M. O'Keeffe, O. M. Yaghi, *PNAS*, 103 (27), 2006, 10186 - 10191.

[133] S. Yuan, J.-S. Qin, C. T. Lollar, H.-C. Zhou, *ACS Cent. Sci.*, 4 (4), 2018, 440 - 450.

[134] J. A. Mason, M. Veenstra, J. R. Long, *Chem. Sci.*, 5, 2014, 32 - 51.

[135] G. Dong, H. Li, V. Chen, *J. Mater. Chem. A*, 1, 2013, 4610 - 4630.

linker rotation and unit cell changes called "breathing" <sup>[136]</sup>) based in their chemical composition, allowing them (in most cases) to accommodate guest molecules which are, in theory, too large in critical diameter to traverse the entrance windows in question (e.g. ZIF-8 and benzene <sup>[137]</sup>).

All these idiosyncrasies mentioned above in combination with seemingly simple production methods sparked the imagination of science and industry alike right from the start, predicting a brilliant future for MOFs as replacement for the "outdated" zeolites in contemporary as well as more traditional application fields, such as the hydrogen/methane storage, CO<sub>2</sub> capture, removal of harmful/toxic chemicals (NO<sub>x</sub>, SO<sub>x</sub>, H<sub>2</sub>S, NH<sub>3</sub>, PH<sub>3</sub>, benzene, mustard gas, pharmaceuticals, nerve agents etc.), heterogeneous catalysis (e.g. aerobic oxidation of alcohols, C-C coupling, hydrogenation of aromatic ketones, ring-opening of epoxides), luminescence (mostly sensing: pH, explosives, bioimaging) or metal corrosion inhibition. <sup>[124, 126, 138]</sup> Unfortunately, this early praise was quite premature and even today, 25 years after their discovery, only a few niche applications in the textile industry (protective clothing for chemical, biological, radiological and nuclear warfare impregnated with MOFs), for respiratory purposes (protection masks), food packaging (MOFs containing/releasing 1-methycyclopropene which retards the ripening of fruits and lengthens their shelf life), sub-atmospheric toxic gas storage, water extraction or antimicrobial coatings for healthcare products has reached market maturity so far or could do so in the nearby future. <sup>[126, 139, 140, 141]</sup>

The one obvious MOF application still missing from the enumerations is the separation of gases which turned out to be kind of a double-edged sword, inasmuch as, while scientific journals reported one new record separation factor for relevant mixtures after the other during the last years (e.g. ZIF-8: SF<sub>propylene/propane</sub> > 150 <sup>[128]</sup>, Zn<sub>2</sub>(bim)<sub>4</sub> nanosheets: SF<sub>H<sub>2</sub>/CO<sub>2</sub></sub> > 200 <sup>[142]</sup>, MOF-74-IM (functionalized with imidazole molecules): SF<sub>O<sub>2</sub>/H<sub>2</sub></sub> > 25 <sup>[143]</sup>), not one metal-organic framework-based process has even come close to replacing cryogenic distillation, scrubbing or countercurrent distillation under real-life conditions so far. By stepping outside the "over"-controlled lab environment the reason for this becomes painfully apparent, because, among other things, without mitigating factors like sweep gas or vacuum on the permeate side of a membrane (both are simply too expensive for a profitable approach) most materials have a hard time meeting the commercial viability limit for the respective separation factor and all gas mixtures in the wild contain MOF-damaging (loss of crystallinity, obstructed channels etc.) impurities such as H<sub>2</sub>S, NO, SO<sub>2</sub>, or water <sup>[144]</sup>.

---

[136] B. Mu, F. Li, Y. G. Huang, K. S. Walton, *J. Mater. Chem.*, 22, 2012, 10172 - 10178.

[137] D. I. Kolokolov, L. Diestel, J. Caro, D. Freude, A. G. Stepanov, *J. Phys. Chem. C*, 118, 2014, 12873 - 12879.

[138] Q. R. Fang, D. G. Yuan, J. Scully, *Inorg. Chem.*, 49, 2010, 11637 - 11642.

[139] N. Notman, *Chem. World*, 14 (5), 2017, 44 - 47.

[140] A. Scott, *Chem. Eng. News*, 95 (24), 2017, 18 - 19.

[141] Editorial, *Nat. Chem.*, 8 (11), 2016, 987.

[142] Y. Peng, Y. Li, Y. Ban, H. Jin, W. Jiao, X. Liu, W. Yang, *Science*, 346 (6215), 2014, 1356 - 1359.

[143] J. Y. Kim, R. Balderas-Xicohtencatl, L. Zhang, S. Kang, M. Hirscher, H. Oh, H. R. Moon, *J. Am. Chem. Soc.*, 139, 2017, 15135 - 15142.

[144] S. Kanehashi, A. Aguiar, H. T. Lu, G. Q. Chen, S. E. Kentish, *J. Membr. Sci.*, 549, 2018, 696 - 692.

## MOF-74

A perfect example for said kind of unfulfilled expectations (especially regarding olefin/paraffin separation) is MOF-74, a family of structures first synthesized/described in 2005 by either YAGHI<sup>[145]</sup> or DIETZEL<sup>[146]</sup> and therefore having more than one name (M-MOF-74 = Yaghi, CPO-27-M = Dietzel,  $M_2(\text{dhtp}) = \text{neutral}$ <sup>[147]</sup>), which was prematurely hailed as the "next big thing" due to calculations and its idiosyncrasies. Most of those are of a structural nature and arise from the combination of divalent metal ions like Mg, Ni, Co, Fe, Cu, Mn or Zn (mixed metal MOF-74s containing Sr, Ba, Ca, Cd + all the others are also possible via one pot synthesis)<sup>[148]</sup> with an unsymmetrical hexavalent linker molecule (2,5-dihydroxyterephthalate) into a honeycomb-like framework with 1,1 nm wide 1D channels and an metal-dependent inner surface areas (Langmuir) of up to  $\sim 2000 \text{ m}^2/\text{g}$ <sup>[134]</sup> (see Fig. 8 and Table 4). The channel corners consist of threefold helical chains (SBU) made from cis-edge-connected oxygen-metal square pyramids, where each ion is coordinated to two hydroxyl as well as three carboxyl groups from several linkers, and are lined with accessible (aimed into the cavities) coordinatively unsaturated metal centers (after activation/solvent or guest removal)<sup>[145, 148, 149]</sup>, aka MOF-74's most sought-after/versatile features.

Among the biggest advantages of having such active sites all over your framework in a very high density is, on the one hand, the possibility for guest molecules (gases like  $\text{NH}_3$ ,  $\text{H}_2\text{S}$ ,  $\text{CO}_2$ ,  $\text{N}_2$  etc.) to undergo direct interactions ranging from strong acid-base, polarization or weak physisorption<sup>[150]</sup> up to  $\pi$ -complexations between the empty antibonding orbital of an olefin's double bond and the metal's outer d atomic orbital (Fig. 8)<sup>[151]</sup> as well as, on the other hand, providing new connection point for a post-synthetic functionalization (i.e. with ethylenediamine<sup>[78]</sup> or imidazole<sup>[143]</sup>). Unfortunately, structural anomalies like these come at the high price of a reduced stability against chemical and environmental influences which, for example, in the case of water will cause a complete pore blockage (phase transformation) after just a few seconds exposure to moist room air<sup>[147]</sup> and therefore necessitates a protective atmosphere ( $\text{N}_2$  or Ar) for the handling/storage of MOF-74 in order to maintain its integrity/activation. A second major problem has to do with the one-dimensionality of the framework's hexagonal channels in combination with them running parallel to the long axis of the rod-shaped crystals (see Fig. 8)<sup>[152]</sup>, because for a gas separation to function properly, their openings

[145] N. L. Rosi, M. Eddaoudi, B. Chen, M. O'Keeffe, O. M. Yaghi, *J. Am. Chem. Soc.*, **127**, **2005**, 1504 - 1518.

[146] P. D. C. Dietzel, Y. Morita, R. Blom, H. Fjellvag, *Angew. Chem. Int. Ed.*, **44**, **2005**, 6354 - 6358.

[147] C. Chmelik, A. Mundstock, P. D. C. Dietzel, J. Caro, *Micropor. Mesopor. Mater.*, **183**, **2014**, 117 - 123.

[148] L. J. Wang, H. Deng, H. Furukawa, F. Gandara, K. E. Cordova, D. Peri, O. M. Yaghi, *Inorg. Chem.*, **53**, **2014**, 5881 - 5883.

[149] P. D. C. Dietzel, R. E. Johnsen, R. Blom, H. Fjellvag, *Chem. Eur. J.*, **14**, **2008**, 2389 - 2397.

[150] B. Supronowicz, A. Mavrandronakis, T. Heine, *J. Phys. Chem. C*, **117**, **2013**, 14570 - 14578.

[151] J. Hou, P. Liu, M. Jiang, L. Yu, L. Li, Z. Tang, *J. Mater. Chem. A*, **7**, **2019**, 23489 - 23511.

[152] I. Strauss, A. Mundstock, D. Hinrichs, R. Himstedt, A. Knebel, C. Reinhardt, D. Dorfs, J. Caro, *Angew. Chem. Int. Ed.*, **57**, **2018**, 7434 - 7439.

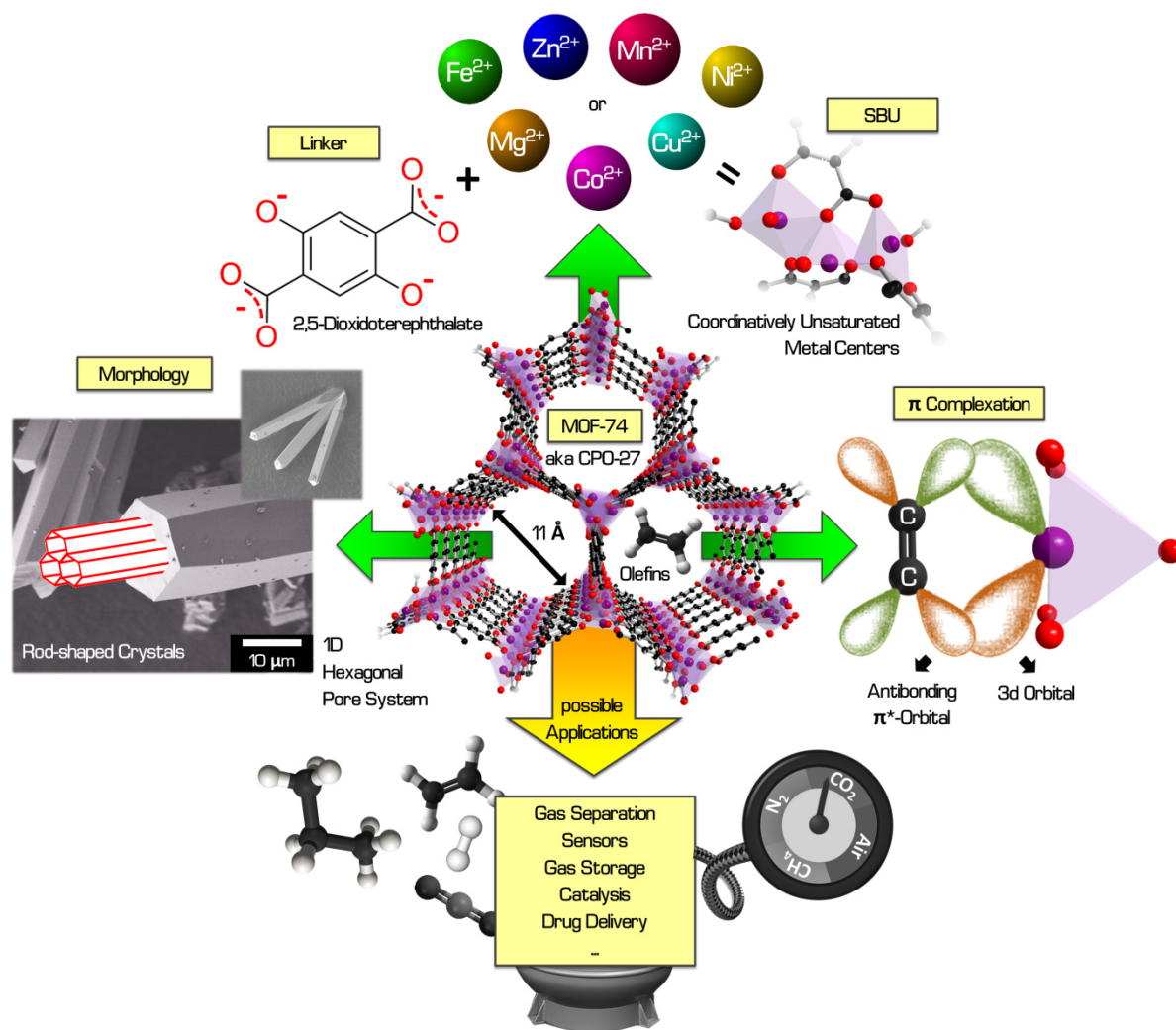


Fig. 8 SEM pictures (Co) as well as schematic visualization of the basic building blocks, crystal structure, idiosyncrasies and possible applications of MOF-74.

need to face the feed gas stream head-on, but particles featuring this kind of morphology rather tend to grow more or less flat on a substrate or orient themselves parallel toward it inside a matrix. <sup>[153, 154]</sup>

In addition to the already mentioned gas separation, which is still pursued regardless of said challenges (H<sub>2</sub>/CO<sub>2</sub> <sup>[78]</sup> with an amine modified Mg-MOF-74, propylene/propane <sup>[30, 153]</sup>, imidazole functionalized MOF-74 for D<sub>2</sub>/H<sub>2</sub> <sup>[143]</sup> etc.), possible applications include gas storage (e.g. CO<sub>2</sub> <sup>[155]</sup>

[153] A. Mundstock, U. Böhme, B. Barth, M. Hartmann, J. Caro, *CIT*, 85 (11), 2013, 1694 - 1699.

[154] A. Sabetghadam, B. Seoane, D. Keskin, N. Duim, T. Rodenas, S. Shahid, S. Sorribas, C. Le Guillouzer, G. Clet, C. Tellez, M. Daturi, J. Coronas, F. Kapteijn, J. Gascon, *Adv. Funct. Mater.*, 26, 2016, 3154 - 3163.

[155] A. R. Millward, O. M. Yaghi, *J. Am. Chem. Soc.*, 127, 2005, 17998 - 17999.

or acetylene <sup>[156]</sup>, electrochemistry (i.e. Mn-MOF-74 as cathode material for Li-O<sub>2</sub> batteries <sup>[157]</sup>), catalysis (oxidation of cyclohexene <sup>[158]</sup>, magnesium sulfite oxidation <sup>[159]</sup> etc.), sensors (e.g. resistive <sup>[129]</sup> or Raman-based <sup>[152]</sup> gas sensing) and drug delivery (i.e. anticancer drugs (computational study) <sup>[160]</sup> or ibuprofen anions in Fe-MOF-74 <sup>[161]</sup>). However, all of these are, once again, purely academic efforts without any real-world implementation so far, not least because of the MOF's high sensitivity towards external factors against which there is, in the case of membrane-based processes, a "simple" (partial) solution.

## Mixed Matrix Membranes

As evinced by the majority of application examples presented so far, the predominant form in which separation-active materials are harnessed today is as membranes <sup>[162]</sup>, followed by packed powder beds for PSA/VSA <sup>[163]</sup> and liquids (i.e. ionic liquids in so-called "liquid membranes") <sup>[164]</sup>, or more precisely plane/spiral-wound flat-sheets and hollow-fibers (highest surface area per unit volume) <sup>[165]</sup> due to mostly economic advantages like their relatively easy workability, low cost/weight/energy/space/maintenance requirements as well as high potential for modularity/process flexibility <sup>[166]</sup>. Unfortunately, the crystalline nature of many highly selective starting materials (MOFs, zeolites, MCMs etc.) entails significant problems regarding a membrane-based use, ranging from the fact that a considerable amount of those can't be grown as a dense layer at all to start with, the very fastidious challenge to synthesize crack/defect-free, at best, nanometer-thick layers over large, curved areas (e.g. onto the inside of a tubular Al<sub>2</sub>O<sub>3</sub> support) with the rest up to the overall lack of flexibility and mechanical stability in such systems, all fueling the perpetual competition between them and the second big player in this field, namely polymeric membranes. <sup>[166, 167, 168]</sup>

---

[156] A. Luna-Triguero, J. M. Vicent-Luna, R. M. Madero-Castro, P. Gomez-Alvarez, S. Calero, *ACS Appl. Mater. Interfaces*, 11 (34), **2019**, 31499 - 31507.

[157] D. Wu, Z. Guo, X. Yin, Q. Pang, L. Zhang, Y.-G. Wang, Q. Li, *Adv. Mater.*, 26 (20), **2014**, 3258 - 3262.

[158] D. Ruano, M. Diaz-Garcia, A. Afayate, M. Sanchez-Sanchez, *Chem. Cat. Chem.*, 7, **2015**, 674 - 681.

[159] M. Li, Q. Guo, L. Xing, L. Yang, T. Qi, S. Zhang, L. Wang, *J. Colloid. Interface Sci.*, 559, **2020**, 88 - 95.

[160] I. Erucar, S. Keskin, *J. Mater. Chem. B*, 5 (35), **2017**, 7342 - 7351.

[161] Q. Hu, J. Yu, M. Liu, A. Liu, Z. Dou, Y. Yang, *J. Med. Chem.*, 57 (13), **2014**, 5679 - 5685.

[162] G. Avci, S. Velioglu, S. Keskin, *ACS Appl. Mater. Interfaces*, 10, **2018**, 33693 - 33706.

[163] N. Alias, K. S. N. Kamarudin, N. A. Ghazali, T. A. T. Mohd, A. Sauki, M. R. Jaafar, *Key Eng. Mater.*, 594 - 595, **2014**, 160 - 167.

[164] F. F. Krull, C. Fritzmann, T. Melin, *J. Membr. Sci.*, 325 (2), **2008**, 509 - 519.

[165] W. J. Koros, G. K. Fleming, *J. Membr. Sci.*, 83, **1993**, 1 - 80.

[166] R. Abedini, A. Nezhadmoghadam, *Pet. Coal*, 52 (2), **2010**, 69 - 80.

[167] A. F. Ismail, L. I. B. David, *J. Membr. Sci.*, 193, **2001**, 1 - 18.

[168] Y. Alqaheem, A. Alomair, M. Vinoba, A. Perez, *Int. J. Polym. Sci.*, **2017**, 4250927.

Their triumphal march started back in the 1960s when LOEB and SOURIRAJAN devised a water desalination process featuring cellulose acetate and steadily gained momentum from there on <sup>[169]</sup>, evidenced by, amongst others, the first commercialized large scale polymer membrane for gas separation purposes (polysulfone hollow fibers for H<sub>2</sub>/CH<sub>4</sub>) developed in 1980 by PERMEA (Air Products) <sup>[168]</sup>. The sheer amount of thriving separation applications, including, for example, hydrogen sulfide removal with cellulose acetate/Pebax (polyether-block-amide), CO<sub>2</sub> capture using polyamides/polyimides, gas dehydration/hydrogen recovery with polydimethylsiloxane (PDMS) or polyethersulfones (PESFs) for various gas mixtures (CO<sub>2</sub>/CH<sub>4</sub>, He/CH<sub>4</sub>, H<sub>2</sub>/N<sub>2</sub>, O<sub>2</sub>/N<sub>2</sub>), proof that polymers can easily compensate for their inherent separation-relevant disadvantages like low permselectivities and plasticization/rigidification issues with advanced mechanical properties (flexibility, long-term stability), easy producibility/malleability/processability/upscalability as well as cost efficiency (e.g. no expensive porous support is needed). <sup>[166, 168]</sup>

Bearing in mind the advantages and shortcomings of the above mentioned competing membrane types, it seems obvious that a combination of both, featuring the unrivalled tailorable selectivity of crystalline materials as well as the superior durability of polymers, could be a match made in heaven and eliminate many of the always recurring separation-relevant problems of the individual components in a single stroke. When PAUL and KEMP added zeolite 5A into PDMS in order to study the immobilizing adsorption in polymeric membranes and discovered that this caused a highly increased diffusion time lag for some small penetrant molecules (CO<sub>2</sub>, CH<sub>4</sub>) compared to others (He, N<sub>2</sub>) in 1973, they unknowingly laid the groundwork for what today is known as mixed matrix membranes (MIMMs). <sup>[170, 171]</sup> These are generally defined as hybrid composite materials comprised of inorganic particles embedded/dispersed (with existing defined internal interfaces) in a continuous organic matrix, whereby the filler is mainly responsible for enhancing the separation-capability by either serving as molecular/affinity sieve or transport barrier while being protected from harmful external influences by the flexible polymeric shell (see Fig. 9). <sup>[172, 173]</sup>

Generally speaking, there are no bounds to the imagination when it comes to the choice of filler material, be it zeolites <sup>[175]</sup>, MOFs <sup>[174]</sup>, carbon molecular sieves <sup>[175]</sup>, mesoporous silica <sup>[176]</sup>, or carbon nanotubes <sup>[177]</sup>, simply because a suitable/adjuvant polymeric counterpart (most of which are multipurpose like polyimides, polysulfones, polyetherimides etc. <sup>[173]</sup> (see Table 5)) with a comparable rudimentary selectivity is easily found or even made and both components can be further modified

---

[169] S. Loeb, S. Sourirajan, *Advances in Chemistry*, 38, 1962, 117 - 132.

[170] D. R. Paul, D. R. Kemp, *J. Polym. Sci.: Polym. Phys.*, 41, 1973, 79 - 93.

[171] T.-S. Chung, L. Y. Jiang, Y. Li, S. Kulprathipanja, *Prog. Polym. Sci.*, 32, 2007, 483 - 507.

[172] R. Lin, B. V. Hernandez, L. Ge, Z. Zhu, *J. Mater. Chem. A*, 6, 2018, 293 - 312.

[173] H. B. Tanh Jeazet, C. Staudt, C. Janiak, *Dalton Trans.*, 41, 2012, 14003 - 14027.

[174] S. Friebe, A. Mundstock, D. Unruh, F. Renz, J. Caro, *J. Membr. Sci.*, 516, 2016, 185 - 193.

[175] T.-H. Wenig, H.-H. Tseng, M.-Y. Wey, *Int. J. Hydrogen Energy*, 35, 2010, 6971 - 6983.

[176] B. Zornoza, S. Iusta, C. Tellez, J. Coronaz, *Langmuir*, 25, 2009, 5903 - 5909.

[177] L. Ge, Z. Zhu, V. Rudolph, *Sep. Purif. Technol.*, 78, 2011, 76 - 82.



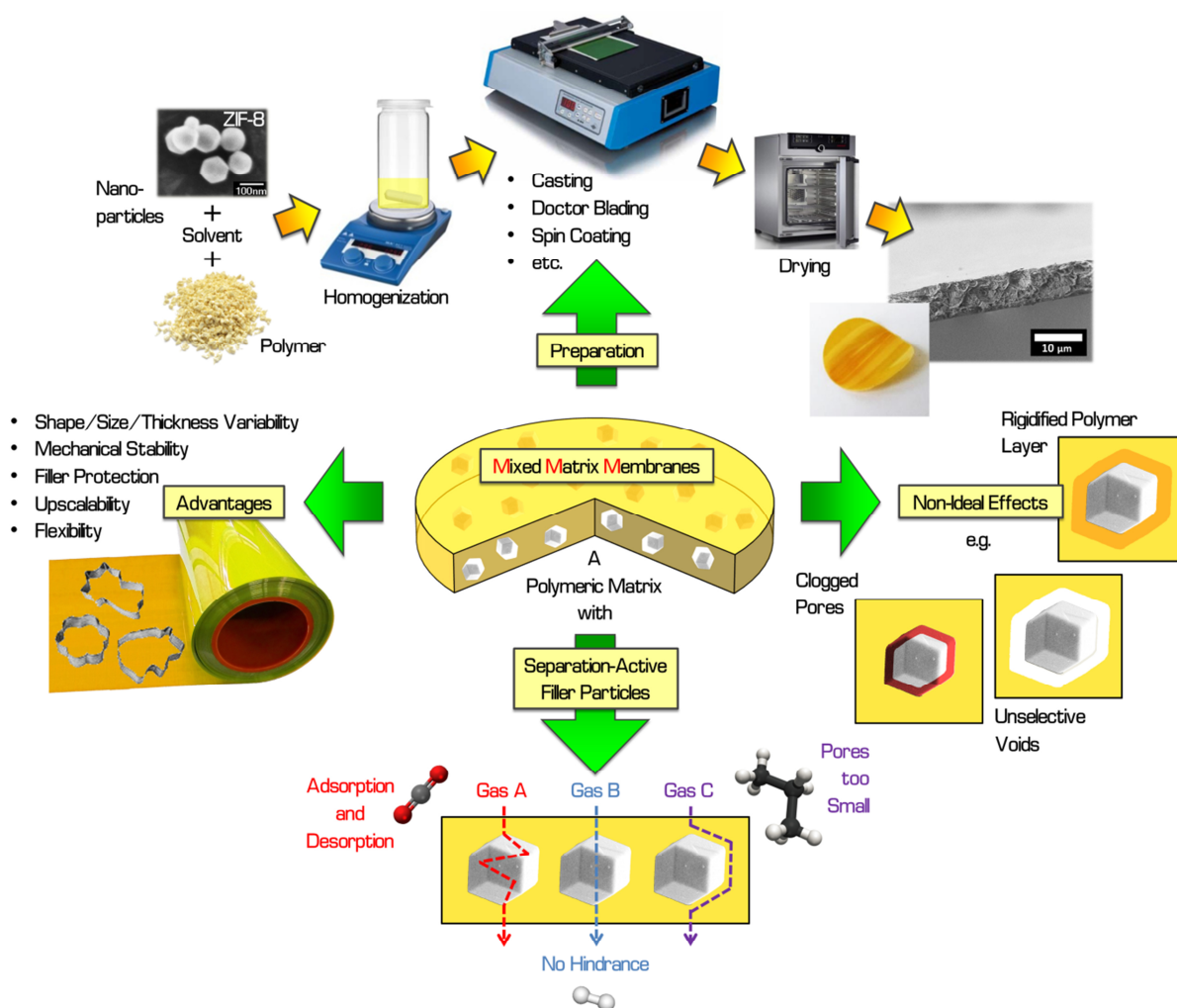


**Fig. 9** Schematic representation of the principle behind mixed matrix membranes, their preparation (flat sheet) and advantages compared to pure crystalline membranes (MOFs, zeolites etc.) as well as matrix/filler interaction-related non-ideal effects.

accordingly. An actual MMM preparation is a multistep process (Fig. 9), including dope (solvent + filler + polymer) production and homogenization (e.g. stirring, ultrasonication), membrane casting/spinning (in the case of hollow fibers), drying (vacuum or not) as well as various pre/post treatments (filtration, degassing, shaping, thermal annealing<sup>[178]</sup> etc.), whose final outcome is determined by a multitude of parameters like type of solvent, dope viscosity, component interaction/similarity, crosslinking, interface morphology or filler amount/dispersion/size.<sup>[172, 179]</sup> The possible problems associated with the latter three alone, i.e. the sedimentation of microparticles or aggregation/recrystallization of nanoparticles<sup>[180]</sup>, which are widely preferred because they allow for

[178] G.-L. Zhuang, M.-Y. Wey, H.-H. Tseng, *Chem. Eng. Res. Des.*, 104, 2015, 319 - 332.

[179] T. T. Moore, W. J. Koros, *J. Membr. Sci.*, 239, 2005, 87 - 98.

[180] A. Knebel, S. Friebe, N. C. Bigall, M. Bazaqui, C. Serre, J. Caro, *ACS Appl. Mater. Interfaces*, 8 (11), 2016, 7536 - 7544.

thinner membranes, provide a good example for why many mixed matrix membranes don't feature an enhanced selectivity as well as permeability (ideal case = perfect filler embedding) compared to the pure polymer.<sup>[179, 181]</sup> Owing to the complexity of the resulting systems, the list of such non-ideal effects in MMMs is quite long and also contains issues like rigidified/compressed polymer regions around the particles (increased selectivity ( $SF \uparrow$ ) + decreased permeability ( $P \downarrow$ )), unselective voids between polymer and filler ( $SF = + P \uparrow$ ), a high free volume at the component interface due to bridging molecules ( $SF \downarrow + P \uparrow$ ) as well as filler pores bottlenecked by ( $SF \uparrow + P \downarrow$ ) or even completely clogged with adsorbed guests/polymer chains ( $SF = + P \downarrow$ ).<sup>[179]</sup>

Amongst the possible reasons for all of this are, for example, the structural influence of the embedded particles on the surrounding polymer (stress due to a high surface area), residual solvents, rigid casting substrates and the dramatic difference in thermal expansion coefficients/drying-related shrinking/mobility/polarity of the organic/inorganic elements which often lead to a disturbed or even non-existing interaction between the two.<sup>[179]</sup> Fortunately, solution approaches in the form of sophisticated activation/preparation procedures (minimized stress due to

**Table 5** Frequently used polymers and some of their literature known MMM variants for diverse binary gas separation applications (data adapted from<sup>[172, 173]</sup>)

Trade name	Polymer type	Exemplary MMM filler materials	Exemplary gas separation applications
Matrimid	Polyimide	MOF-5, HKUST-1, ZIF-8, ZIF-90, MIL-53(AI), NaX	H <sub>2</sub> /CO <sub>2</sub> , CO <sub>2</sub> /CH <sub>4</sub> , CO <sub>2</sub> /N <sub>2</sub> , H <sub>2</sub> /CH <sub>4</sub> , C <sub>3</sub> H <sub>6</sub> /C <sub>3</sub> H <sub>8</sub>
P84	Polyimide	ZIF-4, ZIF-7, ZIF-8, ZIF-67, ZIF-90, HKUST-1, UTSA-280	H <sub>2</sub> /CO <sub>2</sub> , CO <sub>2</sub> /CH <sub>4</sub> , N <sub>2</sub> /O <sub>2</sub> , C <sub>2</sub> H <sub>4</sub> /C <sub>2</sub> H <sub>6</sub> , C <sub>3</sub> H <sub>6</sub> /C <sub>3</sub> H <sub>8</sub>
6FDA-DAM	Polyimide	ZIF-8, ZIF-11, ZIF-90, SFSIX-3-Cu, MCM-41	CO <sub>2</sub> /CH <sub>4</sub> , CO <sub>2</sub> /N <sub>2</sub> , C <sub>2</sub> H <sub>4</sub> /C <sub>2</sub> H <sub>6</sub> , C <sub>3</sub> H <sub>6</sub> /C <sub>3</sub> H <sub>8</sub>
Ultem/PEI	Polyetherimide	ZIF-8, ZIF-90, MIL-53(AI), HKUST-1, silica	CO <sub>2</sub> /N <sub>2</sub> , CO <sub>2</sub> /CH <sub>4</sub> , n-C <sub>4</sub> /CH <sub>4</sub>
Pebax	Polyether block amid	ZIF-7, ZIF-8, ZIF-67, NOTT-300, COF-5, graphite oxide	CO <sub>2</sub> /N <sub>2</sub> , CO <sub>2</sub> /CH <sub>4</sub>
PSF	Polysulfone	ZIF-20, HKUST-1, UiO-66, NH <sub>2</sub> -MIL-53(AI), MIL-101(Cr)	O <sub>2</sub> /N <sub>2</sub> , H <sub>2</sub> /CH <sub>4</sub> , CO <sub>2</sub> /CH <sub>4</sub> , CO <sub>2</sub> /N <sub>2</sub>
PDMS	Polydimethylsiloxane	ZIF-8, HKUST-1, zeolite 4A, carbon, silicalite-1	CO <sub>2</sub> /CH <sub>4</sub> , C <sub>3</sub> H <sub>8</sub> /CH <sub>4</sub> , C <sub>3</sub> H <sub>8</sub> /N <sub>2</sub>
PVac	Polyvinyl acetate	Cu-BDC, Mg-MOF-74, ZIF-8, zeolite 4A	CO <sub>2</sub> /CH <sub>4</sub> , C <sub>3</sub> H <sub>6</sub> /C <sub>3</sub> H <sub>8</sub>
PIM-1	Spirobisindane-based ladder polymer	SFSIX-3-Zn, ZIF-8, MIL-101, UiO-66-NH <sub>2</sub>	C <sub>3</sub> H <sub>6</sub> /C <sub>3</sub> H <sub>8</sub> , CO <sub>2</sub> /CH <sub>4</sub> , CO <sub>2</sub> /N <sub>2</sub>

elevated casting temperatures, melt processing <sup>[182]</sup>, mercury as a casting substrate <sup>[179]</sup> etc.), chemical functionalizations and, especially, crosslinking <sup>[183]</sup> (see Fig. 10) have helped to overcome many of said issues, making MMMs a viable competitor in the field of separation.

This includes, inter alia, areas of application like the purification/dehydration of ethanol <sup>[184]</sup> (using zeolite@poly(vinyl alcohol) <sup>[185]</sup>, silica@Chitosan <sup>[186]</sup>, ZIF-8@Matrimid 5218 <sup>[187]</sup> etc.) and the removal of salt (by e.g. carbon nanotubes@polyethersulfone) <sup>[188]</sup>, pharmaceuticals (i.a. phenolic compounds with Al nanoparticles@cellulose acetate phthalate) <sup>[189]</sup>, heavy metal ions or dyes (for instance Cu (II)/methylene blue through Al<sub>2</sub>O<sub>3</sub>@cellulose acetate-polysulfone) <sup>[190]</sup> from water via membrane distillation/pervaporation. The main focus, however, clearly lies on the mixed matrix membranes' selectivity potential regarding industry-relevant gases, which stems from their unique amalgamation of beneficial traits and is evidenced by the large number of literature known examples for the binary mixtures H<sub>2</sub>/CO<sub>2</sub> (i.a. metal exchanged zeolite X <sup>[75]</sup> or NH<sub>2</sub>-MIL-125 <sup>[174]</sup> in Matrimid), propylene/propane (ZIF-8@6FDA-DAM <sup>[191]</sup>, SIFSIX-3-Zn@PIM-1 <sup>[192]</sup> etc.) and CO<sub>2</sub>/CH<sub>4</sub> (e.g. HKUST-1 @PDMS <sup>[192]</sup>), to name but a few important ones (see Table 5). <sup>[173]</sup>

## Matrimid

As indicated by the previous chapter, one of the most commonly used matrix materials for MMMs are polyimides (PI), a polymer species first reported by BOGERT and RENSHAW in 1908 <sup>[194]</sup>, mass-produced since the 1950's <sup>[195]</sup>, successfully used in a plethora of further application fields ranging from microelectronics to solar cells or aerospace and generally characterized by an imide group-containing backbone featuring, in most cases, aromatic building blocks. <sup>[183]</sup> The combination of these two structural motifs allows for the creation of polymeric precursors which are highly stable on the one hand, clearly evidenced by, for example, their mainly aromaticity-caused high glass transition temperatures, rigidity or oxidative resistance (also helped by the imide bond's electron-deficiency),

---

[182] T. M. Guer, *J. Membr. Sci.*, 93, 1994, 283 - 289.

[183] K. Vanherck, G. Koeckelberghs, I. F. J. Vankelecom, *Prog. Polym. Sci.*, 38, 2014, 874 - 896.

[184] R. Castro-Munoz, F. Galiano, V. Fila, E. Drioli, A. Figolini, *Rev. Chem. Eng.*, 35 (5), 2019, 565 - 590.

[185] Z. Huang, H. M. Guan, W. L. Tan, X. Y. Qiao, S. Kulprathipanja, *J. Membr. Sci.*, 276, 2006, 260 - 271.

[186] Y. L. Liu, C. Y. Hsu, Y. H. Su, J. Y. Lei, *Biomacromolecules*, 6, 2005, 368 - 373.

[187] A. Kudasheva, S. Sorribas, B. Zornoza, J. Coronas, *J. Chem. Technol. Biotechnol.*, 90, 2015, 669 - 677.

[188] H.-G. Choi, M. Son, H. Choi, *Chemosphere*, 185, 2107, 1181 - 1188.

[189] R. Mukherjee, S. De, *J. Hazard. Mater.*, 265, 2014, 8 - 19.

[190] A. Rajeswari, E. J. S. Christy, G. Mary, K. Jayaraj, A. Pius, *J. Environ. Chem. Eng.*, 7 (4), 2019, 103278.

[191] C. Zhang, Y. Dai, J. R. Johnson, O. Karvan, W. J. Koros, *J. Membr. Sci.*, 389, 2012, 34 - 42.

[192] Q. Shen, S. Cong, R. He, X. J. Wang, B. Vander Bruggen, Y. Zhang, *J. Membr. Sci.*, 588, 2019, 117201.

[193] A. Car, C. Stropnik, K. V. Peinemann, *Desalination*, 200, 2006, 424 - 426.

[194] M. T. Bogert, R. R. Renshaw, *J. Am. Chem. Soc.*, 30 (7), 1908, 1135 - 1144.

[195] Y. Zhuang, J. G. Seong, Y. M. Lee, *Prog. Polym. Sci.*, 92, 2019, 35 - 88.

and versatile on the other, due to the fact that an additional incorporation of property-altering (polarity, crosslinkability, selectivity, permeability etc.) groups, side chains or whole sections (block copolymer) is relatively easy.<sup>[183]</sup>

One of the most frequently encountered polyimides in literature, at least when it comes to gas separation, is the glassy (operates below its glass transition temperature ( $T_g$ )) thermoplastic Matrimid 5218, which consists of 3,3'-4,4'-benzophenone tetracarboxylic-dianhydride diaminophenylindane repeating units<sup>[196]</sup> (see Fig. 10) and has been investigated/utilized for that purpose since the late 90's<sup>[197]</sup>. It owes its popularity to a multitude of handy traits, including good solubility in many organic solvents (i.a. dimethylformamide (DMF), tetrahydrofuran (THF), chloroform or dioxane), mechanical toughness, excellent thermal stability ( $T_g \approx 310\text{ }^\circ\text{C}$ <sup>[196]</sup>), low flammability, good

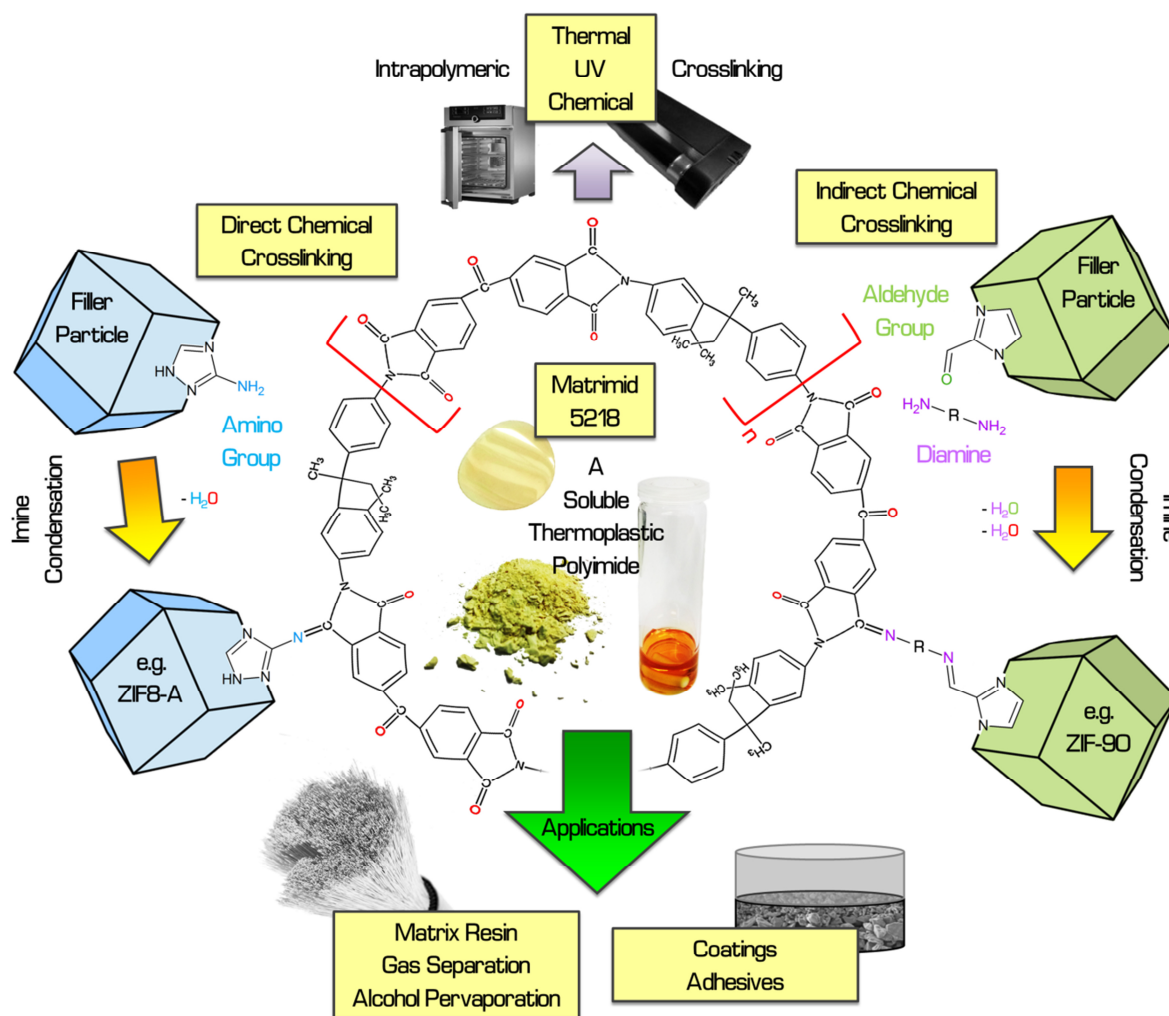


Fig. 10 Chemical structure, common forms (photos of powder/dope/flat sheet membrane) and applications of Matrimid 5218 as well as schematic depiction of various crosslinking methods.

[196] R. Castro-Munoz, V. Fila, *Membranes*, 8 (30), 2018, 8020030.

[197] A. Bos, I. G. M. Puent, M. Wessling, H. Strathmann, *Sep. Purif. Technol.*, 14 (1 - 3), 1998, 27 - 39.

dielectric properties, high radiation resistance as well as relatively high gas separation factors and permeability coefficients compared to other polymeric materials (polycarbonates, polysulfones etc.).<sup>[198, 199]</sup> Furthermore, Matrimid's backbone-contained aldehyde groups additionally facilitate its easy crosslinkability, regardless of whether it is done intrapolymerically via heat treatment (annealing), UV irradiation, bromination or chemical bridging agents like diamines (imine condensation:  $R-C=O + NH_2-R \rightarrow R-C=N-R + H_2O$ ) or between the polymer and functionalized filler particles with amino (e.g. ZIF-8-A<sup>[200]</sup>) or C=O groups (i.e. ZIF-90 + ethylenediamine<sup>[201]</sup>) of their own (see Fig. 10).

This kind of forced interaction not only helps to mitigate or even eliminate a majority of the non-ideal effects in MMMs described above, thereby enhancing the respective separation capabilities towards a far more favorable selectivity/permeability trade-off (when one  $\uparrow$  the other  $\downarrow$ )<sup>[179, 201]</sup>, but also can improve some of the inherent properties of the polymer itself like solvent stability, hydrophilicity and susceptibility to plasticization.<sup>[183]</sup> Especially the latter, generally characterized by a swelling of the polymeric matrix due to the perpetual sorption of penetrants (higher free volume + increased segmental mobility)<sup>[202]</sup>, together with the changes in macroscopic physical properties/morphology over time simply referred to as "aging" (e.g. secondary crystallization by photo-oxidation)<sup>[203]</sup> is one of Matrimid's worst weaknesses with regard to an industrial application. Both phenomena are deeply rooted in the glassy nature of the polymer and eventually result in a gradual deterioration of the membranes' separation performance whose progression is highly dependent on the respective operating conditions (temperature, pressure, gas impurities etc.).<sup>[202, 204]</sup>

Nonetheless, Matrimid 5218 enjoys great popularity within the scientific community, where, amongst other things, it finds niche use as adhesive (Ciba - Product Data), coating (i.e. top layer to suppress linker rotation/gate opening in MOF membranes<sup>[205]</sup> and encapsulation of UiO-66 pallets<sup>[206]</sup>) or sensor component (e.g. capacitive gas phase sensing of alcohols with nano  $NH_2$ -MIL-53(A)@Matrimid layers<sup>[207]</sup>), while its unrivaled main application field remains the membrane/MMM-based gas separation. A few representative examples from the recent literature which perfectly showcase this trend as well as the polyimide's versatility are Matrimid hollow fibers with an ultrathin ZIF-8

---

[198] K. Liang, J. Grebowicz, F. E. Karasz, W. J. MacKnight, *J. Polym. Sci. Pol. Phys.*, 30, 1992, 465 - 476.

[199] C. Nistor, S. Shishatskiy, M. Popa, S. P. Nunes, *Environ. Eng. Manag. J.*, 7, 2008, 653 - 659.

[200] K. Y. Cho, H. An, X. H. Do, H. G. Yoon, H.-K. Jeong, J. S. Lee, K.-Y. Baek, *J. Mater. Chem. A*, 6, 2018, 18912 - 18919.

[201] L. Diestel, N. Wang, A. Schulz, F. Steinbach, J. Caro, *Ind. Eng. Chem. Res.*, 54, 2015, 1003 - 1012.

[202] P. S. Tin, T. S. Chung, Y. Liu, R. Wang, S. L. Liu, K. P. Pramoda, *J. Membr. Sci.*, 225, 2003, 77 - 90.

[203] J. R. White, *C. R. Chimie*, 9, 2006, 1396 - 1408.

[204] B. R. Rowe, B. D. Freeman, D. R. Paul, *Polymer*, 50, 2009, 5565 - 5575.

[205] S. Friebe, A. Mundstock, K. Volgmann, J. Caro, *ACS Appl. Mater. Interfaces*, 9, 2017, 41553 - 41558.

[206] M. I. Hossain, A. Uddh, B. E. Grabicka, K. S. Walton, S. M. C. Ritchie, T. G. Glover, *Ind. Eng. Chem. Res.*, 58 (3), 2019, 1352 - 1362.

[207] S. Sachdeva, S. J. H. Koper, A. Sabetghadam, D. Socol, D. J. Gravesteijn, F. Kapteijn, E. J. R. Sudhoelter, J. Gascon, L. C. P. M. De Smet, *ACS Appl. Mater. Interfaces*, 9 (29), 2017, 24926 - 24935.

membrane on the bore side (propylene/propane)<sup>[208]</sup>, partially Li<sup>+</sup> exchanged Na-ZSM-25 compound materials (CO<sub>2</sub>/CH<sub>4</sub>)<sup>[209]</sup>, Cu-BDC@Matrimid (He/CH<sub>4</sub> + He/N<sub>2</sub>)<sup>[210]</sup> and mixed matrix flat sheet membranes featuring zeolite X filler particles optimized in terms of their ionic potential (H<sub>2</sub>/CO<sub>2</sub>)<sup>[75]</sup>.

### III Measurement Method and Important Physical Quantities

The actual separation capability inherent to (planar) specimen like those mentioned above is, in most cases, scientifically evaluated nowadays using a measurement setup/principle whose basic form and features date back to 1941, when it was originally developed by WICKE and KALLENBACH to investigate the surface diffusion of CO<sub>2</sub> on activated carbon<sup>[211]</sup>. At the heart of this method lies the so-called permeation reactor, a gas-tight vessel made of e.g. stainless steel, Teflon or glass like the original one with four openings (one gas inlet + outlet on each end) and divided by the separation-active membrane in question into two distinct (mirrored) compartments (see Fig. 11).

On the one hand, there is the so-called feed side where the to-be-separated gas mixture (in our case an equimolar binary blend constantly provided by mass flow controllers) or single gas enters the reactor, comes in contact with the separating layer and partially permeates through it in an component-specific ratio, while the majoritarian rest (retentate) simply drains via an outlet. Upon the membrane-facilitated arrival in the other half, generally referred to as permeate side, the analyte (permeate) is transported out of the vessel and towards the analysis method of choice (online gas chromatography (GC), mass spectrometry (MS) or a "bubble counter" flowmeter) using a constant stream of inert sweep gas (mainly N<sub>2</sub>, but also Ar and He).

However, whereas the original purpose of this general setup strictly called for isobaric conditions on both sides in order to minimize the occurrence of other gas transport mechanisms (namely KNUDSEN-, grain boundary- as well as "normal" diffusion - depending on the respective pore diameters) beside the wanted surface diffusion<sup>[211, 212]</sup>, current and industrial viable versions usually operate with higher pressures on the feed side (e.g. generated by a backpressure valve on the outlet (Fig. 11)) as driving force for the permeation/separation, additionally amplified by the sweep-caused, non-existent permeate partial pressure (it's carried away instantaneously) in the other compartment<sup>[213, 214]</sup>. Although this isn't the only benefit of sweep gas, counteracting concentration polarization<sup>[215]</sup> (the

---

[208] M. R. Abdul Hamid, S. Park, Y. M. Lee, H.-K. Jeong, *Ind. Eng. Chem. Res.*, 58 (32), 2019, 14947 -14953.

[209] J. Zhao, K. Xie, L. Liu, M. Liu, W. Qiu, P. A. Webley, *J. Membr. Sci.*, 583, 2019, 23 - 30.

[210] A. Akbari, J. Karimi-Sabet, S. M. Ghoreishi, *Chem. Eng. Process.*, 148, 2020, 107804.

[211] E. Wicke, R. Kallenbach, *Kolloid Z.*, 97, 1941, 135 - 151.

[212] K. Soukup, P. Schneider, O. Solcova, *Chem. Eng. Sci.*, 63, 2008, 1003 - 1011.

[213] A. Sengupta, K. K. Sirkar, *Membrane Science and Technology*, 2, 1995, 499 - 552.

[214] K. Soukup, P. Schneider, O. Solcova, *Chem. Eng. Sci.*, 63, 2008, 4490 - 4493.

[215] M. Nordio, S. Soresi, G. Manzolini, J. Melendez, M. Vant Sint Annaland, D. A. Pacheko Tanaka, F. Gallucci, *Int. J. Hydrogen Energy*, 44, 2019, 4228 - 4239.

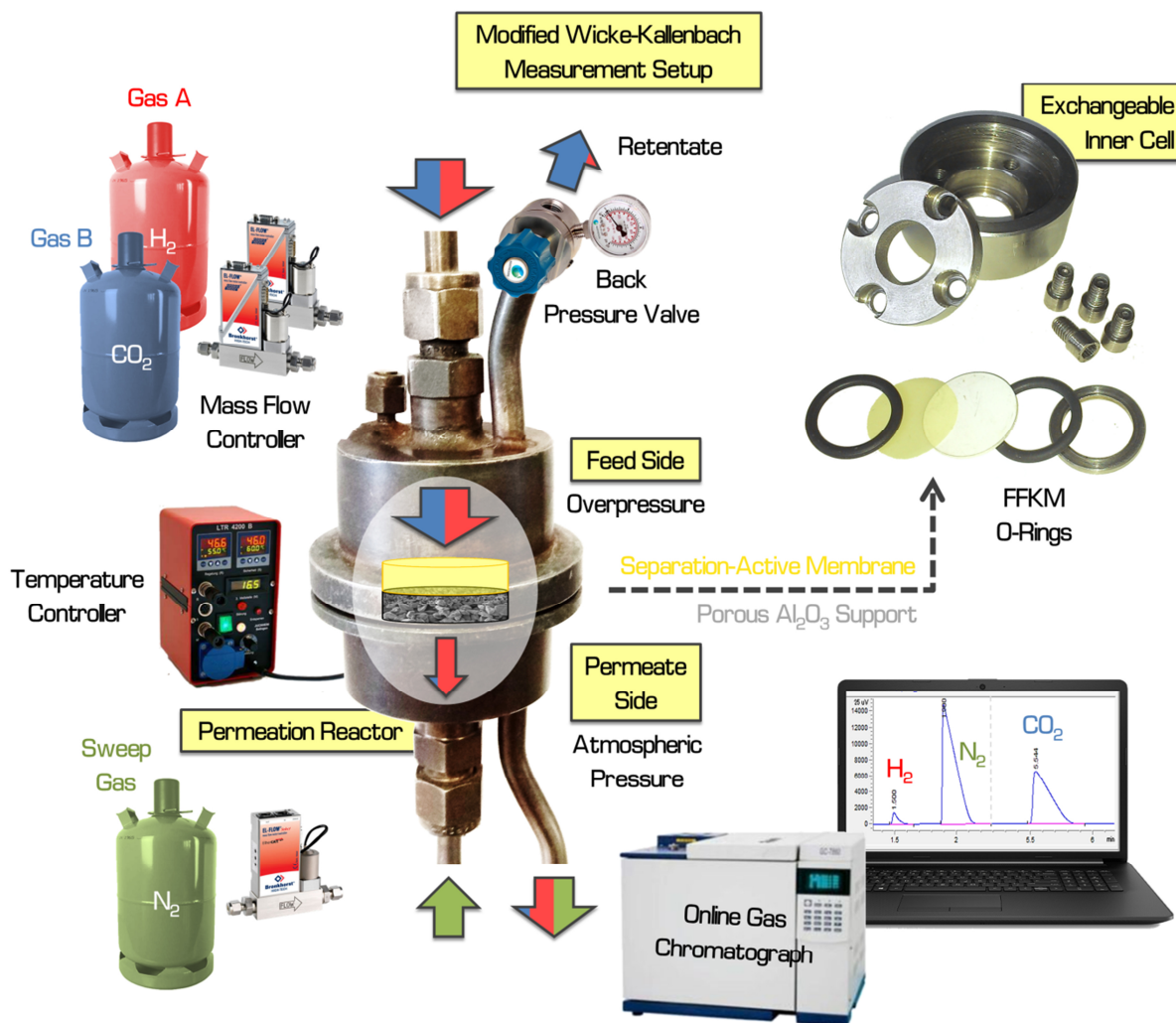


Fig. 11 Schematic visualization of the employed measurement setup (modified Wicke-Kallenbach) including photographs showing the original permeation reactor and exchangeable inner cell.

accumulation of the higher concentrated species on the membrane surfaces, thereby reducing the overall flux), for example, is another one, its use is all but uncontroversial because diluting the freshly separated gas is rather counterproductive in regard to commercialization <sup>[214]</sup> (it increases the overall process costs just like using vacuum) and the often neglected counter-diffusion <sup>[216, 217]</sup> (against the analyte flux → affecting their permeation through support + separation layer) can considerably falsify the measurable values of a membrane's defining physical quantities.

These include, first and foremost, the already abundantly mentioned selectivity/separation factor  $\alpha$ , a numerical measure for the effectiveness of a setup concerning the removal of one distinct part from a mixture, in the simplest case an equimolar binary one made up of the gases  $x$  and  $y$ , which is mathematically defined as the components molar ratio (with  $n_{x \text{ or } y}$  being the respective amount) in

[216] J. Dong, Y. S. Lin, W. Liu, *AIChE Journal*, 46 (10), 2000, 1957 - 1966.

[217] C. Zhao, A. Caravella, H. Xu, A. Brunetti, G. Barbieri, A. Goldbach, *J. Membr. Sci.*, 550, 2018, 365 - 376.

the permeate, divided by the retentate composition <sup>[218]</sup> (Eq. 1).

$$\alpha_{x/y} = \frac{n_{x,permeate} / n_{y,permeate}}{n_{x,retentate} / n_{y,retentate}} \quad (\text{Eq. 1})$$

Due to the fact that the given feed is continuously replenished and usually only a very small share of it (nl -  $\mu\text{l}/\text{min}$  compared to the incoming ml/min) disappears through the membrane, the overall conditions on this side are considered to be "constant" (feed = retentate) throughout the entire process, what, in combination with a preset equimolarity, dramatically simplifies the measurement (halving the necessary analysis effort) as well as Eq. 1 by turning its denominator into a 1.

The second and at least as important fundamental characteristic to detail a systems separation capability is the product of permeance, in itself a species-specific compound quantity calculated via dividing the amount of permeated gas (e.g.  $n_{\text{CO}_2,permeate}$ ) per time  $t$  & membrane area  $A$  (also known as flux) by the pressure difference between the two reactor compartments  $\Delta p$ , with layer thickness  $d$  <sup>[218]</sup> (Eq. 2), collectively referred to as permeability  $P$ .

$$P_x = \frac{n_{x,permeate}}{t \cdot A \cdot \Delta p} \cdot d \quad (\text{Eq. 2})$$

Over the decades, this indicator for how much (or rather little) of the individual feed components actually passes through the material/medium in question under certain circumstances has been expressed in various systems of units (i.a. CGS (centimeter-gram-second) and STP (standard temperature and pressure)), often deliberately chosen such that it complements the respective study focus (performance vs. mechanism) <sup>[219]</sup>, with *barrier* (mol/m s Pa (SI version) <sup>[220]</sup>), coined/named in the 60's after RICHARD MALING BARRER the "founding father of zeolite chemistry and a dominant figure in membrane science" <sup>[221]</sup>, being today's most commonly used unit when it comes to the application-oriented evaluation of polymer-based membranes.

Considering all of this, it becomes apparent that the key factor behind both of these defining physical quantities simply boils down to the question of how exactly the specific gas species enter/exit and travers the separation layers' innards, what in turn materially depends on whether we talk about a dense (e.g. polymers and metals) or porous (MOFs, COFs, zeolites, carbon etc.) substance.

[218] W. J. Koros, Y. H. Ma, T. Shimidzu, *Pure & Appl. Chem.*, 68, 1996, 1479 - 1489.

[219] S. A. Stern, *J. Polymer Sci. Part-A*, 6, 1968, 1933 - 1934.

[220] B. Castro-Dominguez, P. Leelachaikul, S. B. Messaoud, A. Takagaki, T. Sugawara, R. Kikuchi, S. T. Oyama, *Chem. Eng. Res. Des.*, 97, 2015, 109 - 119.

[221] L. V. C. Rees, *Biogr. Mem. Fellows R. Soc.*, 44, 1998, 37 - 49.



Except in the rather rare case of pure molecular sieving, the cross-sectional mass transport of the feed components through the latter generally consists of always the same sequential steps, namely adsorption on the membranes' outer surface → surface diffusion → bulk diffusion inside the porous system → effusion from the pores → desorption from the permeate-side surface <sup>[222]</sup>, breaking down (as a rule of thumb) its overall selectivity into a roughly predictable product of adsorption selectivity and diffusion selectivity <sup>[223]</sup>. Whereas the material flux caused by thermally promoted equalization of a concentration difference (increase in entropy) via random particle movement (BROWNIAN motion), commonly known as diffusion, is gradient-driven (depending on the used model: FICK → concentration, MAXWELL-STEFAN → chemical potential) <sup>[224, 225]</sup>, adsorption/desorption introduces the additional element of direct host-guest interaction (affinity-controlled, e.g. MOF-gas) in the form of chemisorption (stronger chemical bonds) and physisorption based on VAN-DER-WAALS forces (far more common/weaker) <sup>[226]</sup>.

The main difference when dense materials are involved lies on the sorption side of things or, to be more precise, in the so-called solution-diffusion mechanism/model (first proposed in 1866 by GRAHAM <sup>[227]</sup>), which introduces the solubility of a molecular species in a specific matrix <sup>[183]</sup> as a decisive term and adjusts the fundamental dependencies of the affected physical quantities (i.e.  $P = \text{solubility (sorption)} \cdot \text{diffusivity (mobility)}$ ) accordingly <sup>[228]</sup>. In order to get a first impression of what to expect from certain gases, it is possible to use their respective condensabilities as an indicator for how effectively they might dissolve into/through the membrane (in general: larger/easier condensable molecules are better soluble/sorption-dominated) <sup>[229]</sup>, a process strongly dependent on not only temperature (higher  $T$  suppresses adsorption) and interaction strength (mainly vdW forces) but also polymer type, with glassy ones such as Matrimid, for example, exhibiting more or less mobility-dominated permeation patterns (smaller molecules travel faster) due to a stiffer amorphous internal structure <sup>[230]</sup>.

As already outlined in the chapter about mixed matrix membranes, this whole topic only becomes more complicated by introducing the additional variable of porous separation-active filler particles (dispersed phase  $d$ ) into a known dense polymeric material (continuous phase  $c$ ), resulting in the compound permeability ( $P_{MMi}$ ) being a function of the components' individual transport properties

---

[222] R. M. Barrer, *J. Chem. Soc. Faraday Trans.*, 86, 1990, 1123 - 1130.

[223] J. Caro, M. Noack, P. Koelsch, *Adsorption*, 11, 2005, 215 - 227.

[224] J. Kaenger, D. M. Ruthven, *Diffusion in zeolites and other microporous materials*, John Wiley & Sons, New York, 1992.

[225] R. Krishna, J. A. Wesselingh, *Chem. Eng. Sci.*, 52 (6), 1997, 861 - 911.

[226] K. S. W. Sing, D. H. Everett, R. A. W. Haul, L. Moscou, R. A. Pierotti, J. Rouquerol, T. Siemieniowska, *Pure Appl. Chem.*, 57 (4), 1985, 603 - 619.

[227] V. Stannett, *J. Membr. Sci.*, 3, 1978, 97 - 115.

[228] Y. Yampolski, B. Freeman, *Membrane gas separation*, John Wiley & Sons, 2010.

[229] T. C. Merkel, V. I. Bondar, B. D. Freeman, I. Pinnau, *J. Polym. Sci. B Polym. Phys.*, 38, 2000, 415 - 434.

[230] A. Javaid, *Chem. Eng. J.*, 112, 2005, 219 - 226.

( $P_c$  and  $P_d$ ) as well as mixing ratio (e.g. expressed as additive volume fraction  $\varphi_d$ ), at least in the simplest/ideal case of perfect embedment (Maxwell model, Eq. 3).<sup>[179]</sup>

$$P_{MMM} = P_c \left[ \frac{P_d + 2P_c - 2\varphi_d(P_c - P_d)}{P_d + 2P_c + \varphi_d(P_c - P_d)} \right] \quad (\text{Eq. 3})$$

However, because this is rather the exception than the norm, further amendments to this equation concerning possible non-ideal factors like transport restrictions due to interface phenomena, void-related reduction of the effective layer thickness and sieving benefits caused by suppressed linker rotation (each one with a distinct impact on the composites' overall (absolute vs. effective) permeability towards a particular gas)<sup>[179]</sup> are usually needed to better approximate/portray the reality or even predict (for screening purposes) the separation capabilities of a theoretical MMM solely on the basis of its well-studied potential ingredients/predecessors.

For the sake of comparability, most application-oriented studies nowadays present both of the aforesaid key parameters in the form of one logarithmic plot ( $\log \alpha_{x/y}$  against  $\log P_{\text{of the better permeating gas}}$ ) named after LLOYD M. ROBESON, who published his first iterations in 1991 (revised in 2008) after compiling a huge amount of data (extracted from 300+ sources) related to homogeneous polymeric films and a selection of industry-relevant binary gas mixtures (containing  $\text{H}_2$ ,  $\text{CO}_2$ ,  $\text{CH}_4$ ,  $\text{O}_2$ ,  $\text{N}_2$ , He).<sup>[231, 232]</sup> An integral feature of any such graphical overview is the so-called upper bound, a linear line representing the (material type-specific) state-of-the-art separation benchmark for the investigated task at that point in time (its slope seems to be primarily dictated by the dominant transport coefficient)<sup>[232]</sup>, against which every new contender, be it e.g. a carbon, polymer, MOF, zeolite or mixed matrix membrane, is measured.

[231] L. M. Robeson, *J. Membr. Sci.*, 62, 1991, 165 - 185.

[232] L. M. Robeson, *J. Membr. Sci.*, 320, 2008, 390 - 400.

---

## II. Why finding an Olefin/Paraffin-Selective Material is only half the Battle

One particular problem very often associated with the screening for/of new separation-active materials is that, as exemplarily demonstrated by the following three olefin/paraffin-themed publications about one zeolite and three MOFs in total, even if they show great promise in theory or as powder doesn't automatically mean that this kind of behavior is still present/equally pronounced in another form, let alone gives any indication of how difficult it will be to manufacture them into adequate membranes.

Among the most commonly used "pre-membrane" evaluation methods are single component adsorption isotherms and binary mixture breakthrough experiments, both of which were utilized in the first research article featured in this chapter to gain an initial impression of the ethylene/ethane and propylene/propane separation potential inherent to various nanoporous adsorbents in their powder state. While the overall results paint a quite promising picture, ZIF-8 turned out to be paraffin selective and the MOF-74 variants (Co & Mg) included in this study exhibit varying degrees of olefin selectivity, others raised some doubt about their real-world usefulness because, in addition to the experimental separation factors of the latter two being significantly lower than the theoretically predicted ones, they also seem to suffer from a considerable vulnerability to humidity. Dr.-Ing. Ulrike Böhme wrote the majority of this paper as well as conducted all the adsorption/breakthrough experiments together with her two colleagues Dr.-Ing. Benjamin Barth and Carolin Paula. Everything related to the structural characterization under the influence of water was done by Andreas Kuhnt. The author of this thesis co-wrote parts of the publication, developed the synthesis/activation procedures, laid the groundwork for the moisture sensitivity investigation and provided the Co/Mg-MOF-74 samples. By lending their support and expertise, professors Wilhelm Schwieger, Jürgen Caro and Martin Hartmann ensured the timely completion and quality of the manuscript.

Conceived as the logical counterpart to the previous one, the second publication revolves around a comparison between the auspicious adsorption/breakthrough results for compressed Mg-MOF-74 powder and the propylene/propane separation capability of a thin but dense crystalline membrane grown from the same material on a porous  $\text{Al}_2\text{O}_3$  support. What made the preparation of the latter especially challenging is that, owed to the 1D nature of the MOF's channel system, the needlelike crystals need to be arranged/oriented in a very particular way (with the pores as perpendicular as possible to the support surface) inside the layer to allow for an unhindered mass transport through it. Unfortunately, although this was eventually achieved, for the first time ever, by means of synthesis adjustments, the resulting membrane exhibited no propylene/propane selectivity at all due to a previously unknown effect created by adsorption-caused blockage/self-hindrance. The author

---

developed this new synthesis route, prepared all membranes, characterized them (XRD, SEM,  $C_3$  separation performance etc.), provided powder samples and co-wrote the majority of this article together with Prof. Dr. Jürgen Caro, on whose ideas it is based. Dr.-Ing. Ulrike Böhme and Dr.-Ing. Benjamin Barth conducted all tasks related to Mg-MOF-74 powder synthesis as well as characterization (XRD, adsorption isotherms, breakthrough curves etc.) plus contributed to the respective parts in the manuscript. Additional support was rendered by Prof. Dr. Martin Hartmann in the form of very fruitful discussions.

Last but not least, publication number three demonstrates just how crucial membrane quality is for the separation performance by using propylene/propane as a yardstick against which the effectiveness of two pre-synthetic support functionalizations (APTES and PDA), here applied in the type X preparation to mitigate growth-related defects, is measured. Whereas both of these modifications yielded zeolite layers with increased separation factors (compared to the ones fabricated on unaltered  $Al_2O_3$ ), all attempts to improve their selectivity even further by post-synthetic ion exchange ( $Na^+ \rightarrow Co^{2+}$ ) were not only not successful but resulted in severe cracks, most probably thanks to unit cell shrinkage. All XRD, SEM, zeta potential and gas permeation measurements as well as membrane preparations were performed/evaluated by the author, who also wrote the majority of this article. Dr. Nanyi Wang supplied the author with PDA-covered supports and thought him how to handle APTES. Additional support in regard to the contact angle measurements and interpretation of many permeation results was provided by Dr. Sebastian Friebe. Prof. Dr. Jürgen Caro contributed his comprehensive experience with/knowledge about zeolites to the manuscript and thereby helped to improve it considerably.

---

### III Ethene/Ethane and Propene/Propane Separation via the Olefin and Paraffin Selective Metal-Organic Framework Adsorbents CPO-27 and ZIF-8

U. Böhme, B. Barth, C. Paula, A. Kuhnt, W. Schwieger, A. Mundstock, J. Caro, M. Hartmann

*Langmuir*, 29, 2013, 8592 - 8600.

---

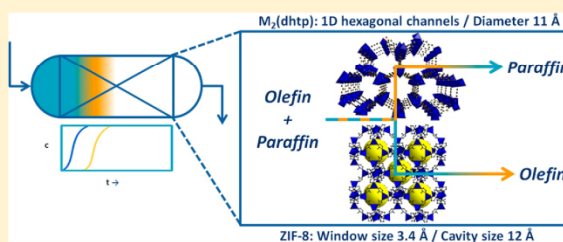
## Ethene/Ethane and Propene/Propane Separation via the Olefin and Paraffin Selective Metal–Organic Framework Adsorbents CPO-27 and ZIF-8

Ulrike Böhme,<sup>†</sup> Benjamin Barth,<sup>†</sup> Carolin Paula,<sup>†</sup> Andreas Kuhn,<sup>‡</sup> Wilhelm Schwieger,<sup>‡</sup> Alexander Mundstock,<sup>§</sup> Jürgen Caro,<sup>§</sup> and Martin Hartmann<sup>\*,†</sup>

<sup>†</sup>Erlangen Catalysis Resource Center (ECRC) and <sup>‡</sup>Chemical Reaction Engineering, Universität Erlangen-Nürnberg, Egerlandstrasse 3, 91058 Erlangen, Germany

<sup>§</sup>Institute of Physical Chemistry and Electrochemistry, Leibniz University Hannover, Callinstraße 3A, 30167 Hannover, Germany

**ABSTRACT:** Two types of metal–organic frameworks (MOFs) have been synthesized and evaluated in the separation of C<sub>2</sub> and C<sub>3</sub> olefins and paraffins. Whereas Co<sub>2</sub>(dhtp) (=Co–CPO-27 = Co–MOF-74) and Mg<sub>2</sub>(dhtp) show an adsorption selectivity for the olefins ethene and propene over the paraffins ethane and propane, the zeolitic imidazolate framework ZIF-8 behaves in the opposite way and preferentially adsorbs the alkane. Consequently, in breakthrough experiments, the olefins or paraffins, respectively, can be separated.



### 1. INTRODUCTION

The separation of the C<sub>2</sub> to C<sub>4</sub> paraffin/olefin mixtures by cryogenic distillation is one of today's indispensable and most energy-intensive processes in the refinery industry. It is, therefore, highly desired to substitute the short chain paraffin/olefin separation by less energy-intensive separation techniques such as adsorption or membrane permeation.

In principle, an adsorptive separation can be accomplished by kinetic or thermodynamic principles. Small differences in the molecular size can cause dramatic changes in the diffusion rates of the mixture components through molecular sieve pores, which lead in their extreme to the molecular sieve effect (size exclusion). Differences in the adsorptive interaction with the adsorbent allow equilibrium-based separations according to different mixed gas adsorption equilibria.

A nice example for the kinetic separation of a propane/propene mixture was given by Li et al.,<sup>1</sup> showing that the uptake rate of propene and propane in a series of zeolitic imidazolate frameworks (ZIFs) can be controlled by the linker size. On ZIF-8, the slightly smaller propene shows a diffusion coefficient which is about 125 times higher than that one of propane (at 30 °C). The adsorption and diffusion of ethene/ethane mixtures in ZIF-8 was explored by <sup>1</sup>H and <sup>13</sup>C MAS NMR spectroscopy and by the combination of pulsed field gradient NMR with magic-angle spinning (MAS PFG NMR). The diffusion selectivity was determined to be  $D_{\text{ethene}}:D_{\text{ethane}} = 5.5$  at a loading of four molecules per cavity.<sup>2</sup> However, the practical exploitation of the different diffusion rates/or the molecular sieve effect seems to be complicated for metal–organic frameworks (MOFs) because of their nonconstant pore size. Framework flexibility can be understood as thermal

vibrations of the MOF window, which open the pores for larger molecules.<sup>3</sup> The gate opening effect also causes a larger pore size and is initiated by the linker distortion.<sup>4</sup> From pioneering in situ X-ray diffraction (XRD) studies, it is known that the methyl imidazolate linkers of ZIF-8 show a swing effect upon gas adsorption; thus the pores open and give access to the cavity.<sup>5</sup> Gücüyener et al. explain the preferred adsorption of ethane in comparison to the only slightly lighter and stiffer ethylene on ZIF-7 also by a gate opening mechanism.<sup>6</sup>

Several reports have shown that the framework structure of ZIF-8 is in fact more flexible rather than static. Although the size of the pore window of ZIF-8 is estimated from crystallographic data to be 0.34 nm, Sanchez and co-workers adsorbed *n*-heptane in ZIF-8;<sup>7</sup> Luebbbers et al. demonstrated that *n*-alkanes with a critical diameter of 0.43 nm are easily adsorbed by ZIF-8.<sup>8</sup> In addition, another chromatographic study showed that more bulky branched alkanes (critical diameter > 0.54 nm) are not able to pass the narrow pore windows of ZIF-8, whereas the linear ones are adsorbed.<sup>9</sup> However, in a recent study by Ferreira et al., it was shown that ZIF-8 can adsorb 2,3-dimethylbutane, with a kinetic diameter of 0.58 nm, but not 2,2-dimethylbutane.<sup>10</sup>

The consideration of framework flexibility is crucial to predicting correct separations on MOF membranes. Permeation studies on ZIF-7,<sup>11</sup> ZIF-8,<sup>12</sup> ZIF-22,<sup>13</sup> and ZIF-90<sup>14</sup> membranes also showed that methane with a critical diameter of 0.38 nm can easily pass the ZIF-8 pore window (0.34 nm),

Received: April 18, 2013

Revised: June 6, 2013

Published: June 10, 2013

and no sharp cutoff exists for hydrocarbons with critical diameters larger than the crystallographic pore size. In recent papers it is shown that also aromatics such as *p*-xylene<sup>15</sup> and benzene<sup>16</sup> are adsorbed in ZIF-8, however, most probably by linker distortion rather than by framework flexibility which is engendered by a shift of the coordination points.

Different from MOFs, zeolites show a more rigid framework with a clear cutoff. Therefore, adsorptive separation of ethylene/ethane mixtures using the molecular sieve effect is possible on zeolites. Zhu et al. found for SiO<sub>2</sub>-DD3R that only propylene (critical diameter 0.43 nm) is adsorbed by DD3R with a pore size of 0.45 nm, but propane (0.45 nm) is excluded from the pores.<sup>17</sup> Breakthrough experiments confirm that DD3R is a very effective molecular sieve for the separation of propylene/propane mixtures.<sup>18</sup> Similar results were obtained by Calero et al.<sup>19</sup> for ITQ-12, which is a pure silica zeolite with eight-ring pores (0.39 × 0.42 nm and 0.24 × 0.54 nm). Krishna and van Baten propose different eight-membered-ring zeolite and MOF structures with pore sizes between 0.34 and 0.46 nm as suitable candidates for the separation of propene/propane mixtures by molecular sieving.<sup>20</sup>

Another concept for the olefin/paraffin separation is the use of thermodynamic control, i.e., of specific adsorbate–adsorbent interactions. Whereas polar, cation-containing zeolites such as 13X show a preference for alkene adsorption,<sup>21,22</sup> nonpolar cation-free zeolites prefer alkane adsorption.<sup>23–25</sup> This preferred alkane over alkene adsorption has been predicted by molecular dynamics calculation of the mixed gas isotherm. Keil et al. predicted a by a factor of 2 stronger ethane than ethene adsorption from an equimolar mixture on carbon nanotubes,<sup>26</sup> but only a slightly stronger ethane than ethene adsorption on silicalite-1.<sup>27</sup>

If the metal component of an MOF structure is freely accessible and coordinatively unsaturated, the olefin becomes enriched due to an adsorption via  $\pi$ -complexation. Early examples are the preferred olefin adsorption on Cu<sub>3</sub>(BTC)<sub>2</sub><sup>28–30</sup> and Ag<sub>2</sub>[Cr<sub>3</sub>O(OOCC<sub>2</sub>H<sub>5</sub>)<sub>6</sub>(H<sub>2</sub>O)<sub>3</sub>]<sub>2</sub>.<sup>31</sup> These experimental findings of a preferred olefin adsorption are in accordance with theoretical results showing that ethene is by a factor of 2 more strongly adsorbed on Cu<sub>3</sub>(BTC)<sub>2</sub> than ethane is.<sup>32</sup> During the past year, a steadily growing number of experiments featuring a series of M–MOF-74, also denoted as M–CPO-27 or more generally M<sub>2</sub>(dhtp) (M = coordinating metal, mostly Co, Ni, Zn, Fe, Mg; dhtp = dihydroxyterephthalate), have been performed. M<sub>2</sub>(dhtp) is a three-dimensional framework with a honeycomb topology, containing one-dimensional channels (Figure 1, top). In its activated state, the metal center is coordinated in distorted square pyramidal fashion by five oxygen atoms, which are part of the organic linker. With a suitable solvent molecule a sixth metal–oxygen bond is formed resulting in a distorted octahedral coordination. The average cross-sectional channel dimensions are ca. 1.1 nm × 1.1 nm.<sup>33</sup> This adsorbent showed a remarkable and promising olefin/paraffin selectivity as a consequence of the one-dimensional hexagonal channels lined with a high concentration of open metal sites (i.e., ~4.5 sites/nm<sup>3</sup> for Mg<sub>2</sub>(dhtp)).<sup>34</sup>

ZIF-8 crystallizes in the sodalite topology, in which every Zn center is coordinated to four nitrogen atoms, forming a tetrahedron (Figure 1, bottom). This leads to six-membered-ring pores with a diameter of 0.34 nm for the pore opening and a total pore diameter of 1.2 nm.<sup>35</sup>

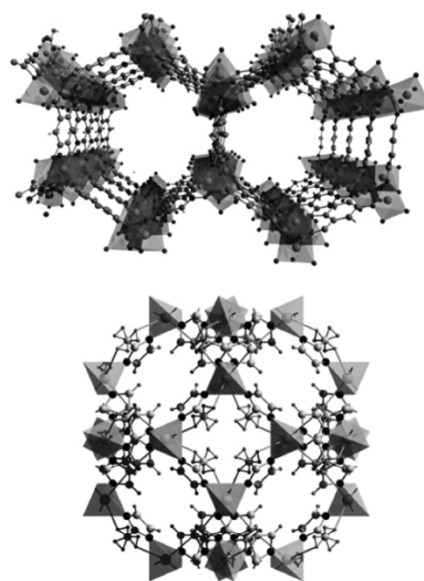


**Figure 1.** Structural representation of M<sub>2</sub>(dhtp) (top) and ZIF-8 (bottom).

It is the aim of this study to prepare two adsorbents with differing olefin/paraffin selectivity. Co<sub>2</sub>(dhtp) as well as Mg<sub>2</sub>(dhtp) in comparison to ZIF-8 will be evaluated as adsorbents in fixed-bed adsorbers, by studying the breakthrough behavior of ethane/ethane and propene/propane mixtures. Particular attention will be paid to the stability of the M<sub>2</sub>(dhtp) structure, which is expected to have a profound effect on the adsorption properties. Theoretical studies hinted at the large potential of Co<sub>2</sub>(dhtp), reporting high (theoretical) separation factors (highest ever reported for MOFs so far)<sup>36</sup> and remarkable ethene/ethane and propene/propane selectivities for the isostructural Fe<sub>2</sub>(dhtp).<sup>37</sup> However, M<sub>2</sub>(dhtp) appears to be sensitive against water, resulting in partial structure degradation.<sup>38</sup>

## 2. EXPERIMENTAL SECTION

### 2.1. Solvothermal Synthesis of the MOFs under Study.

Unless otherwise noted, all procedures were performed under ambient atmosphere and temperature. All reagents were obtained from commercial vendors at reagent grade purity or higher and used without further purification.

**2.1.1. Co<sub>2</sub>(dhtp).** The Co<sub>2</sub>(dhtp) material studied in this work was synthesized according to the reported<sup>39</sup> procedure with minor modifications. A solution of cobalt acetate tetrahydrate (1.229 g, 4.9 mmol) in water (16 mL) was placed in a Teflon-lined stainless steel autoclave with a volume of 23 mL. Dihydroxyterephthalic acid (0.494 g, 3 mmol) was added. The autoclave was sealed and heated at 110 °C for 72 h. After the reaction the resulting brown mixture was filtrated and the filter cake washed with ca. 200 mL of water. The obtained orange solid was solvent exchanged with ethanol in a Soxhlet apparatus for 24 h. The purified product was activated at 150 °C for 16 h in a vacuum. After the activation Co<sub>2</sub>(dhtp) was sensitive to moisture and was, therefore, stored under dry argon.

**2.1.2. Mg<sub>2</sub>(dhtp).** Mg<sub>2</sub>(dhtp) was prepared in a way similar to that described above for Co<sub>2</sub>(dhtp). Magnesium acetate tetrahydrate (5.860 g, 27 mmol) was dissolved in a mixture of *N*-methylpyrrolidone (78 mL) and water (12 mL), and dihydroxyterephthalic acid (2.745 g, 14 mmol) was added. The reaction was carried out in a Teflon-lined 125 mL stainless steel autoclave at 120 °C for 24 h. After filtration and

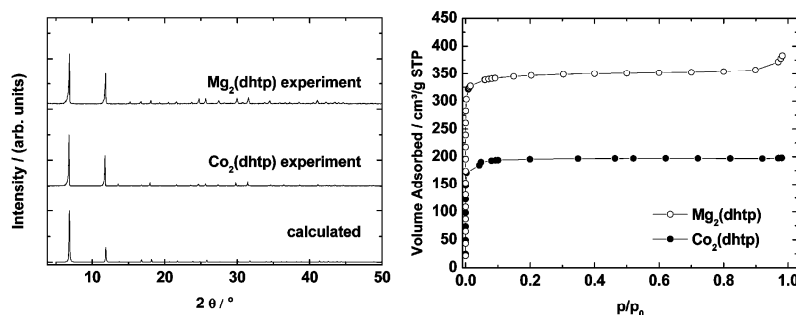


**Figure 2.** X-ray diffraction patterns (left) and nitrogen sorption isotherms at 77 K (right) of activated  $\text{Co}_2(\text{dhtp})$  and  $\text{Mg}_2(\text{dhtp})$ .

solvent exchange the obtained yellow powder was activated at 230 °C in a vacuum for 24 h. Like the cobalt-containing MOF,  $\text{Mg}_2(\text{dhtp})$  is sensitive to moisture. Thus  $\text{Mg}_2(\text{dhtp})$  was stored under argon atmosphere as well.

**2.1.3. ZIF-8.** For a typical ZIF-8 synthesis, a solution of  $\text{Zn}(\text{NO}_3)_2 \cdot 6\text{H}_2\text{O}$  (zinc nitrate hexahydrate, 1 g,  $3.36 \times 10^{-3}$  mol) and HMeIm (2-methylimidazole, 0.552 g,  $6.72 \times 10^{-3}$  mol) in DMF (dimethylformamide, 25 mL) was prepared similar to the procedure reported in ref 35. The synthesis was conducted at 140 °C for 24 h under stirring in a round-bottom flask with reflux condenser. A white powder of crystals with diameters around 10  $\mu\text{m}$  was separated from the solution. The product was Soxhlet-extracted for 48 h with methanol, dried at 60 °C in a vacuum oven for 12 h, and pelletized without binder using a hand-operated mechanical press. The pellets were crushed and sieved. Only particles with diameters between 305 and 250  $\mu\text{m}$  were used in the fixed-bed adsorber in order to avoid a large pressure drop.

The structure and porosity of the adsorbents were determined by powder X-ray diffraction using a PANalytical X'Pert diffractometer (Cu  $K\alpha$  ( $\lambda = 1.54 \text{ \AA}$ )) and nitrogen adsorption measurements (Quantachrome Autosorb 1 at 77 K, respectively). The specific surface area of the samples was calculated employing the BET method. The BET model has been applied in the range  $p/p_0 = 0.00004\text{--}0.015$ . The in situ X-ray diffraction experiments were carried out using an Anton Paar XRK-900 reaction cell at 40.1 °C and 50% relative humidity.

**2.2. Adsorption and Breakthrough Experiments.** The single component adsorption isotherms of ethane, ethene, propane, and propene on  $\text{M}_2(\text{dhtp})$  and ZIF-8 were recorded at different temperatures with a modified Micromeritics ASAP 2010 volumetric adsorption apparatus using the powder samples. All samples were outgassed at 100 °C prior to the measurements under vacuum ( $10^{-4}$  hPa). The breakthrough curves were determined in a home-built fixed-bed flow-type apparatus. The separation column was packed with  $\text{Mg}_2(\text{dhtp})$  ( $m = 0.41$  g),  $\text{Co}_2(\text{dhtp})$  ( $m = 0.75$  g), or ZIF-8 ( $m = 0.54$  g). To prevent a high pressure drop, the ZIF-8 powder was carefully pelletized, crushed, and sieved to obtain particles with diameters between 250 and 305  $\mu\text{m}$ . The  $\text{M}_2(\text{dhtp})$  adsorbents were used as obtained during the synthesis due to their instability toward exposure to air and water (vide infra). Due to their relatively large particle size (up to 100  $\mu\text{m}$ ), the resulting pressure drop was still acceptable.

Thereafter, the samples were in situ activated in the adsorber at 100 °C in flowing helium for 24 h. The feed gas was an equimolar mixture of ethane/ethene and propane/propene with a flow rate of 0.25 mL/min each. The gases are assumed to behave ideally under the prevailing experimental conditions. The dead volume is calculated from the volume of the void space of the packing and the peripheral volume. Therefore, the bulk density of the packing, the real density of the MOFs, and the geometrical dimensions of the apparatus are required. From the dead volume the dead time was calculated.

The gas at the outlet of the fixed-bed adsorber was analyzed online by gas chromatography employing a Rt-Alumina Bond CFC (30 m  $\times$  0.53 mm  $\times$  10  $\mu\text{m}$ ) column using a flame ionization detector (FID).

### 3. RESULTS AND DISCUSSION

#### 3.1. Solvothermal Synthesis of the MOFs under Study.

**3.1.1.  $\text{M}_2(\text{dhtp})$ .** Figure 2 shows the powder X-ray diffraction patterns of the  $\text{Mg}_2(\text{dhtp})$  and  $\text{Co}_2(\text{dhtp})$  powders used for determination of the adsorption isotherms and in the breakthrough adsorption experiments. The XRD patterns of the  $\text{M}_2(\text{dhtp})$  samples after activation are shown in comparison to the theoretical pattern (Figure 2). From the comparison of the XRD data with the pattern reported by Dietzel et al.,<sup>33</sup> it is concluded that our sample is a pure  $\text{M}_2(\text{dhtp})$  phase without any crystalline impurities. The specific BET surface area (Figure 2) was determined to 763 and 1420  $\text{m}^2/\text{g}$  for the Co form and the Mg form, respectively, which is in agreement with the literature (Table 1). The reported surface area of  $\text{M}_2(\text{dhtp})$

**Table 1.** Total Uptake and Specific Surface Areas  $A_{\text{BET}}$  for  $\text{Mg}_2(\text{dhtp})$  and  $\text{Co}_2(\text{dhtp})$

sample	total uptake <sup>a</sup> /( $\text{cm}^3/\text{g}$ )	$A_{\text{BET}}/\text{m}^2/\text{g}$		
		this work	MOF-74 <sup>35</sup>	CPO-27 <sup>39</sup>
$\text{Mg}_2(\text{dhtp})$	382	1420	1206	1743
$\text{Co}_2(\text{dhtp})$	198	763	1000	1341

<sup>a</sup>This work; at  $p/p_0 = 0.98$ .

materials varies largely depending on the metal employed, the synthesis route, and the activation procedure.<sup>40</sup> Part of the lower specific surface area reported for the Co form with respect to the Mg form is due to the lower molecular mass of magnesium (24.3 g/mol) compared to cobalt (58.9 g/mol). It is expected, however, that the accessible surface area and pore volume will largely influence the adsorption and separation properties of the structure under study.

**3.1.2. ZIF-8.** The powder XRD pattern of ZIF-8 is shown in Figure 3 (left). The diffractogram confirms the sodalite structure of our ZIF-8 obtained in a modified synthesis in comparison with the original recipe.<sup>35</sup> The experimental XRD powder pattern is in good agreement with the simulated one, confirming the successful synthesis of this material. The specific BET surface area amounts to 1844  $\text{m}^2/\text{g}$ , which is in the range of typical literature values.<sup>10,32</sup>

**3.2. Adsorption of Pure Paraffins and Olefins.** Figure 4 shows the adsorption isotherms of ethane, ethene, propane, and propene as single gases on our two sorbents  $\text{Mg}_2(\text{dhtp})$  and  $\text{Co}_2(\text{dhtp})$ . Because of the coincidence of the adsorption and desorption isotherms, only the adsorption data points are plotted. Both ethene and propene are adsorbed to a higher extent than the corresponding alkanes ethane and propane. Thus, our expectations were fulfilled: both materials with CPO-



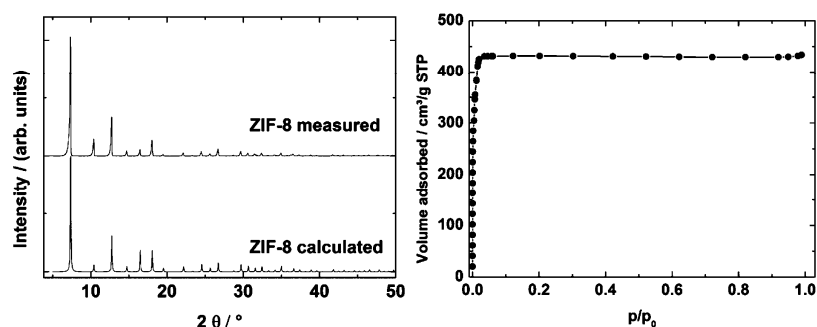


Figure 3. Powder X-ray diffraction patterns (left) and nitrogen sorption isotherms at 77 K (right) of ZIF-8.

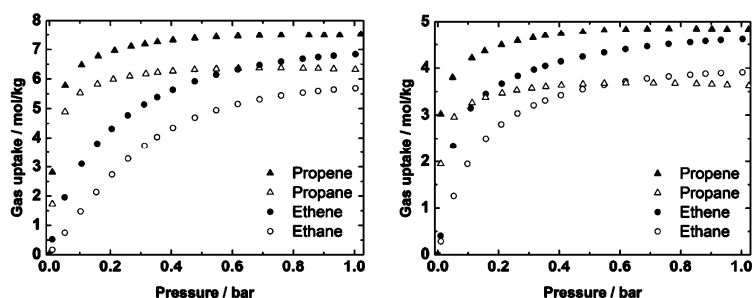


Figure 4. Gas adsorption isotherms of ethene and ethane, and propene and propane, on  $\text{Mg}_2(\text{dhtp})$  (left) and  $\text{Co}_2(\text{dhtp})$  (right) at 295 K.

27/MOF-74 structure are olefin-selective because of the strong  $\pi$ -complexation between the open  $\text{Co}^{2+}$  and  $\text{Mg}^{2+}$  sites and the olefin molecules. Surprisingly, the difference in the amount adsorbed for propane and propene on the one hand and ethane and ethene on the other hand is larger for the  $\text{C}_3$  hydrocarbons than for  $\text{C}_2$ . This experimental finding is in principle in agreement with the paper of Hupp, Snurr, and co-workers.<sup>36</sup> However, in ref 36 the total amounts adsorbed on  $\text{Co}_2(\text{dhtp})$  are somewhat higher than in our study for both  $\text{C}_2$  and  $\text{C}_3$ . This is certainly a consequence of the lower specific surface area found for our sample. In principle, it can be expected that olefin molecules can be adsorbed up to one per open metal site, resulting in a loading of ca. 6 mmol/g as reported by Bae et al.<sup>36</sup> In contrast, for  $\text{Mg}_2(\text{dhtp})$  a significantly higher adsorption capacity of up to 7.8 mmol/g for propene and 6.9 mmol/g for ethene are found in this study, which is somewhat higher than the literature data.<sup>36</sup> The saturation loading clearly depends on the accessible pore volume, which should be similar for all  $\text{M}_2(\text{dhtp})$  adsorbents regardless of the nature of the metal center, and, thus, depends mainly on the sample quality and stability, which, however, might be different.

Further, the complete overlap of adsorption and desorption isotherms confirms that the sorption process is completely reversible at room temperature. In contrast to  $\text{Co}_2(\text{dhtp})$  and  $\text{Mg}_2(\text{dhtp})$ , ZIF-8 shows a preference for the hydrocarbon with the higher molecular weight, i.e., ethane and propane in comparison with ethene and propene. Our finding of a preferred ethane adsorption on ZIF-8 in comparison with ethene is in complete accordance with sorption uptake/desorption experiments on large ZIF-8 crystals with IR detection and grand canonical Monte Carlo simulations.<sup>41,42</sup> The fact that the paraffin is slightly better adsorbed than the corresponding olefin is characteristic of sorbents without specific interactions such as cation-free nonpolar frame-

works.<sup>24,25,43</sup> In ref 44 also a preferred ethane adsorption compared with ethene was observed on ZIF-7 and explained by a gate opening mechanism. The adsorption isotherms of propene and propane (Figure 5) on ZIF-8 are very similar and

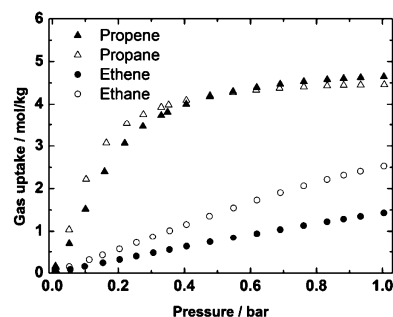


Figure 5. Gas adsorption isotherms of ethene, ethane, propene, and propane on ZIF-8 at 293 K.

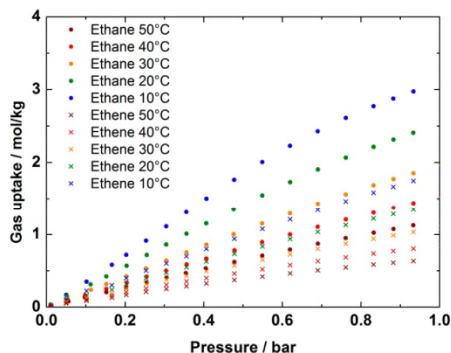
in excellent agreement with a very recent account by Zhang et al.,<sup>45</sup> but significantly higher than the loadings reported in ref 41, which amount to 2.82 and 2.62 mmol/g for propylene and propane, respectively, at 30 °C.

In the pressure range studied, saturation is not reached and the uptake of the  $\text{C}_3$  hydrocarbons is by a factor of ca. 2 higher compared to the significantly smaller hydrocarbons ethane and ethene. Moreover, the ethene and ethane isotherms are almost linear and show Henry-type behavior. The temperature dependent Henry constants are summarized in Table 2. An equilibrium selectivity  $\alpha_2 = K_1/K_2 = 1.85$  is calculated at 20 °C from the Henry constants  $K_1$  and  $K_2$  of the respective adsorption isotherms. The amount of ethene and ethane

**Table 2.** Henry Constants  $K_i$  for ZIF-8 at Different Temperatures

	$T/^\circ\text{C}$				
	10	20	30	40	50
$K_{\text{ethane}}$ ( $\text{cm}^3/(\text{g bar})$ )	72.7	55.4	41.0	33.8	23.5
$K_{\text{ethene}}$ ( $\text{cm}^3/(\text{g bar})$ )	41.2	30.6	23.0	17.6	13.6

adsorbed decreases with increasing temperature (Figure 6), although the preferential adsorption of the alkane with respect to the olefin does not change with temperature.

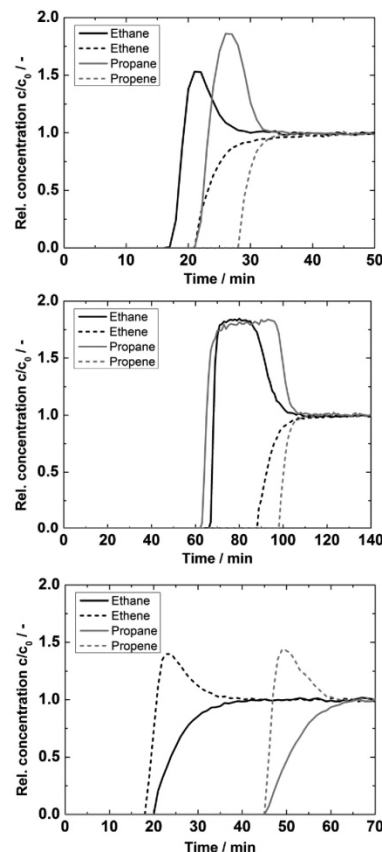
**Figure 6.** Gas adsorption isotherms of ethane and ethene on ZIF-8 at different temperature.

In the case of  $\text{C}_3$  hydrocarbons, the adsorption selectivity is small since the two isotherms almost coincide. From the literature<sup>45</sup> it is known that the amount of *n*-butane and *n*-butene is slightly slower than that of propane and propene, respectively, but the isotherms show an even stronger Langmuir-type behavior than the  $\text{C}_3$  hydrocarbons. Thus, it appears that the interaction strength increases in the order  $\text{C}_2 < \text{C}_3 < \text{C}_4$ . Whether the often suggested gate opening mechanism<sup>6,45</sup> does play a role in small hydrocarbon adsorption in ZIF-8 is at the moment questionable.

### 3.3. Breakthrough Curves in a Fixed-Bed Adsorber.

Breakthrough curves of equimolar mixtures of ethane/ethene and propane/propene have been measured in a fixed bed adsorbed at 22 °C (Figure 7). For both  $\text{Co}_2(\text{dhtp})$  and  $\text{Mg}_2(\text{dhtp})$ , characteristically shaped breakthrough curves are observed. When starting from a clean adsorber, initially both the olefin and the paraffin are completely removed from the feed stream, before the alkane breaks through first. The weaker bound compound gets displaced by the stronger adsorbed one, which leads to the overshoot above the relative concentration  $c/c_0 = 1$  (with  $c_0 = \text{feed concentration}$ ). Similar results have been observed for the separation of  $\text{C}_3$ <sup>46</sup> and iso- $\text{C}_4$ <sup>28</sup> hydrocarbons over  $\text{Cu}_3(\text{BTC})_2$  (HKUST-1). This confirms that the paraffin is displaced by the stronger adsorbed olefin. Thus, in complete accordance with the expectations from the adsorption isotherms,  $\text{Co}_2(\text{dhtp})$  and  $\text{Mg}_2(\text{dhtp})$  turned out to be olefin-selective.

In contrast to the single component isotherms,  $\text{Co}_2(\text{dhtp})$  shows a higher adsorption capacity than  $\text{Mg}_2(\text{dhtp})$  when normalized to the applied adsorbent mass. The breakthrough curves of  $\text{Co}_2(\text{dhtp})$  and  $\text{Mg}_2(\text{dhtp})$  show clear olefin preference because of the  $\pi$ -interaction of the accessible  $\text{M}^{2+}$  site with the olefin molecules. Therefore, the olefin is

**Figure 7.** Breakthrough curves of equimolar mixtures ( $p_{\text{ane}} = p_{\text{ene}} = 500$  hPa) of ethene/ethane and propene/propane in a packed column of preactivated initially clean  $\text{Mg}_2(\text{dhtp})$  ( $m = 0.41$  g, top) and  $\text{Co}_2(\text{dhtp})$  ( $m = 0.75$  g, middle) and ZIF-8 ( $m = 0.54$  g, bottom).

completely separated from the paraffin on  $\text{Co}_2(\text{dhtp})$  and  $\text{Mg}_2(\text{dhtp})$ .

From the breakthrough curves of the olefin/paraffin mixtures, separation factors can be derived.<sup>47</sup> Frontal analysis, viz., integration of the areas in the breakthrough curves, results in separation factors  $\alpha = q(\text{ethene})/q(\text{ethane}) = 1.7$  and  $\alpha = q(\text{propene})/q(\text{propane}) = 2.9$  for  $\text{Co}_2(\text{dhtp})$ . The separation factors derived for  $\text{Mg}_2(\text{dhtp})$  are even lower and amount to 1.4 and 1.7 for ethene/ethane and propene/propane, respectively. These factors are much lower than those reported by Hupp, Snurr, and co-workers derived from mixed gas IAST isotherms calculated from ethane, ethene, propane, and propene single component isotherms. For example, a value of 46 for the (theoretical) propene/propane adsorption selectivity is calculated for  $\text{Co}_2(\text{dhtp})$ .<sup>36</sup> However, in the above-discussed paper, no separation factors are derived from the experimental displacement experiments described.<sup>36</sup> Furthermore, it has to be pointed out that an equimolar mixture of olefin and paraffin with partial pressures of 500 hPa is used in our experiments. Typically, the separation factors increase significantly when more diluted gas streams are employed.<sup>36,48</sup>

While very high separation factors are calculated from single component isotherms, we derive from our breakthrough experiments only values around 2–3. The reasons for this

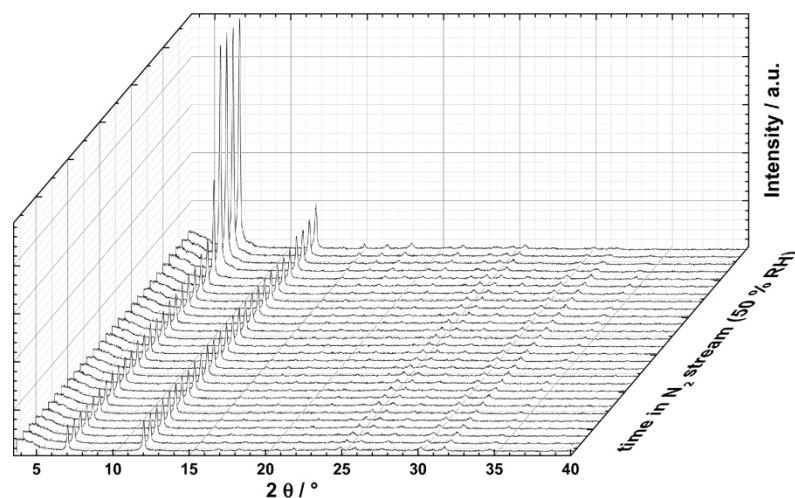


Figure 8. Powder XRD patterns of  $\text{Mg}_2(\text{dhtp})$  as a function of time in a water/ $\text{N}_2$  stream (50% RH). Diffractograms were recorded every 30 min.

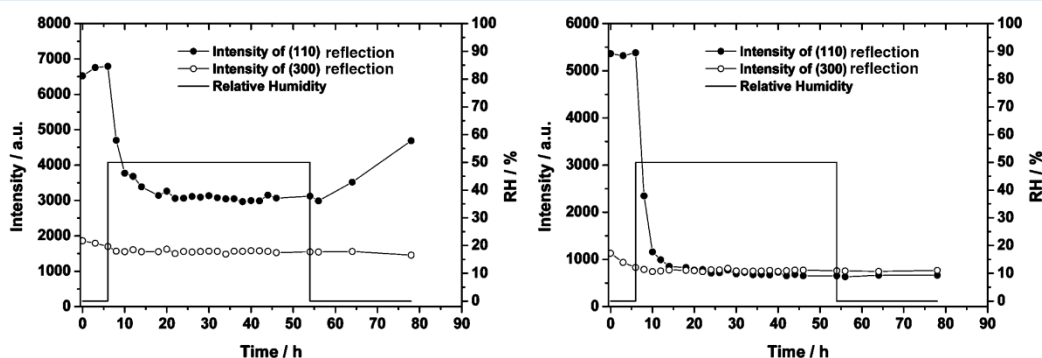


Figure 9. Intensities of the (110) and (300) reflections of  $\text{Co}_2(\text{dhtp})$  and  $\text{Mg}_2(\text{dhtp})$  as a function of time in a nitrogen/water stream.

discrepancy are at present not clear. There could be differences in the quality of the  $\text{Co}_2(\text{dhtp})$  which result in a lower adsorption capacity of our sample, but the XRD and the nitrogen sorption isotherms of our  $\text{Co}_2(\text{dhtp})$  are similar to those reported in refs 36 and 40. Another reason could be different sample activations or even different ways to calculate/determine the adsorption selectivities. Partial destruction of the structure by pelletization and water adsorption also must be considered. Therefore, powder X-ray diffraction patterns were recorded in a controlled  $\text{N}_2$ /water atmosphere at room temperature. After keeping the samples in dry nitrogen for 5 h, a stream of water in nitrogen (50% relative humidity (RH)) was passed over the sample for an additional 50 h before switching back to dry nitrogen (Figure 8). For  $\text{Mg}_2(\text{dhtp})$  and  $\text{Co}_2(\text{dhtp})$ , a clear decrease in intensity is observed for the (110) and (300) reflections (Figure 9). The decrease in intensity of the XRD reflections is accompanied by a strong decrease in the specific  $A_{\text{BET}}$  surface area (from 1420 to  $<200 \text{ m}^2/\text{g}$ ) in the case of  $\text{Mg}_2(\text{dhtp})$  within a few minutes. When the sample is again flushed with dry nitrogen, the intensity of the XRD reflections does not change. The specific surface also does not rise again. This behavior was unexpected since the  $\text{M}_2(\text{dhtp})$  structure is generally considered to be stable against water and even water adsorption isotherms are reported in the literature.<sup>40</sup> The situation is somewhat different for  $\text{Co}_2(\text{dhtp})$ .

While the intensity of the (110) and the (300) reflections is also declining after exposure to water, the decrease in surface area is relatively small (ca.  $200 \text{ m}^2/\text{g}$ ). Moreover, the intensity of those reflections rises again after flushing the sample with dry nitrogen. It is, thus, obvious that both materials are sensitive to water adsorption, which potentially blocks the CUS sites with concomitant decrease in separation potential or partial irreversible structure destruction or change. A possible formation of  $\text{Mg}(\text{OH})_2$  nanocrystals on the outside of the  $\text{Mg}_2(\text{dhtp})$  may block access to the channel system. A detailed <sup>25</sup>Mg NMR study currently underway might help to elucidate this point.<sup>49</sup>

For ZIF-8, a different separation behavior is observed. ZIF-8 appears to be paraffin-selective, and consequently, here first the olefins ethene and propene are detected at the adsorber outlet (Figure 7). It is noted again that the concentration of the olefins at the adsorber outlet exceeds the feed concentration. This overshoot, the so-called roll-up behavior, is due to displacement of the weaker adsorbed olefin by the stronger adsorbed paraffin. The resulting desorption of the olefin results in a further increase of the concentration at the adsorber outlet. The analysis of the breakthrough curves of ZIF-8 shows a clear paraffin preference and gives the separation factors  $\alpha = q(\text{ethene})/q(\text{ethane}) = 0.48$  and  $\alpha = q(\text{propene})/q(\text{propane}) = 0.7$ . In agreement with the single component isotherms, the

uptakes of the  $C_3$  hydrocarbons are significantly higher than those of the  $C_2$  hydrocarbons. Nevertheless, the separations of the propane/propene and the ethane/ethene mixture are nearly the same, which does not fit the different equilibrium selectivities found by the adsorption measurements. The ratio of the diffusion coefficients for propene/propane is about 125,<sup>1</sup> which is 25 times higher than the ratio measured for  $D_{\text{ethene}}/D_{\text{ethane}}$  by Chmelik et al.<sup>2</sup> Thus, the breakthrough curves also reflect the very large difference in diffusivities of propene and propane. Because of the interesting separation potential observed in the breakthrough curves of olefin–paraffin mixtures on ZIF-8, single component adsorption isotherms (Figure 6) and breakthrough curves were recorded at different temperatures (Figure 10). The shape of the breakthrough curves

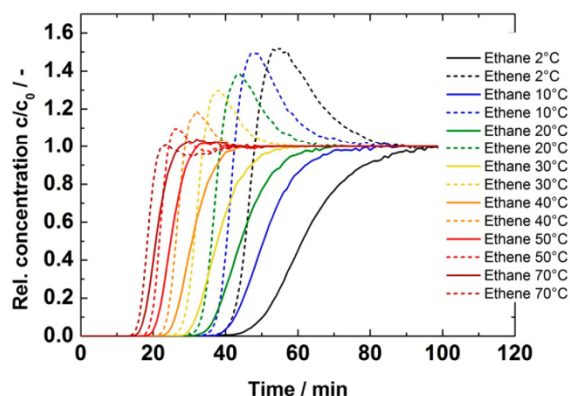


**Figure 10.** Breakthrough curves at different temperatures of equimolar mixtures of ethane/ethene in a packed column of preactivated initially clean ZIF-8.

changes with decreasing temperature, showing a more pronounced displacement of the olefin at lower temperature. The separation factor also increases with decreasing temperature to ca. 0.25 while maintaining the alkane preference.

Very high separation factors for propene/propane of up to 50<sup>50</sup> and 40<sup>51</sup> are reported for supported ZIF-8 membranes. Olson and co-workers<sup>1</sup> reported that propene is much faster adsorbed than the corresponding propane on ZIF-8 at 303 K. From the initial adsorption rates, a ratio for the diffusion coefficients of  $D_{\text{propylene}}:D_{\text{propane}} = 125$  was estimated.<sup>1</sup> Thus, for the separation of propene and propane over ZIF-8, a kinetic separation using pressure swing adsorption (PSA) with short cycle times might be feasible. This will probably not work for the significantly smaller  $C_2$  hydrocarbons where an equilibrium based separation has to be employed. For industrially relevant separations of steam cracker and fluid catalytic cracking unit effluents, the olefin/paraffin ratio is around 10; viz., much smaller concentrations of paraffins must be removed from the excess olefins which are used for the production of polyethylene and polypropylene. Here, ZIF-8 is one of the few adsorbents that adsorb the paraffin preferentially, which might be advantageous for an adsorption based separation process.

#### 4. CONCLUSIONS

Breakthrough curves of equimolar mixtures of ethane/ethene and propane/propene have been measured in a fixed-bed adsorber. In complete accordance with the expectations from the single component adsorption isotherms,  $Co_2$ (dhtp) and

$Mg_2$ (dhtp) turned out to be olefin-selective. As a result, first the alkanes ethane and propane break through. However, the theoretically predicted separation factors are significantly larger than those found in this study. Moreover, both adsorbents appear to be sensitive to water, which might limit their industrial application. In contrast, ZIF-8 is paraffin-selective, and consequently, here first the olefins ethene and propene are detected at the adsorber outlet. This is of particular importance for the industrial separation of ethane/ethene and propane/propene containing streams, which typically contain the olefin in excess (ratio  $\sim 10/1$ ) and the target product is a polymer-grade olefin (purity  $> 99.5\%$ ).

#### ■ AUTHOR INFORMATION

##### Notes

The authors declare no competing financial interest.

#### ■ ACKNOWLEDGMENTS

Financial support of this work by Deutsche Forschungsgemeinschaft (DFG) in the frame of the priority program 1570 is gratefully acknowledged.

#### ■ REFERENCES

- (1) Li, K.; Olson, D. H.; Seidel, J.; Emge, T. J.; Gong, H.; Zeng, H.; Li, J. Zeolitic imidazolate frameworks for kinetic separation of propane and propene. *J. Am. Chem. Soc.* **2009**, *131*, 10368–10369.
- (2) Chmelik, C.; Freude, D.; Bux, H.; Haase, J. Ethene/ethane mixture diffusion in the MOF sieve ZIF-8 studied by MAS PFG NMR diffusometry. *Microporous Mesoporous Mater.* **2012**, *147*, 135–141.
- (3) Haldoupis, E.; Watanabe, T.; Nair, S.; Sholl, D. S. Quantifying large effects of framework flexibility on diffusion in MOFs:  $CH_4$  and  $CO_2$  in ZIF-8. *ChemPhysChem* **2012**, *13*, 3449–3452.
- (4) Pera-Titus, M.; Farrusseng, D. Guest-induced gate opening and breathing phenomena in soft porous crystals: building thermodynamically consistent isotherms. *J. Phys. Chem. C* **2012**, *116*, 1638–1649.
- (5) Fairen-Jimenez, D.; Moggach, S. A.; Wharmby, M. T.; Wright, P. A.; Parsons, S.; Düren, T. Opening the gate: framework flexibility in ZIF-8 explored by experiments and simulations. *J. Am. Chem. Soc.* **2011**, *133*, 8900–8902.
- (6) Gücüyener, C.; van den Bergh, J.; Gascon, J.; Kapteijn, F. Ethane/ethene separation turned on its head: selective ethane adsorption on the metal-organic framework ZIF-7 through a gate-opening mechanism. *J. Am. Chem. Soc.* **2010**, *132*, 17704–1770.
- (7) Demessence, A.; Boissière, C.; Grosso, D.; Horcajada, P.; Serre, C.; Férey, G.; Soler-Illia, G. J. A. A.; Sanchez, C. Adsorption properties in high optical quality nanoZIF-8 thin films with tunable thickness. *J. Mater. Chem.* **2010**, *20*, 7676.
- (8) Luebbers, M. T.; Wu, T.; Shen, L.; Masel, R. I. Effects of molecular sieving and electrostatic enhancement in the adsorption of organic compounds on the zeolitic imidazolate framework ZIF-8. *Langmuir* **2010**, *26*, 15625–15633.
- (9) Chang, N.; Gu, Z. Y.; Yan, X. P. Zeolitic imidazolate framework-8 nanocrystal coated capillary for molecular sieving of branched alkanes from linear alkanes along with high-resolution chromatographic separation of linear alkanes. *J. Am. Chem. Soc.* **2010**, *132*, 13645–13647.
- (10) Ferreira, A. F. P.; Mittelmeijer-Hazeleger, M. C.; Granato, M. A.; Martins, V. F. D.; Rodrigues, A. E.; Rothenberg, G. Sieving di-branched from mono-branched and linear alkanes using ZIF-8: experimental proof and theoretical explanation. *Phys. Chem. Chem. Phys.* **2013**, *15*, 8795–8804.
- (11) Li, Y. S.; Liang, F. Y.; Bux, H.; Feldhoff, A.; Yang, W. S.; Caro, J. Molecular sieve membrane: supported metal-organic framework with high hydrogen selectivity. *Angew. Chem., Int. Ed.* **2010**, *49*, 548–551.
- (12) Bux, H.; Liang, F. Y.; Li, Y. S.; Cravillon, J.; Wiebcke, M.; Caro, J. Zeolitic imidazolate framework membrane with molecular sieving

properties by microwave-assisted solvothermal synthesis. *J. Am. Chem. Soc.* **2009**, *131*, 1600–1601.

(13) Huang, A.; Bux, H.; Steinbach, F.; Caro, J. Molecular-sieve membrane with hydrogen permselectivity: ZIF-22 in LTA topology prepared with 3-aminopropyltriethoxysilane as covalent linker. *Angew. Chem., Int. Ed.* **2010**, *49*, 4958–4961.

(14) Huang, A.; Dou, W.; Caro, J. Steam-stable zeolitic imidazolate framework ZIF-90 membrane with hydrogen selectivity through covalent functionalization. *J. Am. Chem. Soc.* **2010**, *132*, 15562–15564.

(15) Peralta, D. B.; Chaplais, G.; Simon-Masseron, A.; Barthelet, K.; Chizallet, C.; Quoineaud, A.-A.; Pirngruber, G. Comparison of the behavior of metal-organic frameworks and zeolites for hydrocarbon separations. *J. Am. Chem. Soc.* **2012**, *134*, 8115–8126.

(16) Diestel, L.; Bux, H.; Wachsmuth, D.; Caro, J. Pervaporation studies of n-hexane, benzene, mesitylene and their mixtures on zeolitic imidazolate framework-8 membranes. *Microporous Mesoporous Mater.* **2012**, *164*, 288–293.

(17) Zhu, W.; Kapteijn, F.; Moulijn, J. A. Shape selectivity in the adsorption of propane/propene on the all-silica DD3R. *Chem. Commun.* **1999**, 2453.

(18) Gascon, J.; Blom, W.; van Miltenburg, A.; Ferreira, A.; Berger, R.; Kapteijn, F. Accelerated synthesis of all-silica DD3R and its performance in the separation of propylene/propane mixtures. *Microporous Mesoporous Mater.* **2008**, *115*, 585–593.

(19) Gutierrez-Sevillano, J. J.; Dubbeldam, D.; Rey, F.; Valencia, S.; Palomino, M.; Martin-Calvo, A.; Calero, S. Analysis of the ITQ-12 zeolite performance in propane-propylene separations using combination of experiments and molecular simulations. *J. Phys. Chem. C* **2010**, *114*, 14907–14914.

(20) Krishna, R.; van Baten, J. M. A molecular dynamics investigation of the diffusion characteristics of cavity-type zeolites with 8-ring windows. *Microporous Mesoporous Mater.* **2011**, *137*, 83–91.

(21) Grande, C. A.; Gascon, J.; Kapteijn, F.; Rodrigues, A. E. Propane/propylene separation with Li-exchanged zeolite 13X. *Chem. Eng. J.* **2010**, *160*, 207–214.

(22) Da Silva, F.; Rodrigues, A. Propylene/propane separation by vacuum swing adsorption using 13X zeolite. *AIChE J.* **2001**, *47*, 341–357.

(23) Olsen, D. H.; Cambor, M. A.; Villaescusa, L. A.; Kuehl, G. H. Light hydrocarbon sorption properties of pure silica Si-CHA and ITQ-3 and high silica ZSM-58. *Microporous Mesoporous Mater.* **2004**, *67*, 27–33.

(24) Do, D. D.; Do, H. D. Cooperative and competitive adsorption of ethylene, ethane, nitrogen and argon on graphitized carbon black and in slit pores. *Adsorption* **2005**, *11*, 35–50.

(25) Kroon, M. C.; Vega, L. F. Selective paraffin removal from ethane/ethylene mixtures by adsorption into aluminum methylphosphonate- $\alpha$ : a molecular simulation study. *Langmuir* **2009**, *25*, 2148–2152.

(26) Keil, F. J. Molecular simulation of adsorption in zeolites and carbon nanotubes. In *Adsorption and Phase Behaviour in Nanochannels and Nanotubes*; Dunne, L. J., Manos, G., Eds.; Springer Science +Business Media: Dordrecht, The Netherlands, 2010; pp 9–40.

(27) Jakobtorweihen, S.; Hansen, N.; Keil, F. J. Molecular simulation of alkene adsorption in zeolites. *Mol. Phys.* **2005**, *103*, 471–489.

(28) Hartmann, M.; Kunz, S.; Himsl, D.; Tangermann, O.; Ernst, S.; Wagner, A. Adsorptive separation of isobutene and isobutane on Cu<sub>3</sub>(BTC)<sub>2</sub>. *Langmuir* **2008**, *24*, 8634.

(29) Lamia, N.; Jorge, M.; Granato, M. A.; Almeida Paz, F. A.; Chevreau, H.; Rodrigues, A. E. Adsorption of propane, propylene and isobutane on a metal-organic framework: molecular simulation and experiment. *Chem. Eng. Sci.* **2009**, *64*, 3246–3259.

(30) Maes, M.; Alaerts, L.; Vermoortele, F.; Ameloot, R.; Couck, S.; Finsy, V.; Denayer, J. F. M.; De Vos, D. E. Separation of C<sub>5</sub>-hydrocarbons on microporous materials: complementary performance of MOFs and zeolites. *J. Am. Chem. Soc.* **2010**, *132*, 2284–2292.

(31) Uchida, S.; Kawamoto, R.; Tagami, H.; Nakagawa, Y.; Mizuno, N. Highly selective sorption of small unsaturated hydrocarbons by

nonporous flexible framework with silver ion. *J. Am. Chem. Soc.* **2008**, *130*, 12370–12376.

(32) Wang, S.; Yang, Q.; Zhong, C. Adsorption and separation of binary mixtures in a metal-organic framework Cu-BTC: a computational study. *Sep. Purif. Technol.* **2008**, *60*, 30–35.

(33) Dietzel, P. D. C.; Morita, Y.; Blom, R.; Fjellvag, H. An in situ high-temperature single-crystal investigation of a dehydrated metal-organic framework compound and field-induced magnetization of one-dimensional metal-oxygen chains. *Angew. Chem., Int. Ed.* **2005**, *44*, 6354–6358.

(34) Bao, Z.; Alnemrat, S.; Yu, L.; Vasiliev, I.; Ren, Q.; Lu, X.; Deng, S. Adsorption of ethane, ethylene, propane, and propylene on a magnesium-based metal-organic framework. *Langmuir* **2011**, *27*, 13554–13562.

(35) Park, K. S.; Ni, Z.; Côté, A. P.; Choi, J. Y.; Huang, R.; Uribe-Romo, F. J.; Chae, H. K.; O’Keeffe, M.; Yaghi, O. M. Exceptional chemical and thermal stability of zeolitic imidazolate frameworks. *Proc. Natl. Acad. Sci. U.S.A.* **2006**, *103*, 10186–10191.

(36) Bae, Y.-S.; Lee, C. Y.; Kim, K. C.; Farha, O. K.; Nickias, P.; Hupp, J. T.; Nguyen, S. B. T.; Snurr, R. Q. High propene/propane selectivity in isostructural metal-organic frameworks with high densities of open metal sites. *Angew. Chem., Int. Ed.* **2012**, *51*, 1857–1860.

(37) Bloch, E. D.; Queen, W. L.; Krishna, R.; Zadzorny, J. M.; Brown, C. M.; Long, J. R. Hydrocarbon separations in a metal-organic framework with open iron(II) coordination sites. *Science* **2012**, *335*, 1606–1610.

(38) Liu, J.; Benin, A. L.; Furtado, A. M. B.; Jakubczak, P.; Willis, R. R.; LeVan, M. D. Stability effects on CO<sub>2</sub> adsorption for the DOBDC series of metal-organic frameworks. *Langmuir* **2011**, *27*, 11451–11456.

(39) Dietzel, P. D.; Georgiev, P. A.; Eckert, J.; Blom, R.; Strässle, T.; Unruh, T. Interaction of hydrogen with accessible metal sites in the metal-organic frameworks M<sub>2</sub>(dhtp) (CPO-27-M; M = Ni, Co, Mg). *Chem. Commun.* **2010**, *46*, 4962–4964.

(40) Glover, T. G.; Peterson, G. W.; Schindler, B. J.; Britt, D.; Yagi, O. MOF-74 building unit has a direct impact on toxic gas adsorption. *Chem. Eng. Sci.* **2011**, *66*, 163–170.

(41) Deckman, H. W.; Kortunov, P.; Ni, Z.; Paur, C. S. Reyes, S. C.; Santiesteban, J. G.; Zengel, J. Separation of hydrogen from hydrocarbons utilizing zeolitic imidazolate framework materials. U.S. Patent US20090211440, 2009.

(42) Bux, H.; Chmelik, C.; Krishna, R.; Caro, J. Ethene/ethane separation by the MOF membrane ZIF-8: molecular correlation of permeation, adsorption, diffusion. *J. Membr. Sci.* **2011**, *369*, 284–289.

(43) Olsen, D. H.; Cambor, M. A.; Villaescusa, L. A.; Kuehl, G. H. Light hydrocarbon sorption properties of pure silica Si-CHA and ITQ-3 and high silica ZSM-58. *Microporous Mesoporous Mater.* **2004**, *67*, 27–33.

(44) Van den Bergh, J.; Gücüyener, C.; Pidko, E. A.; Hensen, E. J. M.; Gascon, J.; Kapteijn, F. Understanding the anomalous alkane selectivity of ZIF-7 in the separation of light alkane/alkene mixtures. *Chem.—Eur. J.* **2011**, *17*, 8832–8840.

(45) Zhang, C.; Lively, R. P.; Zhang, K.; Johnson, J. R.; Karvan, O.; Koros, W. J. Unexpected molecular sieving properties of zeolitic imidazolate framework-8. *J. Phys. Chem. Lett.* **2012**, *3*, 2130–2134.

(46) Wagener, A.; Rudolph, F.; Schindler, M.; Ernst, S. Trennung von propan/propen-gemischen durch adsorption an metallorganischen koordinationspolymeren. *Chem. Ing. Tech.* **2006**, *78*, 1328–1329.

(47) Yoon, J. W.; Jang, I. T.; Lee, K. Y.; Hwang, Y.; Chang, J. S. Adsorptive separation of propylene and propane on a porous metal-organic framework, copper trimesate. *Bull. Korean Chem. Soc.* **2010**, *31*, 220–223.

(48) Wuttke, S.; Bazin, P.; Vimont, A.; Serre, C.; Seo, Y.-K.; Hwang, Y.-K.; Chang, J. S.; Férey, G.; Daturi, M. Discovering the active sites for C<sub>3</sub> separation in MIL-100(Fe) by using operando IR spectroscopy. *Chem.—Eur. J.* **2012**, *18*, 11959–11967.

(49) Xu, J.; Terskikh, V. V.; Huang, Y. Resolving multiple non-equivalent metal sites in magnesium-containing metal-organic frame-

works by natural abundance  $^{25}\text{Mg}$  solid state NMR spectroscopy. *Chem.—Eur. J.* **2013**, *19*, 4432–4436.

(50) Pan, Y.; Li, T.; Lestari, G.; Lai, Z. Effective separation of propylene/propane binary mixtures by ZIF-8 membranes. *J. Membr. Sci.* **2012**, *390/391*, 93–98.

(51) Kwon, H. T.; Jeong, H.-K. Highly propylene-selective supported zeolite-imidazolate framework (ZIF-8) membranes synthesized by rapid microwave-assisted seeding and secondary growth. *Chem. Commun.* **2013**, *49*, 3854–3856.

## III Propylen/Propan-Trennung im Festbettadsorber und durch Membranpermeation

A. Mundstock, U. Böhme, B. Barth, M. Hartmann, J. Caro

*Chemie Ingenieur Technik*, 85 (11), 2013, 1694 - 1699.

---

Forschungsarbeit

# Propylen/Propan-Trennung im Festbettadsorber und durch Membranpermeation

Alexander Mundstock<sup>1</sup>, Ulrike Böhme<sup>2</sup>, Benjamin Barth<sup>2</sup>, Martin Hartmann<sup>2</sup> und Jürgen Caro<sup>1,\*</sup>

DOI: 10.1002/cite.201300053

*Herrn Prof. Dr. Jörg Kärger zum 70. Geburtstag gewidmet*

Die metallorganische Gerüstverbindung  $Mg_2(dhtp)$  mit dem Linker Dihydroxyterephthalat ist als MOF-74 oder CPO-27 bekannt.  $Mg_2(dhtp)$  wurde in Pulverform für die Messung von Durchbruchskurven im Festbettadsorber und Adsorptionsisothermen sowie als geträgerte dünne Membranschicht für Permeationsmessungen synthetisiert. Die Messung der Durchbruchskurven des binären Propylen/Propan-Gemisches zeigt, dass eine Trennung im Festbettadsorber möglich ist. Es zeigt sich hier eine höhere Affinität des Propylens zum Adsorbens  $Mg_2(dhtp)$ . Obwohl der Einzelgasfluss von Propan höher als der von Propylen ist, weist die  $Mg_2(dhtp)$ -Membran für das binäre Gemisch kein Trennverhalten auf.

**Schlagwörter:** Durchbruchskurve, Metallorganische Gerüstverbindung, Molekularsiebmembran, Propylen/Propan-Trennung

*Eingegangen:* 11. April 2013; *revidiert:* 22. Juli 2013; *akzeptiert:* 09. August 2013

## Propylene/Propane Separation in Fixed-Bed Adsorber and Membrane Permeation

The metal-organic framework  $Mg_2(dhtp)$  with the linker dihydroxyterephthalate is known as MOF-74 or CPO-27.  $Mg_2(dhtp)$  has been synthesized as powder to measure breakthrough curves in a fixed-bed adsorber and adsorption isotherms, and as a supported thin membrane layer for permeation studies. The measurement of the breakthrough curves of the binary propylene/propane mixture shows that separation with the fixed bed adsorber is possible. Propylene shows a higher affinity to  $Mg_2(dhtp)$ . Although the single gas propane flux is slightly higher than the one of propylene, the binary propane/propylene mixture is not separated.

**Keywords:** Breakthrough curve, Metal-organic framework, Molecular sieve membrane, Propylene/propane separation

## 1 Einleitung

Metallorganische Gerüstverbindungen (metal-organic frameworks, MOFs) sind ein neuer Stern am Himmel der nanoporösen Materialien. Positiv geladene Metallionen oder Metalloxydcluster bilden mit negativ geladenen Linkermolekülen offenporige zeolithähnliche Gerüststrukturen. Durch die Vielzahl an möglichen Variationen bietet es sich an,

MOFs für den Einsatz bei Trennproblemen, als Adsorbens oder Membran, und in der Katalyse maßzuschneidern.

Für den erfolgreichen Sprung eines Katalysators oder Adsorbens aus dem Labor in die industrielle Praxis ist die Kenntnis des molekularen Stofftransportes notwendig. Zum Verständnis der Diffusion in Zeolithen und anderen porösen Materialien trugen bahnbrechende Arbeiten von J. Kärger bei [1–4]. Auch liegen inzwischen Pionierarbeiten zum Stofftransport in MOFs vor [5–9]. In Bezug darauf soll in dieser Arbeit gezeigt werden, dass das Zusammenspiel von Gemischadsorption und Gemischdiffusion der Schlüssel zur Erklärung der Durchbruchskurven im Festbettadsorber und der Membranpermeation ist.

$Me_2(dhtp)$ , mit den Metallionen  $Me = Zn^{2+}, Mg^{2+}, Ni^{2+}$  und  $Co^{2+}$  und dem Linker Dihydroxyterephthalat, ist eine häufig untersuchte MOF-Struktur. Das bienenwabenartige

<sup>1</sup>Alexander Mundstock, Prof. Jürgen Caro (juergen.caro@pci.uni-hannover.de), Leibniz Universität Hannover, Institut für Physikalische Chemie und Elektrochemie, Callinstraße 22, 30167 Hannover, Deutschland; <sup>2</sup>Ulrike Böhme, Benjamin Barth, Prof. Martin Hartmann, Friedrich-Alexander-Universität Erlangen-Nürnberg, Erlangen Catalysis Resource Center (ECRC), Egerlandstraße 3, 91058 Erlangen, Deutschland.



eindimensionale Porensystem besitzt einen Durchmesser von 1,1–1,2 nm [10] und ist damit nicht gröÙenselektiv für Moleküle wie Propan und Propylen. Da die Metallionen jedoch exponiert und damit frei zugänglich sind, stellen sie für kleine Moleküle Adsorptionsplätze mit entsprechender Wechselwirkung dar [11–13]. Die Struktur  $\text{Me}_2(\text{dhtp})$  ist als MOF-74 [14] und CPO-27 [15] bekannt. Besonders  $\text{Mg}_2(\text{dhtp})$  gilt für  $\text{CO}_2$  als ein effektives Adsorbens [11, 16], und auch molekuldynamische Rechnungen haben  $\text{Mg}_2(\text{dhtp})$  als leistungsfähiges Material für  $\text{CO}_2$ -selektive Membranen identifiziert [17].  $\text{Ni}_2(\text{dhtp})$  [18] oder  $\text{Co}_2(\text{dhtp})$  [15, 19–22] gelten als vielversprechende Katalysatoren und olefinselektive Adsorbentien.

Wegen der freien Zugänglichkeit der Metallionen für Gastmoleküle und möglicher selektiver Wechselwirkung durch  $\pi$ -Komplexierung gilt die aktivierte MOF-Struktur MOF-74/CPO-27 als aussichtsreicher Kandidat für die adsorptive Olefin/Paraffin-Trennung. In Arbeiten von Deng [23] und Snurr [24] wurde  $\text{Mg}_2(\text{dhtp})$  für die adsorptive Propylen/Propan-Trennung erfolgreich überprüft. Auch die MOF-Struktur HKUST-1 konnte aufgrund der zugänglichen Kupferionen erfolgreich als Adsorbens für die Propylen/Propan-Trennung evaluiert werden [25–27].

An geträgerten MOF-Membranen des Strukturtyps ZIF-8 (zeolitic imidazolate framework Nummer 8) wurden spektakuläre Propylen/Propan-Trennfaktoren von bis zu 50 [28] oder 40 [29] gemessen. Auch eine ZIF-8/Polyimid-Mixed-Matrix-Membran mit 48 Ma-% ZIF-8 im Polymer zeigte einen Propylen/Propan-Trennfaktor von 31 [30]. Ein unter Prozessbedingungen langzeitstabiler Trennfaktor von 5–10 wird als ausreichend bewertet, um die destillative Propylen/Propan-Trennung durch ein Membranverfahren abzulösen [31]. Bloch et al. [32] postulierten, dass  $\text{Me}_2(\text{dhtp})$ -Membranen einschließlich  $\text{Mg}_2(\text{dhtp})$ , unter Beibehaltung der hohen Trennfaktoren einer ZIF-8-Membran, wesentlich höhere FlüÙe haben sollten. Kürzlich wurde gezeigt, dass solche geträgerten dünnen  $\text{Me}_2(\text{dhtp})$ -Schichten herstellbar sind [33]. In dieser Arbeit werden erste Untersuchungen bezüglich der Trennung von Propylen/Propan-Gemischen am MOF  $\text{Mg}_2(\text{dhtp})$  durch Adsorption in einem Festbettadsorber und durch Membranpermeation vorgestellt.

## 2 Experimentelles und Versuchsaufbau

### 2.1 Synthese von $\text{Mg}_2(\text{dhtp})$ , Isothermenmessungen und Aufnahme von Durchbruchskurven im Festbettadsorber

Für die Synthese von  $\text{Mg}_2(\text{dhtp})$  wurde Magnesiumacetat-Tetrahydrat (5,860 g, 27 mmol) in einer Mischung aus *N*-Methylpyrrolidon (78 mL) und Wasser (12 mL) gelöst und Dihydroxyterephthalsäure (2,745 g, 14 mmol) zugegeben. Die Reaktion erfolgte in einem mit Teflon ausgekleideten 125-mL-Edelstahlautoklaven bei 120 °C für 24 h. Nach Filtration und Lösungsmittelaustausch wurde das erhaltene gelbe

Pulver (Kristallgröße 10–100  $\mu\text{m}$ ) bei 230 °C im Vakuum für 24 h aktiviert. Nach der Aktivierung ist  $\text{Mg}_2(\text{dhtp})$  empfindlich gegen Feuchtigkeit [34] und wird daher unter Argonatmosphäre gelagert. Auch die Struktur  $\text{Co}_2(\text{dhtp})$  (Co-MOF-74/CPO-27-Co) erwies sich als extrem empfindlich gegenüber feuchter Luft: nach 30 s Luftexposition bildete sich eine durch Röntgendiffraktion nicht nachweisbare dünne Oberflächenschicht, die jegliche Adsorption verhinderte [35].

Das Röntgenpulverdiffraktogramm von  $\text{Mg}_2(\text{dhtp})$  wurde mit einem PANalytical X'Pert Diffraktometer ( $\text{CuK}\alpha$ ,  $\lambda = 1,54 \text{ \AA}$ ) aufgenommen. Die spezifische Oberfläche der Probe wurde mit der volumetrischen Adsorptionsapparatur ASAP 2010 von Micromeritics durch Stickstoffadsorption bei 77 K ermittelt.

Die Reinstoff-Adsorptionisothermen von Propan und Propylen wurden bei 22 °C mit einem modifizierten ASAP 2010 von Micromeritics aufgenommen. Die Messungen der Durchbruchskurven wurden in einer selbstgebauten Apparatur bei 22 °C durchgeführt. Hierfür wurde eine äquimolare Propylen/Propan-Mischung ( $p_{\text{en}} = p_{\text{an}} = 500 \text{ hPa}$ ) mit einem Gesamtvolumenstrom von  $0,5 \text{ mL min}^{-1}$  über das  $\text{Mg}_2(\text{dhtp})$ -Festbett ( $m_{\text{ads}} = 0,41 \text{ g}$ , unverpresstes Kristallpulver) geleitet. Das Gas am Auslass des Festbettadsorbers wurde online mithilfe eines Gaschromatographen mit Flammenionisationsdetektor (FID) analysiert.

### 2.2 Präparation von geträgerten $\text{Mg}_2(\text{dhtp})$ -Membranen und Permeationsmessungen

Die Präparation der in dieser Arbeit untersuchten geträgerten  $\text{Mg}_2(\text{dhtp})$ -Membranen erfolgte in Anlehnung an eine aus der Literatur bekannten Pulversynthese [23], die jedoch leicht modifiziert wurde. Bei den zur Präparation verwendeten Trägern handelte es sich um Mikrofiltrationsmembranen des Fraunhofer-Instituts für Keramische Technologien und Systeme IKTS, mit der Geometrie  $d = 18 \text{ mm}$ ,  $h = 1 \text{ mm}$ . Trägermaterial ist  $\alpha\text{-Al}_2\text{O}_3$ ,  $d_{50} = 2,5 \mu\text{m}$ , die Trennschicht (Top-Layer) besteht aus  $\alpha\text{-Al}_2\text{O}_3$ ,  $d_{50} = 70 \text{ nm}$ .

Zuerst wurden Magnesiumnitrat-Hexahydrat (1,424 g, 5,16 mmol) und 2,5-Dihydroxyterephthalsäure (334 mg, 1,46 mmol) durch halbstündiges Rühren in 60 mL eines Gemischs aus 15:1:1 (v/v/v) DMF/Ethanol/Wasser (dest.) gelöst. Diese Lösung wurde in den aus Teflon bestehenden Einsatz eines 125-mL-Edelstahlautoklaven (Parr Instruments, Deutschland) überführt. Im Autoklav befand sich der unbehandelte, d. h. weder Funktionalisierung noch Seeding, und senkrecht orientierte  $\text{Al}_2\text{O}_3$ -Träger. Der verschlossene Autoklav wurde anschließend in einem Trockenofen für 28 h auf 120 °C erhitzt. Nach sehr langsamen Abkühlen im geschlossenen Ofen und Öffnen des Autoklaven wurde die Membran schnellstmöglich, d. h. wenig/kein Luftkontakt durch Flüssigkeitsfilm, in ein mit frischem DMF gefülltes und verschließbares 100-mL-Gefäß überführt und durch ständigen Austausch des DMFs gewaschen.

Der erste Aktivierungsschritt der Membran bestand darin, das noch in den Poren befindliche DMF gegen Isopropanol auszutauschen indem die Membran für zwei Tage in Isopropanol gelegt wurde. Der Einbau der Membran in die Permeationszelle erfolgte wegen der hohen Wasserempfindlichkeit des aktivierten Materials unter Schutzgasatmosphäre (Ar) in der Glove-Box. Hierzu wurde zuerst die Membran samt Lösemittel in einen Schlenkkolben überführt, dort unter Vakuum getrocknet und teilaktiviert. Der Schlenkkolben wurde anschließend in die Glove-Box eingeschleust, dort geöffnet, die Membran unter Schutzgasatmosphäre in die Permeationszelle eingebaut und diese dann in einem argongefüllten Behälter zur Messung ausgeschleust. Alle mit den Membranen durchgeführten Permeationsmessungen, sowohl die der Einzelgase als auch die des äquimolaren Propan/Propylen-Gemisches, fanden mit einer modifizierten Wicke-Kallenbach-Apparatur statt. In allen Fällen wurde  $N_2$  als Spülgas auf der Permeatseite der Membran ( $50 \text{ mL min}^{-1}$ , 1 bar) benutzt.

Die Röntgendiffraktogramme der  $Mg_2(\text{dhtp})$ -Membran wurden mit einem D8 Advance Röntgendiffraktometer der Firma Bruker ( $\text{CuK}\alpha$ ,  $\lambda = 1.54 \text{ \AA}$ ) aufgenommen. Die Membran wurde dafür in der Glove-Box in einen, mit einer für Röntgenstrahlen durchlässigen Kuppel, luftdicht verschließbaren Probenhalter (Bruker) überführt und in diesem ausgeschleust und vermessen. Die gezeigten REM-Bilder wurden mit einem JEOL JSM-6700F Feldemissions-Rasterelektronenmikroskop aufgenommen.

### 3 Ergebnisse und Diskussion

#### 3.1 Adsorptionsisothermen und Durchbruchskurven im Festbettadsorber

In Abb. 1 sind das Röntgenpulverdiffraktogramm und die Stickstoffadsorptionsisotherme von aktiviertem  $Mg_2(\text{dhtp})$  dargestellt. Die Übereinstimmung der berechneten und gemessenen Pulverdiffraktogramme belegt die erfolgreiche Synthese von  $Mg_2(\text{dhtp})$ . Die beiden Reflexe mit der höchsten Intensität bei  $2\theta = 6,8^\circ$  bzw.  $11,8^\circ$  können den (110)- bzw. (300)-Ebenen in der Kristallstruktur zugeordnet wer-

den. Das Diffraktogramm von vollständig aktiviertem  $Mg_2(\text{dhtp})$  stimmt gut mit dem aus Strukturdaten berechneten Diffraktogramm überein (Abb. 1). Bei nicht vollständiger Aktivierung, gleichbedeutend mit noch in den Poren vorhandenem Lösungsmittel, werden häufig zusätzliche Reflexe bei  $2\theta = 13,4^\circ$  und  $26,7^\circ$  beobachtet. Aus der Stickstoffadsorptionsisotherme wurde eine spezifische BET-Oberfläche von  $1420 \text{ m}^2 \text{ g}^{-1}$  ermittelt, die mit den in der Literatur bekannten Werten übereinstimmt [36].

In Abb. 2 sind die Reinstoff-Adsorptionsisothermen von Propan und Propylen an  $Mg_2(\text{dhtp})$  dargestellt. Der Sättigungswert der Gasaufnahme liegt für Propylen höher als für Propan. Die höhere Affinität für das Olefin deutet auf eine Koordinationsverbindung in Form eines  $\pi$ -Komplexes zwischen der Doppelbindung und den frei zugänglichen Metallzentren hin. Die aufgenommene Propylenmenge von ca.  $8 \text{ mol kg}^{-1}$  entspricht etwa einer Aufnahme von einem Propylenmolekül pro Magnesiumion, wie sie auch bereits für andere  $\text{Me}_2(\text{dhtp})$  gefunden wurde [23, 24, 32]. Die Isothermendaten von Propylen und Propan an  $Mg_2(\text{dhtp})$  (Abb. 2) stimmen gut mit denen von Bao et al. überein [23]. Aus der Temperaturabhängigkeit der Isothermen wurde nach Clausius-Clapeyron für die Adsorption an  $Mg_2(\text{dhtp})$  eine isostere Adsorptionswärme für Propylen von  $\Delta H = -60,5 \text{ kJ mol}^{-1}$  und für Propan von  $\Delta H = -33,9 \text{ kJ mol}^{-1}$  bestimmt.

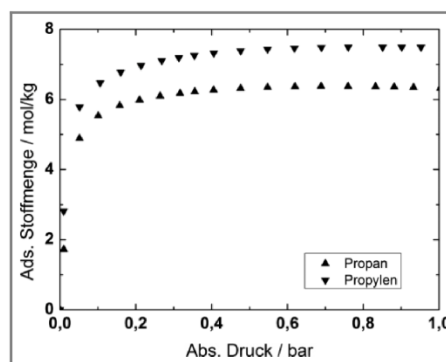


Abbildung 2. Adsorptionsisothermen von Propan und Propylen an  $Mg_2(\text{dhtp})$  bei 295 K.

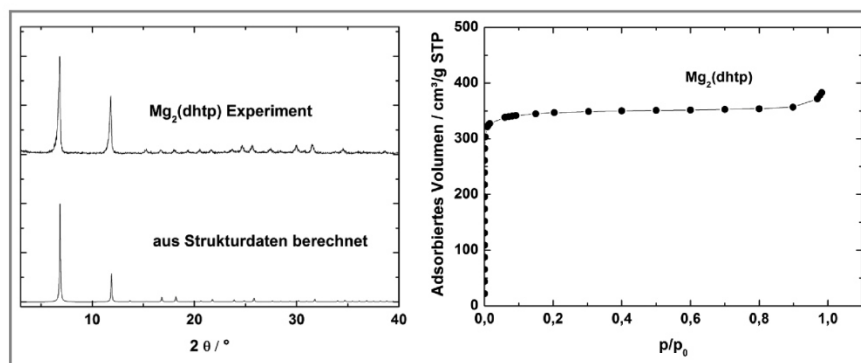


Abbildung 1. Röntgenpulverdiffraktogramme (links) und  $N_2$ -Adsorptionsisotherme bei 77 K (rechts) von  $Mg_2(\text{dhtp})$ .

Für die Messung der Durchbruchskurve wurde ein äquimolares Propylen/Propan-Gemisch über ein Festbett geleitet. Dargestellt ist der auf die Feedkonzentration  $c_0$  normierte Konzentrationsverlauf der Gase am Festbettausgang (Abb. 3). Propan bricht früher durch als Propylen, was auf eine schwächere Wechselwirkung des Alkans mit dem Adsorbens  $Mg_2(dhtp)$  hindeutet. Zudem ist eine Verdrängung des schwächer adsorbierten Paraffins durch das stärker adsorbierte Olefin zu erkennen. Aufgrund der Größe der im Adsorber verwendeten Kristalle von bis zu  $100\ \mu m$  zeigen die Durchbruchskurven außerdem noch einen Diffusionseinfluss. Die Ergebnisse der Durchbruchmessungen sind somit im Einklang mit den Ergebnissen der Reinstoffisothermen (Abb. 2). Der aus der Frontalanalyse berechnete Trennfaktor beträgt ca. 2. Dies entspricht den Ergebnissen für andere MOFs, beispielsweise  $Cu_3(BTC)_2$  [25, 37], jedoch nicht den theoretischen Erwartungen [24]. Aus den Einzelstoffisothermen von Propylen und Propan an  $Mg_2(dhtp)$  wurde nach IAST (ideal adsorbed solution theory) die Gemischadsorptionsisotherme und auf dieser Basis eine Adsorptionstrennselektivität von 4,5 zugunsten des Propylens berechnet.

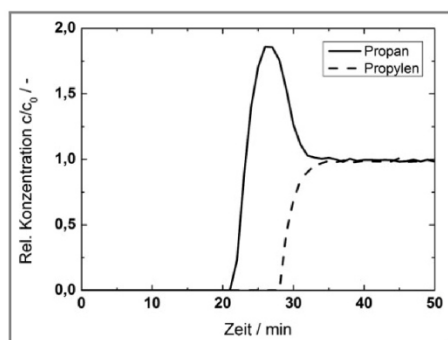


Abbildung 3. Durchbruchskurven eines äquimolaren Propan/Propylen-Gemisches an  $Mg_2(dhtp)$  bei 295 K.

### 3.2 Präparation von geträgerten $Mg_2(dhtp)$ -Membranen und Permeationsmessungen

Erste Versuche zur Präparation dünner  $Me_2(dhtp)$ -Schichten auf Trägern zeigten die damit verbundenen Schwierigkeiten [38, 39]. Entweder waren die Schichten nicht geschlossen und damit für Membrananwendungen nicht verwendbar, oder das eindimensionale Porensystem der aufgewachsenen  $Me_2(dhtp)$ -Schicht war nicht orientiert (statistisch verteilt) oder in einer nicht geeigneten Weise, d. h. mit dem 1D-Porensystem parallel zur Trägeroberfläche, angeordnet. Im Fall von MOFs mit eindimensionalem

Porensystem müssen die MOF-Membranschichten für Membrananwendungen eine Vorzugsorientierung des eindimensionalen Porensystems senkrecht zur Trägeroberfläche besitzen, wie dies erstmals in [40] am Beispiel eines Manganformiats gezeigt wurde.

Die ersten Kristallisationsversuche geträgerter  $Mg_2(dhtp)$ -Schichten zeigten, dass das eindimensionale Porensystem einer ca.  $10\ \mu m$  dicken  $Mg_2(dhtp)$ -Schicht wie im  $Mg_2(dhtp)$ -Pulver statistisch orientiert ist (Abb. 4). Die Pulver-Röntgendiffraktogramme stimmen mit den durch streifenden Einfall gemessenen Diffraktogrammen der  $Mg_2(dhtp)$ -Schichten überein. Eine Orientierung des Porensystems der  $Mg_2(dhtp)$ -Schicht könnte nach dem van-der-Drift-Mechanismus erreicht werden, wonach sich mit zunehmender Schichtdicke durch den Prozess der evolutionären Selektion diejenige Textur ausbildet, die mit der Richtung des schnellsten Kristallwachstums in Richtung Nährstoffgradient weist [41]. Dieses eigentlich für Gasphasenabscheidungen entwickelte Konzept konnte die Ausprägung einer Vorzugsorientierung mit wachsender Kristallisationszeit für Zeolith- [42] und MOF-Schichten [43] erklären. Ein weiteres Schichtwachstum über  $10\ \mu m$  hinaus, das zu einer weiteren Orientierung führen sollte, kam aber in diesem Fall für Membrananwendungen nicht in Frage.

Durch Variation bzw. Anpassung einiger grundlegender Präparationsbedingungen wie Lösemittelzusammensetzung und Kristallisationszeit konnte in weiteren Versuchen eine Vorzugsorientierung des eindimensionalen Porensystems der geträgerten  $Mg_2(dhtp)$ -Schicht bereits für geringe Schichtdicken von  $5\ \mu m$  nach kürzerer Kristallisationszeit erreicht werden (Abb. 5). Der stärkere Reflex der Netzebene (021) im Vergleich zu den Signalen der anderen Netzebenen bedeutet, dass diese Netzebene parallel zur Trägeroberfläche orientiert ist. Wenn alle Kristalle so orientiert wären, entspräche dies einem Neigungswinkel von ca.  $31^\circ$ , bezogen auf die Oberflächennormale (Abb. 5).

Die Evaluation der  $Mg_2(dhtp)$ -Membran durch Einzelgaspermeation ergab ein auf den ersten Blick überraschendes

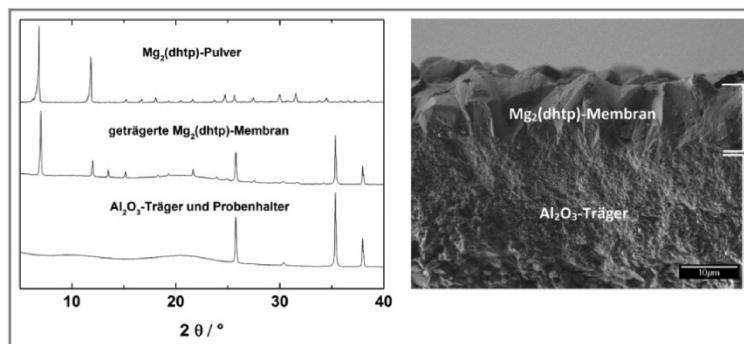
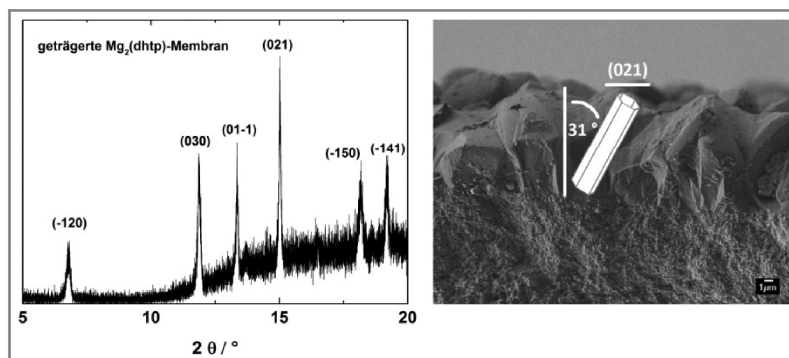


Abbildung 4. Links: Vergleich der Röntgendiffraktogramme von  $Mg_2(dhtp)$  als Pulver und als  $10\ \mu m$  dicke Schicht, aufgewachsen auf dem porösen  $Al_2O_3$ -Träger. Zum Vergleich das Diffraktogramm des  $Al_2O_3$ -Trägers ohne Schicht. Rechts: REM-Bild der  $10\ \mu m$  dicken  $Mg_2(dhtp)$ -Membran auf dem  $Al_2O_3$ -Träger.



**Abbildung 5.** Röntgendiffraktogramm (links) und REM (rechts) einer etwa 5 µm dicken  $Mg_2(dhtp)$ -Schicht. Eine Vorzugsorientierung der 1D-Poren ist angedeutet. Für einen Neigungswinkel von ca.  $31^\circ$  (bezogen auf die Oberflächennormale) der 1D-Kanäle des  $Mg_2(dhtp)$ -Kristalls liegen die Netzebenen (021) parallel zur Oberfläche.

Ergebnis. Die Analyse der Einzelstoff-Flüsse zeigt, dass Propan um den Faktor 2 schneller durch die Membran permeiert als Propylen. Für Propan wurde bei Raumtemperatur  $N_{Propan} \approx 0,054 \text{ mL min}^{-1} \text{ cm}^{-2}$  gemessen, für Propylen  $N_{Propylen} \approx 0,027 \text{ mL min}^{-1} \text{ cm}^{-2}$ . Würde sich das Gemisch Propan/Propylen ideal verhalten, so sollte sich ebenfalls ein Trennfaktor von etwa 2 für die  $Mg_2(dhtp)$ -Membran zugunsten des Propan ergeben. Die Experimente zur Gemischpermeation zeigten aber, dass sich das Gemisch Propan/Propylen an einer  $Mg_2(dhtp)$ -Membran nicht trennen lässt. Es zeigte sich weder eine Propan- noch eine Propylenselektivität. Für alle untersuchten Permeationsparameter, d. h. Druck, Temperatur und Gaszusammensetzung, lag der gemessene Gemischtrennfaktor entgegen optimistischen Voraussagen [32] bei 1, was bedeutet, dass Feed- und Permeatzusammensetzung gleich sind.

Wie es auch für organische Polymermembranen üblich ist, kann das Trennverhalten von Porenmembranen durch das Zusammenspiel von Gemischadsorption und Gemischdiffusion erklärt werden [44]. Der Trennfaktor einer Membran ergibt sich näherungsweise als Produkt aus Adsorptionsselektivität und Diffusionsselektivität [45]. Wie die Adsorptionsisothermen (Abb. 2) belegen, adsorbiert  $Mg_2(dhtp)$  vorzugsweise Propylen über Propan. Dieser Befund ist in Übereinstimmung mit Literaturwerten [22–24]. Diese bevorzugte Propylenadsorption stimmt sowohl mit den Ergebnissen molekuldynamischer Rechnungen überein, wonach Propylen eine um  $20 \text{ kJ mol}^{-1}$  höhere isostere Adsorptionswärme als Propan besitzt [46], als auch mit Messungen nach Clausius-Clapeyron, wonach Propylen an  $Mg_2(dhtp)$  eine um  $25 \text{ kJ mol}^{-1}$  [23] höhere isostere Adsorptionswärme besitzt als Propan. Diese Adsorptionsselektivität zugunsten des Propylens würde ohne Berücksichtigung des Diffusionseinflusses zu einer Propylen-selektiven  $Mg_2(dhtp)$ -Membran führen. Durch die Wechselwirkung des Propylens mit den exponierten Mg-Kationen wird aber die Propylenbeweglichkeit herabgesetzt und kompensiert schließlich die Propylen-Adsorptionsselektivität. Die Mole-

kulardynamik zeigt, dass durch die Wechselwirkung des Propylens mit den Mg-Ionen der Diffusionskoeffizient des Propan um den Faktor zwei höher ist als der des Propylens [44]. Experimentelle Untersuchungen der Stoffaufnahmegeschwindigkeit ergaben tatsächlich, dass der Diffusionskoeffizient des Propylens in  $Mg_2(dhtp)$  kleiner als der des Propan ist [23].

Es kann wie folgt erklärt werden, dass die  $Mg_2(dhtp)$ -Membran überhaupt kein Trennvermögen für das binäre Gemisch Propan/Propylen besitzt. Zu Permeationsbeginn adsorbieren die Propylenmoleküle an den  $Mg^{2+}$ -Zentren bis eine 1:1-Abdek-

kung erreicht ist. Diese relativ fest adsorbierten Propylenmoleküle bilden für nachfolgendes Propan/Propylen-Gemisch lediglich ein Transporthindernis in der 1D-Pore, ändern aber die Gaszusammensetzung nicht. Das Propan/Propylen-Gemisch strömt lediglich gebremst durch die an den  $Mg^{2+}$ -Ionen adsorbierten Propylen-Molekülen, aber unverändert in seiner Zusammensetzung durch die 1D-Pore.

#### 4 Zusammenfassung und Ausblick

$Mg_2(dhtp)$  wurde als Pulver und als geträgerte Membranschicht präpariert. Die Ergebnisse der Festbettmessungen an  $Mg_2(dhtp)$  lassen eine Anwendung dieses Materials für die Olefin/Paraffin-Trennung durch Druckwechseladsorption möglich erscheinen. Der deutliche Verdrängungseffekt spricht dafür,  $Mg_2(dhtp)$ -Materialien in der Verdrängungschromatographie einzusetzen. Es gelang, eine geträgerte Membranschicht zu präparieren, bei der das 1D-Porensystem nicht statistisch zum Träger orientiert ist, sondern eine vorzugsweise senkrechte Orientierung zur Trägeroberfläche besitzt. Der Einzelgasfluss des Propan ist höher als der des Propylens, da Propan die 1D-Poren ohne Wechselwirkung durchströmen kann. Für das binäre Gemisch ergibt die  $Mg_2(dhtp)$ -Membran keine Trennung, da die ersten Propylen-Moleküle an den zugänglichen  $Mg^{2+}$ -Plätzen vergleichsweise fest adsorbiert werden und das Gemisch daraufhin die 1D-Poren der Membran ohne weiteren Trenneffekt passiert.

Wir danken der Deutschen Forschungsgemeinschaft für die finanzielle Unterstützung im Rahmen des Schwerpunktprogramms 1570 *Poröse Medien mit definierter Porenstruktur in der Verfahrenstechnik – Modellierung, Anwendung, Synthese*.

## Literatur

- [1] J. Kärger, D. M. Ruthven, *Diffusion in Zeolites and other Microporous Materials*, Wiley & Sons, New York **1992**.
- [2] J. Kärger, P. Heitjans, R. Haberlandt, *Diffusion in Condensed Matter*, 1st ed., Vieweg Verlag, Wiesbaden **1998**.
- [3] J. Kärger, P. Heitjans, *Diffusion in Condensed Matter: Methods, Materials, Models*, 3rd ed., Springer, Berlin **2013**.
- [4] J. Kärger, D. M. Ruthven, D. N. Theodorou, *Diffusion in Nanoporous Materials*, Wiley-VCH, Weinheim **2012**.
- [5] D. C. Ford, D. Dubbeldam, R. Q. Snurr, V. Künzel, M. Wehring, F. Stallmach, J. Kärger, U. Müller, *Phys. Chem. Lett.* **2012**, *3*, 930.
- [6] F. Hibbe, J. M. van Baten, R. Krishna, C. Chmelik, J. Weitkamp, J. Kärger, *Chem. Ing. Tech.* **2011**, *83*, 2211.
- [7] K. Seehamart, T. Nanok, J. Kärger, C. Chmelik, R. Krishna, S. Fritzsche, *Microporous Mesoporous Mater.* **2010**, *130*, 92.
- [8] C. Chmelik, F. Hibbe, D. Tzoulaki, L. Heinke, J. Caro, J. Li, J. Kärger, *Microporous Mesoporous Mater.* **2010**, *129*, 340.
- [9] D. Tzoulaki, L. Heinke, H. Lim, J. Li, D. Olson, J. Caro, R. Krishna, C. Chmelik, J. Kärger, *Angew. Chem., Int. Ed.* **2009**, *48*, 3525.
- [10] K. Sumida, C. M. Brown, Z. R. Herm, S. Chavan, S. Bordiga, J. R. Long, *Chem. Commun.* **2011**, *47*, 1157.
- [11] D. Britt, H. Furukawa, B. Wang, T. G. Glover, O. M. Yaghi *Proc. Natl. Acad. Sci. U.S.A.* **2009**, *49*, 20637.
- [12] P. D. C. Dietzel, P. A. Georgiev, J. Eckert, R. Blom, T. Strässle, T. Unruh, *Chem. Commun.* **2010**, *46*, 4962.
- [13] K. Sillar, J. Sauer, *J. Am. Chem. Soc.* **2012**, *134*, 18354.
- [14] N. L. Rosi, J. Kim, M. Eddaoudi, B. Chen, M. O'Keefe, O. M. Yaghi, *J. Am. Chem. Soc.* **2005**, *127*, 1504.
- [15] P. D. Dietzel, Y. Morita, R. Blom, H. Fjellvag, *Angew. Chem., Int. Ed.* **2005**, *44*, 6354.
- [16] P. D. Dietzel, V. Besikiotis, R. Blom, *J. Mater. Chem.* **2009**, *19*, 7362.
- [17] R. Krishna, J. M. van Baten, *J. Membr. Sci.* **2011**, *377*, 249.
- [18] D. Peralta, G. Chaplais, A. Simon-Masseron, K. Barthelet, C. Chizallet, A.-A. Quoineaud, G. D. Pirngruber, *J. Am. Chem. Soc.* **2012**, *134*, 8115.
- [19] S. R. Caskey, A. G. Wong-Foy, A. J. Matzger, *J. Am. Chem. Soc.* **2008**, *130*, 10870.
- [20] H.-Y. Cho, D.-A. Yang, J. Kim, S.-Y. Jeong, W.-S. Sahn, *Catal. Today* **2012**, *185*, 35.
- [21] Y. He, R. Krishna, B. Chen, *Energy Environ. Sci.* **2012**, *5*, 9107.
- [22] Y. He, W. Zhou, R. Krishna, B. Chen, *Chem. Commun.* **2012**, *48*, 11813.
- [23] Z. Bao, S. Alnemrat, L. Yu, I. Vasiliev, Q. Ren, X. Lu, S. Deng, *Langmuir* **2011**, *27*, 13554.
- [24] Y.-S. Bae, C. Y. Lee, K. C. Kim, O. K. Farha, P. Nickias, J. T. Hupp, S. T. Nguyen, R. Q. Snurr, *Angew. Chem., Int. Ed.* **2012**, *51*, 1857.
- [25] A. Wagener, M. Schindler, F. Rudolphi, S. Ernst, *Chem. Eng. Technol.* **2007**, *79*, 851.
- [26] M. Jorge, N. Lamia, A. E. Rodrigues, *Colloids Surf., A* **2010**, *357*, 27.
- [27] A. F. P. Ferreira, J. C. Santos, M. G. Plaza, N. Lamia, J. M. Loureiro, A. E. Rodrigues, *Chem. Eng. J.* **2011**, *167*, 1.
- [28] Y. Pan, T. Li, G. Lestari, Z. Lai, *J. Membr. Sci.* **2012**, *390/391*, 93.
- [29] H. T. Kwon, H.-K. Jeong, *Chem. Commun.* **2013**, *49*, 3854–3856.
- [30] C. Zhang, Y. Dai, J. R. Johnson, O. Karvan, W. J. Koros, *J. Membr. Sci.* **2012**, *389*, 34.
- [31] R. W. Baker, in *Membrane Technology in the Chemical Industry* (Eds: S. P. Nunes, K.-V. Peinemann), Wiley-VCH, Weinheim **2006**.
- [32] E. D. Bloch, W. L. Qucen, R. Krishna, J. M. Zdrozny, C. M. Brown, J. R. Long, *Science* **2012**, *335*, 1606.
- [33] D.-J. Lee, Q. Li, H. Kim, K. Lee, *Microporous Mesoporous Mater.* **2012**, *163*, 169.
- [34] U. Böhme, B. Barth, C. Paula, A. Kuhn, W. Schwieger, A. Mundstock, J. Caro, M. Hartmann, *Langmuir* **2012**, *29*, 8592.
- [35] C. Chmelik, A. Mundstock, P. D. C. Dietzel, J. Caro, *Microporous Mesoporous Mater.* **2013**, in press. DOI: 10.1016/j.micromeso.2013.09.002
- [36] D.-A. Yang, H.-Y. Cho, J. Kim, S.-T. Yang, W.-S. Ahn, *Energy Environ. Sci.* **2012**, *5*, 6465.
- [37] M. Hartmann, S. Kunz, D. Himsl, O. Tangermann, S. Ernst, A. Wagener, *Langmuir* **2008**, *24*, 8634.
- [38] A. Betard, D. Zacher, R. A. Fischer, *CrystEngComm* **2010**, *12*, 3768.
- [39] D.-J. Lee, Q. Li, H. Kim, K. Lee, *Microporous Mesoporous Mater.* **2012**, *163*, 169.
- [40] M. Arnold, P. Kortunov, D. Jones, Y. Nedelec, J. Kärger, J. Caro, *Eur. J. Inorg. Chem.* **2007**, *1*, 60.
- [41] A. van der Drift, *Philips Res. Rep.* **1967**, *22*, 267.
- [42] J. Caro, M. Noack, P. Kölsch, *Adsorption* **2005**, *11*, 215.
- [43] H. Bux, A. Feldhoff, J. Cravillon, M. Wiebcke, Y.-S. Li, J. Caro, *Chem. Mater.* **2011**, *23*, 2262.
- [44] C. Chmelik, H. Bux, H. Voß, J. Caro, *Chem. Ing. Tech.* **2011**, *83*, 104.
- [45] R. Krishna, *J. Phys. Chem. C* **2009**, *113*, 19756.
- [46] R. Krishna, J. M. van Baten, *J. Phys. Chem.* **2012**, *116*, 23556.

### III Propane/Propene Permeation through Na-X Membranes: The Interplay of Separation Performance and Pre-Synthetic Support Functionalization

A. Mundstock, N. Wang, S. Friebe, J. Caro

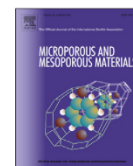
*Microporous and Mesoporous Materials*, 215, 2015, 20 - 28.

---



Contents lists available at ScienceDirect

## Microporous and Mesoporous Materials

journal homepage: [www.elsevier.com/locate/micromeso](http://www.elsevier.com/locate/micromeso)

# Propane/propene permeation through Na-X membranes: The interplay of separation performance and pre-synthetic support functionalization



Alexander Mundstock\*, Nanyi Wang, Sebastian Friebe, Jürgen Caro

Institute of Physical Chemistry and Electrochemistry, Leibniz University Hannover, Callinstr. 22, 30167 Hannover, Germany

### ARTICLE INFO

#### Article history:

Received 16 March 2015  
 Received in revised form  
 7 May 2015  
 Accepted 8 May 2015  
 Available online 16 May 2015

#### Keywords:

FAU membrane  
 Olefin-paraffin separation  
 Support modification  
 Polydopamine modification  
 APTES modification

### ABSTRACT

The influence of different pre-synthetic support modifications on membrane quality for paraffin/olefin and H<sub>2</sub>/CO<sub>2</sub> separation has been investigated. It could be shown that when modifying the alumina support surface by agents like PDA (polydopamine) or APTES (3-aminopropyltriethoxysilane) as molecular linkers between the FAU layer and the alumina support, well intergrown dense membranes with less defects and, therefore, increased separation selectivities can be obtained. As model system, the propane/propene separation has been used. For binary mixtures at room temperature and 1 bar at both sides of the FAU membrane, the mixed gas separation factors of C<sub>3</sub>H<sub>8</sub>/C<sub>3</sub>H<sub>6</sub> are found to be 3.3 for membranes grown on APTES and 2.0 for PDA functionalized supports in comparison to 1.4 for FAU membranes grown on the non-treated neat alumina supports. The improved FAU membrane quality when applying APTES and PDA for support modification in comparison with the neat untreated alumina support, has been proven for the separation of H<sub>2</sub>/CO<sub>2</sub>. Thanks to the relative thin FAU layers (3–4 μm), moderate fluxes can be obtained.

© 2015 Elsevier Inc. All rights reserved.

## 1. Introduction

In today's fuel and plastic addicted world, C<sub>2</sub> to C<sub>4</sub> light hydrocarbons rank among the most important petrochemical commodities. An example is the sheer number of polymers, like polyethylene, polypropylene, polyvinyl chloride and polyester, as well as other basic petrochemicals which can be derived from ethylene and propylene.

Because of their very similar properties the only way to separate paraffin/olefin mixtures is by utilizing their different vapor pressures and thus boiling points (propane: –42.1 °C, propene: –47.7) via cryogenic distillation. This, unfortunately, irreplaceable step is one of today's most energy-intensive processes in the refinery industry, consuming up to 85% of the total energy needed for the entire olefin production [1]. It is, therefore, hardly surprising that there is an ongoing search for a less energy-consuming separation techniques such as adsorption or membrane permeation via porous materials like zeolites or MOFs. Because of the high purity of the olefins needed for polymerization, the desirable high recovery rates

and the accompanying energy, time and capital consuming multi-bed/-step separation/purification procedures (at least a four-bed, five step PSA, VSA or TSA), porous materials with a high paraffin selectivity are sought [2].

A distinction is drawn between separations accomplished by kinetic or thermodynamic principles. On the one hand, even a very small difference in molecular size and critical diameters (propane: ~4.5 Å, propene: ~4.3 Å) [3] can cause dramatic changes in the diffusion rates of the mixture components through molecular sieve pores, resulting in sieve effects (size exclusion) [4,5]. Points of molecular interaction, for example coordinatively unsaturated metal centers or ions within the porous materials can, on the other hand, cause equilibrium-based separations due to different mixed gas adsorption equilibria.

Over the last few years MOFs (metal-organic frameworks) in general and for example MOF-74 (CPO-27) in particular, were considered as great white hope for paraffin/olefin separation and purification of natural gas because of some unique and promising properties [6,7]. MOFs distinguish themselves from other porous materials by their modular setup and framework flexibility while MOF-74 additionally features wide 1D hexagonal channels lined with coordinatively unsaturated metal centers (Co<sup>2+</sup>, Fe<sup>2+</sup>, Mg<sup>2+</sup>). Because of strong π-complexations between these metal sites and

\* Corresponding author. Tel.: +49 5117622943; fax: +49 51176219121.  
 E-mail address: [alexander.mundstock@pci.uni-hannover.de](mailto:alexander.mundstock@pci.uni-hannover.de) (A. Mundstock).

the olefin molecules, MOF-74 shows an olefin-selectivity which can be exploited in e.g. fixed-bed adsorbers [7].

But despite all those promising features, there hasn't been any real breakthrough regarding the paraffin/olefin separation, neither in packed-bed nor membrane-based separations, until now. This is due to a few easily underestimated but none the less very serious disadvantages of MOFs, which are in most cases directly related to their said advantages. For example, separation membranes made out of materials with 1D pore systems like MOF-74 suffer from very specific problems like adsorption founded blockage/self-hindrance and disadvantageous channel orientation [8]. The latter one is especially crucial because of the special geometric requirements in membranes (pores perpendicular to the support) and the very limited possibilities to control the crystal/pore growth orientation. The main deal-breaker, however, is the limited stability against heat, solvents and even humid air in some cases [9] making MOFs a poor choice for industrial applications.

And this is precisely the weak point, where inorganic membranes like metals, carbons or zeolites excel. Due to their high thermal, solvent and environmental stability, as well as other advantages like structural rigidity and 3D uniform pore systems, zeolites have found widespread application as adsorbents and catalysts, potential applications are their use as sensors, electrical insulators, reactors or separators [10–12]. Up until now, various zeolite membranes, e.g. MFI [13,14], LTA [15,16] and FAU [17,18] have been prepared on porous ceramic and metal supports on the lab scale. But despite these successful preparations, only one type of zeolite membranes, namely LTA for the dehydration of different solvents, is used in industrial gas separation and for commercial purposes so far. Because of its strong hydrophilicity and suitable pore sizes, LTA can be used for the de-watering of e.g. bio-ethanol [19], t-butanol [20], tetrahydrofuran [21], i-propanol, acetonitrile, MTBE and ethylene glycol. The more stable zeolite T (erionite-off-rite) is recently considered as a possible and very promising successor to LTA in this regards [22,23].

The still continuous interest in Na-X (Faujasite, FAU, with Si/Al ratio of 1.0–1.5) membranes for gas separation can be mainly attributed to the mentioned stabilities and special structural properties of this framework. Consisting of sodalite cages which are connected through hexagonal prisms, Na-X features 12-membered oxygen ring pores arranged in a 3D system. Due to their relatively large pore diameter of 7.4 Å, this structure is suitable for separating large molecules which cannot be handled by other zeolite membranes [18,24] and using adsorptive interactions. Another known application is the dehydration of organic solvents by steam permeation [25], utilizing the low Si/Al ratio and the resulting hydrophilicity of this structure. Of special interest for a desired paraffin/olefin separation are unsaturated metal ions in the activated de-hydrated state, the possibility of an ion exchange (e.g.  $\text{Co}^{2+}$ ,  $\text{Fe}^{2+}$ ,  $\text{Cu}^{2+}$ ), the concomitant variable pore sizes and the calculated good balance between capacity and selectivity [6]. But despite these advantages, there are so far no reports on paraffin/olefin selective Na-X membranes.

As said before, the growth of Na-X layers on porous supports is not the challenge, whereas growing the Na-X layers as a phase-pure dense membrane without cracks, pinholes or other defects turned out to be very demanding. In the case of Na-X and many other membrane materials this problem arises because of the inhomogeneous nucleation and growth to relatively big crystals on the support surface and the electrostatic rejection between the negatively charged precursor species and the often used alumina ( $\alpha\text{-Al}_2\text{O}_3$ ) supports. Because those defects stand in the way of achieving the membranes highest possible separation selectivities, it is not very surprising that various methods to promote the

heterogeneous growth and nucleation, like seed coating or chemical modification, were developed within the last years.

Two of the more recently developed and most promising pre-synthetic support surface modifications, namely treatments with polydopamine (PDA) and 3-aminopropyltriethoxysilane (APTES), were used in this work to evaluate their impact on Na-X membrane quality in the propane/propene separation as practice-relevant model mixture. PDA has recently emerged as a versatile platform chemical for secondary reactions and possible applications for e.g. in protein immobilization and nanoparticle stabilization [26–28]. Because it is able to form strong covalent (thanks to e.g. free amine groups and its catechol or quinone (under basic conditions) structures) and non-covalent (hydrogen bonds,  $\pi\text{-}\pi$  interactions and metal chelation) bonds to all kinds of organic and inorganic supports [29,30] including e.g. MOF and zeolite crystals, PDA modification of supports is a promising functionalization to obtain denser and defect free membranes with higher selectivity. Almost the same can be said about APTES. Used as a molecular binder to chemically anchor Na-X precursors on the support surface during hydrothermal synthesis, the following crystal growth of an Na-X layer results in dense and phase-pure zeolite membranes [31].

However, we have to state that our final functionalization of the FAU membranes by ion exchange was not successful. All our attempts to replace the sodium ions in the Na-X layers by Co, Fe, Ni and Cu (both solid state ion exchange via gas phase as well as ion exchange in aqueous solution) caused cracks in the FAU layers. The reason of this strange experimental finding is most probably the shrinkage of the crystal lattice/unit cell due to replacing the monovalent sodium ions with smaller divalent ions.

## 2. Experimental

Unless otherwise noted, all procedures were performed under ambient atmosphere. All reagents were obtained from commercial vendors at reagent grade purity or higher and used without further purification.

### 2.1. Support modifications

Besides the standard  $\alpha\text{-Al}_2\text{O}_3$  supports (Fraunhofer IKTS Hermsdorf,  $d = 18$  mm,  $h = 1$  mm,  $d_{50} = 2.5$   $\mu\text{m}$ , top-layer  $d_{50} = 70$  nm) two additionally functionalized versions of these supports were used to grow denser Na-X membranes with less defects and advanced separation capabilities.

3-aminopropyltriethoxysilane (APTES) functionalized  $\alpha\text{-Al}_2\text{O}_3$  supports were prepared according to a previously reported [32] but slightly modified procedure. Two of the porous supports were placed in an APTES (460 mg) toluene (10 mL) mixture within a sealable reaction vial (Schott Duran Bottle) and heated up to 120 °C for 30 min. After subsequently drying in an oven at 60 °C for about 20 min and cooling down in ambient air, the modified supports were ready for further utilization. APTES functionalized nano powder for Zeta potential measurements was prepared in the same way using slightly different amounts of reagents (250 mg  $\text{Al}_2\text{O}_3$  nano powder, 40 mL toluene and 1 g APTES). The resulting suspension was stirred during the whole heating period.

PDA (polydopamine) functionalized  $\alpha\text{-Al}_2\text{O}_3$  supports were also prepared according to a published procedure [33]. Dopamine (DPA) (2 mg/mL) was completely dissolved in 50 mL of 10 mM Tris-HCl (pH 8.5) in an open watch glass ( $d = 180$  mm). The basic supports were simply immersed in this buffered aqueous solution for 24 h at room temperature under continuous stirring. After drying in the ambient atmosphere, the now dark brown supports were used for further membrane preparations. PDA functionalized  $\text{Al}_2\text{O}_3$  powder was prepared by mixing 250 mg  $\text{Al}_2\text{O}_3$  nano powder, 300 mg DPA,



900 mg Tris-(hydroxymethyl)-aminomethane and 40 g water in an open beaker. After 20 h of continuous stirring the remaining liquid was decanted and the dark brown powder was washed with water and dried in air.

## 2.2. Preparation of Na-X membranes

The Na-X membranes on the modified as well as unmodified  $\alpha$ -Al<sub>2</sub>O<sub>3</sub> supports were synthesized by following a previously reported but again slightly modified procedure by Huang et al. [32]. A synthesis solution with a specific molar ratio of 70Na<sub>2</sub>O:1Al<sub>2</sub>O<sub>3</sub>:20SiO<sub>2</sub>:2000H<sub>2</sub>O had to be prepared by mixing a silicate and an aluminate solution at room temperature. The latter one was obtained by dissolving 7.78 g sodium hydroxide (>99%, Merck) and 0.075 g of aluminum foil (Fisher Scientific) as Al source in 25 g deionized water in a sealable reaction vial under stirring. In a second vial the silicate solution was prepared by mixing 4.17 g LUDOX AS-40 colloidal silica (40% SiO<sub>2</sub> in water, Aldrich) as Si source and 22.22 g deionized water. The resulting solution was then vigorously stirred for 2 h at 60 °C. After this period of time the still hot silicate solution was poured into the aluminum solution and both stirred in the closed vial at room temperature till a colorless, clear and homogeneous solution was obtained (ca. 12 h). This was then transferred into a Teflon-lined stainless steel autoclave (Parr Instruments Germany). The treated or non-treated  $\alpha$ -Al<sub>2</sub>O<sub>3</sub> supports were jammed into special Teflon-holders and placed face down in the autoclave/solution too. After in situ growth for 24 h at 75 °C in an oven, the solution was decanted and the resulting membranes and powder were transferred into a sealed vial filled with deionized water for 24 h. Subsequently they were dried in ambient air at 60° in an oven for about 2 h.

## 2.3. Activation and permeation measurements

A full desolvation/activation of membranes and powders was achieved by heating (180 °C) under vacuum over 2 h followed by storage in a sealed Schlenk flask in a glove box (Ar). The assembly of the permeation cells, including the mounting of the membranes, was done under protective gas atmosphere within the glove box.

For the actual permeation measurements, the assembled cells were transferred to sealable vials filled with argon and discharged from the glove box. The installation into the permeation apparatus took place under a nitrogen current to prevent a deactivation of the Na-X membranes. All permeation measurements carried out for this work, single gas as well as equimolar propene/propane mixtures, were done with a modified Wicke-Kallenbach-apparatus. In all cases nitrogen was used as purge gas on the permeate side (50 mL/min, 1 bar).

## 2.4. Ion exchange

All ion exchanges were done, respectively, with Cobalt(II) nitrate hexahydrate, Ni(II) nitrate hexahydrate, Copper(II) nitrate trihydrate and Iron(II) chloride tetrahydrate as "ion sources".

The solid state ion exchanges were simply done by either covering the supported membranes with a sufficient amount of the mentioned metal salts in evacuated glass ampoules or by mixing 150 mg of the FAU powder with the same amount of metal salt in a glass ampoule followed by evacuation. After 24 h the membranes were taken out of the vessels and rinsed with water while the powder was obtained by dissolving the metal salt in water, decanting the created solution and washing the remaining FAU powder a few times with fresh water. Membranes and powders were then dried in an oven under air at 60 °C for 2 h.

The liquid state ion exchanges were done by suspending/inserting the FAU powders/membranes in an aqueous solution of the metal salts (100 mg of salt in 20 mL distilled water) for 24 h at room temperature. Afterward, the solutions were decanted, the remaining membranes and powders washed with water a few times and dried in an oven at 60 °C for 2 h.

## 2.5. XRD, SEM, Zeta potential and contact angle measurement

The XRD patterns of the Na-X samples (powder and membranes) were obtained on a Bruker D8 Advance X-ray Diffractometer using Cu K $\alpha$  ( $\lambda = 1.54 \text{ \AA}$ ) radiation. All shown Scanning Electron Microscopy (SEM) micrographs were taken on a JEOL JSM-6700F with a cold field emission gun operating at 2 kV and 10 iA. The Zeta potential measurements were done with a Malvern Instruments Zetasizer Nano ZS and Multi Purpose Titrator MPT-2. Contact angle pictures were taken on a "home-made" measurement setup and evaluated with the program KSV CAM100.

## 3. Results

### 3.1. Support modification and membrane preparation

As mentioned above and further illustrated in Fig. 1A, when using a pure  $\alpha$ -Al<sub>2</sub>O<sub>3</sub> support without any functionalization for the Na-X membrane preparation, in all cases (12 supported Na-X membranes have been prepared) we have obtained ca. 2  $\mu\text{m}$  thick and defect rich membrane layers. Whether a membrane will be tested in gas separation or is excluded a priori due to too many defects, is evaluated by leakage tests right after the synthesis and in cases of doubt, by subsequent SEM scans. These defects include cracks, pinholes and other flaws which are counterproductive for gas separation and stem most probably from the electrostatic rejection between the negatively charged Na-X ( $\approx -43 \text{ mV}$ , see Fig. 2) and its precursor species and the also negatively charged  $\alpha$ -alumina ( $\approx -32 \text{ mV}$ , see Fig. 2) support at the pH = 11 of the Na-X preparation as for the first time shown by our group in Ref. [31]. Their quantity and quality of occurrence seem to be highly erratic and that's why it was by the end possible to get from 12 preparations only 1 relatively dense Na-X membrane which was used in this work for the permeation studies (Tables 1 and 2).

The only support surface functionalization which one can see with your naked eye, is the PDA layer. Right after the coating and before further membrane preparations, the former white alumina support exhibits a new dark brown (in web version), nearly black color (Fig. 1B).

As one can see in Fig. 1D the membrane grown on a PDA functionalized support (from now on called Na-X/PDA) is, in contrast to the Na-X membrane grown on a pure non-modified support (Fig. 1A), highly crystalline, dense and defect free with a thickness of about 2  $\mu\text{m}$ . It is noteworthy that after functionalization, a PDA layer of 1–2  $\mu\text{m}$  has been formed on top of the alumina support (not shown here) and the functionalized support looks dark brown, nearly black (Fig. 1B). However, after membrane synthesis, this thick PDA layer has been dissolved by the basic reaction solution and the Na-X layer seems to adhere directly to the support without visible PDA intermediate layer. This and the optical transparency of the 2  $\mu\text{m}$  thick Na-X layer cause a slight color change of the Na-X covered support to a lighter, milky kind of brown (Fig. 1C). So the actual functionalization on which the Na-X membrane grows is the strongly bound (covalent and non-covalent) PDA residue on the support surface and in its pores.

The thickest (ca. 3  $\mu\text{m}$ , Fig. 1E) and all in all best looking Na-X membranes grew on the Al<sub>2</sub>O<sub>3</sub> support which had been

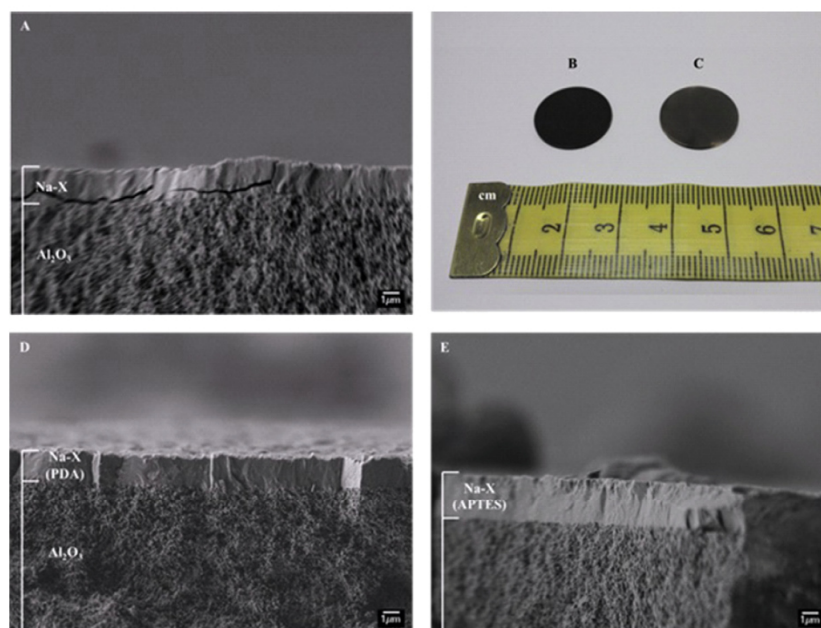


**Fig. 1.** SEM images of (A) defect rich Na-X membrane grown on a pure untreated  $\text{Al}_2\text{O}_3$  support, and photographs of a support modified with PDA (B) before and (C) after Na-X membrane growth, (D) Na-X membrane grown on a support modified with PDA, (E) Na-X membrane grown on a support modified with APTES.

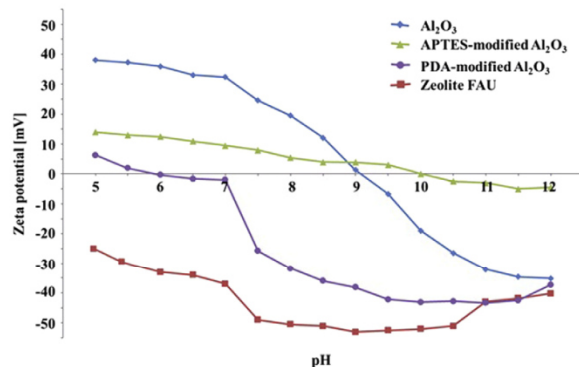


**Fig. 2.** Zeta potential of  $\alpha\text{-Al}_2\text{O}_3$ , APTES-modified  $\text{Al}_2\text{O}_3$ , PDA-modified  $\text{Al}_2\text{O}_3$  and zeolite FAU particles suspended in water as a function of pH at room temperature.

pre-synthetically functionalized with APTES (from now on called Na-X/APTES). They appear to be highly crystalline, continuous and dense layers without any cracks, pinholes or other defect.

### 3.2. Zeta potential and contact angle measurements

As mentioned before, the structural superiority of the Na-X/APTES membranes over the defect rich non-treated Na-X membranes is most probably due to changes in the  $\alpha\text{-Al}_2\text{O}_3$  support surface charge gained by the APTES modification. The most well-known method for determining the surface charges of small particles is the Zeta potential measurement. Fig. 2 shows the Zeta potential as function of pH for the four kinds of nano particles suspended in water which are of particular interest for this work: pure  $\alpha\text{-Al}_2\text{O}_3$ , APTES-modified  $\alpha\text{-Al}_2\text{O}_3$ , zeolite FAU and PDA-modified  $\alpha\text{-Al}_2\text{O}_3$ . Our measured Zeta potentials are in good accordance with published data (e.g. Ref. [31]), however, PDA-modified  $\alpha\text{-Al}_2\text{O}_3$  has not been published before.

**Table 1**

Propane and propene single gas permeation data on the different Na-FAU membranes under study at room temperature.

Support functionalization	$\text{Al}_2\text{O}_3$	$\text{Al}_2\text{O}_3$ Na-X	$\text{Al}_2\text{O}_3$ PDA	$\text{Al}_2\text{O}_3$ PDA Na-X	$\text{Al}_2\text{O}_3$ APTES	$\text{Al}_2\text{O}_3$ APTES Na-X
Average SF propane/propene	1.0	1.7	0.7	2.4	1.0	4.2
Standard deviation of SF	$\pm 0.012$ ( $\approx 1.2\%$ )	$\pm 0.094$ ( $\approx 5.5\%$ )	$\pm 0.043$ ( $\approx 6.1\%$ )	$\pm 0.115$ ( $\approx 4.8\%$ )	$\pm 0.018$ ( $\approx 1.8\%$ )	0.134 ( $\approx 3.2\%$ )
Flux propane $\text{mL min}^{-1} \text{cm}^{-2}$	13.06	1.52	0.03	0.30	2.97	0.39
Flux propene $\text{mL min}^{-1} \text{cm}^{-2}$	13.11	0.87	0.04	0.13	2.99	0.10
Permeance propane $\text{mol/m}^2 \text{s Pa}$	$3.65 \cdot 10^{-6}$	$3.58 \cdot 10^{-7}$	$6.23 \cdot 10^{-9}$	$7.02 \cdot 10^{-8}$	$7.13 \cdot 10^{-7}$	$9.23 \cdot 10^{-8}$
Permeance propene $\text{mol/m}^2 \text{s Pa}$	$3.66 \cdot 10^{-6}$	$2.04 \cdot 10^{-7}$	$8.76 \cdot 10^{-9}$	$2.91 \cdot 10^{-8}$	$7.21 \cdot 10^{-7}$	$2.19 \cdot 10^{-8}$

**Table 2**  
Mixed gas permeation data for an equimolar propane/propene mixture at 1 bar (Wicke Kallenbach technique) at room temperature.

Support functionalization	Al <sub>2</sub> O <sub>3</sub>	Al <sub>2</sub> O <sub>3</sub> Na-X	Al <sub>2</sub> O <sub>3</sub> PDA	Al <sub>2</sub> O <sub>3</sub> PDA Na-X	Al <sub>2</sub> O <sub>3</sub> APTES	Al <sub>2</sub> O <sub>3</sub> APTES Na-X
Mixed gas SF propane/propene (average)	1.0	1.4	0.8	2.0	1.0	3.3
Standard deviation of SF	±0.013 (≈ 1.3%)	±0.091 (≈ 6.5%)	±0.055 (≈ 6.9%)	±0.106 (≈ 5.3%)	±0.021 (≈ 2.1%)	0.132 (≈ 4.0%)
Flux propane mL min <sup>-1</sup> cm <sup>-2</sup>	7.57	0.99	0.02	0.23	1.74	0.34
Flux propene mL min <sup>-1</sup> cm <sup>-2</sup>	7.61	0.70	0.03	0.11	1.77	0.11
Permeance propane mol/m <sup>2</sup> s Pa	1.94 · 10 <sup>-6</sup>	2.32 · 10 <sup>-7</sup>	4.85 · 10 <sup>-9</sup>	5.23 · 10 <sup>-8</sup>	4.11 · 10 <sup>-7</sup>	7.01 · 10 <sup>-8</sup>
Permeance propene mol/m <sup>2</sup> s Pa	1.96 · 10 <sup>-6</sup>	1.64 · 10 <sup>-7</sup>	5.99 · 10 <sup>-9</sup>	2.59 · 10 <sup>-8</sup>	4.19 · 10 <sup>-7</sup>	2.43 · 10 <sup>-8</sup>

When comparing the Zeta potentials for the pure  $\alpha$ -Al<sub>2</sub>O<sub>3</sub> nano powder (Fig. 2, blue line (in web version) with diamonds) with the Na-X particles (Fig. 2, red line (in web version) with squares), at pH ≈ 11 where the Na-X membrane formation takes place, it can be seen that both particles show a highly negative surface charge ( $\alpha$ -Al<sub>2</sub>O<sub>3</sub> ≈ -32 mV and Na-X ≈ -43 mV). Under these circumstances, instead of homogeneously growing together and forming a good groundwork for a dense membrane, support and membrane precursor material repel each other because of their similar surface charges. This directly counteracts a smooth membrane growth and results in the defect rich membranes seen in Fig. 1A with their poor separation qualities.

After the modification with APTES (Fig. 2 green line (in web version) with triangles) the previously negative surface charge of Al<sub>2</sub>O<sub>3</sub> changed to nearly neutral (Zeta potential of APTES/Al<sub>2</sub>O<sub>3</sub> ≈ -3 mV at pH 11), minimizing the electrostatic rejection between the negatively charged FAU precursor species and the modified Al<sub>2</sub>O<sub>3</sub> support. This greatly benefits the homogeneous nucleation and growth of the Na-X membranes (Fig. 1C) and subsequently their capability for separating paraffins from olefins.

A little bit contradictory at the first glance is that at pH 11 PDA-modified Al<sub>2</sub>O<sub>3</sub> (Fig. 2 purple line (in web version) with circles) as well as Na-X show very similar Zeta potentials of about -43 mV and thereby an even higher electrostatic rejection than pure Al<sub>2</sub>O<sub>3</sub> and Na-X but nevertheless the FAU membranes grown on PDA-modified Al<sub>2</sub>O<sub>3</sub> are of higher optical quality (Fig. 1E) but – as shown later – also of moderate paraffin/olefin selectivity (Tables 1 and 2). This phenomenon is probably due to one of PDA's special features mentioned above, namely the ability to chelate metal ions. This, in combination with the abundance of metal ions within the synthesis solution, enables PDA to effectively shield its charge – even despite the elevated temperature – and consequently minimizes or even equalizes the otherwise disruptive electrostatic forces between the functionalized support and the charged FAU precursor species. Furthermore, because most of the chelated metal ions are also Na-X building blocks, the functionalized support surface now additionally features more direct nucleation points for the zeolite layer growth. Together, these two phenomena facilitate an unobstructed growth and almost defect-free membranes.

Looking at the Zeta potential data (Fig. 2), it becomes noticeable that there could be another completely different way to high-quality Na-X membranes, bypassing the need to functionalize the support entirely. At a lower pH of the synthesis solution, e.g. 7 or 8 instead of 11 (as in our case), there should be an electrostatic attraction between the now positively charged Al<sub>2</sub>O<sub>3</sub> support surface and the still negatively charged FAU precursor species, resulting in a very homogeneous nucleation and growth of high quality Na-X membranes. This approach sounds very promising but still has to be evaluated experimentally.

Another very important property of the support surface (pure and modified) as well as FAU itself and its precursor materials, which is crucial for a successful membrane growth, is their

hydrophobicity/hydrophilicity. The easiest way to determine whether a surface is hydrophobic or hydrophilic, is a contact angle measurement. In the present case we tried this method for all the surfaces which are of particular interest for this work: a pure  $\alpha$ -Al<sub>2</sub>O<sub>3</sub> support, a Na-X membrane, and the  $\alpha$ -alumina supports modified with either APTES or PDA. As an example, Fig. 3 shows the contact angle measurement for PDA-modified  $\alpha$ -alumina supports.

As one can see, the biopolymer PDA is strongly hydrophilic, clearly proven by the fitted mean contact angle of 15.08° (Fig. 3). Compared with the PDA-modified  $\alpha$ -Al<sub>2</sub>O<sub>3</sub> support, all other modifications turned out to be even more hydrophilic and the contact angle became near zero thus preventing any reasonable contact angle measurements. From these contact angle data, we can assume that all the supports should be able to interact well with the also strongly hydrophilic Na-X precursor particles. But since PDA-modified supports are slightly less hydrophilic than the other ones, there should be a certain preference, regarding the zeolite growth, in favor of the alternative supports (pure Na-X and Na-X/APTES). This slight disadvantage is most probably once again compensated by the PDA's ability to form strong covalent and noncovalent bonds with Na-X.

### 3.3. Permeation measurements

From the comparison of Tables 1 and 2 it follows that both the single and mixed gas permeation studies reflect the clear trend that PDA and APTES treatments of the support can decisively improve

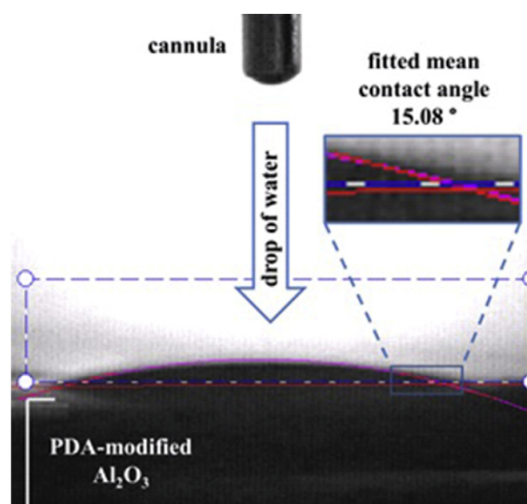


**Fig. 3.** Photograph of a water droplet on the surface of a PDA-modified  $\alpha$ -Al<sub>2</sub>O<sub>3</sub> support and the fitted mean contact angle.

the quality of the resulting Na-X membrane and show a distinct improvement in the propane/propene separation capability compared to the Na-X membrane grown on non-treated supports. Interestingly, all membranes under study are paraffin-selective, i.e. they more or less hold back the olefin. When we assume the validity of the rule of thumb: Permeation Selectivity  $\approx$  Adsorption Selectivity  $\times$  Diffusion Selectivity [31,34–36], the opposite behavior could be expected, namely olefin selectivity. There are numerous adsorption studies of propane/propene mixtures on Na-X zeolite showing a preferential propene adsorption [37–40] due to an interaction between the sodium ions within the activated FAU structure and the olefin double bonds forming strong  $\pi$ -complexations. However, this adsorption selectivity in favor of propene is overcompensated by its reduced mobility. There are a few diffusion studies by the NMR pulsed field gradient technique showing the reduced diffusivity of propene in comparison with propane inside Na-X crystals [41–43]. The slightly smaller critical diameter of propene relative to propane does not play any role in the case of permeation through the large-pore Na-X membrane (7.3 Å pore size).

This interplay of adsorption and diffusion causes a propane selectivity. All in all, Na-X/APTES turned out to be the best paraffin/olefin separating membrane under study in this paper with a mixed gas separation factor ( $SF_{\text{propane/propene}}$ ) of 3.3 (Table 2 and Fig. 4A) which is 2.4 times higher than Na-X and 1.7 times higher than Na-X/PDA. However, this separation factor is too low for an industrial application which requires at least separation factors propane/propene of twice that value. A two-step membrane system, for example, with olefin/paraffin selectivities of 5–10 each would be easily able to split a 50%/50% propane/propene mixture into a 90% propane and 90% propane stream. Streams of this purity could then be further purified in much smaller distillation columns thus reducing the following costs as well as time and energy consumption [44]. On the other hand, membranes with an alkane selectivity are also of interest since the purity requirements as well as the desired recovery rates for paraffins are very high and only attainable through energy and time consuming multi-bed/-step separation/purification processes (pressure-, vacuum- and temperature swing adsorption) and large capital investments [2,45].

Being able to make these processes more efficient or even bypass them entirely, would be a huge success but also presupposes a new kind of paraffin selective porous materials.

The only real but expected difference between the single and mixed gas permeation results are the slightly lower separation factors for the 50:50 mixtures. Possible explanations for this could be paraffin-olefin interactions within the zeolite or a partial pore blockage caused by the adsorbed propene molecules.

The distinct superiority of Na-X/APTES regarding the propane/propene separation is, on the one hand, due to the improved membrane quality because of the APTES functionalization as mentioned above. The second reason for the higher separability of Na-X/APTES in comparison with the other membranes under study, is the poor performance of the Na-X/PDA membrane. As one can see in both Tables 1 and 2 and again illustrated in Fig. 4A, the functionalization with PDA helped us to grow a nearly perfect membrane, but unfortunately, the biopolymer PDA has entered the macro pores of the alumina support where it forms an internal PDA phase inside the pores with propene selectivity (c in Fig. 4A). The dense cross linked biopolymer PDA shows a small but crucial molecular sieve effect and preferably holds back the slightly bigger paraffin. Within the support pores as well as in the interlayer between the alumina support and the Na-X membrane, PDA shows an olefin/paraffin selectivity which counteracts and diminishes the paraffin/olefin selectivity of the Na-X layer (d in Fig. 4A). The poor performance of the “pure” Na-X membrane (b in Fig. 4A) can simply be attributed to the defective Na-X membrane layer. Note that the unmodified alumina support has no selectivity at all (a in Fig. 4A). The highest propane/propene selectivity is found for the Na-X layer grown on APTES-modified supports (f in Fig. 4A). Interestingly, the APTES-modified supports show no selectivity (e in Fig. 4A).

The differences between the fluxes become more visible, if we plot the propane and propene fluxes in logarithmic scales (Fig. 4B). It is not very surprising that the highest fluxes in this work belong to the pure  $\alpha$ - $\text{Al}_2\text{O}_3$  support with its smallest but still huge top layer pores ( $d_{50} = 70$  nm) (a in Fig. 4B) followed by the nearly four times smaller fluxes of the support functionalized with APTES (e in Fig. 4B). This steep fall can be attributed to the APTES molecules attached to the  $\text{Al}_2\text{O}_3$  particles (adsorption on both the support

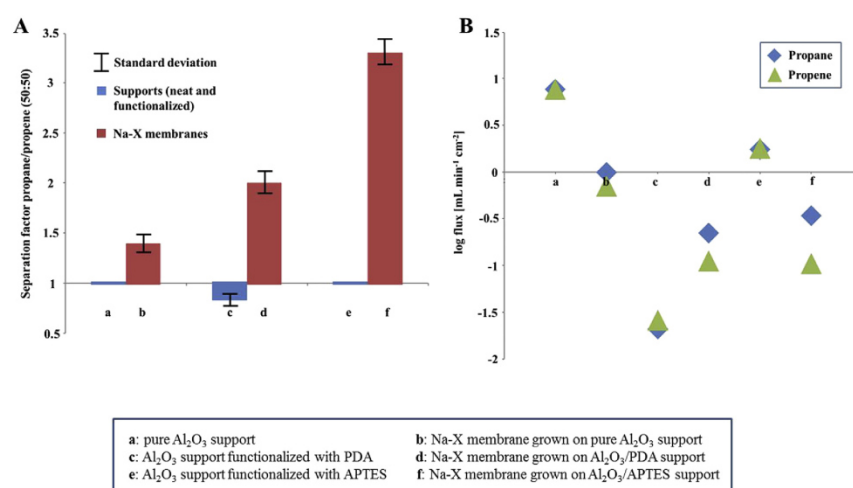


**Fig. 4.** Na-X membranes prepared on the PDA and APTES functionalized supports in comparison with the Na-X membrane prepared on the non-treated supports as well as the pure and the PDA and APTES modified supports without Na-X layer: (A) propane/propene mixed gas (50:50) separation factors (derived from Table 2), and (B) their propane and propene mixed gas fluxes (from Table 2) in logarithmic representation.

surface and in the top layer pores) thus reducing the pore diameter. The lowest fluxes were found on the PDA functionalized supports because of a thick PDA layer (c in Fig. 4B). However, because of the PDA “washing-off” during membrane preparation, the fluxes through the Na-X/PDA are even slightly higher than those through the PDA modified supports, despite the additional zeolite Na-X membrane on top (d in Fig. 4B). Due to its many defects Na-X shows the highest fluxes of all zeolite membranes (b in Fig. 4B) while Na-X/APTES with its relatively thick and flawless zeolite layer is right between the other two (f in Fig. 4B).

An important issue regarding the Na-X membranes grown on functionalized supports is, that their enhanced separation capabilities are based on the expense of a substantially decreased flux (Table 2). This raises the legitimate question of whether it is more efficient to use a single membrane with high separation but low fluxes or a membranes with lower separation but higher fluxes repeatedly in series (Table 3).

As one can see in Table 3, the simulated Na-X membrane two-stage system displays the same separation factor as the single Na-X/PDA membrane (2.0) but its propane permeance is 4.4 times higher. Our best single membrane (Na-X/APTES) still exhibits a higher separation factor, but the two-stage system can compensate (or even overcompensate) for this with its 3.8 times higher propane throughput. Purely in terms of “theoretical” numbers, this two-stage system seems to be a real alternative to a single membrane grown on a functionalized support. Another advantage of two-stage systems is that their recovery rate is significantly better than that of a single-stage one. But nevertheless, the quality problem of the “unmodified” Na-X membranes (only 1 membrane out of 12 prepared was useable for tests) remains, whereas nearly all membranes grown on functionalized supports could be used and showed the mentioned separation capabilities. Additionally, the higher recovery comes at the expense of higher maintenance costs.

As pleasing as the triplication of the propane/propene separation factor for Na-X/APTES or the theoretical two-stage process compared to neat single Na-X membranes may be, it can not change the fact that Na-X is at the lower end of the

propane/propene separation performance scale. Table 4 shows a comparison of recent membrane materials and their olefin/paraffin separation capabilities.

However, as remarkable as some of these numbers may seem, all of these membrane materials are far from being ready for use in any industrial application and one of the main reasons for that is again the long-term stability. We know that Na-X membranes are by far not the last word on the subject of effectively separating olefins from paraffines, but we considered this task suitable, novel and interesting enough to illustrate the very important interplay of separation performance and pre-synthetic support functionalization in the case of Na-X membranes.

To demonstrate that the tremendous improvement in Na-X membrane quality through our pre-synthetic support functionalization is universal and not limited to the propane/propene separation, we used the same membranes to separate H<sub>2</sub> from CO<sub>2</sub> (50:50 mixtures). In literature, a number of H<sub>2</sub>/CO<sub>2</sub> separations through membranes made of zeolites like e.g. MFI (SF<sub>H<sub>2</sub>/CO<sub>2</sub></sub> of 1.8) [50], LTA (SF<sub>H<sub>2</sub>/CO<sub>2</sub></sub> of 6.7) [51] or FAU, including some prepared on APTES-modified supports (ideal SF<sub>H<sub>2</sub>/CO<sub>2</sub></sub> of 8.0) [31], can be found. In comparison, all of our membranes: neat Na-X (SF<sub>H<sub>2</sub>/CO<sub>2</sub></sub> of 8.0), Na-X/APTES (SF<sub>H<sub>2</sub>/CO<sub>2</sub></sub> of 8.9) and Na-X/PDA (SF<sub>H<sub>2</sub>/CO<sub>2</sub></sub> of 10.3), show a notable improvement in H<sub>2</sub>/CO<sub>2</sub> separation capability. Another advantage of our membranes is that they exhibit these increased separation factors even at room temperature, while most of the literature results for FAU were measured at 100 °C.

#### 3.4. Ion exchange

With the aim to modify the adsorptive interaction of propene with the membrane, we tried to cation exchange the Na<sup>+</sup> (being in the Na-X membrane from the synthesis) by bivalent ions like Co<sup>2+</sup>, Ni<sup>2+</sup>, Cu<sup>2+</sup> or Fe<sup>2+</sup>. However, in all cases, after cation exchange the supported X-membrane layer showed severe cracks as you can see in Fig. 5 for Co-X exemplarily for all ion exchanges done in this work, these cracks are up to 2 μm thick and cover the whole membrane. The same crack patterns develop, if we perform the cation exchange via the gas phase, the so called “dry cation

**Table 3**  
Comparison of the gas separation performances of single FAU membranes with a theoretical two-stage process.

System	Single neat Na-X membrane	Single Na-X/PDA membrane	Single Na-X/APTES membrane	Two neat Na-X membranes in series (theoretical)
Mixed gas SF propane/propene	1.4	2.0	3.3	2.0
Permeate composition	58.6% propane 41.4% propene	66.9% propane 33.1% propene	75.9% propane 24.1% propene	67.2% propane 32.8% propene
Enrichment of propane	17.2%	33.8%	51.8%	34.4%
Throughput of propane mol/m <sup>2</sup> s Pa	2.32 · 10 <sup>-7</sup>	5.23 · 10 <sup>-8</sup>	7.01 · 10 <sup>-8</sup>	2.66 · 10 <sup>-7</sup>

**Table 4**  
Comparison of propene/propane separation performances of different membrane types.

Membrane	Temperature	Feed pressure bar	Permeance propene mol/m <sup>2</sup> s Pa	Separation factor propene/propane	Reference
Na-X/APTES	RT	1	2.43 · 10 <sup>-8</sup>	0.3	This study
PEO <sup>a</sup> /AgBF <sub>4</sub> /Al(NO <sub>3</sub> ) <sub>3</sub> complex membrane	RT	1	6.67 · 10 <sup>-9</sup>	10	[46]
Carbon Molecular Sieve membrane <sup>b</sup>	RT	2	3.0 · 10 <sup>-9</sup>	36	[47]
ZIF-8	RT	1	268 · 10 <sup>-10</sup>	70	[48]
HTMOS/O <sub>2</sub> <sup>c</sup> Silica hybrid membrane	270 °C	1	1.0 · 10 <sup>-8</sup>	414 <sup>d</sup>	[49]

<sup>a</sup> Poly(ethylene oxide).

<sup>b</sup> γ-alumina supported.

<sup>c</sup> Hexyltrimethoxysilane with O<sub>2</sub> as oxidant.

<sup>d</sup> Single gas permeation data.

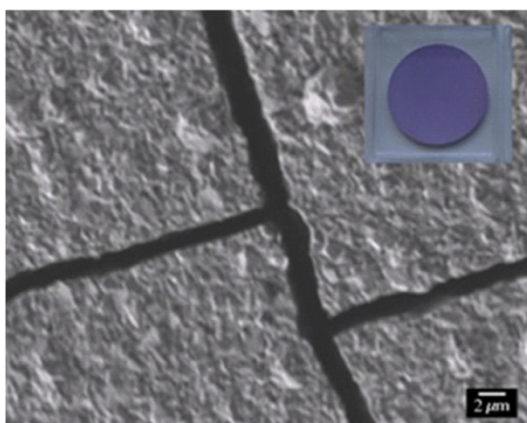


**Fig. 5.** SEM image of a non-activated FAU membrane, grown on an  $\text{Al}_2\text{O}_3$  support functionalized with APTES, after ion exchange with Co (Co-X, liquid state ion exchange). The insert shows a photo of the respective membrane.

exchange". On the other hand, we performed the cation exchange experiments also with Na-X powder (sedimented Na-X from the autoclaves of Na-X membrane synthesis) and apart from the color changes according to the ion source, no significant changes in morphology, crystallinity could be found.

This kind of cracks/crack pattern, wide linear gaps and big intact "floes", could be very specific for a unit cell shrinkage and the accompanying tension in a wide crystal plain linked to a rigid alumina support. To proof this concept, we measured the XRD of the starting Na-X powder and of the cation exchanged  $\text{Co}^{2+}$ ,  $\text{Ni}^{2+}$ ,  $\text{Cu}^{2+}$ , or  $\text{Fe}^{2+}$   $\text{Me}^{2+}$ -X powders (Fig. 6). As shown for Co-X, there is indeed a slight shift of all reflexes to higher angles which means densification of the structure upon ion exchange, but this effect seems to be too small to explain the huge cracks shown in Fig. 5B.

As you can see, nearly all signals, major as well as minor ones, show a slight shift towards larger angles, indicating an overall shrinkage of the unit cell. This phenomenon is most likely due to the improved minimization of the electrostatic repulsion between the FAU framework oxygens through better shielding and balancing by the newly introduced  $\text{Co}(\text{H}_2\text{O})_6^{2+}$  octahedral complexes

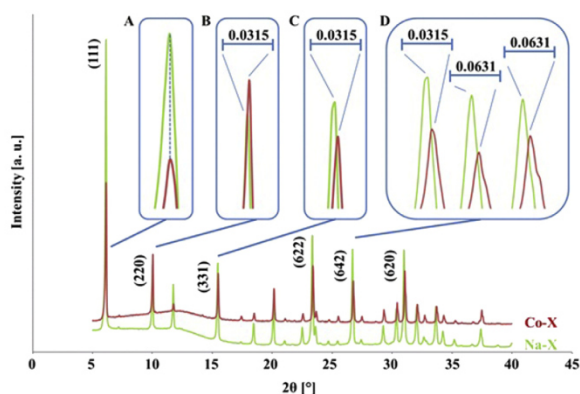


**Fig. 6.** XRD patterns of non-activated i.e. hydrated Na-X and Co-X (obtained by liquid state ion exchange) and (A–D) the resulting changes in the crystal structure (only exemplary and not in scale), the hump at the beginning is due to the amorphous plastic XRD holder.

(pink color). The distinct shift of  $\Delta 2\theta = 0.0315^\circ$  (respectively  $0.0631^\circ = 2 \times 0.0315^\circ$ ) (see Fig. 6B–D) is hereby rather the step size of the used measurement method than the actual shift, which should be somewhere between those steps. A general decrease in signal intensity, like the one seen in Fig. 6, is probably an indication for a slight loss in crystallinity due to the exchange of monovalent sodium ions for divalent cobalt ions. On the other hand, the quantitative analysis of the unit cell of Na-X for cation exchange by Co gave for the Co-X a reduction of the unit cell parameter by only  $a = 0.32\%$ .

There are a few papers reporting the change of the unit cell of Na-X upon dehydration. For example, Caro et al. reported that the de-watering in air of FAU results in a unit cell expansion from 2.478 nm at  $50^\circ\text{C}$  to 2.490 nm at  $100^\circ\text{C}$  [52]. This finding gives the explanation of why FAU membranes excel in water separation but very often fail in shape-selective gas permeation, which presuppose a preceding activation. Due to the damage, mainly cracks, done by this essential step, the membranes lose permselectivity and finally show Knudsen behavior. As long as FAU membranes are still grown on rigid supports with extremely different expansion coefficients, this kind of effects will always have to be born in mind, making the activation one of the most crucial steps in membrane preparation.

#### 4. Conclusions

Three different types of Na-X membranes have been prepared and studied regarding their propane/propene separation capabilities: Na-X layers grown on (i) untreated  $\alpha$ -alumina supports, (ii) APTES-functionalized supports, and (iii) polydopamine based supports. We found that not only the membrane quality and gas fluxes but also the ability to separate these very similar gases highly depend on the kind of pre-synthetic support functionalization used for preparation. Surprisingly, all Na-X membranes showed propane selectivity, that is to say they hold back the olefin because of internal interactions. With its nearly triplicated separation factor of 3.3 and still moderate fluxes compared to neat Na-X membranes, Na-X/APTES appears to be a good example of how even long and well known systems, by applying the right approach, can have quite a few new tricks up their sleeves. In addition to the propane/propene separation, the improved FAU membrane quality by the support modification has been proven for the separation of the  $\text{H}_2/\text{CO}_2$  mixture.

#### Acknowledgments

Financial support by DFG priority program 1570 "Porous media with defined pore structure in chemical engineering - modeling, application, synthesis" (CA 147/17-1 and 2) is acknowledged.

#### References

- [1] A. Van Miltenburg, W. Zhu, F. Kapteijn, J.A. Moulijn, *Chem. Eng. Res. Des.* 84 (5) (2006) 350–354.
- [2] C. Gücüyener, J. van den Bergh, J. Gascon, F. Kapteijn, *JACS* 132 (2010) 17704–17706.
- [3] W. Zhu, F. Kapteijn, J.A. Moulijn, *Chem. Commun.* (1999) 2453–2454.
- [4] K. Li, D.H. Olson, J. Seidel, T.J. Emge, H. Gong, H. Zeng, J. Li, *J. Am. Chem. Soc.* 131 (2009) 10368–10369.
- [5] Z. Song, Y. Huang, L. Wang, S. Li, M. Yu, *Chem. Commun.* 51 (2015) 373–375.
- [6] Y. He, R. Krishna, B. Chen, *Energy Environ. Sci.* 5 (2012) 9107–9120.
- [7] U. Böhme, B. Barth, C. Paula, A. Kuhn, W. Schwieger, A. Mundstock, J. Caro, *M. Hartmann, Langmuir* 29 (2013) 8592–8600.
- [8] A. Mundstock, U. Böhme, B. Barth, M. Hartmann, J. Caro, *Chem. Ing. Tech.* 85 (2013) 1694–1699.
- [9] C. Chmelik, A. Mundstock, P.D.C. Dietzel, J. Caro, *Microporous Mesoporous Mater.* 183 (2014) 117–123.
- [10] J. Caro, M. Noack, *Microporous Mesoporous Mater.* 115 (2008) 215–233.
- [11] A. Tavaloro, E. Drioli, *Adv. Mater.* 11 (1999) 975–996.

- [12] E.E. McLeary, J.C. Jansen, F. Kapteijn, *Microporous Mesoporous Mater.* 90 (2006) 198–220.
- [13] Y.S. Yan, M.E. Davis, G.R. Gavalas, *Ind. Eng. Chem. Res.* 34 (1995) 1652–1661.
- [14] J.M. van de Graaf, E. van der Bijl, A. Stol, F. Kapteijn, J.A. Moulijn, *Ind. Eng. Chem. Res.* 37 (1998) 4071–4083.
- [15] A. Huang, F. Liang, F. Steinbach, T.M. Gesing, J. Caro, *J. Am. Chem. Soc.* 132 (2010) 2140–2141.
- [16] A. Huang, J. Caro, *Chem. Commun.* 46 (2010) 7748–7775.
- [17] K. Kuskabe, T. Kuroda, A. Murata, S. Morooka, *Ind. Eng. Chem. Res.* 36 (1997) 649–655.
- [18] V. Nikolakis, G. Xomeritakis, A. Abibi, M. Dickerson, M. Tsapatsis, D.G. Vlachos, *J. Membr. Sci.* 184 (2001) 209–219.
- [19] K. Sato, K. Aoki, K. Sugimoto, K. Izumi, S. Inoue, J. Saito, S. Ikeda, T. Nakane, *Microporous Mesoporous Mater.* 115 (2008) 184–188.
- [20] T. Gallego-Lizon, E. Edwards, G. Lobiundo, L.F. Santos, *J. Membr. Sci.* 197 (2002) 309–319.
- [21] A. Uritaga, E.D. Gorri, C. Casado, I. Ortiz, *Sep. Purif. Technol.* 32 (2003) 207–213.
- [22] X. Wang, Y. Chen, C. Zhang, X. Gu, N. Xu, *J. Membr. Sci.* 455 (2014) 294–304.
- [23] X. Wang, Z. Yang, C. Yu, L. Yin, C. Zhang, X. Gu, *Microporous Mesoporous Mater.* 197 (2014) 17–25.
- [24] B.H. Jeong, Y. Hasegawa, K.I. Sotowa, K. Kuskabe, S. Morooka, *J. Chem. Eng. Jpn.* 35 (2002) 167–172.
- [25] G. Zhu, Y. Li, H. Zhou, J. Liu, W. Yang, *J. Membr. Sci.* 337 (2009) 47–54.
- [26] Q. Liu, N. Wang, J. Caro, A. Huang, *J. Am. Chem. Soc.* 135 (2013) 17679–17682.
- [27] H. Lee, J. Rho, P.B. Messerschmith, *Adv. Mater.* 21 (2009) 431–434.
- [28] D. Ling, W. Park, Y.I. Park, N. Lee, F. Li, C. Song, S.G. Yang, S.H. Choi, K. Na, T. Hyeon, *Angew. Chem. Int. Ed.* 50 (2011) 11360–11365.
- [29] F. Pan, H. Jia, S. Qiao, Z. Jiang, J. Wang, B. Wang, Y. Zhong, *J. Membr. Sci.* 341 (2009) 279–285.
- [30] H. Lee, S.M. Dellatore, W.M. Miller, P.B. Messerschmith, *Science* 318 (2007) 426–430.
- [31] A. Huang, N. Wang, J. Caro, *J. Membr. Sci.* 389 (2012) 272–279.
- [32] A. Huang, F. Liang, F. Steinbach, J. Caro, *J. Membr. Sci.* 350 (2010) 5–9.
- [33] R. Lui, M. Mahurin, C. Li, R.R. Unocic, H.J. Gao, S.J. Pennycook, S. Dai, *Angew. Chem. Int. Ed.* 50 (2011) 6799–6802.
- [34] C. Chmelik, H. Bux, H. Voß, J. Caro, *Chem. Ing. Tech.* 83 (2011) 104–112.
- [35] H. Bux, C. Chmelik, R. Krishna, J. Caro, *J. Membr. Sci.* 369 (2011) 284–289.
- [36] R. Krishna, *J. Phys. Chem. C* 113 (2009) 19756–19781.
- [37] A. van Miltenburg, J. Gascon, W. Zhu, F. Kapteijn, J.A. Moulijn, *Adsorption* 14 (2008) 309–321.
- [38] F.A. Da Silva, A.E. Rodrigues, *Ind. Eng. Chem. Res.* 38 (1999) 2051–2057.
- [39] N. Lamia, M.A. Granato, P. Gomes, C.A. Grande, L. Wolff, P. Leflaive, D. Leinekugel-le-Cocq, A.E. Rodrigues, *Sep. Sci. Technol.* 44 (2009) 1485–1509.
- [40] Y.-H. Huang, J.W. Johnson, A.I. Liapis, O.K. Cresser, *Sep. Technol.* 4 (1994) 165–166.
- [41] J. Kärger, D.M. Ruthven, *Diffusion in Zeolites and Other Microporous Solids*, Wiley, New York, 1992.
- [42] M. Gratz, M. Wehring, P. Galvosas, F. Stellmach, *Microporous Mesoporous Mater.* 125 (2009) 30–34.
- [43] A. Malka-Edery, K. Abdalla, P. Grenier, F. Meunier, *Adsorption* 7 (2001) 17–25.
- [44] R.W. Baker, *Membrane Technology in the Chemical Industry*, Wiley-VCH, 2006.
- [45] F.A. Da Silva, A.E. Rodrigues, *AIChE J.* 47 (2001) 341–357.
- [46] D. Song, Y.S. Kang, S.W. Kang, *J. Membr. Sci.* 474 (2015) 273–276.
- [47] X. Ma, B.K. Lin, X. Wei, J. Knief, Y.S. Lin, *Ind. Eng. Chem. Res.* 52 (2013) 4296–4305.
- [48] H.T. Kwon, H.-K. Jeong, *Chem. Eng. Sci.* 124 (2015) 20–26.
- [49] E. Matsuyama, A. Ikeda, M. Sasaki, M. Nomura, *Sep. Purif. Technol.* 128 (2014) 25–30.
- [50] C. Algieri, P. Bernado, G. Golemme, G. Barbieri, E. Drioli, *J. Membr. Sci.* 222 (2003) 181–190.
- [51] A. Huang, J. Caro, *J. Mater. Chem.* 21 (2011) 11424–11429.
- [52] J. Caro, D. Albrecht, M. Noack, *Sep. Purif. Technol.* 66 (2009) 143–147.

### III. Material Optimizations and their Impact on the H<sub>2</sub>/CO<sub>2</sub> Separation Capability

Not having to "reinvent the wheel" every time a newish problem needs solving has always had a certain appeal and the perfect proof for this is the field of zeolite/MOF membrane-based gas separation with its brimming toolbox of pre- (e.g. support functionalization) as well as post-synthetic (ion exchange, introduction of new functional groups, composites etc.) material optimizations, some of whose direct effect on the hydrogen/carbon dioxide selectivity will be addressed in the two publications featured in the present chapter.

The first one uses a series of type X-built/containing layer systems, ranging from neat crystalline films grown on un- as well as pre-modified (APTES or PDA) Al<sub>2</sub>O<sub>3</sub> supports over sandwich composites crowned by polymeric (Matrimid) covers to full-fledged MMIMs, and their respective separation capabilities towards H<sub>2</sub>/CO<sub>2</sub> to illustrate that, despite the zeolites' fundamental lack of functionalization points like e.g. organic framework components, improvement through adaptation is still feasible even for the long-known "boiling stones". Special attention was paid to the mobile counterions (Na<sup>+</sup> in the initial state) within the FAU structure, or rather the possibility to create several more selective powder variants by simply exchanging them (PbX, CuX, NiX and CoX → higher ionic potential = stronger CO<sub>2</sub> interaction/adsorption), which were then subsequently used as fillers in novel Matrimid-based mixed matrix membranes. All the work related to zeolite membrane/powder preparation, support functionalization, ion exchange, XRD/SEM characterization and permeation measurements as well as the writing of this article were done by the author. Dr. Sebastian Friebe fabricated the mixed matrix/multilayer membranes, conducted the EDXS experiment and helped with the evaluation of the gas separation results. Thanks to Prof. Dr. Jürgen Caro's resourcefulness, the paper constantly evolved and finally found its way to the right journal.

MOF-74's most important asset when it comes to separation issues, on the other hand, are its coordinatively unsaturated metal centers since they not only constitute a gas interaction point but also a highly reactive functionalization hot spot, demonstrated and utilized in the second study by post-synthetically introducing amino groups (via ethylenediamine) into the wide 1D channels of a membrane made from the Mg variant. The resulting optimized material, which was additionally grown on MgO-seeded supports to minimize defects, possesses a greatly improved H<sub>2</sub>/CO<sub>2</sub> selectivity in comparison to unmodified Mg-MOF-74 layers due to a combination of very strong host-guest interactions (-NH<sub>2</sub> ↔ CO<sub>2</sub>) and reduced effective pore size. Dr. Nanyi Wang performed all the membrane preparations/functionalizations, XRD/SEM/IR experiments and permeation measurements as well as wrote the paper. She was assisted by the author of this thesis, who helped with developing/improving the synthesis methods, data interpretation, image editing and the writing process. Professors Yi Liu and Aisheng Huang used their extensive combined firsthand knowledge



about gas separation, MOFs and their modification to further improve the manuscript. Additional guidance and support during the whole creative process (planning/executing/writing) came from Prof. Dr. Jürgen Caro.

---

### III On comparing Permeation through Matrimid-Based Mixed Matrix and Multilayer Sandwich FAU Membranes: H<sub>2</sub>/CO<sub>2</sub> Separation, Support Functionalization and Ion Exchange

A. Mundstock, S. Friebe, J. Caro

*International Journal of Hydrogen Energy*, 42, **2017**, 279 - 288.

---



ELSEVIER

Available online at [www.sciencedirect.com](http://www.sciencedirect.com)

ScienceDirect

journal homepage: [www.elsevier.com/locate/he](http://www.elsevier.com/locate/he)

# On comparing permeation through Matrimid<sup>®</sup>-based mixed matrix and multilayer sandwich FAU membranes: H<sub>2</sub>/CO<sub>2</sub> separation, support functionalization and ion exchange

Alexander Mundstock<sup>\*\*</sup>, Sebastian Friebe, Jürgen Caro<sup>\*</sup>

Institute of Physical Chemistry and Electrochemistry, Leibniz University Hannover, Callinstr. 3A, 30167 Hannover, Germany

## ARTICLE INFO

### Article history:

Received 19 April 2016

Received in revised form

31 August 2016

Accepted 15 October 2016

Available online 9 December 2016

### Keywords:

H<sub>2</sub>/CO<sub>2</sub> separationFAU/Matrimid<sup>®</sup> MMMs

Ion exchange

FAU membrane

Support modification

## ABSTRACT

A series of supported membranes with zeolite FAU either as a thin layer or as powder in Matrimid as Mixed Matrix Membrane (MMM) have been prepared and evaluated in the H<sub>2</sub>/CO<sub>2</sub> separation. In addition to neat NaX membrane layers, we developed two novel composite materials, namely FAU/Matrimid<sup>®</sup> Mixed Matrix Membranes (MMMs) as well as NaX/Matrimid<sup>®</sup> multilayer/sandwich membranes, all of them supported by porous alumina plates. The influence of different pre-synthetic support modifications (APTES = 3-aminopropyltriethoxysilane, PDA = polydopamine) on the quality of neat supported NaX membranes grown as layer on these modified supports has been investigated studying the H<sub>2</sub>/CO<sub>2</sub> separation performance. It could be shown that NaX membrane layers grown on modified supports show a remarkably increased quality and correspondingly higher H<sub>2</sub>/CO<sub>2</sub> separation factors  $\alpha$  (H<sub>2</sub>/CO<sub>2</sub>) ( $\alpha$  = 8.0 for neat NaX,  $\alpha$  = 8.9 for NaX/APTES and  $\alpha$  = 10.3 for NaX/PDA). In the preparation of MMMs, the separation performance could be improved by ion exchanged Na-FAU powders. Exchanging the Na<sup>+</sup> of the as-synthesized NaX particles for metal ions with higher ionic potentials like Co<sup>2+</sup>, results in enhanced mixed gas separation factors  $\alpha$  in the H<sub>2</sub>/CO<sub>2</sub> separation (NaX/Matrimid<sup>®</sup> MMM  $\alpha$  = 4.0 and CoX/Matrimid<sup>®</sup> MMM  $\alpha$  = 5.6).

© 2016 Hydrogen Energy Publications LLC. Published by Elsevier Ltd. All rights reserved.

## Introduction

In academic literature one can find a wide variety of CO<sub>2</sub>- and H<sub>2</sub>-selective membranes for syngas purification at different pressures like e.g. FAU [1], ZIF-8/Matrimid<sup>®</sup> Mixed Matrix Membranes (MMM) [2] and polyvinylalcohol-polysiloxan/

fumed silica MMMs [3], but their problems are insufficient selectivity and/or stability. Prominent examples for this issue are palladium based membranes, which are known for permeating H<sub>2</sub> at an almost infinite selectivity [4]. However, they suffer from sulfur poisoning, hydrogen embrittlement and the difficult scale up of [5]. These problems triggered

\* Corresponding author. Fax: +49 51176219121.

\*\* Corresponding author. Fax: +49 51176219121.

E-mail addresses: [alexander.mundstock@pci.uni-hannover.de](mailto:alexander.mundstock@pci.uni-hannover.de) (A. Mundstock), [Juergen.caro@pci.uni-hannover.de](mailto:Juergen.caro@pci.uni-hannover.de) (J. Caro).  
<http://dx.doi.org/10.1016/j.ijhydene.2016.10.161>

0360-3199/© 2016 Hydrogen Energy Publications LLC. Published by Elsevier Ltd. All rights reserved.

increased research and development efforts towards alternative materials with a special focus on polymers and MMMs [1,6,7]. Even though the polymers show lower selectivities than inorganic membranes, their commercially far more viable upscalability, high degree of variability (different polymers/fillers) and high mechanical-/pressure-stability more than compensate for this. Especially MMMs ingeniously combine the processability of polymers and the superior gas separation properties of inorganic materials. The key challenge now is to find the right materials.

One of the more promising candidates is zeolite faujasite (FAU) – either as filler in MMM or as supported membrane layer. Zeolite FAU is usually synthesized as NaX with Si/Al ratio of 1.2–1.5. Consisting of sodalite cages which are connected through hexagonal prisms, NaX features 12-membered oxygen ring pores (pore diameter  $\approx 7.4$  Å) in a 3D pore system. Of special interest for a desired  $H_2/CO_2$  separation are metal ions in the activated de-hydrated state ( $CO_2$  - ion interactions), the possibility of an ion exchange (e.g.  $Co^{2+}$ ,  $Ni^{2+}$ ,  $Cu^{2+}$ ), high gas capacity as well as the overall high stability (chemical, thermal) inherent to zeolites. Potential applications for supported NaX membranes are e.g.  $H_2/CO_2$  separation [1], propane/propene separation [8], dehydration of organic solvents by steam permeation [9] and separating large molecules which cannot be handled by other zeolite membranes [10,11]. Growing neat, phase-pure dense NaX membranes without cracks, pinholes or other defects is very demanding due to inhomogeneous nucleation on the support surface and the electrostatic rejection between the negatively charged precursor species and the often used alumina ( $\alpha-Al_2O_3$ ) supports [1,8]. This problem can be solved by pre-synthetic support surface modifications with “molecular binders” like e.g. polydopamine (PDA) [1,12] and 3-aminopropyltriethoxysilane (APTES) [1,8]. Both serve as molecular binder to chemically anchor NaX precursors on the support surface during hydrothermal synthesis, resulting in dense and phase-pure zeolite membranes. In this work, to get a complete picture, we evaluated both, the impact of these modifications on the membrane quality as well as on the  $H_2/CO_2$  separation capabilities of supported NaX membranes.

Among the polymers frequently used for commercial gas separation (e.g. polysulfones, polycarbonates, poly(arylethers), poly(arylketones) [13,14]), polyimides are of particular interest because of their high chemical, thermal and mechanical stability and high gas selectivity [15,16]. Especially Matrimid<sup>®</sup>, one of the most frequently studied polyimides, shows permeability and selectivity properties falling close to upper bound regions of various Robeson plots [17,18]. Therefore, Matrimid<sup>®</sup> is a suitable basis for MMMs with different filler materials e.g. carbon molecular sieves [19], carbon nanotubes [20] as well as metal–organic frameworks [21,22] which have been implemented so far for various tasks, including the  $H_2/CO_2$  separation [2,6,7,23]. Recent progress in ZIF-enabled membranes and the barriers that must be overcome to advance ZIF-enabled membranes beyond the laboratory level are discussed in the reviews [24,25]. In this work we prepared and evaluated novel FAU/Matrimid<sup>®</sup> MMMs using ion exchanged FAU particles as inorganic filler and investigated their impact/influence on the  $H_2/CO_2$  separation performance.

Recently, there have been reports on how coating ZIF (–8 and –90) membranes with an additional Matrimid<sup>®</sup> top layers dramatically increases their  $H_2/CH_4$  selectivity [26]. This improvement is most likely due to a suppressed linker distortion in the ZIF/polymer contact zone and the accompanying enhanced sieving capabilities. To verify whether a similar enhancement can be achieved in the case of zeolite membranes, maybe due to a “defect healing” or synergistic effects, we additionally coated several of the NaX/PDA membranes with a layer of neat Matrimid<sup>®</sup> and measured the  $H_2/CO_2$  separation capabilities of this multilayer/sandwich membrane.

## Experimental

Unless otherwise noted, all procedures were performed under ambient atmosphere. All reagents were obtained from commercial vendors at reagent grade purity or higher and used without further purification.

Depending on the task at hand, two different kinds of porous  $\alpha-Al_2O_3$  supports (Fraunhofer IKTS Hermsdorf, diameter  $d = 18$  mm, thickness  $h = 1$  mm) have been used in this work, featuring either a medium top layer pore diameter of  $d_{50} = 2.5$   $\mu m$  (called rough/large-pored (r)) or  $d_{50} = 70$  nm (called fine/fine-pored (f)).

### Support modifications

As described in the following, the supports (f) with the fine top layer have been functionalized by APTES and PDA:

- (i) 3-aminopropyltriethoxysilane (APTES) functionalized  $\alpha-Al_2O_3$  supports were prepared according to a previously reported [27] but slightly modified procedure. Two of the porous supports were placed in an APTES (460 mg) toluene (10 mL) mixture within a sealable reaction vial (Schott Duran Bottle) and heated up to 120 °C for 30 min. After subsequently drying in an oven at 60 °C for about 20 min and cooling down in ambient air, the modified supports were ready for further utilization.
- (ii) Polydopamine (PDA) functionalized  $\alpha-Al_2O_3$  supports were also prepared according to a published procedure [28]. Dopamine (DPA) (2 mg/mL) was completely dissolved in 50 mL of 10 mM Tris–HCl (pH 8.5) in an open watch glass ( $d = 180$  mm). The neat supports were simply immersed in this buffered aqueous solution for 24 h at room temperature under continuous stirring. After drying in the ambient atmosphere, the now dark brown supports were used for further membrane preparations.

### Preparation of supported NaX and multilayer sandwich membranes

The crystallization of NaX membrane layers on the modified as well as unmodified  $\alpha-Al_2O_3$  supports has been achieved by following a previously reported but again slightly modified procedure by Huang et al. [27]. A synthesis solution with a

specific molar ratio of  $70\text{Na}_2\text{O}:1\text{Al}_2\text{O}_3:20\text{SiO}_2:2000\text{H}_2\text{O}$  was prepared by mixing a silicate and an aluminate solution at room temperature. The latter one was obtained by dissolving 7.78 g sodium hydroxide (>99%, Merck) and 0.075 g of aluminum foil (Fisher Scientific) as Al source in 25 g deionized water in a sealable reaction vial under stirring. In a second vial the silicate solution was prepared by mixing 4.17 g LUDOX AS-40 colloidal silica (40%  $\text{SiO}_2$  in water, Aldrich) as Si source and 22.22 g deionized water. The resulting solution was then vigorously stirred for 2 h at 60 °C. After this period of time the still hot silicate solution was poured into the aluminum solution and the resulting mixture was stirred in the closed vial at room temperature till a colorless, clear and homogeneous solution was obtained (ca. 12 h). This was then transferred into a Teflon-lined stainless steel autoclave (Parr Instruments Germany). The treated or non-treated  $\alpha\text{-Al}_2\text{O}_3$  supports were jammed into special Teflon-holders and placed face down in the autoclave/solution too. After in situ growth for 24 h at 75 °C in an oven, the solution was decanted of and the resulting membranes were transferred into a sealed vial filled with deionized water for 24 h (washing step). Subsequently they were dried in ambient air at 60 °C in an air conditioned oven for about 2 h. In this membrane synthesis, also NaX powder has been formed which sedimented at the bottom of the autoclave. This powder has been used for ion exchange and MMM preparation.

The preparation of the FAU sandwich membranes was done as follows. First of all Matrimid® 5218 was solved in Dichloromethane. This mixture was stirred overnight and sonicated at the following day to remove air bubbles. After the sonification, the polymer solution was casted on top of the neat FAU membrane with the help of an Eppendorf pipette. This sandwich membrane was stored under dichloromethane atmosphere and activated as described below.

#### **Ion exchange of NaX powder for MMM preparation**

All ion exchanges were done, respectively, with Cobalt (II) nitrate hexahydrate, Nickel (II) nitrate hexahydrate, Copper (II) nitrate trihydrate and Lead (II) nitrate as “ion sources”.

The liquid state ion exchanges were done by suspending the FAU powders (100 mg each) in an aqueous solution of the metal salts (100 mg of salt in 20 ml distilled water) for 24 h at room temperature. Afterward, the solutions were decanted, and the powders were washed with water a few times and dried in an oven at 60 °C for 2 h.

#### **Preparation of supported mixed matrix membranes (MMM) with ion exchanged FAU powder**

The supported Mixed Matrix Membranes (MMMs) were produced by a simple casting approach. Therefore, the Matrimid® 5218 and the dried (still hydrated) ion-exchanged FAU ( $\text{Na}^+$ ,  $\text{Pb}^{2+}$ ,  $\text{Co}^{2+}$ ,  $\text{Ni}^{2+}$ ,  $\text{Cu}^{2+}$ ) powders (10 wt%) were weighed in a glass bottle. After that 1 mL Dichloromethane was added, the glass bottle was closed and the resulting mixture was stirred overnight. At the following day the mixture was casted on a rough  $\alpha\text{-Al}_2\text{O}_3$  support (2.5  $\mu\text{m}$  pores; Fraunhofer IKTS, former Hermsdorfer HITK, Germany) with the help of an Eppendorf pipette. After casting, the MMMs were stored in an

atmosphere of Dichloromethane to allow a slow solvent evaporation. At the end the membranes were activated at 180 °C in vacuum for several hours and subsequently stored in a glove box (Ar).

#### **Activation and permeation measurements**

A full dehydration/activation of membranes and powders was achieved by heating (180 °C) under vacuum over 2 h followed by storage in a sealed Schlenk flask in a glove box (Ar). The assembly of the permeation cells, including the mounting of the membranes, was done under protective gas atmosphere within the glove box.

For the actual permeation measurements, the assembled cells were transferred to sealable vials filled with argon and discharged from the glove box. The installation into the permeation apparatus took place under a nitrogen current to prevent a deactivation of the membranes. All permeation measurements carried out for this work, single gas as well as equimolar  $\text{H}_2/\text{CO}_2$  mixtures, were done with a modified Wicke-Kallenbach-apparatus at room temperature following the Wicke Kallenbach principle with equal gas pressure on feed and permeate side of the membrane. As feed we used an equimolar 50 ml/min stream (25 mL  $\text{H}_2$  and 25 mL  $\text{CO}_2$ ). As sweep we used  $\text{N}_2$  with a flow rate of 50 ml/min. Since the flux of the polymer-based MMMs is only 1/50 of the flux of the neat NaX membrane, the sweep gas rate was adjusted accordingly (1 ml/min  $\text{N}_2$  for polymer-based membranes).

#### **XRD and SEM**

The XRD patterns of the Na-X samples (powder and membranes) were obtained on a Bruker D8 Advance X-ray Diffractometer using  $\text{Cu K}_\alpha$  ( $\lambda = 1.54 \text{ \AA}$ ) radiation. All shown Scanning Electron Microscopy (SEM) micrographs were taken on a JEOL JSM-6700F with a cold field emission gun operating at 2 kV and 10  $\mu\text{A}$ .

## **Results and discussion**

#### **Support modification by APTES and PDA, NaX membrane layer preparation**

As shown in a previous paper [8], there are huge problems to prepare defect-free NaX membranes on our standard  $\alpha\text{-Al}_2\text{O}_3$  supports – even when using identical synthesis protocols. All NaX membrane preparations on the neat supports resulted in a ca. 2  $\mu\text{m}$  thick and defect-rich membrane layer. These defects include all kinds of cracks, pinholes and other flaws which are counter-productive for gas separation and stem most probably from the electrostatic rejection between the negatively charged NaX precursor macro molecules ( $\approx -43 \text{ mV}$  [8]) and the also negatively charged  $\alpha\text{-alumina}$  ( $\approx -32 \text{ mV}$  [8]) support at the pH 11 (NaX preparation condition) as for the first time shown by our group in Refs. [1,8]. The quantity and quality of the defect occurrence seems to be highly erratic, what results in the widely fluctuating membrane quality mentioned above. Eventually, only approximately 1 out of 10 preparations resulted in relatively dense

neat NaX membranes, which were used for the permeation studies in this work (Table 1).

In comparison, all membranes grown on Al<sub>2</sub>O<sub>3</sub> supports which had been pre-synthetically functionalized with APTES (from now on called NaX/APTES) are dense and nearly defect-free (no cracks, pinholes or other defects could be observed, see Fig. 1A). This is most probably due to the fact that APTES-modified  $\alpha$ -Al<sub>2</sub>O<sub>3</sub> has, in stark contrast to the unmodified/neat material, a nearly neutral surface charge (Zeta potential of APTES/Al<sub>2</sub>O<sub>3</sub>  $\approx$  -3 mV at pH 11 [8]), minimizing the electrostatic rejection between the negatively charged FAU precursor species and the modified Al<sub>2</sub>O<sub>3</sub> support. This then greatly benefits the homogeneous nucleation and growth of the Na-X membranes and, subsequently, their capability for separating H<sub>2</sub> from CO<sub>2</sub> and results also in a slightly thicker (ca. 3  $\mu$ m) NaX layer.

Also support modification by a PDA layer was successful. A little bit contradictory at the first glance is that an enhanced membrane quality (Fig. 1B) and the improved H<sub>2</sub>/CO<sub>2</sub> selectivity (Table 1) are achieved despite the Al<sub>2</sub>O<sub>3</sub>/PDAs highly negative Zeta potential ( $\approx$  -43 mV at pH 11 [8]) and the subsequent electrostatic rejection between the modified support and NaX, which is even higher than the one between the neat support and the NaX zeolite. The positive effect of PDA coating of the support for the subsequent growth of the NaX layer is probably due to one of PDAs special features, namely the ability to chelate metal ions. Along with the abundance of metal ions within the synthesis solution, which enables PDA to effectively shield its charge and consequently minimize or even equalize the otherwise disruptive electrostatic forces between the functionalized support and the charged FAU precursor species. Because most of the chelated metal ions are also NaX building blocks, the functionalized support surface now additionally features more direct nucleation points for the zeolite layer growth. Together, these two phenomena facilitate an unobstructed growth and almost defect-free membranes [8].

The NaX powder, later on used for ion exchange and MMM preparations, was obtained as a sedimentation by-product from the membrane syntheses. It consists of polycrystalline microparticles with a size range of  $\approx$  1–4  $\mu$ m (diameter) which are distinguished by their high crystallinity and overall quality, as proven by accompanying XRD measurements (Fig. 3 black line).

#### Multilayer membrane preparation

The preparation of the multilayer sandwich membranes, consisting of an NaX membrane layer grown on a PDA-

functionalized support and subsequently covered with a Matrimid<sup>®</sup> layer, turned out to be rather challenging due to a lack of interaction between polymer and zeolite. In most cases, the Matrimid<sup>®</sup> cover completely peels off from the supported NaX membrane during the drying, thus partially damaging the latter in the process. Various adjustments to the polymer casting procedure eventually enabled us to prepare several intact multilayer sandwich membranes of the desired composition, as shown in Fig. 2A.

The greatly differing thickness of the individual layers (crystalline NaX  $\approx$  2–3  $\mu$ m and Matrimid<sup>®</sup>  $\approx$  10–15  $\mu$ m) is due to the applied preparation techniques and their accompanying problems as described earlier. Fig. 2B shows that, despite the improved casting procedure, the overall adherence between polymer and zeolite layers is still limited to a small number of “anchor points” scattered throughout the “cavernous” border region. Obviously, the inorganic NaX layer and the Matrimid<sup>®</sup> – despite the latter's hydrophilicity – do not match. This finding differs from known published results which showed that polymer coatings easily adhere on MOF (Metal–Organic Framework) layers [26].

The mentioned few “anchor points” (see Fig. 2B left side), where a much better interaction between zeolite and polymer can be found, are possibly due to small defects (cracks and pinholes) and impurities within the surface of the zeolite membrane. Those “former” defect sites, now sealed by a plug of Matrimid<sup>®</sup>, could provide a better “grip” for the polymer (e.g. a filled crack) and consequently a much needed minimum of interaction between the two layers.

#### Ion exchange of the NaX powder for MMM preparation

Ion exchanged FAU particles have been used as inorganic filler phase in mixed matrix membranes (MMM). The ion exchanged particles show, apart from the expected color changes according to the ion source, no significant changes in XRD patterns (Fig. 3). However, all ion exchanged FAU powders seem to suffer from a slight loss of crystallinity compared to the NaX source material, as indicated by the overall decrease in signal intensity, due to the forced exchange of monovalent sodium ions for multivalent metal ions.

#### Mixed matrix membrane preparation

The hydrated ion exchanged FAU powder crystals have been used as inorganic filler phase (10 wt%) in supported (pressure

**Table 1 – Mixed gas permeation data on supported (fine  $\alpha$ -Al<sub>2</sub>O<sub>3</sub>, top-layer pore  $d_{50}$  = 70 nm) for an equimolar H<sub>2</sub>/CO<sub>2</sub> mixture (Knudsen separation factor  $\approx$  4.7) at 1 bar (Wicke Kallenbach technique), room temperature and 50 ml/min N<sub>2</sub> sweep.**

Support	Al <sub>2</sub> O <sub>3</sub>	Al <sub>2</sub> O <sub>3</sub>	Al <sub>2</sub> O <sub>3</sub>	Al <sub>2</sub> O <sub>3</sub>	Al <sub>2</sub> O <sub>3</sub>	Al <sub>2</sub> O <sub>3</sub>
Modification	–	–	APTES	APTES	PDA	PDA
Membrane	–	NaX	–	NaX	–	NaX
Mixed gas $\alpha$ (H <sub>2</sub> /CO <sub>2</sub> )	4.6	8.0	5.7	8.9	6.3	10.3
Flux H <sub>2</sub> mL min <sup>-1</sup> cm <sup>-2</sup>	6.3	4.5	5.8	0.7	0.0042	0.09
Flux CO <sub>2</sub> mL min <sup>-1</sup> cm <sup>-2</sup>	1.4	0.6	1.0	0.08	0.0007	0.009
Permeance H <sub>2</sub> mol/m <sup>2</sup> s Pa	$4.4 \cdot 10^{-7}$	$3.1 \cdot 10^{-7}$	$4.0 \cdot 10^{-7}$	$5.1 \cdot 10^{-8}$	$2.9 \cdot 10^{-10}$	$6.4 \cdot 10^{-9}$
Permeance CO <sub>2</sub> mol/m <sup>2</sup> s Pa	$9.8 \cdot 10^{-8}$	$3.9 \cdot 10^{-8}$	$7.1 \cdot 10^{-8}$	$5.7 \cdot 10^{-9}$	$4.6 \cdot 10^{-11}$	$6.2 \cdot 10^{-10}$

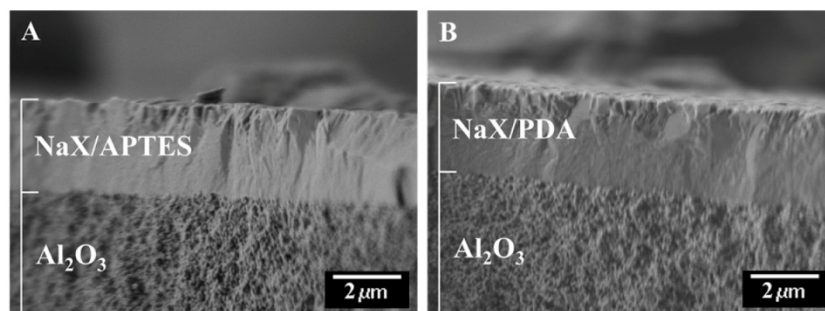


Fig. 1 – SEM cross sections of supported NaX membranes grown on  $\alpha$ -alumina supports which have been treated with (A) 3-aminopropyltriethoxysilane (APTES) and (B) with polydopamine (PDA).

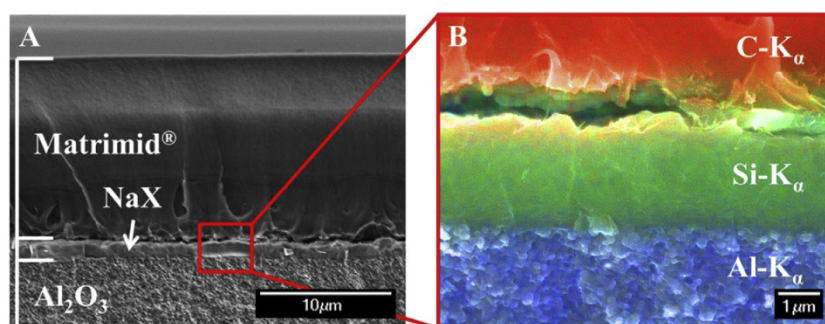


Fig. 2 – SEM images (A) of Matrimid<sup>®</sup>/FAU multilayer membrane and magnified cameo (EDX) (B) of the border regions.

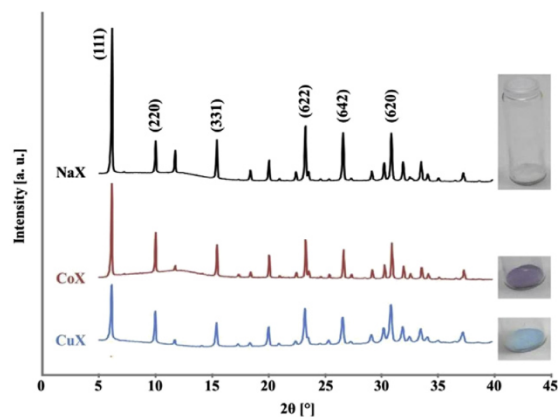


Fig. 3 – XRD patterns and photos of the original NaX as well as ion exchanged FAU powders (obtained by liquid state ion exchange). The hump at low  $2\theta$  angles is due to the amorphous plastic XRD sample holder.

stability) Matrimid<sup>®</sup>-based MMMs. The results of the MMM preparations (casting and drying), thin glassy looking polymer layers with distinct discolorations (compared to the pure yellow of neat Matrimid<sup>®</sup>) due to the differently colored embedded FAU particles on top of the white corundum supports, are shown in Fig. 4. At first glance, the particles appear to be evenly distributed over the entire area, with exception of the fringe.

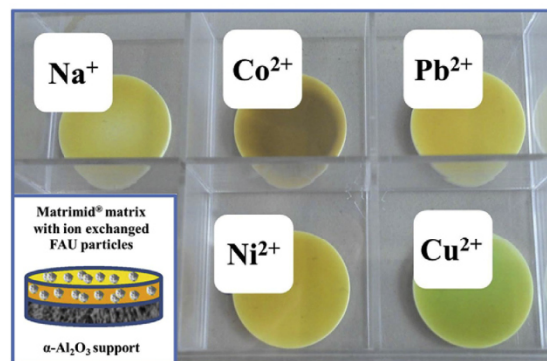


Fig. 4 – Photo of the Matrimid<sup>®</sup>-based MMMs prepared with ion exchanged FAU particles (10 wt%).

The average thickness of these casted MMM layers on top of the alumina support, as estimated respectively from several SEM cross section images, is around 100  $\mu\text{m}$ . Fig. 5 exemplarily shows the transitional area between loaded polymer layer and support for a CoX/Matrimid<sup>®</sup> MMM. The majority of the embedded FAU particles seem to be located at exactly that border (see Fig. 5A). This is probably due to the sedimentation by gravity forces during the long drying time (2 h).

The corresponding element map (Fig. 5B) is further proof that the performed ion exchange was successful. By utilizing the element distribution obtained via EDX measurements, we were additionally able to determine that, in the special case of

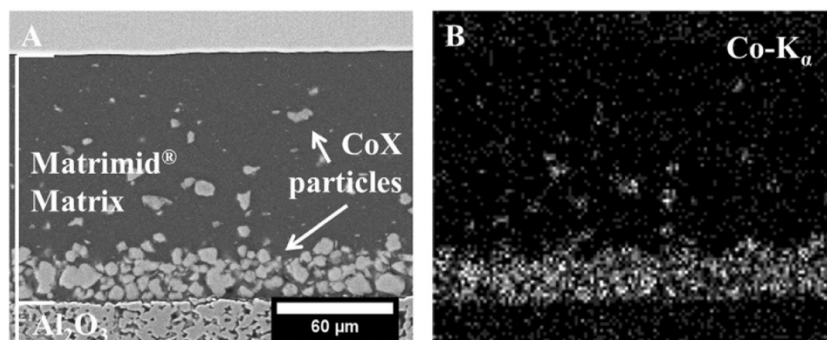


Fig. 5 – SEM image (A) of CoX/Matrimid® MMM and the corresponding Co element map (EDX) (B).

CoX as an example, around 75% of the initial Na<sup>+</sup> ions were exchanged with Co<sup>2+</sup> ion during the fluid state ion exchange (atomic % of Na<sup>+</sup> ≈ 0.28 and Co<sup>2+</sup> ≈ 0.41 after ion exchange). This value is in good agreement with literature data [29,30].

#### Permeation measurements on supported NaX and multilayer membranes

An examination of the results summarized in Table 1, regarding the mixed gas permeation studies done with supported NaX membranes, clearly reflects the known trend that APTES and PDA treatments of the support can not only decisively improve the quality of the resulting NaX membranes but also subsequently ensure a distinct improvement in the H<sub>2</sub>/CO<sub>2</sub> separation capability compared to the NaX

membranes grown on non-treated supports (e.g. Ref. [10]) (fine-pored α-Al<sub>2</sub>O<sub>3</sub> ceramic discs exhibit their own basic gas separation capability (Knudsen, see Table 1)). All membranes under study are hydrogen-selective, i.e. they more or less hold back the CO<sub>2</sub>, what is in accordance with the well-known rule of thumb: Permeation Selectivity ≈ Adsorption Selectivity × Diffusion Selectivity [1,31–34]. This behavior is basically due to the strong electrostatic potential of the FAU structure as well as the easily accessible site II (SII) sodium ions located near the six-membered oxygen rings, which are able to interact with various polar molecules [1,33]. In the special case of CO<sub>2</sub>, these adsorption complexes are due to quadrupole–monopole interactions between it and single unsaturated Na<sup>+</sup> ions within the super-cages of the activated FAU structure. A strong adsorption like this inevitably entails

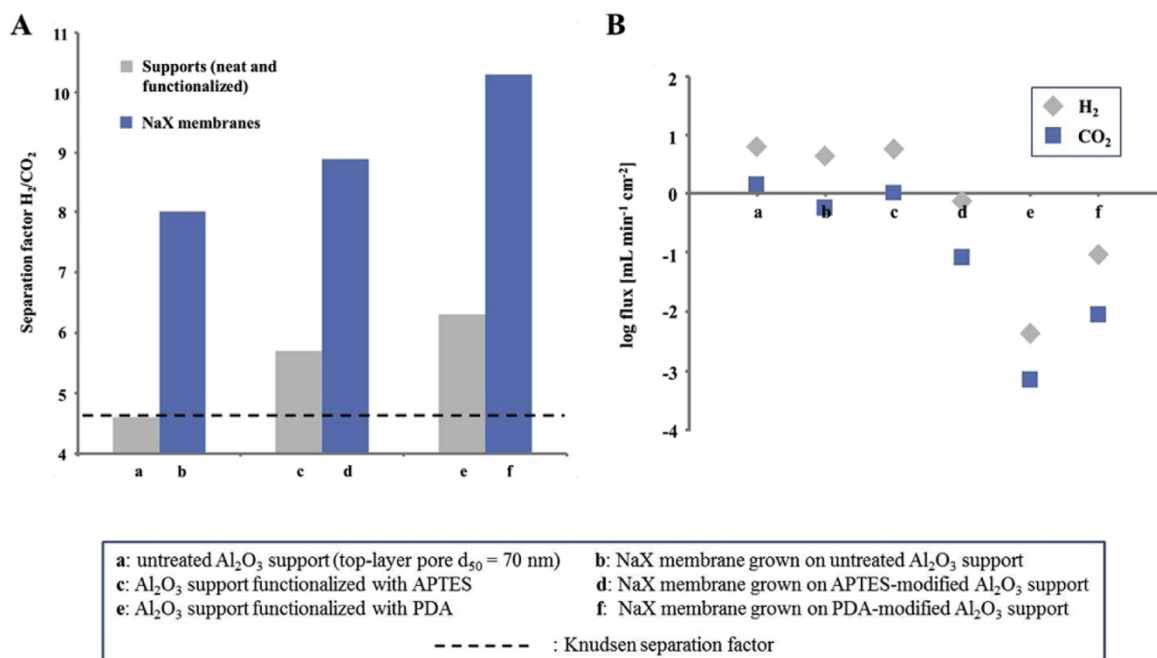


Fig. 6 – Neat supported NaX layer membranes prepared on the untreated as well as PDA and APTES functionalized supports in comparison with the untreated and modified supports without NaX layer: (A) H<sub>2</sub>/CO<sub>2</sub> mixed gas (50:50) separation factors (derived from Table 1), and (B) their H<sub>2</sub> and CO<sub>2</sub> mixed gas fluxes (derived from Table 1) in logarithmic representation.



**Table 2 – Mixed gas permeation data of supported (rough  $\alpha$ -Al<sub>2</sub>O<sub>3</sub>, pore  $d_{50} = 2.5 \mu\text{m}$  in top layer) Matrimid<sup>®</sup>-based MMMs (thickness  $\approx 100 \mu\text{m}$ ) containing ion exchanged MeX crystals for an equimolar H<sub>2</sub>/CO<sub>2</sub> mixture at 1 bar (Wicke Kallenbach technique), room temperature and 1 ml/min N<sub>2</sub> sweep.**

Support	Al <sub>2</sub> O <sub>3</sub>	Al <sub>2</sub> O <sub>3</sub>	Al <sub>2</sub> O <sub>3</sub>	Al <sub>2</sub> O <sub>3</sub>	Al <sub>2</sub> O <sub>3</sub>	Al <sub>2</sub> O <sub>3</sub>	Al <sub>2</sub> O <sub>3</sub>
Matrix	–	Matrimid <sup>®</sup>	Matrimid <sup>®</sup>	Matrimid <sup>®</sup>	Matrimid <sup>®</sup>	Matrimid <sup>®</sup>	Matrimid <sup>®</sup>
Filler	–	–	NaX	PbX	CuX	NiX	CoX
Mixed gas $\alpha$ (H <sub>2</sub> /CO <sub>2</sub> )	1.0	3.0	4.0	4.8	5.2	5.6	5.6
Permeance H <sub>2</sub> mol/m <sup>2</sup> s Pa	$4.8 \cdot 10^{-08}$	$5.7 \cdot 10^{-11}$	$1.7 \cdot 10^{-10}$	$7.1 \cdot 10^{-11}$	$9.8 \cdot 10^{-11}$	$8.7 \cdot 10^{-11}$	$7.7 \cdot 10^{-11}$
Permeance CO <sub>2</sub> mol/m <sup>2</sup> s Pa	$4.7 \cdot 10^{-08}$	$1.9 \cdot 10^{-11}$	$4.3 \cdot 10^{-11}$	$1.5 \cdot 10^{-11}$	$1.9 \cdot 10^{-11}$	$1.6 \cdot 10^{-11}$	$1.4 \cdot 10^{-11}$
Ionic radius <sup>a</sup>	–	–	Na <sup>+</sup>	Pb <sup>2+</sup>	Cu <sup>2+</sup>	Ni <sup>2+</sup>	Co <sup>2+</sup>
pm	–	–	102	119	73	69	75
Ionic potential	–	–	0.0098	0.0168	0.0274	0.0290	0.0267
e/pm	–	–	–	–	–	–	–

<sup>a</sup> Empirical ionic radii of the exchanged two-valent metal ions (coordination number 6, derived by the comparison of bond length in ionic, metallic and covalent crystals and molecules) [39].

a decreased diffusion, causing lower CO<sub>2</sub> permeation than found for other small molecules like H<sub>2</sub>, N<sub>2</sub> or CH<sub>4</sub> [1,35]. Besides these well-known one-on-one interactions (cation-CO<sub>2</sub>), CO<sub>2</sub> additionally seems to be able to simultaneously adsorb on two neighboring cations at once (cation-CO<sub>2</sub>-cation) [36,37], creating an even stronger adsorption.

All in all, NaX/PDA turned out to be the best supported FAU membrane for separating H<sub>2</sub> from CO<sub>2</sub> from the neat supported NaX membranes under study with a mixed gas separation factor ( $\alpha$  H<sub>2</sub>/CO<sub>2</sub>) of 10.3 (Table 1 and Fig. 6A), which is not only higher than the ones for neat supported NaX ( $\alpha$  (H<sub>2</sub>/CO<sub>2</sub>) = 8.0) and NaX/APTES ( $\alpha$  (H<sub>2</sub>/CO<sub>2</sub>) = 8.9), but also exceeds the known literature values (see Table 3). This superiority of Na-X/PDA is caused, on the one hand, by the improved membrane quality due to the PDA functionalization, as mentioned above. The second reason for the higher separation capabilities of NaX/PDA in comparison with the other membranes under study, is possibly the residual PDA within the support pores itself. As one can see in Table 1, even the PDA-modified support, without a NaX membrane layer grown on top, shows a clearly increased selectivity compared to the Knudsen separation factor of the microporous neat support. This phenomenon is most likely due to strong interactions between CO<sub>2</sub> and PDA (free amine groups [38]) on the one hand and a furthermore reduced CO<sub>2</sub> permeability because of the 1–2  $\mu\text{m}$  thick polymeric top layer (small chaotic pores) and narrowed top layer support pores (due to intruded PDA ( $d_{50} = 70 \text{ nm}$  without)) on the other hand. The latter two aspects are also responsible for the very low (lowest measured) fluxes (Fig. 6B).

While lacking the mentioned PDA top layer, which was dissolved during membrane preparation, NaX/PDA still features the PDA residue within the topmost support pores in addition to the highly selective zeolite membrane. This combination results in the high H<sub>2</sub>/CO<sub>2</sub> separation capability with  $\alpha$  (H<sub>2</sub>/CO<sub>2</sub>) = 10.3 and low fluxes.

The slightly improved gas separation capabilities of the APTES-modified support in comparison with the neat support can also be attributed to extra interactions between free amine groups and CO<sub>2</sub>. But in contrast to PDA, the APTES monolayer isn't able to seal hermetically the support pores.

This is clearly proven by the very similar gas fluxes through both supports (see Table 1 and a/c in Fig. 6B).

As mentioned before, the sole purpose of adding a Matrimid<sup>®</sup> top layer to the NaX/PDA membranes was to use possible “defect healing” effects like sealed cracks to further enhance their the H<sub>2</sub>/CO<sub>2</sub> separation performance. Unfortunately, adding a polymeric top layer nearly halved the separation factor (multilayer membrane  $\alpha$  (H<sub>2</sub>/CO<sub>2</sub>) = 5.4, see Table 3) compared to the starting membrane (NaX/PDA  $\alpha$  (H<sub>2</sub>/CO<sub>2</sub>) = 10.3) rather than increasing it. Possible explanations for this are the previously mentioned very weak interaction between Matrimid<sup>®</sup> and NaX as well as further defects in the zeolite membrane caused during the casting and drying/shrinking of the polymeric top layer. The “defect healing” could also have a negative effect in the form of not only sealing existent cracks and pinholes but also widening them in the process. The permeances of the multilayer membranes (H<sub>2</sub> =  $1.9 \cdot 10^{-10} \text{ mol/m}^2 \text{ s Pa}$ , see Table 3) are, as expected, lower than the ones of the starting NaX/PDA (H<sub>2</sub> =  $6.4 \cdot 10^{-9} \text{ mol/m}^2 \text{ s Pa}$ ) membranes due to the additional dense polymeric top layer.

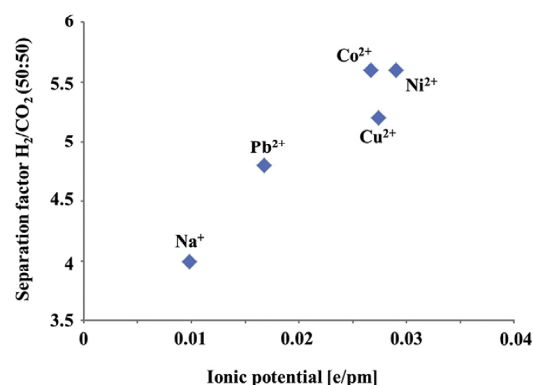


**Fig. 7 – Influence of the ionic potential (derived from Table 2) on the H<sub>2</sub>/CO<sub>2</sub> separation factor of Matrimid<sup>®</sup>-based MMMs containing different ion exchanged MeX particles as filler.**

### Permeation measurements on FAU/Matrimid<sup>®</sup> mixed matrix membranes

The second series of H<sub>2</sub>/CO<sub>2</sub> separation tests, this time performed with supported FAU/Matrimid<sup>®</sup> MMMs (large-pore  $\alpha$ -Al<sub>2</sub>O<sub>3</sub> ceramic discs without own gas separation capability (see Table 2)), clearly show, on the one hand, that the separation performance of the neat polymer Matrimid<sup>®</sup> can easily be enhanced by embedding NaX particles. On the other hand, one can see that using ion exchanged FAU particles (Pb<sup>2+</sup>, Co<sup>2+</sup>, Ni<sup>2+</sup>, Cu<sup>2+</sup>) instead of the source zeolite (Na<sup>+</sup>) to prepare those MMMs always (in all studied cases) resulted in improved separation capabilities (Table 2). These improvements in H<sub>2</sub>/CO<sub>2</sub> selectivity are anything but random and follow a clear trend:  $\alpha$  (H<sub>2</sub>/CO<sub>2</sub>): Na<sup>+</sup> < Pb<sup>2+</sup> < Cu<sup>2+</sup> < Ni<sup>2+</sup>  $\approx$  Co<sup>2+</sup>.

The decisive factor, which determines whether one ion exchanged FAU crystal is better suited for H<sub>2</sub>/CO<sub>2</sub> separation than another, seems to be the so called “ionic potential”. This indicator for the charge density at the surface of an ion (ionic charge/ionic radius see Table 2 and Fig. 7) provides evidence

for how strong the interaction between the ion in question and gases like CO<sub>2</sub> may be. In the special case of H<sub>2</sub>/CO<sub>2</sub> separation, this stronger interaction between carbon dioxide and the zeolite within the matrix in turn should induce a higher H<sub>2</sub> selectivity.

The veracity of this assumption is shown in Fig. 7. As one can see, the H<sub>2</sub>/CO<sub>2</sub> separation factor of the FAU/Matrimid<sup>®</sup> MMMs rises, as expected, with increasing ionic potential of the exchanged bivalent metal ions in the FAU filler, and ions with similar ionic potentials show comparable influences. Similar observations, but with other ions, have already been reported in the literature [37,40]. Due to the dense glassy Matrimid<sup>®</sup> matrix, all MMMs displayed very similar, regardless of the used ions within the inorganic phase, very low fluxes/permeances and comparable only with the PDA layer mentioned earlier (Table 2).

A comparison between the H<sub>2</sub>/CO<sub>2</sub> separation performances of our Matrimid<sup>®</sup>-based MMM and literature data shows that our approach is quite promising. Although our FAU/Matrimid MMM system is not quite the best yet in terms

**Table 3 – Comparison of H<sub>2</sub>/CO<sub>2</sub> separation performances of different supported membrane types.**

Membrane	Temperature °C	Feed pressure bar	Permeance H <sub>2</sub> mol/m <sup>2</sup> s Pa	Separation factor H <sub>2</sub> /CO <sub>2</sub>	Reference
Supported NaX <sup>a</sup>	20	1.0	6.4 · 10 <sup>-9</sup>	10.3	This study
Supported FAU <sup>b</sup>	100	1.0	5.0 · 10 <sup>-7</sup>	8.0 <sup>c</sup>	[1]
Supported LTA	20	1.0	2.3 · 10 <sup>-7</sup>	6.7	[41]
Supported MFI	25	3.0	7.9 · 10 <sup>-6</sup>	1.7	[42]
CoX/Matrimid <sup>®</sup> (10 wt% CoX)	20	1.0	7.7 · 10 <sup>-11</sup>	5.6	This study
MOF-5/Matrimid <sup>®</sup> (5 wt% MIL-53)	25	6.0	7.9 · 10 <sup>-11</sup>	0.9 <sup>b</sup>	[6]
MIL-53/Matrimid <sup>®</sup> (37.5 wt% MIL-53)	35	2.0	3.3 · 10 <sup>-10</sup>	2.0 <sup>b</sup>	[7]
ZIF-8/Matrimid <sup>®</sup> (60 wt% ZIF-8)	35	2.7	1.1 · 10 <sup>-10</sup>	7.0	[2]
Zeolite 4A/PDMS (40 wt% Zeolite 4A)	35	7.0	<sup>d</sup>	3.5 <sup>c</sup>	[43]
NaX/PDA with Matrimid <sup>®</sup> cover	20	1.0	1.9 · 10 <sup>-10</sup>	5.4	This study

<sup>a</sup> Prepared on PDA-modified supports.  
<sup>b</sup> Prepared on APTES-modified supports.  
<sup>c</sup> Ideal separation factor.  
<sup>d</sup> 10,000 Barrer.

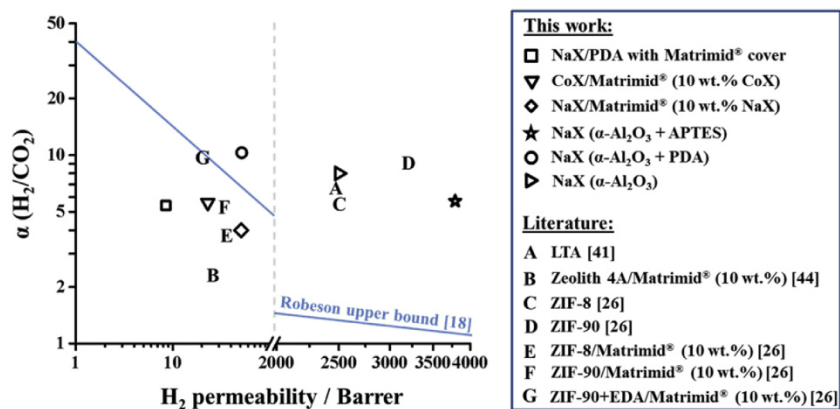


**Fig. 8 – Hydrogen permeabilities and separation factors  $\alpha$  (H<sub>2</sub>/CO<sub>2</sub>) for all membranes under study relative to an assortment of comparative membranes and the Robeson upper bound [18,44].**

of separation factor and permeance (see e.g. ZIF-8/Matrimid<sup>®</sup> in Table 3) it offers a lot of potential and room for improvement. Some possible ways to enhance the current separation performances are e.g. smaller FAU particles for a better distribution within the matrix, a higher ion exchange rate, higher particle crystallinity after ion exchange as well as an increased volume fraction of the inorganic phase within the matrix to maximize the occurring effects.

For an even better comparison and benchmarking of our membranes, we use the established Robeson plot [18]. It follows from Fig. 8 that some of our preparations are above the upper bound. In the field of high-permeability membranes, the NaX layer grown on APTES-modified alumina supports, as well as the NaX layer grown on the non-modified alumina supports show a much better performance than the existing polymers. The MMMs show medium permeability and medium H<sub>2</sub>/CO<sub>2</sub> selectivity, but their advantage is a cheap preparation and easy scale up.

## Conclusions

Different types of supported FAU membranes have been prepared: (i) neat NaX membrane layers on chemically supported Al<sub>2</sub>O<sub>3</sub> carriers, (ii) multilayer NaX/Matrimid<sup>®</sup> sandwich membranes, and (iii) FAU/Matrimid<sup>®</sup> Mixed Matrix Membranes (MMM). Said membranes have been evaluated in the H<sub>2</sub>/CO<sub>2</sub> separation. They all showed a certain H<sub>2</sub> selectivity, that is to say they hold back CO<sub>2</sub> because of differently pronounced internal interactions. We found that the NaX membrane quality highly depends on the kind of pre-synthetic alumina support functionalization (no treatment, APTES or PDA functionalization). Both PDA and APTES coating of the alumina supports result in higher selectivity of the FAU membrane and a better reproducibility of FAU membrane formation. Compared with the pure Matrimid<sup>®</sup>, the Matrimid<sup>®</sup>-based MMM containing 10 wt% cation exchanged FAU powder as filler showed an almost doubled mixed gas separation factor  $\alpha$  (H<sub>2</sub>/CO<sub>2</sub>), which seems to be proportional to the ionic potential of the ions in the FAU filler.

## Acknowledgements

Financial support by DFG priority program 1570 “Porous media with defined pore structure in chemical engineering – modeling, application, synthesis” (CA 147/17-1 and 2) (organized by F. Keil, TU Hamburg-Harburg) and by the EU for financing the project M<sup>4</sup>CO<sub>2</sub> (Energy efficient MOF-based mixed matrix membranes for CO<sub>2</sub> capture, organized by F. Kapteijn and J. Gascon, Delft) under the 7th Framework Program, Grant agreement No. 608490 is acknowledged.

## REFERENCES

- [1] Huang A, Wang N, Caro J. Seeding-free synthesis of dense zeolite FAU membranes on 3-aminopropyltriethoxysilane-functionalized alumina supports. *J Membr Sci* 2012;389:272–9.
- [2] Ordonez JC, Balkus KJ, Ferraris JP, Musselman IH. Molecular sieving realized with ZIF-8/Matrimid<sup>®</sup> mixed-matrix membranes. *J Membr Sci* 2010;361:28–37.
- [3] Xin R, Ho WSW. Crosslinked polyvinylalcohol–polysiloxane/fumed silica mixed matrix membranes containing amines for CO<sub>2</sub>/H<sub>2</sub> separation. *J Membr Sci* 2011;367:91–102.
- [4] Ramasubramanian K, Zhao Y, Ho WSW. CO<sub>2</sub> capture and H<sub>2</sub> purification: prospects for CO<sub>2</sub>-selective membrane processes. *AIChE J* 2013;59:1033–45.
- [5] Gabitto J, Tsouris C. Sulfur poisoning of metal membranes for hydrogen separation. *Int Rev Chem Eng* 2009;1:394–411.
- [6] Ren H, Jin J, Hu J, Liu H. Affinity between metal–organic frameworks and polyimides in asymmetric mixed matrix membranes for gas separations. *Ind Eng Chem Res* 2012;51:10156–64.
- [7] Hsieh JO, Balkus KJ, Ferraris JP, Musselman IH. MIL-53 frameworks in mixed-matrix membranes. *Micropor Mesopor Mater* 2014;196:165–74.
- [8] Mundstock A, Wang N, Friebe S, Caro J. Propane/propene permeation through Na-X membranes: the interplay of separation performance and pre-synthetic support functionalization. *Micropor Mesopor Mater* 2015;215:20–8.
- [9] Zhu G, Li Y, Zhou H, Liu J, Yang W. Microwave synthesis of high performance FAU-type zeolite membranes: optimization, characterization and pervaporation dehydration of alcohols. *J Membr Sci* 2009;337:47–54.
- [10] Nikolakis V, Xomeritakis G, Abibi A, Dickerson M, Tsapatsis M, Vlachos DG. Growth of a faujasite-type zeolite membrane and its application in the separation of saturated/unsaturated hydrocarbon mixtures. *J Membr Sci* 2001;184:209–19.
- [11] Jeong BH, Hasegawa Y, Sotowa KI, Kuskabe K, Morooka S. Separation of mixtures of benzene and n-alkanes using an FAU-type zeolite membrane. *J Chem Eng Jpn* 2002;35:167–72.
- [12] Lee H, Dellatore SM, Miller WM, Messerschmidt PB. Mussel-inspired surface chemistry for multifunctional coatings. *Science* 2007;318:426–30.
- [13] Robeson LM. Polymer membranes for gas separation. *Curr Opin Solid State Mater Sci* 1999;4:549–52.
- [14] Mohamad IN, Rohani R, Mastar@Mastar MS, Nor MTM, Jahim J Md. Permeation properties of polymeric membranes for biohydrogen purification. *Int J Hydrogen Energy* 2016;41:4474–88.
- [15] Ceceopieri-Gomez ML, Palacios-Alquisira J, Domingues JM. On the limits of gas separation in CO<sub>2</sub>/CH<sub>4</sub>, N<sub>2</sub>/CH<sub>4</sub> and CO<sub>2</sub>/N<sub>2</sub> binary mixtures using polyimide membranes. *J Membr Sci* 2007;293:53–65.
- [16] Powell CE, Qiao GG. Polymeric CO<sub>2</sub>/N<sub>2</sub> gas separation membranes for the capture of carbon dioxide from power plant flue gases. *J Membr Sci* 2006;211:1–49.
- [17] Lang LY, Chung T-S, Li DF, Cao C, Kulprathipanja S. Fabrication of Matrimid/polyethersulfone dual-layer hollow fiber membranes for gas separation. *J Membr Sci* 2004;240:91–103.
- [18] Robeson LM. The upper bound revisited. *J Membr Sci* 2008;320:390–400.
- [19] Vu DQ, Koros WJ, Miller SJ. Mixed matrix membranes using carbon molecular sieves: I. Preparation and experimental results. *J Membr Sci* 2003;211:311–34.
- [20] Kim S, Chen L, Johnson JK, Marand E. Polysulfone and functionalized carbon nanotube mixed matrix membranes for gas separation: theory and experiment. *J Membr Sci* 2007;284:147–58.
- [21] Zhang Y, Musselman IH, Ferraris JP, Balkus Jr KJ. Gas permeability properties of Matrimid<sup>®</sup> membranes containing

- the metal-organic framework Cu–BPY–HFS. *J Membr Sci* 2008;170–81.
- [22] Fan H, Xia H, Kong C, Chen L. Synthesis of thin amine-functionalized MIL-53 membrane with high hydrogen permeability. *Int J Hydrogen Energy* 2013;38:10795–801.
- [23] Abedini R, Omidkhah M, Dorosti F. Hydrogen separation and purification with poly (4-methyl-1-pentyne)/MIL 53 mixed matrix membrane based on reverse selectivity. *Int J Hydrogen Energy* 2014;39:7897–909.
- [24] Seoane B, Coronas J, Gascon I, Benavides ME, Karvan O, Caro J, et al. Metal–organic framework based mixed matrix membranes: a solution for highly efficient CO<sub>2</sub> capture? *Chem Soc Rev* 2015;44:2421–54.
- [25] Zhang C, Koros WJ. Zeolitic imidazolate framework-enabled membranes: challenges and opportunities. *J Phys Chem Lett* 2015;6:3841–9.
- [26] Diestel L, Wang N, Schwiedland B, Steinbach F, Giese U, Caro J. MOF based MMMs with enhanced selectivity due to hindered linker distortion. *J Membr Sci* 2015;492:181–6.
- [27] Huang A, Liang F, Steinbach F, Caro J. Preparation and separation properties of LTA membranes by using 3-aminopropyltriethoxysilane as covalent linker. *J Membr Sci* 2010;350:5–9.
- [28] Lui R, Mahurin M, Li C, Unocic RR, Gao HJ, Pennycook SJ, et al. Dopamine as a carbon source: the controlled synthesis of hollow carbon spheres and yolk-structured carbon nanocomposites. *Angew Chem Int Ed* 2011;50:6799–802.
- [29] Nibou D, Amokrane S, Lebaili N. Use of NaX porous materials in the recovery of iron ions. *Desalination* 2010;250:459–62.
- [30] Maes A, Cremers A. Ion exchange of synthetic zeolite X and Y with Co<sup>2+</sup>, Ni<sup>2+</sup>, Cu<sup>2+</sup> and Zn<sup>2+</sup> ions. *J Chem Soc Faraday Trans* 1975;71:265–77.
- [31] Chmelik C, Bux H, Voß H, Caro J. Adsorption and diffusion – basis for molecular understanding of permeation through molecular sieve membranes. *Chem Ing Tech* 2011;83:104–12.
- [32] Bux H, Chmelik C, Krishna R, Caro J. Ethene/ethane separation by the MOF membrane ZIF-8: molecular correlation of permeation, adsorption, diffusion. *J Membr Sci* 2011;369:284–9.
- [33] Krishna R. Describing the diffusion of guest molecules inside porous structures. *J Phys Chem C* 2009;113:19756–81.
- [34] Go Y, Lee JH, Shamsudin IK, Kim J, Othman MR. Microporous ZIF-7 membranes prepared by *in-situ* growth method for hydrogen separation. *Int J Hydrogen Energy* 2016;41:10366–73.
- [35] Weh K, Noack M, Sieber I, Caro J. Permeation of single gases and gas mixtures through faujasite-type molecular sieve membranes. *Micropor Mesopor Mater* 2002;54:27–36.
- [36] Pulido A, Nachtigall P, Zukal A, Domínguez I, Cejka J. Adsorption of CO<sub>2</sub> on sodium-exchanged ferrierites: the bridged CO<sub>2</sub> complexes formed between two extraframework cations. *J Phys Chem C* 2009;112:2928–35.
- [37] Pirngruber GD, Raybaud P, Cejka J, Zukal A. The role of the extra-framework cations in the adsorption of CO<sub>2</sub> on faujasite Y. *Phys Chem Chem Phys* 2010;12:13534–46.
- [38] Pan F, Jia H, Qiao S, Jiang Z, Wang J, Wang B, et al. Bioinspired fabrication of high performance composite membranes with ultrathin defect-free skin layer. *J Membr Sci* 2009;341:279–85.
- [39] Huheey JE, Keiter EA, Keiter RL. *Anorganische Chemie: Prinzipien von Struktur und Reaktivität*. 5th ed. De Gruyter; 2014.
- [40] Yu L, Gong J, Zeng C, Zhang L. Synthesis of binderless zeolite X microspheres and their CO<sub>2</sub> adsorption properties. *Sep Purif Technol* 2013;118:188–95.
- [41] Huang A, Caro J. Facile synthesis of LTA molecular sieve membranes on covalently functionalized supports by using diisocyanates as molecular linkers. *J Mater Chem* 2011;21:11424–9.
- [42] Algieri C, Bernado P, Golemme G, Barbieri G, Dioli E. Permeation properties of a thin silicalite-1 (MFI) membrane. *J Membr Sci* 2003;222:181–90.
- [43] Rezakamezi M, Shahidi K, Mohammadi T. Hydrogen separation and purification using crosslinkable PDMS/zeolite A nanoparticles mixed matrix membranes. *Int J Hydrogen Energy* 2012;37:14576–89.
- [44] Ahmad J, Hägg A-B. Development of matrimid/zeolite 4A mixed matrix membranes using low boiling point solvent. *Sep Purif Technol* 2013;115:190–7.

---

### III Amine-Modified Mg-MOF-74/CPO-27-Mg Membrane with Enhanced H<sub>2</sub>/CO<sub>2</sub> Separation

N. Wang, A. Mundstock, Y. Liu, A. Huang, J. Caro

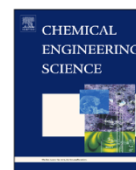
*Chemical Engineering Science*, 124, 2015, 27 - 36.

---



Contents lists available at ScienceDirect

Chemical Engineering Science

journal homepage: [www.elsevier.com/locate/ces](http://www.elsevier.com/locate/ces)

## Amine-modified Mg-MOF-74/CPO-27-Mg membrane with enhanced H<sub>2</sub>/CO<sub>2</sub> separation



Nanyi Wang<sup>a</sup>, Alexander Mundstock<sup>a</sup>, Yi Liu<sup>a</sup>, Aisheng Huang<sup>b,\*</sup>, Jürgen Caro<sup>a,\*</sup>

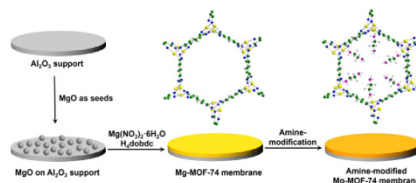
<sup>a</sup> Institute of Physical Chemistry and Electrochemistry, Leibniz University Hannover, Callinstr. 22, D-30167 Hannover, Germany

<sup>b</sup> Institute of New Energy Technology, Ningbo Institute of Material Technology and Engineering, CAS, 1219 Zhongguan Road, 315201 Ningbo, PR China

### HIGHLIGHTS

- Amination of the open metal sites in Mg-MOF-74 leads to retardation of CO<sub>2</sub> and doubles the selectivity for H<sub>2</sub>/CO<sub>2</sub> separation.
- The size of Mg-MOF-74 crystals in membrane can be reduced after optimization of synthesis solution.
- Only by using MgO as seeds, a dense and continuous Mg-MOF-74 layer could be obtained.
- The selectivity of the Mg-MOF-74 membrane for H<sub>2</sub>/CO<sub>2</sub> is far above the Robeson bound.

### GRAPHICAL ABSTRACT



### ARTICLE INFO

#### Article history:

Received 8 October 2014  
 Received in revised form  
 17 October 2014  
 Accepted 20 October 2014  
 Available online 27 October 2014

#### Keywords:

Metal-organic framework  
 Mg-MOF-74 membrane  
 Amine-modification  
 Gas separation

### ABSTRACT

Mg-MOF-74 has attracted intense attention due to its high CO<sub>2</sub> uptake ability. In this work, a new strategy by using magnesium oxide as seeds was developed to synthesize a dense, defect-free Mg-MOF-74 membrane with hydrogen-selectivity. The mixed gas separation factor of H<sub>2</sub>/CO<sub>2</sub> mixture could be improved by the post-modification of the Mg-MOF-74 membrane with ethylenediamine, since the modification with amine groups enhanced the strong adsorption of CO<sub>2</sub> molecules, which reduces the permeance of CO<sub>2</sub>. The separation factors for both as-synthesized and amino-functionalized Mg-MOF-74 membranes reduce gradually with increasing temperature. After amination of the open Mg sites, the separation performance of the Mg-MOF-74 membrane was remarkably enhanced, and the H<sub>2</sub>/CO<sub>2</sub> selectivity increased from 10.5 to 28 at room temperature.

© 2014 Elsevier Ltd. All rights reserved.

### 1. Introduction

As a high-quality and clean energy carrier, hydrogen has attracted renewed and increasing attention around the world in recent years. Currently, the majority of hydrogen is produced by steam-methane reforming (SMR) followed by a water-gas shift (WGS) strategy. Before hydrogen can be used in fuel cell, it has to be purified from the resulting SMR gas mixture which mainly

contains CO<sub>2</sub>. Also in the pre-combustion technology of CO<sub>2</sub> sequestration, H<sub>2</sub>-selective membranes are desired. In the case of pre-combustion CO<sub>2</sub> capture, H<sub>2</sub>-selective membranes can be applied at moderate temperatures (150–250 °C) in a one-step separation process. This approach offers the advantages that (i) the mixture of CO<sub>2</sub> and H<sub>2</sub> has already a high pressure, and that (ii) the application of selective H<sub>2</sub>-permeable membranes can deliver CO<sub>2</sub> at high pressure, thus reducing compression costs. Therefore, the separation of H<sub>2</sub> from CO<sub>2</sub> is of high interest. Compared with conventional separation methods such as pressure swing adsorption (PSA), membrane separation is the most promising alternative because of its low energy consumption, ease of operation, and cost effectiveness (Rostrup-Nielsen and

\* Corresponding authors. Tel.: +49 511762 3175; fax: +49 511 762 1912.

E-mail addresses: [huangaisheng@nimte.ac.cn](mailto:huangaisheng@nimte.ac.cn) (A. Huang),

[juergen.caro@pci.uni-hannover.de](mailto:juergen.caro@pci.uni-hannover.de) (J. Caro).

<http://dx.doi.org/10.1016/j.ces.2014.10.037>

0009-2509/© 2014 Elsevier Ltd. All rights reserved.

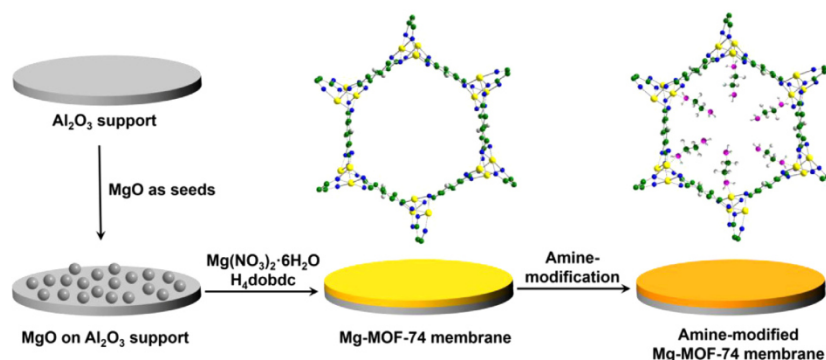


Fig. 1. Scheme of the synthesis of Mg-MOF-74 membrane on MgO-seeded Al<sub>2</sub>O<sub>3</sub> supports and amine-modification of the as-prepared Mg-MOF-74 membrane.

Rostrup-Nielsen, 2002; Brown et al., 2014; Rodenas et al., 2014). Inorganic membranes like zeolites, Pt-alloys and carbon are of special interest since – different to organic polymer membranes – they can be operated under harsh separation conditions. In the recent 20 years, various hydrogen permselective inorganic membranes have been developed for the separation of H<sub>2</sub> from CO<sub>2</sub> (Shiflett and Foley, 1999; Uemiyama et al., 1991; Ockwig and Nenoff, 2007; de Vos and Verweij, 1998; Hong et al., 2008; Huang et al., 2010). However, the preparation of highly H<sub>2</sub>-permselective membranes is still a challenge.

Metal–organic frameworks (MOFs), which consist of metal ions or metal oxide clusters interconnected by anionic organic linkers, have attracted intense attention for potential applications in catalysis, separation, gas adsorption and gas storage due to their well-defined pore structure and specific adsorption affinities. (Yaghi et al., 2003; Seo et al., 2000; Ranjan and Tsapatsis, 2009; Lu and Hupp, 2010; Hermes et al., 2005; Zhao et al., 2009; Yoo et al., 2009; Li et al., 2010; Huang et al., 2012; Liu et al., 2013) Magnesium dioxobenzene dicarboxylate (Mg-MOF-74 or Mg/dobdc, also known as CPO-27-Mg, hereafter termed Mg-MOF-74) (Rosi et al., 2005), one of the iso-structural compounds of M<sub>2</sub>(dhtp)(H<sub>2</sub>O)<sub>2</sub>·8H<sub>2</sub>O (M-MOF-74, M=Ni, Co, Zn, Mg, Mn, dhtp=dihydroxyterephthalic) (Dietzel et al., 2005, 2008, 2006; Britt et al., 2009) is under intense investigation due to its significantly high CO<sub>2</sub> adsorption capacities. (Ranjan and Tsapatsis, 2009; Dietzel et al., 2009) Mg-MOF-74 is built up by the linkage of the Mg<sup>2+</sup> ions with 2,5-dioxido-1,4-benzenedicarboxylate (DOBDC), where the metal ions build a distorted octahedron and the carboxylate groups act as ligand of the metal cations, to form a well-defined hexagonal, one-dimensional (1D) pore structure with a pore diameter of about 11 Å (Caskey et al., 2008; Bétard et al., 2010).

Attributing to the unique feature of its framework structure, where metal cations are bonded with five oxygen atoms to form a square-pyramid coordination, and the unsaturated metal sites in the center of the square plane are free to interact with CO<sub>2</sub> molecules, Mg-MOF-74 has a high CO<sub>2</sub> adsorption capacity (380 mg CO<sub>2</sub>/g at room temperature under dry conditions) (Yazaydin et al., 2009). Due to its high gas adsorption ability, many studies have been focused on the gas separation efficiency of Mg-MOF-74 (Mason et al., 2011; Yang et al., 2012; Dietzel et al., 2010; Herm et al., 2012; Yu and Balbuena, 2013; Böhme et al., 2013; Mundstock et al., 2013).

Although there are numerous studies of Mg-MOF-74 powders on the gas adsorption incl. simulation (Kong et al., 2012; Dzubak et al., 2012; Remy et al., 2013), to date no Mg-MOF-74 membrane with successful gas separation performance has been reported. In a first attempt, a supported Mg-MOF-74 membrane with a mean tilt angle of 31° of the 1D pore system from the

direction perpendicular to the membrane surface could be developed (Mundstock et al., 2013). Lee et al. (2012) have prepared a Ni-MOF-74 membrane by using the layer-by-layer synthesis technique with a H<sub>2</sub>/CO<sub>2</sub> selectivity of 9.1 at 25 °C. Bae and Long (2013) used Mg-MOF-74 nanocrystals in mixed-matrix membranes to improve the CO<sub>2</sub>/N<sub>2</sub> selectivity of the polymer membrane. In the present work, we have developed a new strategy by using magnesium oxide as seeds to synthesize a dense, defect-free Mg-MOF-74 membrane for gas separation. Moreover, the post-synthesis modification with ethylenediamine, which was developed by Choi et al. (2012), was employed to improve its gas separation efficiency (Fig. 1). When preparing supported MOF membranes with a 1D pore system, the orientation of the pores in a suitable direction remains a challenge as addressed for the first time for the Mn formate membrane (Arnold et al., 2007).

## 2. Experimental

### 2.1. Materials

Chemicals were used as received. 2,5-dihydroxyterephthalic acid (H<sub>4</sub>dobdc, 98%, Aldrich), magnesium nitrate hexahydrate (99%, Sigma-Aldrich), magnesium oxide (99.9%, ChemPur), polyethyleneimine (branched, avg MW ~ 25000 by LS, Aldrich), ethylenediamine (≥ 99%, Sigma-Aldrich), toluene (≥ 99.8%, Acros), *N,N*-dimethylformamide (DMF, water < 50 ppm, Acros), ethanol (≥ 99.8%, Sigma-Aldrich). Porous α-Al<sub>2</sub>O<sub>3</sub> disks (Fraunhofer Institute IKTS, former HITK/Inoceramic, Hermsdorf, Germany: 18 mm in diameter, 1.0 mm in thickness, 70 nm particles in the top layer) were used as supports.

### 2.2. Preparation of Mg-MOF-74 membranes

#### 2.2.1. Seeding on the support surface

The seeding suspension was prepared by adding 1.5 g MgO and 1.2 g polyethyleneimine (PEI) in 100 mL water. PEI was used to ensure that the MgO particles (< 50 nm) adhered to the support surface. The suspension was then stirred overnight, and the α-Al<sub>2</sub>O<sub>3</sub> supports were dipped in the seeding suspension by using an automatic dip-coating device with a dip- and withdraw-speed of 300 and 100 mm/min, respectively. The seeded supports were then air-dried at 100 °C overnight.

#### 2.2.2. Synthesis of Mg-MOF-74 membrane

The Mg-MOF-74 membrane was prepared by a solvothermal reaction. Mg(NO<sub>3</sub>)<sub>2</sub>·6H<sub>2</sub>O (0.2375 g, 0.925 mmol) and H<sub>4</sub>dobdc (0.1011 g, 0.509 mmol) were added to a 15 mL solution which was

prepared by mixing DMF, water and ethanol with a volumetric ratio of 15:1:1. The MgO-coated supports were then placed vertically in a Teflon-lined stainless steel autoclave which was filled with the synthesis solution and then heated at 120 °C in an air-conditioned oven for 24 h. After solvothermal reaction, the Mg-MOF-74 membranes were washed with DMF three times, and then dried in air overnight.

### 2.2.3. Post-modification of the membrane

The as-prepared Mg-MOF-74 membranes were treated with ethylenediamine (0.5 g in 10 mL toluene) at 110 °C for 2 h under reflux in argon atmosphere. The membranes were then directly removed from the solution and dried in argon at room temperature.

## 2.3. Characterization

Scanning electron microscopy (SEM) micrographs were taken on a JEOL JSM-6700F with a cold field emission gun operating at 2 kV and 10 μA. The X-ray diffraction (XRD) patterns were recorded at room temperature under ambient conditions with Bruker D8 ADVANCE X-ray diffractometer with CuKα radiation at 40 kV and 40 mA. FT-IR spectrums were recorded with a Tensor 27 instrument (Bruker) through KBr pellets using Ar/Xe laser line with λ=633 nm.

## 2.4. Evaluation of single gas permeation and mixed gas separation

The as-prepared and amine-modified Mg-MOF-74 membranes synthesized on MgO-seeded α-Al<sub>2</sub>O<sub>3</sub> supports at 120 °C for 24 h were evaluated by single gas permeation and mixture gas separation with Wicke–Kallenbach (Huang et al., 2010). For the measurements of gas separation performances, the supported Mg-MOF-74 membrane was sealed in a permeation module with silicone O-rings. The mounting of the membranes into the housing was done in a glove box under argon to avoid the influence of humid air. According to the Wicke–Kallenbach technique, on both sides of the membrane was atmospheric pressure, N<sub>2</sub> was used on the permeate side as sweep gas, except for the measurement of N<sub>2</sub> permeance where CH<sub>4</sub> was used as sweep gas. The flow rate on the feed side was kept constant for each gas with 50 mL min<sup>-1</sup>, and the flow rate on the permeate side was kept at 50 mL min<sup>-1</sup> as well. The fluxes of both the feed and sweep gas were controlled by mass flow controllers, and a calibrated gas chromatograph (HP6890) was used to detect the gas concentrations on the permeate side. The gas chromatograph (GC) was calibrated every week anew with standard gas mixtures. The accuracy of the GC analysis of our H<sub>2</sub>/CO<sub>2</sub> mixture with TCD detection is about ± 5 vol%. The permeance  $P$  is obtained by division of the flux by the transmembrane pressure difference, as shown in Eq.(1), where  $n$  is the amount of gas in mol,  $A$  is the membrane area,  $t$  is the permeation time, and  $\Delta p$  is the pressure difference. The separation factor  $\alpha_{ij}$  of a binary mixture permeation is defined as the quotient of the molar ratios of the components ( $i, j$ ) in the permeate, divided by the quotient of the molar ratio of the components ( $i, j$ ) in the retentate, as show in Eq. (2). Since less than 1% of the feed gas pass the membrane, the retentate composition is de facto identical with the feed composition.

$$P = \frac{n}{A \times t \times \Delta p} \quad (1)$$

$$\alpha_{ij} = \frac{y_{i,perm}/y_{j,perm}}{y_{i,ret}/y_{j,ret}} \quad (2)$$

Originally, the Wicke–Kallenbach method has been developed for the determination of CO<sub>2</sub> surface diffusion with N<sub>2</sub> as sweep gas (Wicke and Kallenbach, 1941). It could happen therefore in our

case that the adsorption of nitrogen on the permeate side of the membrane would falsify the separation factor, also the counter-diffusion of the sweep gas to the feed side can happen. Therefore, to prove the feasibility of the Wicke–Kallenbach technique, gas permeation measurements were also carried out without sweep gas. In one scenario, the feed side was at 1 bar, and the permeate side was at reduced pressure (vacuum). In another case, scenario 2, the pressure on the feed side was 2 bar, and the pressure on the permeate side was 1 bar. It was found that the fluxes of the components of the feed gases were increased in scenario 1 and decreased in scenario 2. This experimental finding can be understood by modified concentrations gradients over the membrane as driving force for permeation. However, the mixture separation factors kept almost unchanged (less than ± 5%).

We have also excluded another source of experimental errors. Before every gas permeation measurement, the membranes were first activated in situ at 100 °C by using 50 mL min<sup>-1</sup> H<sub>2</sub> in the Wicke–Kallenbach permeation apparatus. All permeation data were collected in steady state of permeation after at least 5 h equilibration time. Sometimes, after 5 h equilibration time we waited for another 12 h. Since there was no change in the permeation data, we assume that the H<sub>2</sub>/CO<sub>2</sub> mixed gas system was in steady state after 5 h.

The apparent activation energy  $E_{act}$  of permeation can be calculated according to the Arrhenius equation (Eq. (3)), where  $P_i$  is the permeance of component  $i$ ,  $P_i^0$  is the pre-exponential factor,  $R$  is the ideal gas constant (8.314 J mol<sup>-1</sup> K<sup>-1</sup>), and  $T$  is the temperature in Kelvin. Then  $E_{act}$  has been determined through the slope of the plot, which is obtained from the straight line of  $\ln P_i$  against  $T^{-1}$  (Li et al., 2010) (see Section 3.4. Results of single gas permeation and mixture gas separation).

$$P_i = P_i^0 \exp\left(-\frac{E_{act}}{RT}\right) \quad (3)$$

## 3. Results and discussion

### 3.1. Effects of the synthesis solution on the membrane preparation

We first tried to grow a Mg-MOF-74 membrane following Caskey's recipe with a solution composition of 3.3 equiv. Mg(NO<sub>3</sub>)<sub>2</sub>·6H<sub>2</sub>O: 1 equiv. H<sub>4</sub>dobdc (Caskey et al., 2008). However, we failed to prepare a continuous Mg-MOF-74 membrane after solvothermal synthesis for 24 h at 120 °C. As shown in Fig. 2(a), the crystals are too large to intergrow to a continuous layer, and big inter-crystalline gaps are easily observed in the Mg-MOF-74 layer. In order to control the size of the Mg-MOF-74 crystal and to avoid inter-crystalline voids, we modified the chemical composition of the synthesis solution by adjusting the ratio of Mg<sup>2+</sup> and the dobdc<sup>4-</sup> linker. By use of the new recipe with a solution composition of 1.8 equiv. Mg(NO<sub>3</sub>)<sub>2</sub>·6H<sub>2</sub>O:1 equiv. H<sub>4</sub>dobdc, the size of Mg-MOF-74 crystals can be remarkably reduced, and thus the crystals become well intergrown and form a dense Mg-MOF-74 membrane on the alumina support (Fig. 2(b)). XRD pattern of the Mg-MOF-74 membrane further confirms that the as-synthesized layer is a pure Mg-MOF-74 phase after the adjustment of the synthesis solution.

Due to the poor heterogeneous nucleation of Mg-MOF-74 crystals on the alumina support surface, it is difficult to form a continuous Mg-MOF-74 layer simply by in-situ hydrothermal synthesis. Fig. 3(a) shows the Mg-MOF-74 membrane prepared directly on the un-modified alumina support. It can be seen that the crystals don't grow into a dense membrane layer, and inter-crystalline gaps can be observed between the Mg-MOF-74 crystals. Therefore, we tried to improve their intergrowth by pre-coating



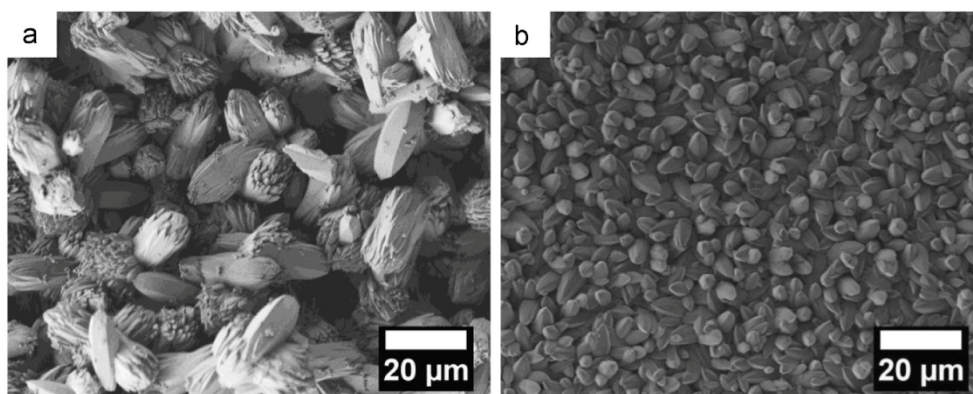


**Fig. 2.** Top view SEM images of Mg-MOF-74 membranes prepared on  $\alpha$ - $\text{Al}_2\text{O}_3$  supports (a) before and (b) after the optimization of the synthesis solution (a cross-section of membrane (b) is shown in Fig. 6(b)).

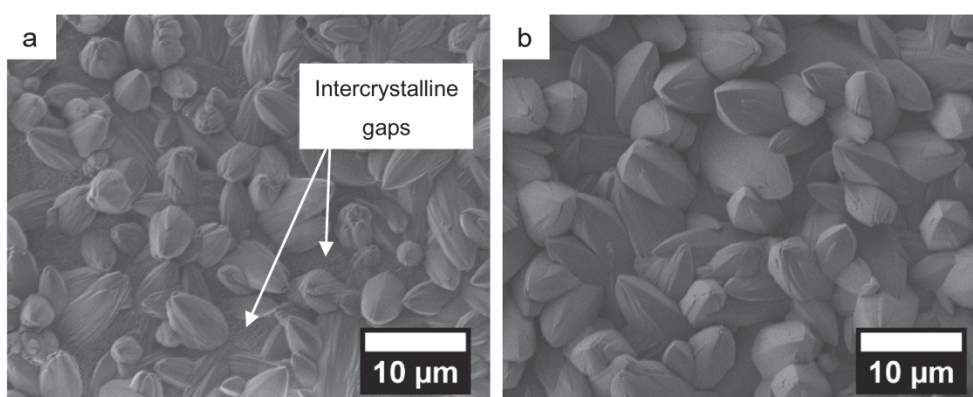


**Fig. 3.** Top view SEM images of Mg-MOF-74 membranes prepared (a) directly on the  $\alpha$ - $\text{Al}_2\text{O}_3$  support and (b) on MgO-seeded  $\alpha$ - $\text{Al}_2\text{O}_3$  support at 120 °C for 24 h.

the alumina substrate surface with MgO seeds, which are expected to promote both nucleation and growth of the Mg-MOF-74 layer. As shown in Fig. 3(b), the membranes prepared on MgO-seeded  $\alpha$ - $\text{Al}_2\text{O}_3$  supports are indeed dense and no inter-crystalline voids can be observed. In the present work, MgO powders (< 50 nm) were coated on the surface of the support with the help of PEI, and served as nucleation centers which released  $\text{Mg}^{2+}$  ions into the synthesis solution, thus promoting the following growth of the Mg-MOF-74 crystals. After the synthesis of the membranes, the MgO seeds have transformed fully into the Mg-MOF-74. On the one hand, we cannot see any MgO seeds from the cross-section view of the membrane. On the other hand, the XRD patterns (Fig. 4) also indicate that the peaks of MgO disappeared after the membrane was grown on the support. Before choosing the MgO as seeds, we have also tried using Mg-MOF-74 nano crystals as seeds. However, these membrane preparations on the Mg-MOF-74-seeded supports, either by seeding in DMF or in ethanol, were not successful. The crystals grew too fast to large 10  $\mu\text{m}$  sized crystals, and intercrystalline cracks were unavoidable.

### 3.2. Effects of the synthesis time

With the secondary growth method, the effect of the synthesis time on the membrane microstructure was followed. Fig. 5 shows SEM images of the Mg-MOF-74 membranes prepared on MgO-seeded  $\alpha$ - $\text{Al}_2\text{O}_3$  supports for different synthesis times at 120 °C. As shown in Fig. 5(a), after 12 h, the alumina support surface has been covered by separate Mg-MOF-74 crystals. As the synthesis

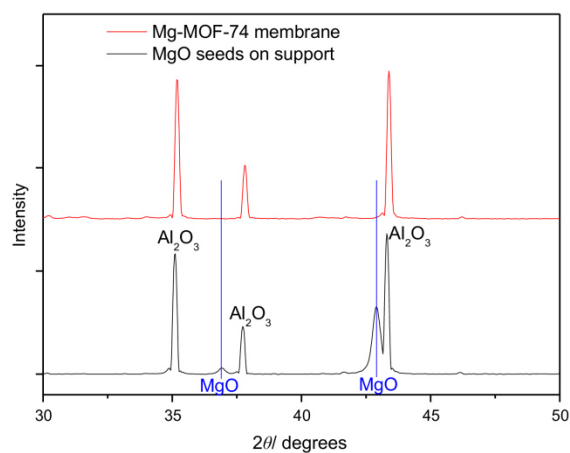


**Fig. 4.** XRD patterns of MgO seeds on the  $\text{Al}_2\text{O}_3$  support and synthesized Mg-MOF-74 membranes.

time increases to 20 h, more Mg-MOF-74 crystals are attached to the substrate and gradually form a thin and continuous layer, although there are still observable inter-crystalline gaps between the Mg-MOF-74 crystals (Fig. 5(b)). A dense Mg-MOF-74 membrane can be formed if the synthesis time increases up to 24 h. It can be seen that the support surface was completely covered by

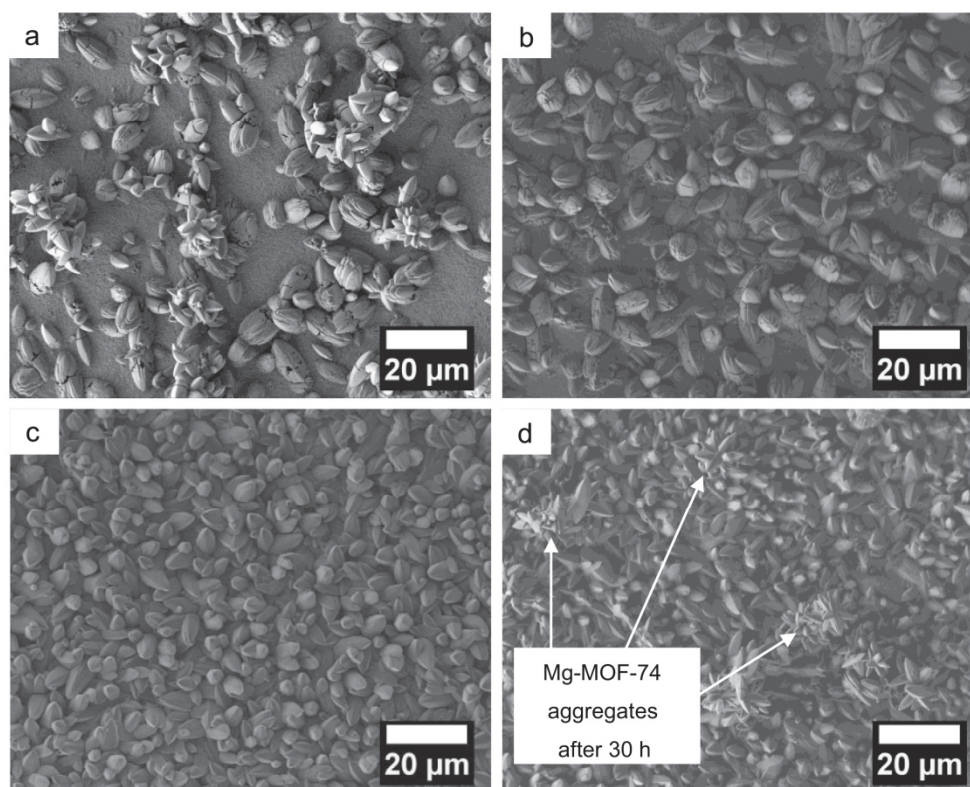


Fig. 5. Top view SEM images of Mg-MOF-74 membranes prepared on MgO-seeded  $\alpha$ - $\text{Al}_2\text{O}_3$  supports at 120 °C for different synthesis times: (a) 16 h, (b) 20 h, (c) 24 h and (d) 30 h (for the XRD see Fig. 6).

uniform Mg-MOF-74 crystals with a grain size of about 10  $\mu\text{m}$ , and no cracks or other macroscopic defects are visible (Fig. 5(c)). By further extending the synthesis time to 30 h, more Mg-MOF-74 crystals agglomerate on the as-prepared membrane, resulting in a rough membrane surface (Fig. 5(d)). The evolution of the Mg-MOF-74 membrane formation is also characterized by XRD, as shown in Fig. 6, compared with the XRD patterns of Mg-MOF-74 powder (Fig. 6(a)). After an elapse of 16 h, the first peaks of the Mg-MOF-74 crystals have been detected on the support surface (Fig. 6(b)). The heights of the Mg-MOF-74 diffraction peaks relative to the  $\alpha$ - $\text{Al}_2\text{O}_3$  support increase with synthesis time, which indicates that the thickness of the membrane increases with time. After 24 h, the heights of the Mg-MOF-74 peaks relative to the  $\alpha$ - $\text{Al}_2\text{O}_3$  support remain unchanged, which indicates that the Mg-MOF-74 crystals completely have covered the surface of the substrate (Fig. 6e). We conclude therefore, that 24 h at 120 °C is the optimum synthesis condition for the preparation of Mg-MOF-74 membranes.

Unfortunately, in this special case, it is impossible to draw from the XRD any conclusions about the crystal and – therefore – channel orientation in the membrane by simply comparing the XRD patterns of the isotropic powder and the membrane (Fig. 6(a) and (e)). This is due to the fact that all dominant peaks in the powder XRD pattern can be allocated to Miller indices  $(-1\ 2\ 0)$ ,  $(0\ 3\ 0)$  and  $(-1\ 5\ 0)$  with  $l$  values of 0. Therefore, the formation of a “crystallographic preferred orientation” (CPO) index (Jeong et al., 2002) gives no information on the channel orientation in  $l$  direction. It has to be mentioned, that our XRD of the supported Mg-MOF-74 is similar to the XRD of Ni-MOF-74 and Zn-MOF-74 grown on alumina support (Bétard et al., 2010).

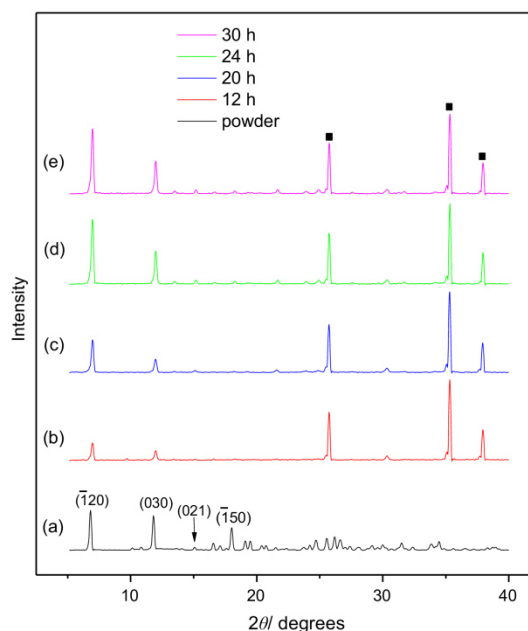


Fig. 6. XRD patterns of Mg-MOF-74 membranes prepared on MgO-seeded  $\alpha$ - $\text{Al}_2\text{O}_3$  supports at 120 °C for different synthesis times: (b) 16 h, (c) 20 h, (d) 24 h and (e) 30 h, compared with (a) the XRD patterns of Mg-MOF-74 powder. (■):  $\text{Al}_2\text{O}_3$  support, (not marked): Mg-MOF-74 (for the SEM see Fig. 5).

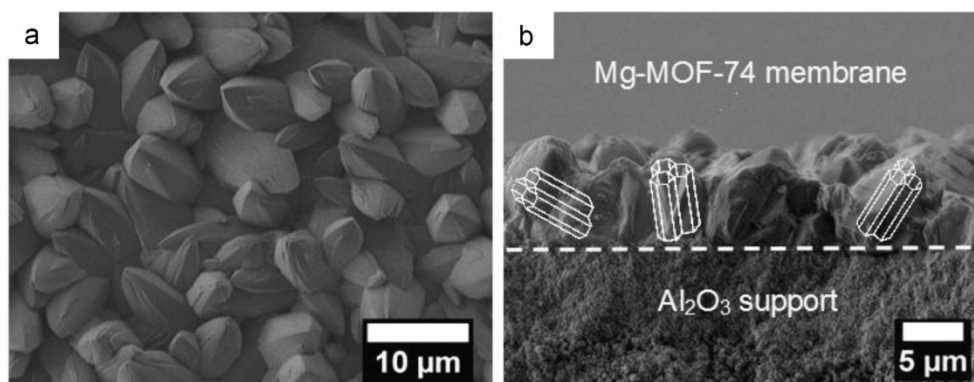


Fig. 7. (a) Top view and (b) cross-section SEM images of the Mg-MOF-74 membrane prepared on MgO-seeded  $\alpha$ - $\text{Al}_2\text{O}_3$  supports at 120 °C for 24 h. The white channels in (b) stand for the orientation of the 1 D pores in Mg-MOF-74 crystals.

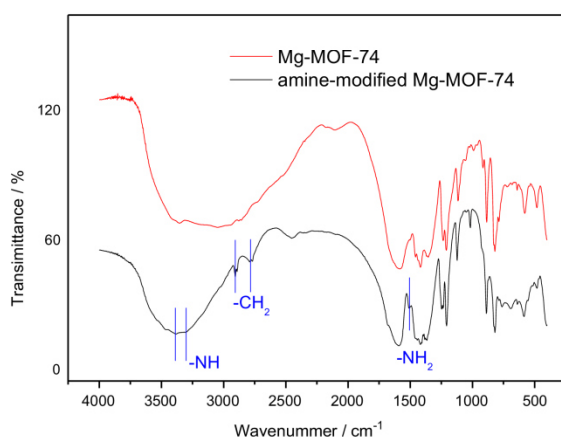


Fig. 8. FT-IR spectra of as-prepared and amine-modified Mg-MOF-74 crystals at room temperature.

Fig. 7 shows the Mg-MOF-74 membrane prepared on a MgO-seeded support for 24 h at 120 °C. From the cross-section view (Fig. 7(b)), the membrane is well intergrown with a thickness of about 10  $\mu\text{m}$ . The shown membrane top view and the cross-section (Fig. 7) indicate that the crystals in the membrane show no statistical arrangement on the support but rather a tilted orientation with their trigonal axis perpendicular to the support. Thanks to this, a major part of all the 1D channels, which run along the  $c$ -axis of the trigonal structure, should be available for gas separation. Because of this tilted orientation of the  $c$ -axis, a huge amount of crystal planes and edges without an  $l \neq 0$  value such as  $(-1\ 2\ 0)$  and  $(0\ 3\ 0)$  are present and dominate the XRD as another reason for the above mentioned problematic orientation determination via XRD.

### 3.3. Effects of the post-modification

The Mg-MOF-74 membranes prepared on MgO-seeded  $\alpha$ - $\text{Al}_2\text{O}_3$  supports were then post-modified with ethylenediamine. Fig. 8 shows the FT-IR spectra of non-modified and ethylenediamine-modified Mg-MOF-74 membranes. Both two samples contain a broad band at around 3450  $\text{cm}^{-1}$ , which can be assigned to O-H stretching vibrations of adsorbed water, and most of the bands in the region from about 1600 to 800  $\text{cm}^{-1}$  are due to the stretching of the aromatic ring. Although lots of bands in the fingerprint region cannot be recognized clearly due to the overlapping of

functional groups, some remarkable bands can still be distinguished. Compared with the FT-IR spectrum of non-modified Mg-MOF-74, the FT-IR spectrum of ethylenediamine-modified Mg-MOF-74 contains characteristic bands at 3370, 3285, 2932, 2814 and 1545  $\text{cm}^{-1}$ , which match well with the FT-IR spectrum of ethylenediamine (Bétard et al., 2010; Su et al., 2010; Chang et al., 2003; Sabo et al., 2006). The bands shown at 3370, 3285 and 1545  $\text{cm}^{-1}$  are related to  $\text{NH}_2$  vibration in the primary amine group. The absorptions of the  $\text{CH}_2$  groups of the aliphatic chains of ethylenediamine are observed at 2935 and 2814  $\text{cm}^{-1}$  and are attributed to the asymmetric and symmetric stretching vibrations and deformation vibrations. The presence of  $-\text{NH}_2$  and  $-\text{CH}_2$  of the aliphatic chain after the amine modification confirms that ethylenediamine has been successfully grafted onto the Mg-MOF-74 crystals according to the recipe given in Choi et al. (2012). Judged by the SEM image and XRD pattern (not shown here), both the morphology and structure of the Mg-MOF-74 membrane remain unchanged after the amine-modification.

### 3.4. Results of single gas permeation and mixture gas separation

The single gas permeances on the as-prepared and amine-modified Mg-MOF-74 membranes at 25 °C and 1 bar as a function of the kinetic diameter of the gas molecules are shown in Fig. 9, and the inset gives the mixture separation factors for  $\text{H}_2$  over other gases from their equimolar mixtures. The single gas permeances and ideal separation factors are summarized in Table 1, and the permeation data for mixed gases are listed in Table 2.

It follows from Fig. 9 to Table 1 that the single gas permeances of the as-prepared Mg-MOF-74 membrane follow the order:  $\text{H}_2 > \text{CH}_4 > \text{N}_2 > \text{CO}_2$ , with a  $\text{H}_2$  permeance of  $1.2 \times 10^{-7} \text{ mol m}^{-2} \text{ s}^{-1} \text{ Pa}^{-1}$ . The mixture separation factor of  $\text{H}_2/\text{CO}_2$  with 10.5 is much higher than those of  $\text{H}_2/\text{CH}_4$  (5.4) and  $\text{H}_2/\text{N}_2$  (3.8) (inset in Fig. 9). This surprising experimental finding can be described by the diffusivity-solubility model of permeation (Krishna and van Baten, 2011). According to the rough estimate “permeation selectivity = adsorption selectivity  $\times$  diffusion selectivity”, a strong  $\text{CO}_2$  adsorption over  $\text{H}_2$  could lead to a  $\text{CO}_2$ -selective membrane. As reported previously (Yazaydin et al., 2009), Mg-MOF-74 shows very high  $\text{CO}_2$  capture ability due to the unsaturated  $\text{Mg}^{2+}$  site, thus  $\text{CO}_2$  can be stored in the pore structure Mg-MOF-74 especially. However, this strong  $\text{CO}_2$  adsorption reduces the  $\text{CO}_2$  mobility over proportional so that the Mg-MOF-74 membrane shows by the end a  $\text{H}_2$  over  $\text{CO}_2$  selectivity.

It is known that  $\text{CO}_2$  interacts electronically also with amines (Langeroudi et al., 2009; Serna-Guerrero et al., 2008; Planas et al., 2013). It was our concept, therefore, to further enhance the  $\text{H}_2/\text{CO}_2$  selectivity by increasing the adsorptive interaction of  $\text{CO}_2$  by

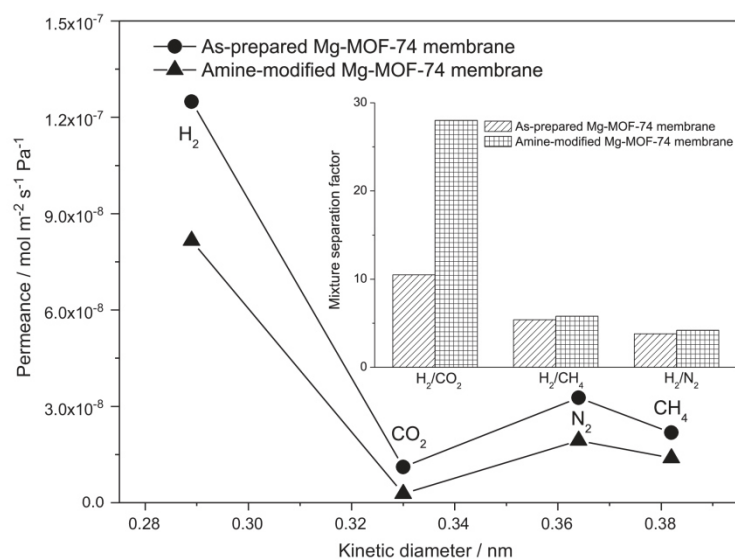


Fig. 9. Single gas permeances on the as-prepared and amine-modified Mg-MOF-74 membranes at 25 °C and 1 bar as a function of the kinetic diameter. The inset shows the mixture separation factors for H<sub>2</sub> over other gases from equimolar mixtures (for the temperature dependence of the H<sub>2</sub>/CO<sub>2</sub> mixed gas selectivities see Fig. 10).

Table 1

Single gas permeation performances of the as-prepared and amine-modified Mg-MOF-74 membrane at 25 °C and 1 bar.

Gas <sub><i>ij</i></sub>	KC*	As-prepared Mg-MOF-74 membrane			Amine-modified Mg-MOF-74 membrane		
		Permeances ( <i>i</i> ) (mol m <sup>-2</sup> s <sup>-1</sup> Pa <sup>-1</sup> )	Permeances ( <i>j</i> ) (mol m <sup>-2</sup> s <sup>-1</sup> Pa <sup>-1</sup> )	Ideal separation factor	Permeances ( <i>i</i> ) (mol m <sup>-2</sup> s <sup>-1</sup> Pa <sup>-1</sup> )	Permeances ( <i>j</i> ) (mol m <sup>-2</sup> s <sup>-1</sup> Pa <sup>-1</sup> )	Ideal separation factor
H <sub>2</sub> /CO <sub>2</sub>	4.7	1.24 × 10 <sup>-7</sup>	1.1 × 10 <sup>-8</sup>	11	8.2 × 10 <sup>-8</sup>	2.8 × 10 <sup>-9</sup>	29
H <sub>2</sub> /CH <sub>4</sub>	2.8		2.2 × 10 <sup>-8</sup>	5.6		1.4 × 10 <sup>-8</sup>	5.8
H <sub>2</sub> /N <sub>2</sub>	3.7		3.5 × 10 <sup>-8</sup>	3.5		1.9 × 10 <sup>-8</sup>	4.3

\* KC: Knudsen constant.

Table 2

Mixed gas separation performances of the as-prepared and amine-modified Mg-MOF-74 membrane at 25 °C and 1 bar with 1:1 binary mixtures.

Gas <sub><i>ij</i></sub>	KC*	As-prepared Mg-MOF-74 membrane			Amine-modified Mg-MOF-74 membrane		
		Permeances ( <i>i</i> ) (mol m <sup>-2</sup> s <sup>-1</sup> Pa <sup>-1</sup> )	Permeances ( <i>j</i> ) (mol m <sup>-2</sup> s <sup>-1</sup> Pa <sup>-1</sup> )	Mixture separation factor	Permeances ( <i>i</i> ) (mol m <sup>-2</sup> s <sup>-1</sup> Pa <sup>-1</sup> )	Permeances ( <i>j</i> ) (mol m <sup>-2</sup> s <sup>-1</sup> Pa <sup>-1</sup> )	Mixture separation factor
H <sub>2</sub> /CO <sub>2</sub>	4.7	1.0 × 10 <sup>-7</sup>	9.8 × 10 <sup>-9</sup>	10.5	7.6 × 10 <sup>-8</sup>	2.7 × 10 <sup>-9</sup>	28
H <sub>2</sub> /CH <sub>4</sub>	2.8	1.1 × 10 <sup>-7</sup>	2.1 × 10 <sup>-8</sup>	5.4	7.5 × 10 <sup>-8</sup>	1.3 × 10 <sup>-8</sup>	5.8
H <sub>2</sub> /N <sub>2</sub>	3.7	1.2 × 10 <sup>-7</sup>	3.3 × 10 <sup>-9</sup>	3.8	7.6 × 10 <sup>-8</sup>	1.8 × 10 <sup>-8</sup>	4.2

\* KC: Knudsen constant.

amine-modification of prepared Mg-MOF-74 membrane. As expected, after the amine-modification, due to the narrowed pore size of MOF-74 the single gas permeances of H<sub>2</sub>, CH<sub>4</sub> and N<sub>2</sub>, decreased slightly by only a factor of 1.5, 1.6, and 1.8, respectively. However, the CO<sub>2</sub> permeance has been reduced by a factor of 4 from 1.1 × 10<sup>-8</sup> mol m<sup>-2</sup> s<sup>-1</sup> Pa<sup>-1</sup> to 2.8 × 10<sup>-9</sup> mol m<sup>-2</sup> s<sup>-1</sup> Pa<sup>-1</sup>. As a result, the mixed separation factors of H<sub>2</sub> against CH<sub>4</sub> and N<sub>2</sub> remained almost unchanged after the amine-functionalization, but the mixture separation factor of H<sub>2</sub>/CO<sub>2</sub> dramatically increased from 10.5 to 28.

Due to the large pore size of about 11 Å, the size-based molecular sieve effect of Mg-MOF-74 was negligible. After the amine-modification, the pore size of the membrane was narrowed,

but the pores are still large enough for the passage of small molecules like H<sub>2</sub>, CH<sub>4</sub>, N<sub>2</sub> and CO<sub>2</sub>. Therefore, the mixture separation factors of H<sub>2</sub>/CH<sub>4</sub> and H<sub>2</sub>/N<sub>2</sub> do not change much when the membrane is modified by the diamine. On the contrary, the surface modification with amine groups has enhanced the strong adsorption of CO<sub>2</sub> molecules, which in turn reduces the permeance of CO<sub>2</sub>, leading to an increase of the separation performance of H<sub>2</sub> over CO<sub>2</sub>. As reported previously (Choi et al., 2012), one side of the amine group of ethylenediamine is bound to the open coordination sites of the Mg in the framework structure by direct ligation, while the amine group on the other side remains free in space (Hwang et al., 2008). Fig. 10 shows the mixture separation factors for equimolar H<sub>2</sub>/CO<sub>2</sub> mixtures and the single

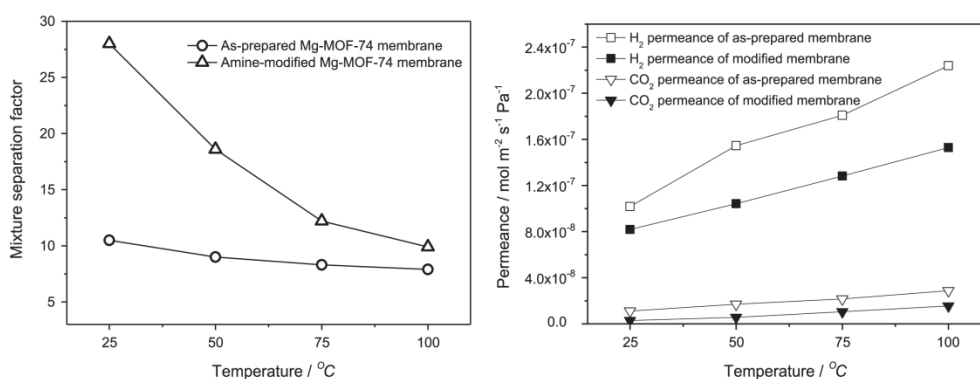


Fig. 10. Mixture separation factors for H<sub>2</sub>/CO<sub>2</sub> from equimolar mixture (left) and single gas permeances of H<sub>2</sub> and CO<sub>2</sub> (right) on the as-prepared and amine-modified Mg-MOF-74 membranes at 1 bar as a function of temperature.

Table 3

Activation energies of H<sub>2</sub> and CO<sub>2</sub> permeation for Mg-MOF-74 membrane before and after amine-modification.

	Activation energy $E_{act}$ (kJ mol <sup>-1</sup> )
H <sub>2</sub> before amine-modification	7.65
H <sub>2</sub> after amine-modification	7.71
CO <sub>2</sub> before amine-modification	11.4
CO <sub>2</sub> after amine-modification	20.9

gas permeances of H<sub>2</sub> and CO<sub>2</sub> on the as-prepared and amine-modified Mg-MOF-74 membranes at 1 bar as a function of temperature from 25 to 100 °C. For both the as-synthesized and amino-functionalized Mg-MOF-74 membranes the separation factors reduce gradually with increasing temperature. However, the reduction of the separation factors for the modified Mg-MOF-74 membrane was more remarkable since rising temperature has reduced the preferential adsorption of CO<sub>2</sub> on the amine groups. This trend is a good argument, that the interplay of adsorption and diffusion dominates the gas separation performance, rather than the size-based molecular sieving mechanism. As temperature increases, less CO<sub>2</sub> becomes adsorbed and more gas molecules can go through in the resulting free volume, leading to an increase in the hydrogen permeance and a reduction of the H<sub>2</sub>/CO<sub>2</sub> selectivity. The grafted ethylenediamine was also proven to be stable at 100 °C, since the heating process of 1 °C min<sup>-1</sup> from 25 to 100 °C is also reversible. The apparent activation energies  $E_{act}$  for H<sub>2</sub> and CO<sub>2</sub> permeation before and after modification, which are shown in Table 3, were obtained by fitting the data between 25 and 100 °C. Whereas the activation energy of H<sub>2</sub> permeation remains unchanged by the amination process, the activation energy of CO<sub>2</sub> has been almost doubled. This experimental finding can be explained by both steric effects (pore narrowing) and energetic effects (amine-CO<sub>2</sub> interaction). Our activation energies of H<sub>2</sub> and CO<sub>2</sub> permeation are similar to literature data of other microporous membranes for H<sub>2</sub>/CO<sub>2</sub> separation, like CVD modified DDR zeolite membrane developed by Kanezashi et al. (2008) (the activation energy for H<sub>2</sub> and CO<sub>2</sub> are 9.62 and 12.8, respectively), but different to CVI modified silica membrane by Koutsonikolasa et al. (2009) (the activation energy for H<sub>2</sub> and CO<sub>2</sub> are 15.8 and 7.4, respectively).

As shown in a Robeson plot (Robeson 1991; Robeson 2008) in Fig. 11, the H<sub>2</sub>/CO<sub>2</sub> selectivities and H<sub>2</sub> permeances of both the as-synthesized and the amine-modified Mg-MOF-74 membranes exceed by far the “upper-bound” for polymeric membranes, and the H<sub>2</sub>/CO<sub>2</sub> selectivity after amine-modification increases with

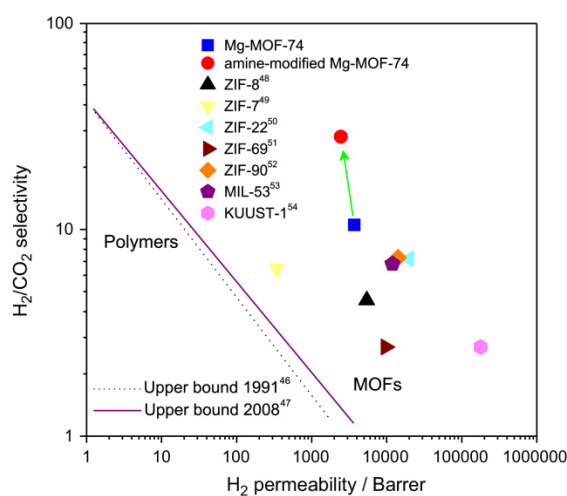


Fig. 11. H<sub>2</sub>/CO<sub>2</sub> selectivity versus H<sub>2</sub> permeability for as-prepared and amine-modified Mg-MOF-74 membranes at 25 °C and 1 bar, compared with the previously reported MOF membranes. The upper bound lines for polymeric membranes are based on Robeson (1991) and Robeson (2008).

only a slight decrease of the permeability. Furthermore, also compared with other MOF membranes, our amine-modified MOF-74 membrane is a promising material for the H<sub>2</sub>/CO<sub>2</sub> separation (Fig. 11 and Table 4). As shown in Fig. 11, compared with the existing polymer membranes, the amine-modified MOF-74 membrane exhibits a both much higher H<sub>2</sub>/CO<sub>2</sub> selectivity and H<sub>2</sub> permeability which recommends amine-modified MOF-74 powder also a promising candidate for the preparation of mixed matrix membranes (MMM) (Mahajan and Koros, 2000). The MMM concept avoids the difficulty to prepare and scale up pure supported MOF membranes and can be produced more easily as spiral wound or hollow fiber module, compared to the pure MOF membranes.

As a proof of the good reproducibility of the MgO-seeding synthesis method and amine-modification, Table 5 shows the results of gas permeation performance for four tested amine-modified Mg-MOF-74 membranes prepared following identical synthesis method. The selectivities of H<sub>2</sub>/CO<sub>2</sub> and H<sub>2</sub> and CO<sub>2</sub> permeance at room temperature do not scatter more than ± 10%, which indicates the good reproducibility of the Mg-MOF-74 membranes.

**Table 4**

H<sub>2</sub>/CO<sub>2</sub> selectivity versus H<sub>2</sub> permeability for as-prepared and amine-modified Mg-MOF-74 membranes at 25 °C and 1 bar, compared with the previously reported MOF membranes.

MOF membranes	Thickness (μm)	H <sub>2</sub> permeance (mol m <sup>-2</sup> s <sup>-1</sup> Pa <sup>-1</sup> )	H <sub>2</sub> permeability* (Barrer)	H <sub>2</sub> /CO <sub>2</sub> selectivity	References
Mg-MOF-74	10	1.2 × 10 <sup>-07</sup>	3.7 × 10 <sup>3</sup>	10.5	This study
Amine-modified Mg-MOF-74	10	8.2 × 10 <sup>-08</sup>	2.5 × 10 <sup>3</sup>	28	This study
ZIF-8	30	6.0 × 10 <sup>-08</sup>	5.4 × 10 <sup>3</sup>	4.5	Bux et al. (2009)
ZIF-7	1.5	7.7 × 10 <sup>-08</sup>	3.5 × 10 <sup>2</sup>	6.5	Li et al. (2010)
ZIF-22	40	1.7 × 10 <sup>-07</sup>	2.0 × 10 <sup>4</sup>	7.2	Huang et al. (2010)
ZIF-69	50	6.5 × 10 <sup>-08</sup>	9.7 × 10 <sup>3</sup>	2.7	Liu et al. (2010)
ZIF-90	20	2.4 × 10 <sup>-07</sup>	1.4 × 10 <sup>4</sup>	7.3	Huang et al. (2010)
MIL-53	8	5.0 × 10 <sup>-07</sup>	1.2 × 10 <sup>4</sup>	6.8	Hu et al. (2011)
KUUST-1	60	1.0 × 10 <sup>-06</sup>	1.8 × 10 <sup>5</sup>	2.7	Guo et al. (2009)

\* Permeability is calculated as the membrane permeance multiplied by the membrane thickness. 1 Barrer = 3.348 × 10<sup>-16</sup> mol m/(m<sup>2</sup> s Pa).

**Table 5**

Gas permeances of H<sub>2</sub> and CO<sub>2</sub> and mixture separation factors of H<sub>2</sub>/CO<sub>2</sub> from equimolar mixtures at room temperature and 1 bar of 4 tested Mg-MOF-74 membranes.

H <sub>2</sub> permeance (mol m <sup>-2</sup> s <sup>-1</sup> Pa <sup>-1</sup> )	CO <sub>2</sub> permeance (mol m <sup>-2</sup> s <sup>-1</sup> Pa <sup>-1</sup> )	Mixture separation factor H <sub>2</sub> /CO <sub>2</sub>
1 8.2 × 10 <sup>-8</sup>	2.8 × 10 <sup>-9</sup>	28
2 9.0 × 10 <sup>-8</sup>	3.1 × 10 <sup>-9</sup>	30
3 7.4 × 10 <sup>-8</sup>	2.8 × 10 <sup>-9</sup>	25
4 7.5 × 10 <sup>-8</sup>	2.9 × 10 <sup>-9</sup>	26

#### 4. Conclusion

Phase-pure and compact Mg-MOF-74 membranes have been prepared successfully on MgO-seeded porous Al<sub>2</sub>O<sub>3</sub> supports at 120 °C for 24 h after optimization of the synthesis solution. The mixture separation factor of H<sub>2</sub>/CO<sub>2</sub> was much higher than those of H<sub>2</sub>/CH<sub>4</sub> and H<sub>2</sub>/N<sub>2</sub>, especially at lower temperature. After amine-functionalization of the Mg-MOF-74 membrane by using ethylenediamine, the separation performance of H<sub>2</sub>/CO<sub>2</sub> was remarkably enhanced and the mixture separation performance increased from 10.5 to 28 at room temperature. This increase is ascribed to two effects: (i) One amino group of the diamine is docked to the open Mg site, thus the diamine narrows the effective pore size which retards for steric reasons the carbon dioxide (kinetic diameter 3.3 Å) permeation stronger than the hydrogen one (2.9 Å), and (ii) the other amino group interacts with CO<sub>2</sub> thus reducing its mobility.

#### Acknowledgements

Financial support by EU CARENA (FP7-NMP-2010-LARGE-4, Nr. 263007), and Chinese Academy of Science Visiting Professorship for Senior International Scientists (Grant No. 2013T1G0047) is acknowledged.

#### References

Arnold, M., Kortunov, P., Jones, D., Nedellec, Y., Kärger, J., Caro, J., 2007. Oriented crystallization on supports and anisotropic mass transport of the metal organic framework manganese formate. *Eur. J. Inorg. Chem.* 1, 60–64.

Bae, T., Long, J.R., 2013. CO<sub>2</sub>/N<sub>2</sub> separations with mixed-matrix membranes containing Mg<sub>2</sub>(dobdc) nanocrystals. *Energy Environ. Sci.* 6, 3565–3569.

Bétard, A., Zander, D., Fischer, R.A., 2010. Dense and homogeneous coatings of CPO-27-M type metal-organic frameworks on alumina substrates. *CrystEngComm* 12, 3768–3772.

Böhme, U., Barth, B., Paula, C., Kuhnt, A., Schwieger, W., Mundstock, A., Caro, J., 2013. Martin Hartmann, Ethene/ethane and propene/propane separation via the olefin and paraffin selective metal-organic framework adsorbents CPO-27 and ZIF-8. *Langmuir* 29, 8592–8600.

Britt, D., Furukawa, H., Wang, B., Glover, T.G., Yaghi, O.M., 2009. Highly efficient separation of carbon dioxide by a metal-organic framework replete with open metal sites. *Proc. Natl. Acad. Sci.* 106, 20637–20640.

Brown, A.J., Brunelli, N.A., Eum, K., Rashidi, F., Johnson, J.R., Koros, W.J., Jones, C.W., Nair, S., 2014. Interfacial microfluidic processing of metal-organic framework hollow fiber membranes. *Science* 345, 72–75.

Bux, H., Liang, F., Li, Y., Cravillon, J., Wiebcke, M., Caro, J., 2009. Zeolitic imidazolate framework membrane with molecular sieving properties by microwave-assisted solvothermal synthesis. *J. Am. Chem. Soc.* 131, 16000–16001.

Caskey, S.R., Wong-Foy, A.G., Matzger, A.J., 2008. Dramatic tuning of carbon dioxide uptake via metal substitution in a coordination polymer with cylindrical pores. *J. Am. Chem. Soc.* 130, 10870–10871.

Chang, A.C.C., Chuang, S.S.C., Gray, M., Soong, Y., 2003. In-situ infrared study of CO<sub>2</sub> adsorption on SBA-15 grafted with gamma-(aminopropyl)triethoxysilane. *Energy Fuels* 17, 468–473.

Choi, S., Watanabe, T., Bae, T., Sholl, D.S., Jones, C.W., 2012. Modification of the Mg/DOBDC MOF with amines to enhance CO<sub>2</sub> adsorption from ultradilute gases. *J. Phys. Chem. Lett.* 3, 1136–1141.

de Vos, R.M., Verweij, H., 1998. High-selectivity, high-flux silica membranes for gas separation. *Science* 279, 1710–1711.

Dietzel, P.D.C., Besikiotis, V., Blom, R., 2009. Application of metal-organic frameworks with coordinatively unsaturated metal sites in storage and separation of methane and carbon dioxide. *J. Mater. Chem.* 19, 7362–7370.

Dietzel, P.D.C., Georgiev, P.A., Eckert, J., Blom, R., Strässle, T., Unruh, T., 2010. Interaction of hydrogen with accessible metal sites in the metal-organic frameworks M<sub>2</sub>(dhtp) (CPO-27-M; M=Ni, Co, Mg). *Chem. Commun.* 46, 4962–4964.

Dietzel, P.D.C., Johnsen, R.E., Blom, R., Fjellvag, H., 2008. Structural changes and coordinatively unsaturated metal atoms on dehydration of honeycomb analogous microporous metal-organic frameworks. *Chem. A Eur. J.* 14, 2389–2397.

Dietzel, P.D.C., Morita, Y., Blom, R., Fjellvag, H., 2005. An in situ high-temperature single-crystal investigation of a dehydrated metal-organic framework compound and field-induced magnetization of one-dimensional metal-oxygen chains. *Angew. Chem. Int. Ed.* 44, 6354–6358.

Dietzel, P.D.C., Panella, B., Hirscher, M., Blom, R., Fjellvag, H., 2006. Hydrogen adsorption in a nickel based coordination polymer with open metal sites in the cylindrical cavities of the desolvated framework. *Chem. Commun.* 9, 959–961.

Dzubak, A.L., Lin, L., Kim, J., Swisher, J.A., Poloni, R., Maximoff, S.N., Smit, B., Gagliardi, L., 2012. Ab initio carbon capture in open-site metal-organic frameworks. *Nat. Chem.* 4, 810–816.

Guo, H., Zhu, G., Hewitt, I.J., Qiu, S., 2009. "Twin copper source" growth of metal-organic framework membrane: Cu<sub>3</sub>(BTC)<sub>2</sub> with high permeability and selectivity for recycling H<sub>2</sub>. *J. Am. Chem. Soc.* 131, 1646–1647.

Herm, Z.R., Krishna, R., Long, J.R., 2012. CO<sub>2</sub>/CH<sub>4</sub>, CH<sub>4</sub>/H<sub>2</sub> and CO<sub>2</sub>/CH<sub>4</sub>/H<sub>2</sub> separations at high pressures using Mg<sub>2</sub>(dobdc). *Microporous Mesoporous Mater.* 151, 481–487.

Hermes, S., Schroder, F., Chelmoski, R., Woll, C., Fischer, R.A., 2005. Selective nucleation and growth of metal-organic open framework thin films on patterned COOH/CF<sub>3</sub>-terminated self-assembled monolayers on Au(111). *J. Am. Chem. Soc.* 127, 13744–13745.

Hong, M., Li, S., Falconer, J.L., Noble, R.D., 2008. Hydrogen purification using a SAPO-34 membrane. *J. Membr. Sci.* 307, 277–283.

Hu, Y., Dong, X., Nan, J., Jin, W., Ren, X., Xu, N., Lee, Y.M., 2011. Metal-organic framework membranes fabricated via reactive seeding. *Chem. Commun.* 47, 737–739.

Huang, A., Bux, H., Steinbach, F., Caro, J., 2010. Molecular-sieve membrane with hydrogen permselectivity: ZIF-22 in LTA topology prepared with 3-aminopropyltriethoxysilane as covalent linker. *Angew. Chem. Int. Ed.* 49, 4958–4961.

Huang, A., Dou, W., Caro, J., 2010. Steam-stable zeolitic imidazolate framework ZIF-90 membrane with hydrogen selectivity through covalent functionalization. *J. Am. Chem. Soc.* 132, 15562–15564.

Huang, A., Liang, F., Steinbach, F., Caro, J., 2010. Preparation and separation properties of LTA membranes by using 3-aminopropyltriethoxysilane as covalent linker. *J. Membr. Sci.* 350, 5–9.

- Huang, A., Wang, N., Kong, C., Caro, J., 2012. Organosilica-functionalized zeolitic imidazolate framework ZIF-90 membrane with high gas-separation performance. *Angew. Chem. Int. Ed.* 51, 10551–10555.
- Hwang, Y.K., Hong, D.Y., Chang, J.S., Jung, S.H., Seo, Y.K., Kim, J., Vimont, A., Daturi, M., Serre, C., Ferey, G., 2008. Amine grafting on coordinatively unsaturated metal centers of MOFs: consequences for catalysis and metal encapsulation. *Angew. Chem. Int. Ed.* 47, 4144–4148.
- Jeong, H.K., Krohn, J., Sujaoti, K., Tsapatsis, M., 2002. Oriented molecular sieve membranes by heteroepitaxial growth. *J. Am. Chem. Soc.* 124, 12966–12968.
- Kanezashi, M., O'Brien-Abraham, J., Lin, Y.S., Suzuki, K., 2008. Gas permeation through DDR-type zeolite membranes at high temperatures. *AIChE J.* 54, 1478–1486.
- Kong, X., Scott, E., Ding, W., Mason, J.A., Long, J.R., Reimer, J.A., 2012. CO<sub>2</sub> dynamics in a metal–organic framework with open metal sites. *J. Am. Chem. Soc.* 134, 14341–14344.
- Koutsonikolas, D., Kaldish, S., Sakellariopoulos, G.P., 2009. A low-temperature CVI method for pore modification of sol–gel silica membranes. *J. Membr. Sci.* 342, 131–137.
- Krishna, R., van Baten, J.M., 2011. In silico screening of metal–organic frameworks in separation applications. *Phys. Chem. Chem. Phys.* 13, 10593–10616.
- Langeroudi, E.G., Kleitz, F., Iliuta, M.C., Larachi, F., 2009. Grafted amine/CO<sub>2</sub> interactions in (Gas–liquid–solid adsorption/absorption equilibria). *J. Phys. Chem. C* 113 (52), 21866–21876.
- Lee, D., Li, Q., Kim, H., Lee, K., 2012. Preparation of Ni-MOF-74 membrane for CO<sub>2</sub> separation by layer-by-layer seeding technique. *Microporous Mesoporous Mater.* 163, 169–177.
- Li, Y., Bux, H., Feldhoff, A., Li, G., Yang, W., Caro, J., 2010. Controllable synthesis of metal–organic frameworks: from MOF nanorods to oriented MOF membranes. *Adv. Mater.* 22, 3322–3326.
- Li, Y., Liang, F., Bux, H., Feldhoff, A., Yang, W., Caro, J., 2010. Molecular sieve membrane: supported metal–organic framework with high hydrogen selectivity. *Angew. Chem. Int. Ed.* 49, 548–551.
- Li, Y., Liang, F., Bux, H., A., Yang, W., Caro, J., 2010. Zeolitic imidazolate framework ZIF-7 based molecular sieve membrane for hydrogen separation. *J. Membr. Sci.* 354, 48–54.
- Liu, Q., Wang, N., Caro, J., Huang, A., 2013. Bio-inspired polydopamine: a versatile and powerful platform for covalent synthesis of molecular sieve membranes. *J. Am. Chem. Soc.* 135, 17679–17682.
- Liu, Y., Hu, E., Khan, E.A., Lai, Z., 2010. Synthesis and characterization of ZIF-69 membranes and separation for CO<sub>2</sub>/CO mixture. *J. Membr. Sci.* 353, 36–40.
- Lu, G., Hupp, J.T., 2010. Metal–organic frameworks as sensors: a ZIF-8 based Fabry–Perot device as a selective sensor for chemical vapors and gases. *J. Am. Chem. Soc.* 132, 7832–7833.
- Mahajan, R., Koros, W.J., 2000. Factors controlling successful formation of mixed-matrix gas separation materials. *Ind. Eng. Chem. Res.* 39, 2692–2696.
- Mason, J.A., Sumida, K., Herm, Z.R., Krishna, R., Long, J.R., 2011. Evaluating metal–organic frameworks for post-combustion carbon dioxide capture via temperature swing adsorption. *Energy Environ. Sci.* 4, 3030–3040.
- Mundstock, A., Böhme, U., Barth, B., Hartmann, M., Caro, J., 2013. Propylene/propane separation in fixed-bed adsorber and membrane permeation. *Chem. Ing. Tech.* 85, 1694–1699.
- Ockwig, N.W., Nenoff, T.M., 2007. Membranes for hydrogen separation. *Chem. Rev.* 107, 4078–4110.
- Planas, N., Dzubak, A.L., Poloni, R., Chiang, L., McManus, A., McDonald, T.M., Neaton, J.B., Lange, J.R., Smit, B., Gagliardi, L., 2013. The mechanism of carbon dioxide adsorption in an alkylamine-functionalized metal–organic framework. *J. Am. Chem. Soc.* 135, 7402–7405.
- Ranjan, R., Tsapatsis, M., 2009. Microporous metal organic framework membrane on porous support using the seeded growth method. *Chem. Mater.* 21, 4920–4924.
- Remy, T., Peter, S.A., Van der Perre, S., Valvekens, P., de Vos, D.E., Baron, G.V., Denayer, J.F.M., 2013. Selective dynamic CO<sub>2</sub> separations on Mg-MOF-74 at low pressures: a detailed comparison with 13X. *J. Phys. Chem. C* 117, 9301–9310.
- Robeson, L.M., 1991. Correlation of separation factor versus permeability for polymeric membranes. *J. Membr. Sci.* 62, 165–185.
- Robeson, L.M., 2008. The upper bound revisited. *J. Membr. Sci.* 320, 390–400.
- Rodenas, T., van Dalen, M., García-Pérez, E., Serra-Crespo, P., Zornoza, B., Kapteijn, F., Gascon, J., 2014. Visualizing MOF mixed matrix membranes at the nanoscale: towards structure–performance relationships in CO<sub>2</sub>/CH<sub>4</sub> separation over NH<sub>2</sub>-MIL-53(Al)@PI. *Adv. Funct. Mater.* 24, 249–256.
- Rosi, N.L., Kim, J., Eddaoudi, M., Chen, B.L., O'Keeffe, M., Yaghi, O.M., 2005. Rod packings and metal–organic frameworks constructed from rod-shaped secondary building units. *J. Am. Chem. Soc.* 127, 1504–1518.
- Rostrup-Nielsen, J.R., Rostrup-Nielsen, T., 2002. Large-scale hydrogen production. *CATTECH* 6, 150–159.
- Sabo, M., Boehlmann, W., Kaskel, S., 2006. Titanium terephthalate (TT-1) hybrid materials with high specific surface area. *J. Mater. Chem.* 16, 2354–2357.
- Seo, J.S., Whang, D., Lee, H., Jun, S.I., Oh, J., Jeon, Y.J., Kim, K., 2000. A homochiral metal–organic porous material for enantioselective separation and catalysis. *Nature* 404, 982–986.
- Serna-Guerrero, R., Da'na, E., Sayari, A., 2008. New insights into the interactions of CO<sub>2</sub> with amine-functionalized silica. *Ind. Eng. Chem. Res.* 47, 9406–9412.
- Shiflett, M.B., Foley, H.C., 1999. Ultrasonic deposition of high-selectivity nanoporous carbon membranes. *Science* 285, 1902–1905.
- Su, F., Lu, C., Kuo, S., Zeng, W., 2010. Adsorption of CO<sub>2</sub> on amine-functionalized Y-type zeolites. *Energy Fuels* 24, 1441–1448.
- Uemiya, S., Matsuda, T., Kikuchi, E., 1991. Hydrogen permeable palladium–silver alloy membrane supported on porous ceramics. *J. Membr. Sci.* 56, 315–325.
- Wicke, E., Kallenbach, R., 1941. Die Oberflächendiffusion von Kohlendioxid in aktiven Kohlen 97, 135–151.
- Yaghi, O.M., O'Keeffe, M., Ockwig, N.W., Chae, H.K., Eddaoudi, M., Kim, J., 2003. Reticular synthesis and the design of new materials. *Nature* 423, 705–714.
- Yang, D., Cho, H., Kim, J., Yang, S., Ahn, W., 2012. CO<sub>2</sub> capture and conversion using Mg-MOF-74 prepared by a sonochemical method. *Energy Environ. Sci.* 5, 6465–6473.
- Yazydın, A.Ö., Snurr, R.Q., Park, T., Koh, K., Liu, J., LeVan, M.D., Benin, A.I., Jakubczak, P., Lanuza, M., Galloway, D.B., Low, J.J., Willis, R.R., 2009. Screening of metal–organic frameworks for carbon dioxide capture from flue gas using a combined experimental and modeling approach. *J. Am. Chem. Soc.* 131, 18198–18199.
- Yoo, Y., Lai, Z., Jeong, H., 2009. Fabrication of MOF-5 membranes using microwave-induced rapid seeding and solvothermal secondary growth. *Microporous Mesoporous Mater.* 123, 100–106.
- Yu, J., Balbuena, P.B., 2013. Water effects on postcombustion CO<sub>2</sub> capture in Mg-MOF-74. *J. Phys. Chem. C* 117 (7), 3383–3388.
- Zhao, Z., Li, Z., Lin, Y., 2009. Adsorption and diffusion of carbon dioxide on metal–organic framework (MOF-5). *Ind. Eng. Chem. Res.* 48, 10015–10020.

## IV. An Example for the Love-Hate Relationship between MOFs and Humidity

As argued throughout this thesis, there are a few distinct issues standing between the majority of MOFs and their successful and widespread application in the real world, with one of the most important being the vulnerability to industrial (e.g.  $H_2S$ ) as well as ambient "hazards" like ordinary water, which is either very hard to get out again in the most optimistic case (necessitating the use of resource-consuming activation methods) or simply damages/destroys the material.

The sole publication featured in this chapter revolves around a very interesting example where both of these phenomena go hand in hand, namely Co-MOF-74 who not only changes color (dark red/black  $\rightarrow$  light red/orange) but also suffers from surface blockade most probably due to a phase transformation after being exposed to room air and its natural level of humidity for a very short period of time. Fortunately, IR microscopy-based gas uptake measurements revealed that a methanol atmosphere can be used to anneal the crystalline material, what eventually reopens the channel system and thereby restores the MOF's ability to accommodate guests like propane. Dr. Christian Chmelik was responsible for the IR microscopy/gas uptake experiments and wrote the majority of this article. Everything related to the MOF synthesis, SEM investigation and humidity response study via XRD, as well as much of the experimental planning was done by the author of this thesis. Prof. Dr. Pascal D. C. Dietzel used his profound knowledge about the material in question to help with the interpretation of the obtained results and put them into context. The initial idea behind this paper and its final touches came from Prof. Dr. Jürgen Caro.

---

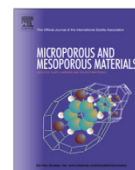


## IV.I Idiosyncrasies of $\text{Co}_2(\text{dhtp})$ : In Situ-Annealing by Methanol

C. Chmelik, A. Mundstock, P. D. C. Dietzel, J. Caro

*Microporous and Mesoporous Materials*, 183, **2014**, 117 - 123.

---

Idiosyncrasies of Co<sub>2</sub>(dhtp): In situ-annealing by methanolChristian Chmelik<sup>a,\*</sup>, Alexander Mundstock<sup>b</sup>, Pascal D.C. Dietzel<sup>c</sup>, Jürgen Caro<sup>b</sup><sup>a</sup> Faculty of Physics and Geosciences, University of Leipzig, Linnéstr. 5, 04103 Leipzig, Germany<sup>b</sup> Institute of Physical Chemistry and Electrochemistry, Leibniz University Hannover, Callinstr. 3A, 30167 Hannover, Germany<sup>c</sup> Department of Chemistry, University of Bergen, Postboks 7803, N-5020 Bergen, Norway

## ARTICLE INFO

## Article history:

Received 16 April 2013

Received in revised form 4 June 2013

Accepted 3 September 2013

Available online 12 September 2013

## Keywords:

Co<sub>2</sub>(dhtp)

Co-MOF-74

CPO-27-Co

IR microscopy

Phase transformation

## ABSTRACT

Structural instability in humid surroundings is one of the major drawbacks of many metal organic frameworks (MOFs) compared to zeolites. In this study we investigate the pronounced sensitivity of MOF Co<sub>2</sub>(dhtp) (Co-MOF-74 or CPO-27-Co) towards humid air. Guest uptake in big Co<sub>2</sub>(dhtp) crystals has been studied by IR microscopy. We found that already a short exposure of 30 s to moist air causes a surface blockage, completely preventing the adsorption of even small guest molecules. It could be confirmed in complementary PXRD measurements that the interior of the crystals remains intact during such short exposure times. Indications for a loss of crystallinity were evidenced only for notably longer exposure times (4 h). Most remarkably, the defects could at least be partially annealed in methanol atmosphere. Reversible adsorption of hydrocarbons in initially blocked crystals was found after exposing the crystals to methanol vapor for about 0.5 h.

© 2013 Elsevier Inc. All rights reserved.

## 1. Introduction

The metal organic framework (MOF) structure of the composition M<sub>2</sub>(dhtp)(H<sub>2</sub>O)<sub>2</sub>·H<sub>2</sub>O (dhtp<sup>4-</sup> = dioxidoterephthalate derived from H<sub>4</sub>dhtp as dihydroxyterephthalic acid, M = Zn, Co, Ni, Mg, Mn, Fe, Cu; the compounds in the series are typically also labeled as M-MOF-74, CPO-27-M, or M<sub>2</sub>(dobdc)) became one of the most studied MOFs for the storage and separation of gas molecules because of the high concentration of coordinatively unsaturated metal sites. The structure was first published as MOF-74 with zinc [1], quickly followed by isostructural compounds with Co [2] and other metals like Ni [3], Mg [4,5], Mn [6], Fe [7,8] and Cu [9]. M<sub>2</sub>(dhtp) has a honeycomb-like one-dimensional pore structure with a pore size of about 1.1–1.2 nm [10]. Especially Mg<sub>2</sub>(dhtp) became known as a prominent adsorbent for CO<sub>2</sub> [11–13]. MOFs with coordinatively unsaturated metal sites like Ni<sub>2</sub>(dhtp) or Fe<sub>2</sub>(dhtp) present promising properties for usage as adsorbents for olefins [14–16] and as catalysts [17]. The cobalt containing structure Co<sub>2</sub>(dhtp) has been identified as a promising candidate for the adsorptive separation of ethylene/ethane, propylene/propane and ethyne/ethylene mixtures [16,18], for selective CO<sub>2</sub> adsorption [5] and as catalyst [19].

The Zn<sub>2</sub>(dhtp) structure is believed to belong to the most stable MOFs; in the steam stability map for several MOF structures, MOF-74/CPO-27 shows a relative high structural stability as found by

XRD measurements which correlates with a high energy of activation of 42.0 kcal/mol for ligand displacement by a water molecule determined by molecular modeling [20]. On the other hand, it was reported by Mertens et al. that Co<sub>2</sub>(dhtp) is very sensitive to moisture [21], and damage of Co<sub>2</sub>(dhtp) in humid surroundings was also detected by Matzger et al. [22].

IR microscopy has been developed into a powerful tool for the determination of mixed gas adsorption isotherms and mixed gas diffusion coefficients in individual crystals of nanoporous materials [23,24]. Furthermore, in the IR micro-imaging mode it allows to record the spatial evolution of the intracrystalline concentration of guest molecules during a sorption process. This ability provides direct access to a quantification of fluxes through the outer surface of individual crystals and, thus, to a characterization of possibly existing outer surface resistances towards mass transfer [25]. In addition to the resistance exerted by the intracrystalline diffusion inside the pore network, such barriers may notably influence or even dominate the uptake of guest molecules [26,27].

In this paper the uptake of methanol and several small alkanes and alkenes into individual crystals of Co<sub>2</sub>(dhtp) was characterized by IR microscopy. We report the surprising finding of an in situ-annealing of Co<sub>2</sub>(dhtp) which was damaged before by a 30 s-contact with humid air. While in air exposed crystals no uptake of guest molecules could be found, after subjecting the sample to a methanol atmosphere the channel network could be opened again for guest uptake. The IR microscopy data are correlated with a series of complementary XRD experiments.

\* Corresponding author. Tel.: +49 3419732531; fax: +49 3419732549.

E-mail address: [chmelik@physik.uni-leipzig.de](mailto:chmelik@physik.uni-leipzig.de) (C. Chmelik).

## 2. Experimental

Unless otherwise noted, all procedures were performed under ambient atmosphere and temperature. All reagents were obtained from commercial vendors at reagent grade purity or higher and used without further purification.

### 2.1. Co<sub>2</sub>(dhtp) synthesis, XRD preparation, annealing and characterization

For IR microscopy, relatively big crystals (>200 μm) had to be synthesized. In consideration of the very nature of the Co<sub>2</sub>(dhtp) idiosyncrasies examined in this study, these had to be prepared, handled and stored with special care to avoid any contact with humid air.

The Co<sub>2</sub>(dhtp) material studied in this work was synthesized following a previously reported [19] but slightly modified procedure. Co(NO<sub>3</sub>)<sub>2</sub>·6H<sub>2</sub>O (cobalt nitrate hexahydrate, 750 mg, 2.58 mmol) and DOT (2,5-dihydroxy benzenedicarboxylic acid, 144 mg, 0.73 mmol) were dissolved in a 1:1:1 (v/v/v) mixture of DMF–ethanol–water (60 mL) and stirred for several minutes. The homogeneous solution was then transferred to a 125 mL Teflon-lined stainless steel autoclave (Parr Instruments (Germany)) and placed in an oven at 121 °C for 24 h. After reaction under autogenous pressure, the autoclaves were cooled down very slowly (over 12 h) to room temperature. The mother liquor, along with the red-orange crystalline product, was then transferred from the autoclave into a 100 mL sealable reaction vial (Schott Duran Bottle). Here the mother liquor was replaced step after step with fresh DMF without exposing the crystals to air. The Co<sub>2</sub>(dhtp) was then washed several times with new DMF and subsequently with fresh methanol, using the same replacement method like before. The latter was used to remove the DMF guest molecules incorporated in the crystals by suspending the product for three days, during which the methanol was replaced four times. A fully desolvation/activation of the compound was achieved by heating (180 °C) under vacuum over 2 h, yielding some dark-purple (nearly black) crystalline porous material. In this activated state, Co<sub>2</sub>(dhtp) is highly air and moisture sensitive and was stored, therefore, in a sealed Schlenk flask under vacuum in a glove box (Ar).

The annealing was done by exposing the air contacted material for 24 h to a methanol atmosphere in an exsiccator filled with methanol and evacuated.

### 2.2. IR microscopy

The methodology of IR microscopy for sorption and diffusion measurements has been described in detail elsewhere [23,28]. In short, it is based on following the intensity of characteristic IR bands of the guest molecules, which is known to be proportional to their concentration. Our setup consists of a Bruker HYPERION 3000 IR microscope which is attached to a Bruker VERTEX 80v FTIR spectrometer. For the measurement, some dozen crystals were introduced into the IR cell employing two different procedures: (i) Filling the cell outside the glove box which includes contact to humid air for about 30 s; (ii) Filling the cell inside the glove box under Ar atmosphere. Then, the cell was connected to the static vacuum system. For activation, the crystals were heated to 180 °C with a heating rate of 5 K/min and kept under vacuum at this elevated temperature for 2 h.

A scheme of the IR measurements is shown in Fig. 1. For the measurement, the IR cell is then mounted on the movable x–y sample stage of the microscope. After selection of an individual Co<sub>2</sub>(dhtp) crystal in visible mode, all IR measurements were run in IR transmission mode at 298 K. Adsorption or desorption steps were

initiated by step-changes in the gas phase surrounding the crystals by altering the gas pressure inside the attached vacuum system. The uptake is followed by recording time-resolved IR spectra either by using the integral mode to obtain integral uptake curves or the IR micro-imaging mode to obtain transient intracrystalline concentration profiles (spatial resolution up to 2.7 × 2.7 μm<sup>2</sup>).

For further analysis, the uptake curves for each uptake step were normalized as  $c_{\text{norm}}$  to run from zero at  $t = 0$  s to unity for infinite time (equilibrium) and fitted with an analytical solution of Fick's 2nd law for diffusion limited uptake in a system with one-dimensional channels [29]:

$$c_{\text{norm}} = \frac{c(t) - c(t=0)}{c(t=\infty) - c(t=0)} = 1 - \frac{8}{\pi^2} \sum_{n=0}^{\infty} \frac{1}{(2n+1)^2} \exp\left(-\frac{(2n+1)^2 \pi^2 D_T t}{l^2}\right) \quad (1)$$

The transport diffusivity  $D_T$  is included as free fitting parameter,  $l$  denotes the channel (crystal) length. For the fits the sum was calculated until  $n_{\text{max}} = 100$ . Please note that Eq. (1) is valid only if the influence of external mass transfer resistances is negligible and the diffusivity does not depend on the guest loading in the considered concentration step.

### 2.3. XRD and SEM

For the XRD experiments Co<sub>2</sub>(dhtp) as environmentally sensitive material was transferred to an airtight specimen holder with a dome like X-ray transparent cap (Bruker). The controlled air exposures were achieved by simply unscrewing the cap and placing the holder on a well-ventilated spot. After some time the open holder was placed back in the glove-box, evacuated. The XRD patterns of the Co<sub>2</sub>(dhtp) samples were obtained on a Bruker D8 Advance X-ray Diffractometer using Cu K<sub>α</sub> ( $\lambda = 1.54 \text{ \AA}$ ) radiation.

The morphology of the Co<sub>2</sub>(dhtp) crystals was studied by scanning electron microscopy (SEM). SEM micrographs were taken on a JEOL JSM-6700F with a cold field emission gun operating at 2 kV and 10 μA.

## 3. Results

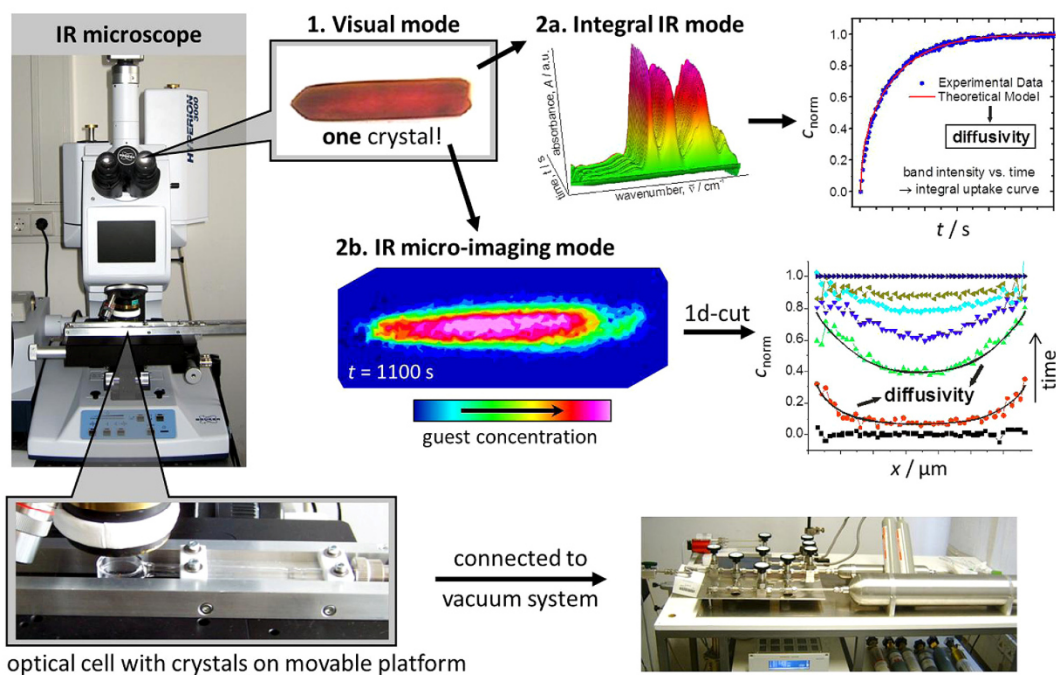
### 3.1. Synthesis

Fig. 1 shows SEM images of the synthesized Co<sub>2</sub>(dhtp) material used in our XRD and IR experiments. Habit and crystal size of our Co<sub>2</sub>(dhtp) are similar to the CPO-27-Co synthesized by microwave heating by Cho et al. [19]. The sample consists of single-phase hexagonal column-structured particles with large aspect ratios (Fig. 2A). It is noticeable that the powder consists, to a large extent, of crystal fragments, showing a wide particle size distribution with lengths ranging from 10 to 100 μm and widths from 5 up to 20 μm (see Fig. 2B). The rarely seen intact Co<sub>2</sub>(dhtp) crystals were up to 300 μm long and 50 μm wide.

The XRD pattern of the Co<sub>2</sub>(dhtp) sample prepared under the synthesis, storage and activation conditions mentioned above is shown in Fig. 6A. Apart from the amorphous underground caused by the gastight specimen holder, the XRD of our Co<sub>2</sub>(dhtp) is in good agreement with the pattern reported by Dietzel et al. [3] showing that our sample is Co<sub>2</sub>(dhtp) with, however, a non-identified peak at about 7°.

### 3.2. IR microscopy

The uptake of different small guest molecules in large individual Co<sub>2</sub>(dhtp) crystals was studied by IR microscopy. Considering



**Fig. 1.** Schematics of the IR microscopy experiments. One individual crystal is selected for the uptake study in the visual mode. The uptake can be recorded as function of time in, (2a) integral mode (one averaged signal from the entire crystal) or, (2b) IR micro-imaging mode (with spatial resolution within the crystal).

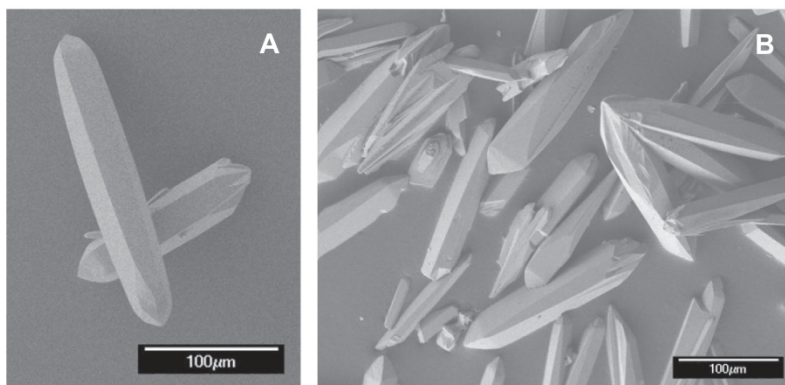


**Fig. 2.** SEM images of the  $\text{Co}_2(\text{dhtp})$  material used in our XRD and IR studies.

the quite large channel diameter of about 11 Å for the dehydrated  $\text{Co}_2(\text{dhtp})$  sample, rapid filling of the pore space is to be expected with time constants of not more than a couple of minutes. However, when the crystals are loaded into the IR cell following procedure 1 (which includes a short contact with humid air) no uptake at all could be observed for small alkanes and alkenes, such as ethane, propane, ethene and propene. Only methanol was found to enter into the channels, although following a rather unusual time-dependence (see blue bullets in Fig. 3A). Initially the uptake rate is very small indicating a process which would take more than 2 h to be equilibrated. Moreover, the curve exhibits a linear slope which is to be expected for processes being limited by a strong transport resistance (barrier) at the crystal surface. Then, after about 17 min a sudden, step-like increase in mass transfer is

observed finishing the remaining uptake in less than 1 min. This experiment was repeated for five different crystals, including a variation of the pressure step (0–0.2 kPa and 0–1 kPa). All curves follow the same trend and show a pronounced step-like increase occurring after about 15–40 min. This behavior changes notably when the IR cell is loaded following procedure 2 (avoiding contact with humid air). Now, the methanol uptake curve exhibits a “normal” shape and the process is finished after 100 s, already (red squares in Fig. 3A). Assuming diffusion-limited uptake a fit according to Eq. (1) translates into an apparent transport diffusivity of  $D_T = 2 \times 10^{-10} \text{ m}^2 \text{ s}^{-1}$  and lies within the expected range.

Obviously, the route of sample treatment can change the uptake performance dramatically. Already a short contact with humid air might block the crystal interior for the uptake of guest molecules.

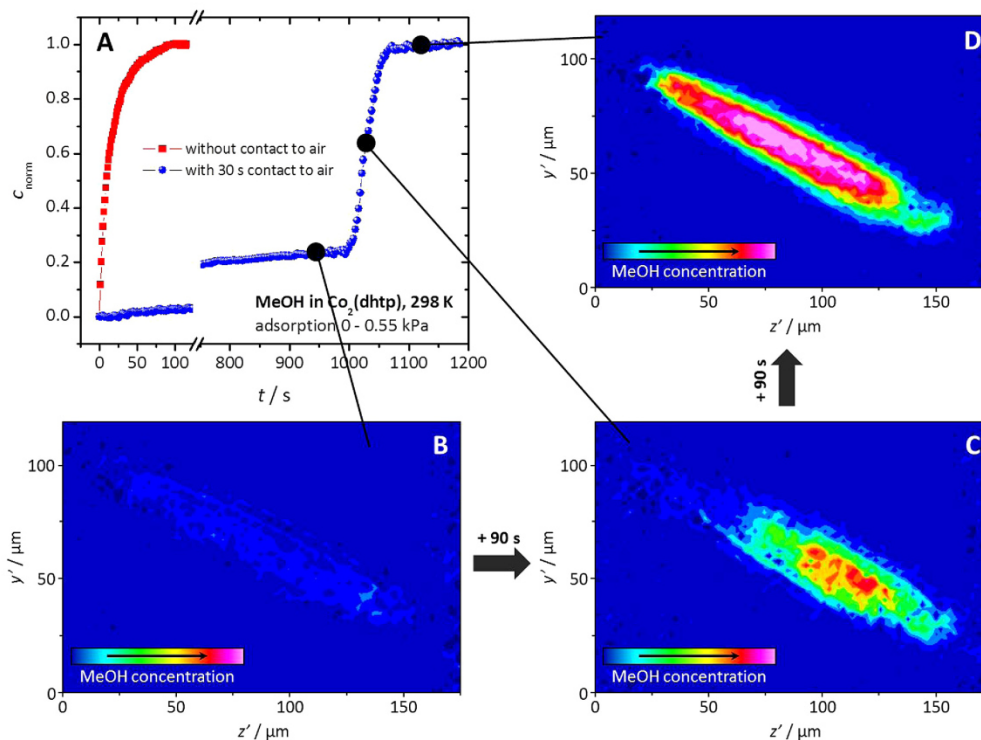


**Fig. 3.** (A) Uptake curves of methanol in a  $\text{Co}_2(\text{dhtp})$  crystal for the pressure step from 0 to 0.55 kPa at 298 K. The uptake in crystals which were exposed to humid air for about 30 s while filling into the IR cell proceeds slow and follows a very unusual step-like trend (blue bullets). Only for crystals where contact with humid air was entirely avoided “normal” uptake behavior could be observed (red squares). Please note the break in the time axis between 125 s and 750 s and the different scaling afterwards. (B–D) Time evolution of the methanol concentration during uptake into an individual  $\text{Co}_2(\text{dhtp})$  crystal. The three images were taken in intervals of about 90 s and show the internal distribution of methanol molecules (B) just before, (C) during and (D) after the step-increase. (For interpretation of the references to color in this figure legend, the reader is referred to the web version of this article.)

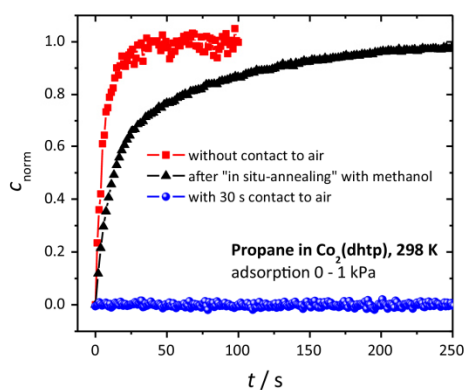


**Fig. 4.** Uptake curves of propane in a  $\text{Co}_2(\text{dhtp})$  crystal for pressure steps of 0–1 kPa at 298 K. No uptake could be detected in crystals which were exposed to humid air for about 30 s while filling into the IR cell (blue bullets). However, uptake was found after “in situ-annealing” with methanol (black triangles). Fastest uptake rates were found in crystals where contact with humid air was entirely avoided (red squares). (For interpretation of the references to color in this figure legend, the reader is referred to the web version of this article.)

This conforms to the observation by FitzGerald et al. who discussed the dramatic effect of brief exposure to air on the IR spectra of CPO-27 materials during hydrogen adsorption [30].

Three features can be noted concerning the uptake of methanol in the air exposed sample: (i) the uptake rate is severely retarded and, (ii) exhibits a linear curve shape while, (iii) no difference in the absolute loading was noted for crystals from both series. These findings indicate that a transport barrier has been formed on the external surface while the crystal interior remained unaffected. A comparable effect has already been reported for another MOF of type  $\text{Zn}(\text{tbip})$  [31]. The sudden step-like increase in the uptake rate indicates that methanol has the capability to remove the formed barrier. Having in mind that methanol is used as solvent in many MOF syntheses one might speculate that some kind of in situ-annealing occurs in presence of a methanol atmosphere, e.g., a recrystallization of the damaged surface layer.

Following methanol uptake into the crystals from series 1 by IR micro-imaging confirms the conclusions made based on the integral uptake rate. In the time before the step-increase the concentration profiles are flat as expected for barrier-limited uptake (Fig. 3B). The limiting elementary step for the guest molecules is to overcome the strong surface barrier. Once entered into the channels the molecules can diffuse fast and immediately distribute over the entire crystal, leading to the observed uniform concentration. After in situ-annealing of the damaged surface layer on at least one of both crystal ends molecules quickly fill the pore space. Apparently, in the current example the layer on the lower right crystal end was removed first. As a consequence, in Fig. 3C we find only the right half of the crystal filled. The methanol diffusion front entered the crystal only from this end and did reach approximately the crystal centre. A short time later the entire crystal is filled and

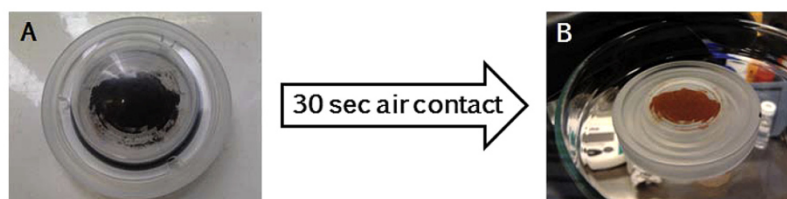


**Fig. 5.** When activated  $\text{Co}_2(\text{dhtp})$  crystals (A) are exposed to humid air for a short time (B) the color changes from dark-purple to light red upon adsorption of water at the coordinatively unsaturated metal centres inside the channels. (For interpretation of the references to color in this figure legend, the reader is referred to the web version of this article.)

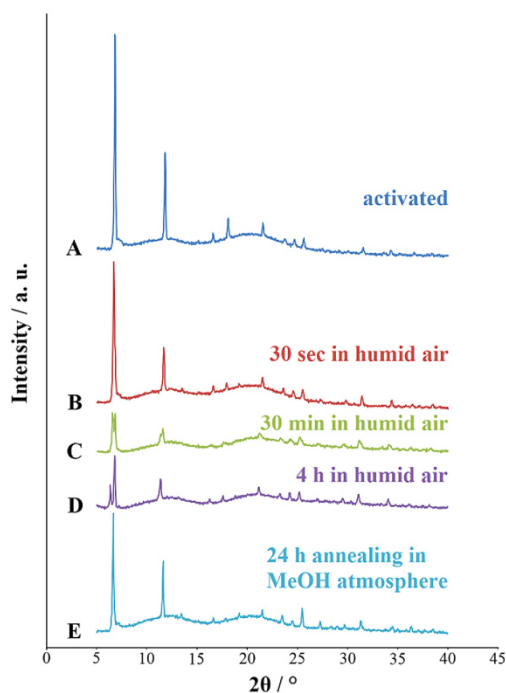


**Fig. 6.** Series of powder XRD measurements investigating the influence of exposure to humid air and methanol atmosphere on the structure of  $\text{Co}_2(\text{dhtp})$ .

we observe a homogeneous equilibrium distribution of methanol (Fig. 3D). Please note that the images were recorded in transmission mode and display, strictly speaking, the product of local concentration and sample thickness. The greenish shadow around the crystal is a result of the crystal shape (decreasing thickness towards the ends).

Following the hypothesis of in situ-annealing one should expect that also other molecules might adsorb into the  $\text{Co}_2(\text{dhtp})$  sample which had been loaded following procedure 1 after exposure to methanol atmosphere. Indeed, after removal of methanol at  $100^\circ\text{C}$  for 2 h rapid uptake of short alkanes and alkenes was found. Fig. 4 compares the uptake curves of propane in a crystal of series 1 (contact to humid air for about 30 s) before (blue bullets) and after (black triangles) in situ-annealing in methanol atmosphere with uptake into a crystal from series 2 (red squares; no contact with air). Although the contact with a methanol atmosphere made the channel network accessible to other guest molecules, we see that the uptake rate is smaller than in crystals of series 2. There are two possible reasons to explain this finding: (i) the contact with methanol atmosphere did not entirely remove the damaged

surface layer or, (ii) during the contact time with methanol the surface layer could be removed only on one of the two crystal ends (see Fig. 3C). Implying a constant crystal length, sealing one of the two faces would retard the uptake time by a factor of four, which is approximately the difference seen in Fig. 4.

### 3.3. XRD

The powder diffraction patterns reflect the state of the bulk  $\text{Co}_2(\text{dhtp})$  substance and how it reacts to exposure to air. A Pawley profile fit of the activated substance yields lattice constants which indicate that the compound is indeed solvent free (see Table 1). After 30 s exposure of the desolvated  $\text{Co}_2(\text{dhtp})$  to surrounding air at room temperature, the color of the activated sample changes from the dark-purple (nearly black) to light red (Fig. 5). This color change, which remains until a new activation, is most likely due to adsorption of water at the coordinatively unsaturated metal centres lining the 1D hexagonal channels of the structure.

The XRD (Fig. 6B) confirms this interpretation. Predominating the pattern are the reflections of a partially hydrated phase with the first two reflections shifted slightly towards lower diffraction angles. The peaks of the original dehydrated phase (Fig. 5A) have diminished significantly in intensity and only the strongest peak remains clearly visible as shoulder of its analogue of the hydrated structure. Indications for any further structural change cannot be found. This result does not refute the conclusion from the IR measurements that short contact with humid air damages a small region on the surface whereas the interior remains unaffected. Changes in a small fraction of the material (such as a layer on the surface) can hardly be detected in conventional XRD experiments. However, if with increasing exposure time the damage or structural change proceeds further it might finally become visible in the XRD data.

Indeed, further details of the changes resulting from continued contact with humid air can already be noticed in the XRD taken after 30 min exposure time (Fig. 6C). These changes become even more pronounced after 4 h of exposure time (Fig. 6D) while afterwards the pattern remains virtually unchanged as indicated by comparison to the measurement after 72 h. First, instead of a single peak at about  $6.8^\circ$ , we observe two peaks in this low angle range, one which is shifted further towards smaller angles ( $\sim 6.4^\circ$ ) and another which remains at the position which it assumed initially. The interpretation of these findings is complicated by the bad signal to noise ratio of the data, which in this case (cobalt compound and time resolved measurements) regrettably cannot be improved using the available laboratory X-ray instrumentation. One interpretation is as phase mixture:

- (i) The stationary peak is caused by a fraction of isolated islands (crystallites) of the material where the pore cannot be accessed from the outer surface (e.g., due to internal blockage or stacking faults). Hence, this fraction stays in its initial activated or solvated state independent of the changes in the surrounding atmosphere.

**Table 1**

Comparison of Co<sub>2</sub>(dhtp) lattice parameters of the activated sample and the sample which was exposed to humid air for 4 h and then annealed under methanol atmosphere for 24 h with data of Ref. [3].

Co <sub>2</sub> (dhtp) sample	a/Å	c/Å
<i>This study</i>		
Activated (Fig. 6A)	25.984(3)	6.851(3)
4 h in air, followed by 24 h exposure to methanol (Fig. 6E)	26.127(4)	6.729(2)
<i>Data from Ref. [3]</i>		
Dehydrated (468 K)	25.95258(101)	6.81854(38)
Hydrated	26.15786(84)	6.71822(25)

- (ii) The pronounced shift of the reflection towards lower angles results from a Co<sub>2</sub>(dhtp) phase with more notably different dimensions of the unit cell than generally expected for Co<sub>2</sub>(dhtp)-type structures in various levels of hydration [3].

An alternative interpretation is that the original CPO-27 structure type phase in space group R-3 transforms into a lower symmetry phase which will result in a split of the reflections. Such phase transformations from space group R-3 to P-1 upon solvent removal occur for the structurally related STA-12 materials [32]. In addition, CPO-27-Zn also passes through a shortly existing phase with possible P-1 symmetry during removal of water [3]. Indeed, we can obtain a satisfactory profile fit of a triclinic unit cell to the present pattern, but we do not consider this as sufficient proof because of the small number of observed reflections in the pattern.

In both cases, the resulting change in the channel-size would be too small to affect the methanol uptake rates as drastically as observed.

Furthermore, the peak intensity in Fig. 6C and D is reduced significantly relative to the other patterns. This could be an indication that a part of our crystalline sample is transformed into a predominantly amorphous material. (It shall be noted that small variations in the amount of sample in the X-ray beam, which might occur when the sample holder is moved and opened for exposure to air, can not be excluded and might also cause such an effect. However, the effect is so large in the present case that it would necessitate the majority of the material to have left the irradiated area. In addition, the subsequent methanol annealed sample exhibits significantly stronger intensities again.)

After annealing the sample under methanol atmosphere for 24 h the diffractogram returns to a pattern typical for the CPO-27 structure again. The lattice parameters obtained from a Pawley profile fit correspond well with those of fully hydrated CPO-27-Co (Table 1). The relative maximum intensities of the first reflections of the activated and annealed sample also change qualitatively as reported for the hydrated and dehydrated compound [3], further corroborating this interpretation.

The behavior of the material on prolonged exposure to atmosphere is intriguing and warrants further study, as it exemplifies that the structure of the coordination network compound can be dramatically affected by the environment the sample finds itself in. In respect to the observations we have made during the diffusion measurements, these are best interpreted on the basis of the pattern in Fig. 6B which shows no dramatic change to the bulk crystalline phase. We therefore think that the most sensible explanation for the diffusion hindrance we initially observed is surficial blockage of the pore entrances, which is not visible in the powder diffraction patterns, by reaction products formed upon short exposure to air (and the humidity contained therein). The blockage is subsequently removed by exposure to methanol vapor. Thus,

whichever process is actually leading to blocked access to the pore, it appears to be reversible in methanol. In addition, air exposed samples of Co<sub>2</sub>(dhtp) can be reversibly hydrated and dehydrated [2], indicating access to the pores, while nitrogen adsorption of air exposed samples is generally diminished.

#### 4. Conclusions

Big crystals of MOF Co<sub>2</sub>(dhtp) (Co-MOF-74 or CPO-27-Co) have been prepared and studied by IR microscopy. We found that this structure is extremely sensitive towards humid surrounding air. Even 30 s exposure to air caused a surface blockage of the pore entrances preventing the adsorption of any guest molecules. However, the air exposed samples can be transformed back into the activated state by in situ exposure to methanol. After annealing by contact with methanol, Co<sub>2</sub>(dhtp) adsorbs reversibly hydrocarbons. If the sample is carefully manipulated inside a glove box into the IR cell, the effect of damage is not observed.

#### Acknowledgements

Financial support by DFG priority program SPP 1570 "Porous media with defined pore structure in chemical engineering – modeling, application, synthesis" is acknowledged. Prof. F. Keil is thanked for organizing this DFG Priority program. Further, we thank ENMIX, the "European Nanoporous Materials Institute of Excellence", for support.

#### References

- [1] N.L. Rosi, J. Kim, M. Eddaoudi, B. Chen, M. O'Keefe, O.M. Yaghi, *J. Am. Chem. Soc.* 127 (2005) 1504–1518.
- [2] P.D.C. Dietzel, Y. Morita, R. Blom, H. Fjellvåg, *Angew. Chem. Int. Ed.* 44 (2005) 6354–6358.
- [3] P.D.C. Dietzel, R.E. Johnsen, R. Blom, H. Fjellvåg, *Chem. Eur. J.* 14 (2008) 2389–2397.
- [4] P.D.C. Dietzel, R. Blom, H. Fjellvåg, *Eur. J. Inorg. Chem.* 23 (2008) 3624–3632.
- [5] S.R. Caskey, A.G. Wong-Foy, A.J. Matzger, *J. Am. Chem. Soc.* 130 (2008) 10870–10871.
- [6] W. Zhou, H. Wu, T. Yildirim, *J. Am. Chem. Soc.* 130 (2008) 15268–15269.
- [7] E.D. Bloch, L.J. Murray, W.L. Queen, S. Chavan, S.N. Maximoff, J.P. Bigi, R. Krishna, V.K. Peterson, F. Grandjean, G.J. Long, B. Smit, S. Bordiga, C.M. Brown, J.R. Long, *J. Am. Chem. Soc.* 133 (2011) 14814–14822.
- [8] M. März, R.E. Johnsen, P.D.C. Dietzel, H. Fjellvåg, *Micropor. Mesopor. Mater.* 157 (2012) 62–74.
- [9] R. Sanz, F. Martinez, G. Orcajo, L. Wojtas, D. Briones, *Dalton Trans.* 42 (2013) 2392–2398.
- [10] K. Sumida, C.M. Brown, Z.R. Herm, S. Chavan, S. Bordiga, J.R. Long, *Chem. Commun.* 47 (2011) 1157–1159.
- [11] D. Britt, H. Furukawa, B. Wang, T.G. Glover, O.M. Yaghi, *PNAS* (2009) 20637–20640.
- [12] P.D.C. Dietzel, V. Besikiotis, R. Blom, *J. Mater. Chem.* 19 (2009) 7362–7370.
- [13] R. Krishna, J.M. van Baten, *Phys. Chem. Chem. Phys.* 13 (2011) 10593–10616.
- [14] D. Peralta, G. Chaplais, A. Simon-Masseron, K. Barthelet, C. Chizallet, A.-A. Quoineaud, G.D. Pirngruber, *J. Am. Chem. Soc.* 134 (2012) 8115–8126.
- [15] E.D. Bloch, W.L. Queen, R. Krishna, J.M. Zadrozny, C.M. Brown, J.R. Long, *Science* 335 (2012) 1606–1610.
- [16] Y. He, R. Krishna, B. Chen, *Energy Environ. Sci.* 5 (2012) 9107–9120.
- [17] L. Mitchell, B. Gonzalez-Santiago, J.P.S. Mowat, M.E. Gunn, P. Williamson, N. Acerbi, M.L. Clarke, P.A. Wright, *Catal. Sci. Technol.* 3 (2013) 606–617.
- [18] Y. He, W. Zhou, R. Krishna, B. Chen, *Chem. Commun.* 48 (2012) 1831–1831.
- [19] H.-Y. Cho, D.-A. Yang, J. Kim, S.-Y. Jeong, W.-S. Sahn, *Catal. Today* 185 (2012) 35–40.
- [20] J.J. Low, A.I. Benin, P. Jakubczak, J.F. Abrahamian, S.A. Faheem, R.R. Willis, *J. Am. Chem. Soc.* 131 (2009) 15834–15842.
- [21] S. Hausdorf, F. Baitalov, T. Bohle, D. Rafaja, F.O.R.L. Mertens, *J. Am. Chem. Soc.* 132 (2010) 10978–10981.
- [22] A.C. Kizzie, A.G. Wong-Foy, A.J. Matzger, *Langmuir* 27 (2011) 6368–6373.
- [23] C. Chmelik, J. Kärger, *Chem. Soc. Rev.* 39 (2010) 4864–4884.
- [24] H. Bux, C. Chmelik, J.M. van Baten, R. Krishna, J. Caro, *Adv. Mater.* 22 (2010) 4741–4743.
- [25] F. Hibbe, C. Chmelik, L. Heinke, S. Pramanik, J. Li, D.M. Ruthven, D. Tzoulaki, J. Kärger, *J. Am. Chem. Soc.* 133 (2011) 2804–2807.
- [26] L. Heinke, J. Kärger, *Phys. Rev. Lett.* 106 (2011) 074501.
- [27] D.S. Sholl, *Nat. Chem.* 3 (2011) 429–430.

- [28] C. Chmelik, H. Bux, J. Caro, L. Heinke, F. Hibbe, T. Titze, J. Kärger, *Phys. Rev. Lett.* 104 (2010) 085902.
- [29] J. Kärger, D.M. Ruthven, D.N. Theodorou, *Diffusion in Nanoporous Materials*, Wiley-VCH, Weinheim, 2012.
- [30] S.A. FitzGerald, B. Burkholder, M. Friedman, J.B. Hopkins, C.J. Pierce, J.M. Schloss, B. Thompson, J.L.C. Rowsell, *J. Am. Chem. Soc.* 133 (2011) 20310–20318.
- [31] C. Chmelik, F. Hibbe, D. Tzoulaki, L. Heinke, J. Caro, J. Li, J. Kärger, *Microporous Mesoporous Mater.* 129 (2010) 340–344.
- [32] S.R. Miller, G.M. Pearce, P.A. Wright, F. Bonino, S. Chavan, S. Bordiga, I. Margiolaki, N. Guillou, G. Férey, S. Bourrelly, P.L. Llewellyn, *J. Am. Chem. Soc.* 130 (2008) 15967–15981.
-



---

## V. Conclusions

### VI Summary

The crucial question this thesis and its six associated publications set out to help answer was whether permeation through membranes made from or containing certain nanoporous materials with potentially beneficial "out-of-the-box" properties as well as synthetically modified/introduced functionalities could, someday in the near future, become at least a feasible alternative to some of the resource-intensive gas separation methods currently applied in the industry, including necessary evils like cryogenic distillation and scrubbing.

Both of these latter procedures directly relate to the practice-relevant binary model systems focused on in the present study, namely olefins/paraffins and hydrogen/carbon dioxide, which were primarily chosen due to their diversity as well as civilizational relevance in the face of today's ever-growing energy hunger, climate change/pollution or the omnipresence of polymers. Because addressing such fundamentally different separation issues (various critical diameters, polarizabilities, reactivities etc.) calls, at best, for multipurpose affinity sieves featuring adaptable/functionalizable interaction point, the choice of material fell on the well-known zeolite type X (mobile/exchangeable counterions in a rigid 3D pore system) and the promising metal-organic framework 74 (11 nm wide 1D channels lined with unsaturated metal centers).

In order to pre-evaluate the ethylene/ethane and propylene/propane separation potential of the MOF in question, two of its metal variants (Mg, Co) plus ZIF-8 (a staple in this regard) as reference were at first characterized via powder-based adsorption as well as breakthrough experiments in a fixed-bed adsorber, followed by the actual  $C_3$  permeation measurements on a supported Mg-MOF-74 membrane grown using a newly developed preparation route to accommodate for the one-dimensional pores' special orientation requirements (perpendicular to the  $Al_2O_3$  disk surface/parallel to the gas flow direction). While the first results still gave reason for hope because they clearly revealed/showcased MOF-74's pronounced adsorption selectivity towards the respective olefins (the exact opposite of how zeolitic imidazolate framework ZIF-8 behaves), it soon became apparent that all real measurable separation factors were either significantly lower than the predicted ones (e.g.  $SF_{propylene/propane} = 2.9$  instead of 46 [theoretical] for Co-MOF-74 powder) or simply 1, as in the case of said layer which was, most probably, further handicapped by an host-guest interaction-caused partial channel blockage.

When it comes to neat zeolite type X membranes (FAU structure), on the other hand, the main hurdle to overcome isn't the right orientation of the 3D pore system but rather their propensity for defect-richness, a direct consequence of adverse growth issues (electrostatic rejection between precursor species  $\leftrightarrow$  corundum, inhomogeneous nucleation etc.) addressed/circumvented in the present work via a pre-synthetic support surface modification with certain bridge/anchor molecules

---

(poly-dopamine or 3-aminopropyltriethoxysilane), resulting in substantially enhanced separation capabilities towards both model gas systems ( $SF_{\text{propylene/propane}} = 14$  (NaX)  $\rightarrow$  3.3 (APTES/NaX) and  $SF_{\text{H}_2/\text{CO}_2} = 8.0$  (NaX)  $\rightarrow$  10.3 (PDA/NaX)). A way to stay well clear of this kind of problematic entirely in the first place is incorporating type X particles into polymer-based mixed matrix membranes, what also allows for the zeolite's ion exchangeability to be utilized (grown membranes crack during an exchange process) as a setscrew for the materials overall gas selectivity (e.g.  $SF_{\text{H}_2/\text{CO}_2} = 4.0$  (NaX@Matrimid)  $\rightarrow$  5.6 (CoX@Matrimid), 10 wt% faujasite in each case) due to the seemingly direct correlation between the ionic potential of the contained mobile counterions and the  $\text{CO}_2$ /filler interaction strength.

The logical starting points for any pore optimization in the case of MOF-74, in turn, are its coordinatively unsaturated metal centers, as is exemplarily shown/evidenced in the present work through their successful post-synthetic amination in a defect free layer of the Mg variant (synthesized on MgO seeded supports) via ethylenediamine which not only narrows the material's huge pore size but also heightens the  $\text{CO}_2$  adsorption, almost tripling the already present separation preference ( $SF_{\text{H}_2/\text{CO}_2} = 10.5$  (Mg-MOF-74)  $\rightarrow$  28 (amino-functionalized Mg-MOF-74) as a result. Unfortunately, such a high level of functionalizability is a double edged sword at best, insofar that, for example, a mere 30 s exposure to ambient air is enough to cause a complete surface blockage in Co-MOF-74 (rooted in a humidity-driven phase transformation) and thereby render the whole pore system useless until it is reopened by a cumbersome annealing process requiring a MeOH atmosphere, once again shining a spotlight on one of the metal-organic frameworks' most damning handicaps in regard to an widespread implementation/application, namely their pronounced vulnerability to certain environmental factors like the ubiquitous moisture.

## V.I Discussion and Outlook

Observant readers may have noticed that the predominant sentiment towards MOFs in particular and their possible realworld application in this thesis is one of huge theoretical potential (porosity, tailorability, switchability, catalytic activity etc.), normally followed by a long list of problems and idiosyncrasies which throw a monkey wrench in nearly all aspirations. Because a lot of those obstacles have already been exhaustively discussed throughout the previous pages, this chapter mainly focuses on a few additional ones and the crucial role they altogether play in why metal-organic frameworks may never will be more than a niche material, especially when it comes to the field of gas separation.

Unsurprisingly, two of the key aspects are money and competitiveness, with the first one representing a considerable hurdle for supported membranes right from the start due to a multitude of cost-boosting factors like the multilayered (coarse/microfiltration/ultrafiltration for a reduced flow resistance, fired at least 3 times) ceramic support itself ( $> 700$  € per noninstalled  $\text{m}^2$ ),

sophisticated synthesis/preparation/testing/activation/storage equipment (needed in some way or the other for every membrane type), huge areas of separation-active material + "waste powder" (i.a. some MOF linkers come with a price tag of several hundred euros per mg) as well as long-term stability and defect density issues. Although a polymer-based mixed matrix membrane has the upper hand in regard to the cost side of things, leaking hollow fibers, for example, can be mended in situ without replacing the whole reactor, this is somewhat of an inconsequential win because both systems struggle to meet the industrial selectivity and permeability thresholds (commercial viability for e.g.  $H_2/CO_2$ :  $SF \geq 30$  and  $P \approx 500$  Barrer,  $C_3H_6/C_3H_8$ :  $SF \approx 35$ ) required to replace the respective currently used state of the art separation processes.

The second layer of problems is more academic in nature with far reaching consequences for promising selective materials (i.a. chances for application) and a direct result of the way gas separation experiments are conducted in the scientific community today, or rather the multitude of different process parameters (single/mixed gas, pressure, temperature, no/which/how much sweep gas or vacuum etc.) - each one able to effect the membrane's physical quantities tremendously - for which there are sadly no standardized (as close to the praxis relevant ones as possible) values, leading to a lack of comparability even between publications with the same general topic. Furthermore, the scarcity of literature about the negative effects of industry-relevant impurities/byproducts like e.g.  $H_2S$ ,  $SO_2$  or  $NH_3$  on novel systems' performance and stability (e.g. collapsed/blocked MOF structures  $\rightarrow$  decreased separation capability) unnecessarily hampers their sensible evaluation regarding a possible realworld implementation as well as the much needed but often neglected exchange between industry and the ivory tower.

Although they are anything but immune to these kinds of hazards, the harmful gases can still reach the embedded filler particles despite the surrounding matrix while some of the polymers tend to plasticize (decrease in density) over time, MMMs, in summary, seem to be the best and most future proof platform right now when it comes to membrane-based gas separation. But whether they someday manage to replace cryogenic distillation and scrubbing depends in part on a successful reorientation of the related research efforts towards either a much more focused approach (a few universally stable MOFs (Zr, Ti), dedicated high throughput polymers, pore and interface optimization etc.) or, better still, reallocating the majority of the resources currently dedicated to metal-organic frameworks (to many structures without purpose) into more promising fields (i.a. graphene, polymers from  $CO_2$ , cold fusion).

Let's hope that it won't take another 150 years to find a viable solution.

---

## Appendix

### List of Abbreviations

$\alpha$	selectivity
APTES	3-aminopropyltriethoxysilane
BEA	beta zeolite
CAU	Christian-Albrecht-University of Kiel
CCSU	carbon capture, storage and utilization
CD	cryogenic distillation
CGS	centimeter-gram-second
CHP	combined heat and power unit
COF	covalent organic framework
CPO	coordination polymer of Oslo
CVD	chemical vapor deposition
DDR	deca-dodecasil 3R zeolite
DMF	dimethylformamide
DUT	Dresden University of Technology
ECBM	enhanced coalbed methane recovery
EDXS	energy-dispersive X-ray spectroscopy
EOR	enhanced oil recovery
ESGR	enhanced shale gas recovery
FAU	faujasite zeolite
FC	fuel cell
GC	gas chromatography
HKUST	Hong-Kong University of Science and Technology
IR	infrared
LTA	Linde type A zeolite
MCM	Mobile composition of matter
MFI	pentasil zeolite (Mobile five ring)
MIL	matériaux de l'institut Lavoisier
MOF	metal-organic framework
MOR	mordenite zeolite

---

---

MMM	mixed matrix membrane
MS	mass spectrometry
MTO	methanol-to-olefins
P	permeability
PCP	porous coordination polymers
PCN	porous coordination networks
PDA	polydopamine
PDMS	polydimethylsiloxane
PE	polyethylene
PESF	polyethersulfones
PSLE	post-synthetic linker exchange
PP	polypropylene
PS	polystyrol
PSA	pressure swing adsorption
PSME	post-synthetic metal exchange
PVC	polyvinylchloride
PVD	physical vapor deposition
SBU	secondary building unit
SEM	scanning electron microscopy
SF	separation factor
SOD	sodalite
SMR	steam methane reforming
SNG	synthetic natural gas
STP	standard temperature and pressure
TCNQ	tetra-cyanoquinodimethane
THF	tetrahydrofuran
TTF	tetrathiafulvalene
TSA	temperature swing adsorption
UiO	Universitetet i Oslo
VSA	vacuum swing adsorption
WGS	water-gas shift
XRD	X-ray diffraction

---

---

## Publications

1. **MOF-in-COF molecular sieving membrane for selective for selective hydrogen separation**, H. Fan, M. Peng, I. Strauss, A. Mundstock, H. Meng, J. Caro, *Nat. Commun.*, 12 (38), 2021, 1 - 10.  
DOI: 10.1038/s41467-020-20298-7
  2. **Role of the metal cation in the dehydration of the microporous metal-organic frameworks CPO-27-M**, M. H. Rosnes, B. Pato-Doldan, R. E. Johnson, A. Mundstock, J. Caro, P. D. C. Dietzel, *Micropor. Mesopor. Mater.*, 309, 2020, 110503.  
DOI: 10.1016/j.micromeso.2020.110503
  3. **UiO-66 and UiO-66-NH<sub>2</sub> based sensors: Dielectric and FTIR investigations on the effect of CO<sub>2</sub> adsorption**, I. Strauss, K. Chakarova, A. Mundstock, M. Mihaylov, K. Hadjivanov, N. Guschanski, J. Caro, *Micropor. Mesopor. Mater.*, 302, 2020, 110227.  
DOI: 10.1016/j.micromeso.2020.110227
  4. **High-Flux Vertically Aligned 2D Covalent Organic Framework Membrane with Enhanced Hydrogen Separation**, H. Fan, M. Peng, I. Strauss, A. Mundstock, H. Meng, J. Caro, *J. Am. Chem. Soc.*, 142 (15), 2020, 6872 - 6877.  
DOI: 10.1021/jacs.0c00972
  5. **Methanol-to-Olefins in a Membrane Reactor within situ Steam Removal - The Decisive Role of Coking**, F. Rieck genannt Best, A. Mundstock, G. Dräger, P. Rusch, N. C. Bigall, H. Richter, J. Caro, *ChemCatChem*, 12 (1), 2020, 273 - 280.  
DOI: 10.1002/cctc.201901222
  6. **Low Thermal Conductivity in Thermoelectric Oxide-Based Multiphase Composites**, M. Wolf, K. Menekse, A. Mundstock, R. Hinterding, F. Nietschke, O. Oeckler, A. Feldhoff, *J. Electron. Mater.*, 48 (11), 2019, 7551 - 7561.  
DOI: 10.1007/s11664-019-07555-2
  7. **Metal-Organic Framework Co-MOF-74-Based Host-Guest Composites for Resistive Gas Sensing**, I. Strauss, A. Mundstock, M. Treger, K. Lange, S. Hwang, C. Chmelik, P. Rusch, N. C. Bigall, T. Pichler, H. Shiozawa, J. Caro, *ACS Appl. Mater. Inter.*, 11 (15), 2019, 14175 - 14181.  
DOI: 10.1021/acsami.8b22002
  8. **Covalent Organic Framework-Covalent Organic Framework Bilayer Membranes for Highly Selective Gas Separation**, H. Fan, A. Mundstock, A. Feldhoff, A. Knebel, J. Gu, H. Meng, J. Caro, *J. Am. Chem. Soc.*, 140 (32), 2018, 10094 - 10098.  
DOI: 10.1021/jacs.8b05136
-

- 
9. **Polymer-Stabilized Percolation Membranes Based on Nanosized Zeolitic Imidazole Framework for H<sub>2</sub>/CO<sub>2</sub> Separation**, J. Sanchez-Lainez, S. Friebe, B. Zarnozza, A. Mundstock, I. Strauss, C. Tellez, J. Caro, J. Coronas, *ChemNanoMat*, 4 (7), **2018**, 698 - 703.  
DOI: 10.1002/cnma.201800126
  
  10. **Frontispiz: The Integration of Guest Molecules with Co-MOF-74: A Vis/NIR Raman and Approach**, I. Strauss, A. Mundstock, D. Hinrichs, R. Himstedt, A. Knebel, C. Reinhardt, D. Dorfs, J. Caro, *Angew. Chem. Int. Ed.*, 57 (25), **2018**, 7434 - 7439.  
DOI: 10.1002/anie.201801966
  
  11. **Frontispiz: Vis/NIR- und Raman-Untersuchung der Wechselwirkung von Gastmolekülen mit Co-MOF-74**, I. Strauss, A. Mundstock, D. Hinrichs, R. Himstedt, A. Knebel, C. Reinhardt, D. Dorfs, J. Caro, *Angew. Chem.*, 130, **2018**, 7556 - 7561.  
DOI: 10.1002/ange.201882562
  
  12. **Cover Feature: Hierarchical Nanostructures of Metal-Organic Frameworks Applied in Gas Separating ZIF-8-on-ZIF-67 Membranes**, A. Knebel, P. Wulfert-Holzmann, S. Friebe, J. Pavel, I. Strauss, A. Mundstock, F. Steinbach, J. Caro, *Chem. Eur. J.*, 24 (22), **2018**, 5728 - 5733.  
DOI: 10.1002/chem.201705562
  
  13. **An azine-linked covalent organic framework ACOF-1 membrane for highly selective CO<sub>2</sub>/CH<sub>4</sub> separation**, H. Fan, A. Mundstock, J. Gu, H. Meng, J. Caro, *J. Mater. Chem. A*, 6 (35), **2018**, 16849 - 16853.  
DOI: 10.1039/c8ta05641b
  
  14. **Continuous Separation of light olefin/paraffin mixtures in ZIF-4 by pressure swing adsorption and membrane separation**, M. Hovestadt, S. Friebe, L. Helmich, M. Lange, J. Möllmer, R. Gläser, A. Mundstock, M. Hartmann, *Molecules*, 23 (4), **2018**, 889.  
DOI: 10.3390/molecules.23040889
  
  15. **On the better Understanding of the Surprisingly High Performance of Metal-Organic Framework-Based Mixed-Matrix Membranes Using the Example of UiO-66 and Matrimid**, S. Friebe, A. Mundstock, K. Volgmann, J. Caro, *ACS Appl. Mater. Inter.*, 9 (47), **2017**, 41553 - 41558.  
DOI: 10.1021/acsami.7b13037
  
  16. **On comparing permeation through Matrimid-based mixed matrix and multilayer sandwich FAU membranes: H<sub>2</sub>/CO<sub>2</sub> separation, support functionalization and ion exchange**, A. Mundstock, S. Friebe, J. Caro, *Int. J. Hydrogen. Energ.*, 42 (1), **2017**, 279 - 288.  
DOI: 10.1016/j.ijhydene.2016.10.161
-

- 
17. **An Untrodden Path: Versatile Fabrication of Self-Supporting Polymer-Stabilized Percolation Membranes (PSPMs) for Gas Separation**, S. Friebe, A. Mundstock, D. Scheider, J. Caro, *Chem. Eur. J.*, 23 (27), 2017, 6522 - 6526.  
DOI: 10.1002/chem.201701266
  18. **NH<sub>2</sub>-ML-125 as membrane for carbon dioxide sequestration: Thin supported MOF layers contra Mixed-Matrix-Membranes**, S. Friebe, A. Mundstock, D. Unruh, F. Renz, J. Caro, *J. Membr. Sci.*, 516, 2016, 185 - 193.  
DOI: 10.1016/j.memsci.2016.06.015
  19. **Deuterium/hydrogen permeation through different molecular sieve membranes: ZF, LDH, zeolite**, S. Friebe, N. Wang, L. Diestel, Y. Liu, A. Schulz, A. Mundstock, J. Caro, *Micropor. Mesopor. Mater.*, 216, 2015, 127 - 132.  
DOI: 10.1016/j.micromeso.201503034
  20. **Propene/propane permeation through Na-X membranes: The interplay of separation performance and pre-synthetic support functionalization**, A. Mundstock, N. Wang, S. Friebe, J. Caro, *Micropor. Mesopor. Mater.*, 215, 2015, 20 - 28.  
DOI: 10.1016/j.micromeso.2015.05.019
  21. **Amine-modified Mg-MOF-74/CPO-27-Mg membrane with enhanced H<sub>2</sub>/CO<sub>2</sub> separation**, N. Wang, A. Mundstock, Y. Liu, A. Huang, J. Caro, *Chem. Eng. Sci.*, 124, 2015, 27 - 36.  
DOI: 10.1016/j.ces.2014.10.037
  22. **Idiosyncrasies of Co<sub>2</sub>(dhtp): In situ-annealing by methanol**, C. Chmelik, A. Mundstock, P. D. C. Dietzel, J. Caro, *Micropor. Mesopor. Mater.*, 183, 2014, 117 - 123.  
DOI: 10.1016/j.micromeso.2013.09.002
  23. **Propylen/Propan-Trennung im Festbettadsorber und durch Membranpermeation**, A. Mundstock, U. Böhme, B. Barth, M. Hartmann, J. Caro, *CIT*, 85 (11), 2013, 1694 - 1699.  
DOI: 10.1002/cite.201300053
  24. **Ethene/ethane and propylene/propane separation via the olefin and paraffin selective metal-organic framework adsorbents CPO-27 and ZIF-8**, U. Böhme, B. Barth, C. Paula, A. Kuhnt, W. Schwieger, A. Mundstock, J. Caro, M. Hartmann, *Langmuir*, 29 (27), 2013, 8592 - 8600.  
DOI: 10.1021/la401471g
  25. **NHC-based self-assembled monolayers on solid gold substrates**, T. Weidner, J. E. Baio, A. Mundstock, C. Große, S. Karthäuser, C. Bruhn, U. Siemeling, *Aust. J. Chem.*, 64 (8), 2011, 1177 - 1179.  
DOI: 10.1071/CH11173
-



---

## Oral Presentations

**Metal-Organic Frameworks (MOFs) in Mixed-Matrix-Membranen für die energieeffiziente Trennung von Stoffgemischen (MOMa), A. Mundstock, J. Caro, *Third semi-annual Progress Meeting, Research and development project together with Evonik Creavis GmbH, 2020*, Marl, Germany.**

**Metal-Organic Frameworks (MOFs) in Mixed-Matrix-Membranen für die energieeffiziente Trennung von Stoffgemischen (MOMa), A. Mundstock, J. Caro, *Second semi-annual Progress Meeting, Research and development project together with Evonik Creavis GmbH, 2019*, Enschede, The Netherlands.**

**Metal-organic Frameworks (MOFs) in Mixed Matrix Membranes (MMMs), A. Mundstock, J. Caro, *Creative Quantum GmbH, 2019*, Berlin, Germany.**

**Metal-Organic Frameworks (MOFs) in Mixed-Matrix-Membranen für die energieeffiziente Trennung von Stoffgemischen (MOMa), A. Mundstock, J. Caro, *First semi-annual Progress Meeting, Research and development project together with Evonik Creavis GmbH, 2019*, Hannover, Germany.**

**MOF-75-based Gas Sensors, I. Strauss, A. Mundstock, J. Caro, *Porous Materials in Hannover Workshop, 2019*, Hannover, Germany.**

**Metal-Organic Frameworks (MOFs) in Mixed-Matrix-Membranen für die energieeffiziente Trennung von Stoffgemischen (MOMa), A. Mundstock, J. Caro, *Kick-off Meeting, Research and development project together with Evonik Creavis GmbH, 2019*, Marl, Germany.**

**Research Project for Evonik Creavis GmbH, A. Mundstock, S. Friebe, A. Knebel, J. Caro, *Closing Reports, Work packages I - VI, 2016 - 2018*, Marl/Hannover, Germany.**

**New nanoporous materials with optimized pore structure in the olefin/paraffin separation by permeation and adsorption, A. Mundstock, J. Caro, *DFG-Colloquium, SPP 1570, 2014*, Frankfurt, Germany.**

**New nanoporous materials with optimized pore structure in the olefin/paraffin separation by permeation and adsorption, A. Mundstock, J. Caro, *Solvay GmbH, 2012*, Hannover, Germany.**

**New nanoporous materials with optimized pore structure in the olefin/paraffin separation by permeation and adsorption, A. Mundstock, J. Caro, *DFG-Colloquium, SPP 1570, 2012*, Frankfurt, Germany.**

---

## Poster Presentations

**Tetrathiafulvalene Doped Cobalt containing Metal-Organic Framework for Resistive Gas Sensing**, I. Strauss, A. Mundstock, H. Shiozawa, M. Treger, K. Lange, S. Hwang, C. Chmelik, P. Rusch, N. Bigall, T. Pichler, J. Caro, *EuroMOF*, 2019, Paris, France.

**Tetrathiafulvalene Doped Cobalt containing Metal-Organic Framework for Gas Detection Applications**, I. Strauss, A. Mundstock, H. Shiozawa, M. Treger, K. Lange, S. Hwang, C. Chmelik, P. Rusch, N. Bigall, T. Pichler, J. Caro, *Deutsche Zeolith-Tagung*, 2019, Dresden, Germany.

**On the interaction of guest molecules with Co-MOF-74**, I. Strauss, A. Mundstock, D. Hinrichs, R. Himstedt, A. Knebel, C. Reinhardt, D. Dorfs, J. Caro, *Bunsentagung*, 2018, Leibniz Universität Hannover, Germany.

**Investigations of guest interaction with Co-MOF-74**, I. Strauss, A. Mundstock, D. Hinrichs, A. Knebel, C. Reinhardt, D. Dorfs, J. Caro, *EuroMOF*, 2017, Delft, The Netherlands.

**NH<sub>2</sub>-MIL-125 as membrane for carbon dioxide sequestration: Thin supported MOF layers contra Mixed-Matrix-Membranes**, S. Friebe, A. Mundstock, D. Unruh, F. Renz, J. Caro, *International Zeolite Membrane Meeting*, 2016, Dalian, China.

**NH<sub>2</sub>-MIL-125 as membrane for carbon dioxide sequestration: Thin supported MOF layers contra Mixed-Matrix-Membranes**, S. Friebe, A. Mundstock, D. Unruh, F. Renz, J. Caro, *Deutsche Zeolith-Tagung*, 2016, Gießen, Germany.

**Deuterium/hydrogen permeation through different molecular sieve membranes: ZIF, LDH, zeolite**, S. Friebe, N. Wang, L. Diestel, Y. Liu, A. Schulz, A. Mundstock, J. Caro, *Deutsche Zeolith-Tagung*, 2015, Oldenburg, Germany.

**The idiosyncrasies of M<sub>2</sub>(dhtp)**, A. Mundstock, C. Chmelik, U. Böhme, P. D. C. Dietzel, M. Hartmann, J. Caro, *Bunsentagung*, 2014, Hamburg, Germany.

**The idiosyncrasies of M<sub>2</sub>(dhtp)**, A. Mundstock, C. Chmelik, U. Böhme, P. D. C. Dietzel, M. Hartmann, J. Caro, *International MOF Symposium*, 2013, Dresden, Germany.

---

## Patent Applications

**Herstellungsverfahren für ein Material mit hoher nichtlinearer optischer Suszeptibilität zweiter Art**, I. Strauss, A. Mundstock, H. Fan, T. Koehler, F. Marlow, J. Caro, 2020, EZN (Erfinderzentrum Norddeutschland GmbH) Ref.-Nr.: 16898.

**Verfahren zur Herstellung einer Polymerstabilisierten Perkolationsmembran**, S. Friebe, A. Mundstock, J. Caro, *EP17151687*, 2017, EZN (Erfinderzentrum Norddeutschland GmbH) Ref.-Nr.: 16501.

---

## Curriculum Vitae

Name	Alexander Mundstock
Date/place of birth	12.01.1984, Zeitz
Nationality	German
since 2019	<p>LUH's head of operations and lead scientist for a research and development project in cooperation with Evonik Creavis GmbH.</p> <p>Project title: "<i>Metal-Organic Frameworks (MOFs) in Mixed-Matrix-Membranen für die energieeffiziente Trennung von Stoffgemischen (MOMa)</i>"</p> <p>Funded by the German Federal Ministry for Economic Affairs and Energy (BMWf funding code O3ET1557A).</p>
2016 - 2018	<p>Lead scientist for an industry-paid research project at the Leibniz University Hannover.</p> <p>Client: Evonik Creavis GmbH</p>
2012 - 2020	<p>Dissertation at the Institute of Physical Chemistry and Electrochemistry at the Leibniz University Hannover.</p> <p>Supervisor: Prof. Dr. Jürgen Caro</p> <p>Doctoral thesis title: "<i>Preparation and Characterization of Nanoporous Membranes with Optimized Pore Structure for the Separation of Practice-Relevant Binary Gas Mixtures</i>"</p>
2004 - 2011	<p>Study of Nanostructure and Molecular Sciences (Nanostrukturwissenschaften) at the University of Kassel.</p> <p>Degree: Diplom-Nanostrukturwissenschaftler (Dipl.-NanoSc.)</p> <p>Supervisor: Prof. Dr. Ulrich Siemeling</p> <p>Diploma thesis title: "<i>N-heterocyclische Carbene als Adsorbatspezies für selbstorganisierende Monolagen</i>"</p>
2003	Basic military service in the German Bundeswehr.
2003	Abitur at the Christopherus Gymnasium Droyßig with advanced studies in English and Biology.